Catalogued

Report No. FAA-RD-74-3

REMOTE SENSING WIND AND WIND SHEAR SYSTEM

Donald W. Beran

February 1974

Interim Report Covering Phase I and II
for Period April 1972 – December 1973

Document is available to the public through
the National Technical Information Service,
Springfield, Virginia 22151

Prepared for

DEPARTMENT OF TRANSPORTATION
FEDERAL AVIATION ADMINISTRATION
Systems Research and Development Service
Washington, D.C. 20591

DISCLAIMERS

The contents of this report reflect the views of the (NOAA/ERL, Wave Propagation Laboratory) which is responsible for the facts and the accuracy of the data presented herein. The contents do not necessarily reflect the official views or policy of the Department of Transportation. This report does not constitute a standard, specification or regulation.

The Environmental Research Laboratories, National Oceanic and Atmospheric Administration, U. S. Department of Commerce, does not approve, recommend or endorse any proprietary product or proprietary material mentioned in this publication. No reference shall be made to the Environmental Research Laboratories, or to this publication furnished by the Environmental Research Laboratories, in an advertising or sales promotion which would indicate or imply that the Environmental Research Laboratories approves, recommends or endorses any proprietary product or proprietary material mentioned herein, or which has as its purpose an intent to cause directly or indirectly the advertised product to be used or purchased because of this Environmental Research Laboratories publication.

Technical Report Documentation Page

1. Report No. FAA-RD-74-3	2. Government Accession No.	3. Recipient's Catalog No.
4. Title and Subtitle REMOTE SENSING WIND AND WIND SHEAR SYSTEM		5. Report Date January 1974
		6. Performing Organization Code NOAA/ERL, WPL R45x8
7. Author(s) Donald W. Beran		8. Performing Organization Report No.
9. Performing Organization Name and Address NOAA/ERL Wave Propagation Laboratory Boulder, Colorado 80302		10. Work Unit No. (TRAIS)
		11. Contract or Grant No. DOT-FA72WAI-281
12. Sponsoring Agency Name and Address DOT/FAA Aviation Weather Systems Branch Federal Aviation Administration Washington, D. C. 20590		13. Type of Report and Period Covered Interim report covering Phase I and II for period April 1972-December 1973
		14. Sponsoring Agency Code
15. Supplementary Notes		

16. Abstract The background for, and developmental history of acoustic Doppler is followed by a detailed study of winds that effect landing operations. A climatology of critical boundary layer wind shear and a study of optimum averaging times for reported winds show that the occurrence of severe wind shear is regional and not to be expected more than a small percentage of the time. Analysis of several ground based remote wind sensing devices suggests that the acoustic Doppler system is presently optimum. Weaknesses in any given device may, however, dictate that a joint sensor approach must be used to insure continual real time operation. The selection of an optimum antenna configuration and details of the hardware used during experimental tests at Stapleton International Airport are discussed in Chapter 4. Calibration of the Acoustic Doppler Wind System was accomplished by comparison with winds taken by anemometers suspended beneath balloons, tower mounted anemometers and slow ascent radiosondes. Agreement with all of these wind measurements was very good. Results from the operational tests at Stapleton indicate the Acoustic Doppler System can perform in the high noise environment of an airport. The effect of the high noise in terms of percentage of lost record has not yet been determined.

17. Key Words Acoustic Doppler Wind Shear Remote Sensing		18. Distribution Statement Document is available to the public through National Technical Information Service, Springfield, Virginia 22151.	
19. Security Classif. (of this report) Unclassified	20. Security Classif. (of this page) Unclassified	21. No. of Pages 115	22. Price

Form DOT F 1700.7 (8-72) Reproduction of completed page authorized

USCOMM - ERL

Foreword

This report contains the work of several individuals. Where an entire Chapter or Section was prepared by a single author or group of authors, they have been credited for their work in the by-line at the beginning of their Section. Chapter 3 contains the work of authors who are experts in particular remote sensing techniques. The timing of the project was such that these sections were written over one year before the final publication of this manuscript. The subject matter, remote sensing of winds by various techniques, is a rapidly advancing field and those interested in the latest developments are urged to contact the individual authors for the most recent developments.

Individuals who have contributed to other portions of the Report are Dr. F. F. Hall, Mr. B. Willmarth, Mr. E. Owens, Mr. J. Wescott, Mr. J. Keeler, Mr. D. Hunter. Their contributions are gratefully acknowledged. In addition, appreciation for the valuable assistance of Mrs. N. Alspaugh and Mr. W. Neff during preparation of the manuscript is expressed.

CONTENTS

		Page
CHAPTER 1	REMOTE SENSING OF WIND SHEAR AND THE THEORY AND DEVELOPMENT OF ACOUSTIC DOPPLER	1.1
1.1	Introduction	1.1
1.2	Theory	1.1
1.2.1	The Scattering Equation	1.1
1.2.2	The Absorption of Sound	1.2
1.2.3	Doppler	1.3
1.3	History of Development	1.3
	References (Chapter 1)	1.5
CHAPTER 2	WIND STUDIES	
2.1	A Climatological Study of Wind Shear in the Lower Layers of the Atmosphere	2.1
2.1.1	Introduction	2.1
2.1.2	Background	2.1
2.1.2.1	Operational Implications and the Representation of Wind Shear	2.1
2.1.2.2	Wind Shear and its effect on Aircraft Operations	2.2
2.1.2.3	Averaging Time	2.2
2.1.2.4	Models of Wind Shear and its Extreme	2.2
2.1.3	Method of Analysis	2.4
2.1.3.1	Frequency Distribution of Vector Fields: The Bivariate Frequency Table	2.4
2.1.3.2	Criteria for Extreme Wind Shear	2.6
2.1.3.3	Data Set and its Limitations	2.7
2.1.4	Results of Investigation	2.8
2.1.4.1	Denver Case Study	2.8
2.1.4.2	Meteorological Conditions During Extreme Wind Shear; Synopsis of Results	2.8
2.1.4.3	Conclusions Using all Stations	2.9
	References (Chapter 2, Section 1)	2.10
	Appendix A (Tabular & Graphical Results)	2.13
	Appendix B (Recommendations)	2.22
2.2	Optimum Averaging Times for Short Term Prediction of Winds in the Boundary Layer	2.24
2.2.1	Introduction	2.24
2.2.2	Optimum Sensor Location	2.25
2.2.3	Method of Analysis	2.25
2.2.4	Data Processing	2.26
2.2.5	Results	2.26
2.2.6	Conclusions and Summary	2.34
	References (Chapter 2, Section 2)	2.35
CHAPTER 3	A COMPARISON OF METHODS FOR THE REMOTE DETECTION OF WINDS IN THE AIRPORT ENVIRONMENT	3.1
3.1	Foreword and Summary	3.1
3.1.1	Introduction	3.1
3.1.2	Major Advantages and Disadvantages	3.2
3.1.3	Combined Sensor Approach	3.3
3.2	Short Range Radar for Wind Measurements at an Airport	3.4
3.2.1	Introduction	3.4
3.2.2	Radar Reflectivity Values	3.5
3.2.2.1	Reflectivity Factors for Rain	3.5
3.2.2.2	Reflectivity Factors for Clouds and Fog	3.5
3.2.2.3	Reflectivity Factor for Water Drops	3.6
3.2.2.4	Reflectivity Factor for Atmospheric Aerosols	3.6
3.2.2.5	Reflectivity Values for Refractive Index Fluctuations	3.6
3.2.3	Wind Field Measurements From Doppler Radar	3.7
3.2.3.1	Vertical Velocity	3.7
3.2.3.2	Horizontal Velocity	3.7
3.2.4	Radar System for Airport Wind Measurements	3.8
3.2.4.1	Pulse Doppler Radar	3.8
3.2.4.2	FM/CW Radar	3.9
3.2.4.3	Pseudorandom Coded Radar	3.9
3.2.5	Conclusions	3.11
	References (Chapter 3, Section 2)	3.12

CONTENTS (Continued)

3.3	Wind Profiles by Laser Scattering	3.14
3.3.1	Introduction	3.14
3.3.2	Laser Scattering Fundamentals	3.14
3.3.2.1	Doppler Frequency Shifts	3.14
3.3.2.2	Aerosol Scattering Intensity	3.15
3.3.2.3	Two Beam Interference	3.15
3.3.3	Operational Implication	3.16
3.3.3.1	Wind Shear Measurement Limitations	3.16
3.3.3.2	Safety Considerations	3.16
3.3.3.3	Possible Systems	3.16
3.3.4	Comparison With Other Wind Shear Sensors	3.17
3.3.5	Performance of Practical Laser Doppler Systems	3.17
3.3.5.1	Existing Systems	3.17
3.3.5.2	Comparison of Possible Systems	3.18
3.3.6	Research Recommendations	3.18
3.3.6.1	Ranging	3.18
3.3.6.2	Atmospheric Turbulence Effects	3.18
3.3.7	Conclusions	3.19
	References (Chapter 3, Section 3)	3.19
3.4	Measurement of Wind Velocity by Eddy Correlation Methods	3.20
3.4.1	Introduction and Summary	3.20
3.4.1.1	Principle of Operation	3.21
3.4.1.2	Passive Techniques	3.21
3.4.1.3	Active Techniques	3.22
3.4.2	Statistical Character of Atmospheric Eddies	3.28
3.4.3	Accuracy	3.29
3.4.4	Geometrical Configurations for Field Applications	3.29
3.4.5	Experimental Results	3.30
3.4.6	Safety Considerations	3.33
3.4.7	Conclusions	3.35
	References (Chapter 3, Section 4)	3.35
3.5	Passive Detection of Wind Profile With Ground Based Pressure Sensors	3.36
3.5.1	Introduction	3.36
3.5.2	Theory	3.36
3.5.3	Spectrum of Wall Pressure in Turbulent Flow	3.36
3.5.4	Phase Spectrum and Convection Velocity	3.37
3.5.5	Proposed Configuration of System	3.39
3.5.6	Conclusions	3.40
	References (Chapter 3, Section 5)	3.40
3.6	Acoustic Angle of Arrival Wind Sensing Techniques	3.41
3.6.1	Introduction	3.41
3.6.2	Theory	3.41
3.6.3	Conclusions	3.42
	References (Chapter 3, Section 6)	3.42
CHAPTER 4	ACOUSTIC DOPPLER SYSTEM DEVELOPMENT	4.1
4.1	Antenna Configuration Studies	4.1
4.1.1	Monostatic, Spaced Antennas	4.1
4.1.2	Monostatic, Clustered Antennas	4.1
4.1.3	Bistatic, Fanned or Wide Beam	4.1
4.1.4	Monostatic-Bistatic Configuration	4.2
4.1.5	Bistatic, Multiple Transmitters	4.2
4.1.6	Conclusions	4.2
4.2	Basic Components Required	4.2
4.2.1	Antenna Sub-System	4.3
4.2.2	Acoustic Sounder Sub-System	4.4
4.2.3	Computer Sub-System	4.5
4.2.4	Display Sub-System	4.8

CONTENTS (Continued)

		Page
CHAPTER 5	SYSTEM CALIBRATION	5.1
5.1	Introduction	5.1
5.2	Haswell Calibration Tests	5.1
5.3	Table Mountain Calibration Tests	5.1
5.4	Results and Conclusions on the Calibration Tests	5.6
CHAPTER 6	AIRPORT OPERATIONAL TESTS	6.1
6.1	Introduction	6.1
6.2	Site Selection	6.1
6.3	Installation	6.1
6.4	Results	6.1
CHAPTER 7	SUMMARY	7.1

ILLUSTRATIONS

Figure	Title	Page
1.1	Wave Vector Diagram	1.3
1.2	Vertical Velocity Field	1.4
1.3	Bistatic Test Configuration	1.4
1.4	Doppler vs BLP Winds	1.5
1.5	Table Mountain Field Setup	1.5
1.6	Doppler vs BLP Winds	1.5
1.7	Doppler Derived Isotachs	1.5
2.1.1	Wind Vector Components	2.4
2.1.2	Bivariate Frequency Table Format	2.5
2.1.3	Bivariate Frequency Table	2.5
2.1.4	Integration Limits for Frequency of Occurrence	2.5
2.1.5	Overlay for Bivariate Frequency Table	2.6
2.1.6	Overlay for Extreme Wind Shear	2.9
2.1.7a	Extreme Wind Shears (sfc.-150 m)	2.10
2.1.7b	Extreme Wind Shears (150-300 m)	2.10
	Appendix A - Fig. A1 to A10 - Monthly Summary of Wind Shear Data	2.14-2.16
2.2.1	Schematic of Forecasting Problems	2.26
2.2.2	RMSE of Wind vs 5 min Running Variance	2.27
2.2.3	30 m High Variance Wind	2.28
2.2.4	91 m High Variance Wind	2.28
2.2.5	152 m High Variance Wind	2.29
2.2.6	30 m High Variance Azimuth	2.29
2.2.7	91 m High Variance Azimuth	2.30
2.2.8	152 m High Variance Azimuth	2.30
2.2.9	30 m Low Variance Wind	2.31
2.2.10	91 m Low Variance Wind	2.31
2.2.11	152 m Low Variance Wind	2.32
2.2.12	30 m Low Variance Azimuth	2.32
2.2.13	91 m Low Variance Azimuth	2.33
2.2.14	152 Low Variance Azimuth	2.33
3.2.1	VAD Wind Field Measurement	3.7
3.2.2	Doppler Radar Measured Eddy Flow Field	3.8
3.2.3	Pulsed Doppler Velocity Measurements	3.9
3.2.4	FM/CW Radar Clear Air Returns	3.10
3.2.5	Radar Reflectivity Factors	3.12
3.4.1	Laser Configuration for Eddy Correlations	3.23
3.4.2	Max Range vs S/N, CO_2 Laser	3.26
3.4.3	Max Range vs S/N, CO_2 Laser	3.27
3.4.4	Max Range vs Energy Per Pulse	3.27
3.4.5	Max Range vs S/N, N_2 Laser	3.28
3.4.6	Covariance vs Delay for Separated Sensors	3.29
3.4.7	Conical Scan Wind Measuring Configuration	3.30
3.4.8	Passive Vertical Parallel Beams Eddy Correlations	3.31
3.4.9	Active Laser Eddy-Correlation	3.32
3.4.10	Pulsed Laser Eddy Correlation	3.32
3.4.11	Eddy Correlation Wind Velocities	3.33
3.4.12	Wind Velocities from Eddy Correlation	3.34

Figure	Title	Page
3.5.1	Theoretical Wall Pressure	3.37
3.5.2	Composite Plot of Normalized Power Spectra	3.37
3.5.3	Optimized Longitudinal Correlation Coefficient	3.38
3.5.4	Reciprocal Longitudinal Scale α vs Wave Number	3.38
3.5.5	Convection Velocity and Wavelength	3.39
3.5.6	Suggested Airport Arrangement	3.39
4.1	Bistatic Antenna Configuration	4.1
4.2	Multi-Transmitter Bistatic Antenna Configuration	4.2
4.3	Acoustic Doppler Wind System	4.3
4.4	Antenna Sub-System	4.3
4.5	Searchlight Beam Pattern	4.3
4.6	Off Axis Parabolic Horn	4.3
4.7	Off Axis Parabolic Horn Beam Pattern	4.4
4.8	Bunker Installation	4.4
4.9	Acoustic Sounder Sub-System	4.5
4.10	Timing Diagram	4.6
4.11	Computer Hardware	4.7
4.12	Computer Software	4.7
4.13	Tower Display	4.8
4.14	Tower Display, Block Diagram	4.8
5.1	Table Mountain Field Layout	5.2
5.2	Radiosonde vs Doppler Wind	5.4
5.3	" " " "	5.4
5.4	" " " "	5.4
5.5	" " " "	5.4
5.6	" " " "	5.5
5.7	" " " "	5.6
5.8	Scatter Diagram of Radiosonde vs Doppler Wind	5.6
5.9	Time-Height Section of Doppler Winds	5.7
6.1	Stapleton Airport Layout	6.1
6.2	Stapleton Radiosonde Wind vs Doppler Wind	6.2
6.3	" " " " "	6.2
6.4	" " " " "	6.2

TABLES

No.	Title	Page
2.1.1	Low Level Wind Shear Station Selection	2.8
2.1.2	Extreme Wind Shear Cases for Synoptic Analysis	2.9
2.1.3	Percentage Occurrence of Wind Shear	2.9
	Chapter 2 Appendix	
A-1	Percentage of Extreme Wind Shear by Month	2.17 - 2.21
2.2.1	Averaged High and Low 5 min Variance by Level	2.26
2.2.2	T-Test Results (High Variance)	2.35
2.2.3	T-Test Results (Low Variance)	2.35
3.1	Ratings of Remote Sensors	3.2
3.2.1	Reflectivity of Uniform Droplets	3.6
3.2.2	Pulse Doppler Radar Parameter	3.9
3.2.3	FM/CW Parameters	3.10
3.2.4	Potential FM/CW Radar	3.10
3.2.5	Pseudorandom Radar	3.11
5.1	Table Mountain Data Log 72T	5.3

CHAPTER 1

REMOTE SENSING OF WIND SHEAR AND THE THEORY AND DEVELOPMENT OF ACOUSTIC DOPPLER

1.1 INTRODUCTION

Wind shear, resulting from either a change in the speed or direction of the wind with height, can affect aircraft safety, especially in the critical takeoff and landing configurations. Analysis of this problem has demonstrated that unexpected wind shear along the path of a landing or departing aircraft could result in a variety of hazardous situations (see Chapter 2 of this report for a complete bibliography on this subject). Governing bodies such as the International Commission on Aircraft Operations (ICAO) and the Federal Aviation Administration (FAA) have recognized wind shear as a potential hazard to the safety of aircraft. The work reported on here is one action being taken by the FAA to solve the problem.

Lack of a good understanding of the nature, characteristics, and distribution of low-level shears has made it difficult to deal with this potential hazard on an operational basis. The only routine measurements of low level winds are made by radiosondes or rawinsondes taken, at most, a few times per day at major airports. These wind measurements lack both the time and spatial resolution necessary in near real time operations. This lack of complete information has hampered both the efforts to provide aircraft with a warning of hazardous winds, and those to establish a comprehensive climatology of low-level wind shear.

New ground based remote sensing techniques hold promise of solving this difficult wind measuring problem. Several devices have been tested (a discussion of each is contained in Chapter 3 of this report) and have demonstrated the ability to measure a vertical profile of the winds within 1 km of the ground. In terms of "stage of development" and overall ability to provide the necessary wind information, the acoustic Doppler system is the present leader in the field.

The primary thrust of the work reported here was to advance the development of the acoustic Doppler system to a point where an experimental model of an operational system could be installed at an airport for real time testing. This work is described in Chapters 4, 5, and 6 of this report. In addition, the problems of determining an optimum average time, to be used in predicting the wind a few minutes after an observation, and the development of a climatology of wind shear are presented in Chapter 2. The remainder of this chapter is devoted to theory relevant to the operation of an acoustic sounder, the Doppler principle, and the history of the development of the acoustic Doppler wind measuring system.

1.2 THEORY

1.2.1 The Scattering Equation. The knowledge that propagating sound waves are scattered by various properties in the atmosphere is not new, as is evidenced by Tyndall's observations, using the sound from a fog horn (Tyndall, 1874). Much later, the experimental work of Gilman et al. (1946) and Kallistratova (1959a, 1959b) led to a clearer understanding of the theory of sound scattering Kelton and Bricout (1964) were the first to demonstrate that the scattered sound was strong enough to determine the Doppler shift produced by wind induced motion of the air. Australian scientists under the direction of McAllister (1968) showed that the scattered echoes, if properly displayed, could be useful for study of atmospheric motions. Shortly after this, Little (1969) outlined many potential uses of acoustic methods for remotely probing the lower atmosphere. Later experimental efforts confirmed Little's prediction that an acoustic sounder could be useful in the study of inversion structure (Beran, 1970a; Emmanuel et al., 1972; Hall et al., 1971; Beran et al., 1971a), the measurement of wind (Beran et al., 1971b; Beran and Clifford, 1971) and the monitoring of wave motions and momentum transport (Hooke et al., 1971 and Beran et al., 1972). One of the early proposals for an operational application, the use of an acoustic sounder to monitor the environment near an airport was made by Beran (1971) and led to the project described in this report.

Theoretical studies of the scatter of sound by turbulent velocity fluctuations in the atmosphere have been conducted by several workers (Lighthill, 1953; Kraichnan, 1953; Batchelor, 1957). Later, the effects of both velocity and temperature fluctuations were considered by Tatarskii (1961, 1971) and Monin (1961).

Following this work, we can write the equation for the scatter of sound in dry air as

$$d\sigma = \frac{2\pi k^4 V \cos^2\theta}{\left[\frac{E(K)}{C^2}\cos^2\frac{\theta}{2} + \frac{\phi(K)}{4T^2}\right]^{-1}}\, d\Omega \qquad (1.1)$$

where $d\sigma$ is the fraction of the incident acoustic power which is scattered by irregularities in volume V (the scattering volume) through an angle θ into a cone of solid angle $d\Omega$. The wave number of the acoustic wave is $k = 2\pi/\lambda$; $K = 2k(\sin\theta/2)$ is the effective wave number at which an acoustic sounder scattering through angle θ interrogates the medium. The speed of sound and the mean temperature in the scattering volume are given by C and T, respectively, and the spectral intensity of the wind fluctuations is given by E(K), and the temperature fluctuations by $\phi(K)$, at wave number K.

If we assume that a Kolmogorov spectrum of turbulence represents the true atmospheric processes, Equation 1.1 can be reduced to

$$\sigma(\theta) = \frac{0.03k^{1/3}\cos^2\theta\,(\sin\frac{\theta}{2})^{-\frac{11}{3}}}{\left[\frac{C_v^2}{C^2}\cos^2\frac{\theta}{2} + 0.13\frac{C_T^2}{T^2}\right]^{-1}} \qquad (1.2)$$

where $\sigma(\theta)$ is now the scattered power per unit volume, per unit incident flux per unit solid angle at an angle θ from the initial direction of propagation. Values of C_v and C_T are obtained from the structure functions for wind,

$$D_W = \overline{\left[W(x) - W(x + r)\right]^2} = C_v^2 \; r^{2/3} , \qquad (1.3)$$

and for temperature,

$$D_T = \overline{\left[T(x) - T(x + r)\right]^2} = C_T^2 \; r^{2/3} . \qquad (1.4)$$

The values W(x) and T(x) are the instantaneous wind speed and temperature, respectively, at point x. W(x + r) and T (x + r) are the corresponding instantaneous values at point (x + r).

The equations given above do not take account of Doppler effects due to the transport of small eddies by large-scale eddies, and there is no term to include the effect of humidity fluctuations. The assumption that the turbulence is isotropic is also rather restrictive when applied to the real atmosphere where horizontal layers can contain a large degree of anisotropy.

For the application considered in this report, acoustic Doppler, the limitations inherent in the scattering equation are, fortunately, less important. It is critical only that the scattered energy be large enough so its frequency can be tracked; knowing the exact cause and magnitude of the atmospheric effects is, for the most part, unimportant.

The scattering equation does contain information that must be considered in the design of a Doppler sounder, particularly with regard to the particular antenna configuration to be employed. For example, the scatter equation tells us that:

1) the scattered acoustic power varies relatively weakly with wavelength ($\sigma \propto \lambda^{-1/3}$);

2) the scattered power is the sum of two terms, one related to wind fluctuations and one due to temperature fluctuations;

3) both wind and temperature scattering terms are multiplied by $\cos^2\theta$, which means that no power will be scattered at an angle of 90°;

4) the wind term includes a $\cos^2(\theta/2)$ multiplying term, or the wind fluctuations produce no scatter in the backward direction ($\theta = 180°$); and

5) both the wind and temperature components of the scatter are multiplied by a $(\sin\theta/2)^{-11/3}$ factor, or most of the scatter is in the forward hemisphere.

In practice, items 2 and 4 imply that a bistatic system (transmitter and receiver separated) will receive stronger signals than a monostatic system (transmitter and receiver collocated), an important consideration for achieving long ranges with a minimum of transmitted power. Item number 3 further suggests that the intersecting angle between the transmitter and receiver should never be equal to 90° where no energy will be scattered. These factors are important considerations in the development of an optimum antenna configuration, as will be demonstrated later in this report.

1.2.2 The Absorption of Sound. The subject of sound absorption has been extensively treated by several authors and a reasonably complete bibliography can be found in papers by Harris and Tempest (1965) and Harris (1966, 1968). Briefly, it is conventional to divide the attenuation coefficient for sound absorption into a so-called classical term and a molecular term. Studies by Delsasso and Leonard (1953) and Beran (1970b) indicate that a third term, called excess attenuation, may also be of importance when considering losses along a one-way transmission path or in a bistatic system.

Classical absorption is a function of viscosity, heat conduction, molecular diffusion, and radiation of heat. It is normally at least one order of magnitude less than the absorption due to molecular effects and as such can be neglected. Molecular absorption, on the other hand, can be as great as spreading losses (proportional to the distance squared) and is an important consideration. This type of absorption is due to the relaxation process involving a lag in the adjustment of the vibrational energy of O_2 molecules during the passage of a sound wave. Excess absorption is thought to be largely due to the scattering of sound out of a transmitted beam and not a true absorption phenomena.

Molecular absorption, the predominant term, is a function of the temperature and moisture content of the air through which the sound wave is propagating and of the frequency of the sound wave. In general, the molecular absorption increases rapidly as the frequency is increased, suggesting that the lower the carrier frequency, the better. This assumption must be modified when one also considers that ambient background noise increases rapidly at lower frequencies. In practive, the selection of an optimum carrier frequency must be a trade-off between the absorption at high frequency and the high noise levels at low frequencies.

1.2.3 Doppler. If the scattering volume referred to in Section 1.2.1 is in motion as a result of the ambient wind, the frequency of the scattered sound will be Doppler shifted. The amount of shift will be a function of the wind speed and the angle from which it is observed.

The diagram shown in Figure 1.1 can be used to develop an equation relating the Doppler shift to the antenna configuration and the wind speed. Sound transmitted from an antenna at T and having a frequency f_o insonifies some scattering volume at O. If this scattering volume is moving with a velocity, $\vec{V}$ the frequency of the sound wave received at point R will be some new value, f_s, and we can calculate a difference frequency, $\Delta f = f_s - f_o$, proportional to $\vec{V}$. If we express the transmitted frequency as a wave vector $\vec{K}_o$ and the scattered wave as $\vec{K}_s$ the difference frequency, or Doppler shift can be written in vector notation as

$$\Delta f = \frac{1}{2\pi} (\vec{K}_s - \vec{K}_o) \cdot \vec{V} \qquad (1.5)$$

where $\vec{V}$ is the wind component in the plane formed by the transmitter and receiver beams. Writing Equation 1.5 in terms of the wavelength λ_o of the carrier wave, the angle β between the total wind vector $\vec{V}$ in the plane and the component being measured, and the scattering angle θ, we have

$$\Delta f \approx \frac{2V}{\lambda_o} \sin(\frac{\theta}{2}) \cos \beta \qquad (1.6)$$

where $V \cos \beta$ is now the magnitude of the wind resolved along the vector $\vec{K}_s - \vec{K}_o$. Note that the direction of this component is along the bisector of the angle formed by the intersection of the two beams. It will become the radial component only when the transmitter and receiver are collocated in a monostatic system.

Replacing λ_o by C/f_o in Equation 1.6, where C is the speed of sound, and solving for the magnitude of the wind component in the plane, we have

$$V \cos \beta = V' = \frac{C}{2 \sin(\frac{\theta}{2})} \left[\frac{\Delta f}{f_o}\right] . \qquad (1.7)$$

Second and third order terms have been neglected in the derivation of Equation 1.7.

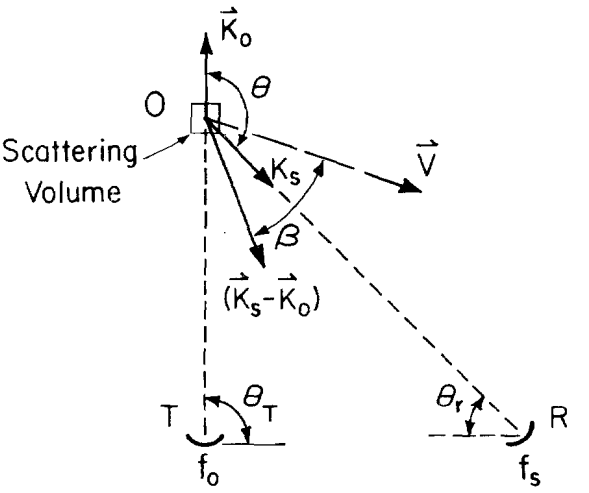

Figure 1.1 Wave vector diagram showing the component of the wind measured by a Doppler shift.

Atmospheric refraction effects can alter the geometry shown in Figure 1.1. Wind shear and a temperature gradient along the path of the sound wave can change the apparent location of the scattering volume. This will also result in a shift in the axis of resolution of the Doppler component and an error in the magnitude of the derived wind. These effects are considered in detail by Beran and Clifford (1971) and by Georges and Clifford (1972). It was concluded from these studies that a worst case error for a system with 1 km range would be of the order of 5%.

The basic physical principles outlined in this and the previous sections govern the range of possible sounder configurations that can be employed. Several possibilities can be envisioned. These are discussed more fully in the following section, and in Chapter 4 where final experimental configuration for Doppler wind measurements is selected.

1.3 HISTORY OF DEVELOPMENT

The first experimental demonstration that the acoustic Doppler shift from scattered sound was related to the ambient wind was made by Kelton and Bricout (1964). While adequately demonstrating the principle, their work was limited to measurements only a few meters above the ground. The full potential of the technique for measuring winds at greater heights was not exploited.

Further development of the technique did not take place until after McAllister (1968) had shown that a vertically pointed monostatic sounder could be used to reveal the intricate patterns of boundary layer structure. Using an experimental setup similar to that employed by McAllister, a vertical profile of the vertical wind component was derived in an experiment near Boulder, Colorado (Beran et al., 1971).

This was achieved by gating the returned echo at successive heights on each pulse of a vertically pointed monostatic system. The spectrum in each of these height gates was then determined and the spectra from several (5 to 10) gates on succeeding pulses were averaged together. This averaging was necessary in order to achieve a greater degree of spectral stability. The first moment of the resulting spectrum was then subtracted from the original carrier frequency and this value was converted to the wind speed component along the monostatic beam. This procedure was repeated until a time height cross section of vertical winds were derived, resulting in the pattern of isotachs shown in Figure 1.2. The left side of the figure shows the pattern displayed by the facsimile recording from the acoustic sounder; the right side is the corresponding vertical velocity field determined from the acoustic Doppler shift. This experiment demonstrated that realistic and continuous patterns of vertical velocity could be measured with the acoustic Doppler technique. It did not, however, verify that the magnitude of the winds were correct.

A second experiment was designed with the dual purpose of testing the ability of the sounder to measure a component of the horizontal wind and to verify the measurement through comparison with accepted standard wind sensors.

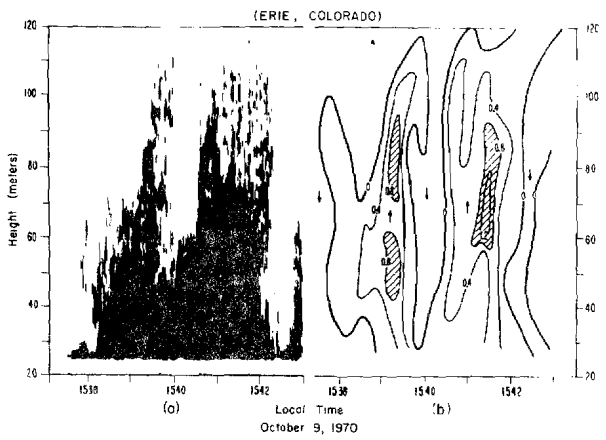

Figure 1.2 Acoustic echoes (left) and Doppler derived vertical velocity field during thermal plume activity. Contour interval is 0.4 m/sec, regions of vertical velocity >0.8 m/sec are shaded, arrows indicate direction of vertical component.

A bistatic sounder configuration was used for this test (see Figure 1.3). The sound pulse was transmitted from the vertically pointed antenna and the scattered sound received at the tilted antenna. A second phase of this test employed the tilted antenna in the monostatic mode. The results of these tests made it possible to draw conclusions about the differences between winds measured with a tilted monostatic system where the measured component is along the beam and near the horizontal, and a bistatic configuration where the measured component is directed along the bisector at the intersection of the two antenna beams. Winds measured by both systems were compared with a kytoon mounted anemometer, part of the National Center of Atmospheric Research (NCAR) Boundary Layer Profiler (BLP) tethered at an altitude near the intersection of the two beams. Figure 1.4 shows the comparison of the winds measured by the Doppler method (DOP) and by the anemometer (BLP). The correlation coefficient of 0.94 suggests excellent agreement. The results also indicated that a low powered monostatic system could lose signal during times of weak C_T activity while the bistatic system received the expected, much stronger, signals and did not suffer from the problem of signal fading.

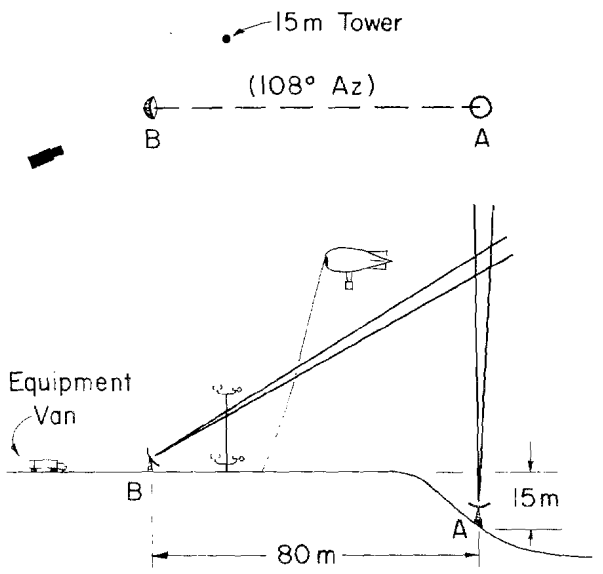

Figure 1.3 Plan and elevation view of bistatic test configuration.

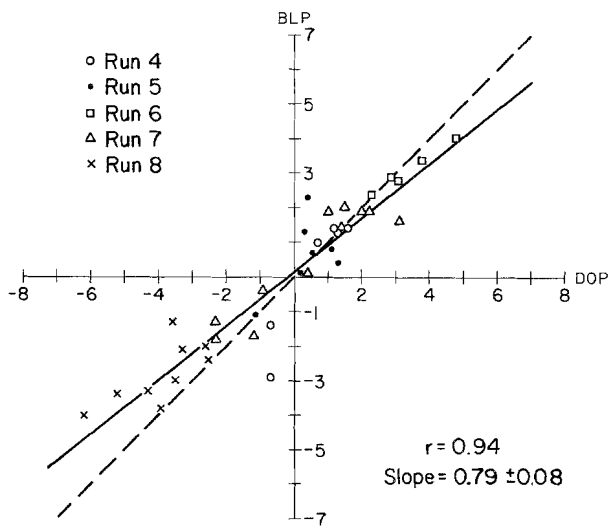

Figure 1.4 Scatter diagram of measured (1 min averages) for 5 separate runs. Boundary Layer Profile winds are plotted on the BLP axis, Doppler winds on the DOP axis.

The next series of tests was designed to measure the total wind component and to explore methods of measuring a vertical profile of the horizontal wind. To do this the sounder configuration used previously was expanded to include a third antenna pointed at the common volume of the first two and located on a line normal to the plane of the first two (see Figure 1.5). Bistatic measurements were again compared with the anemometer and the scatter diagram of the two sets of wind measurements is shown in Figure 1.6.

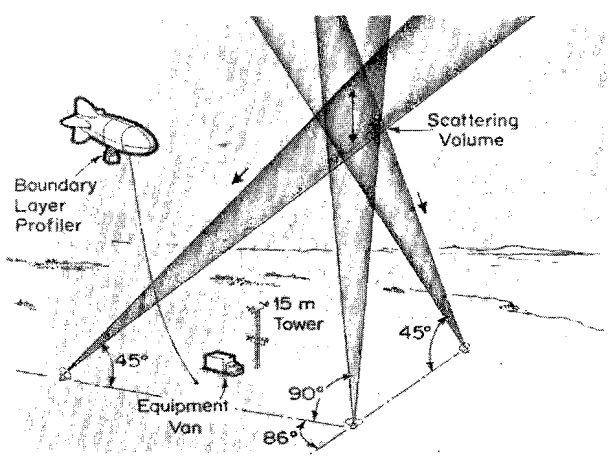

Figure 1.5 Schematic of the field setup for testing the three axis Doppler wind technique. Antenna spacing was varied from 150 to 200 m.

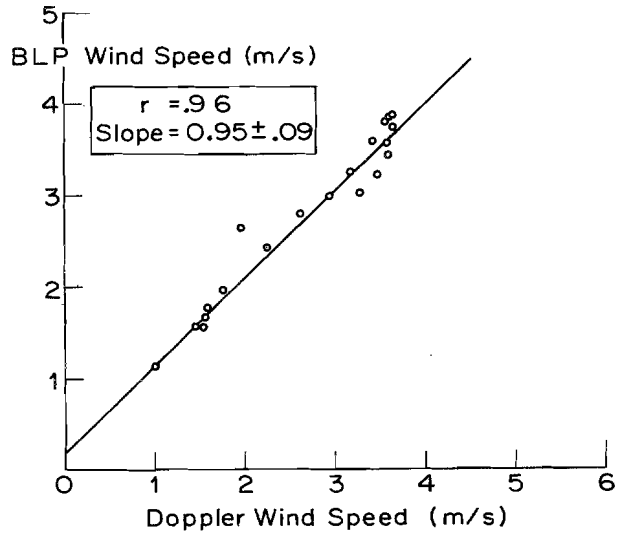

Figure 1.6 Scatter diagram of Doppler vs BLP winds.

Using the same configuration as that shown in Figure 1.5, we first attempted to measure a vertical profile of the horizontal wind. This was done by operating the three separate antennas in a monostatic mode and gating each of the signals to produce the Doppler spectrum at successive equal heights. In this way, three wind components directed along their respective beam axes were generated at each height gate. These components were then averaged on succeeding pulses for periods of from 3 to 5 min, or a time long enough so horizontal homogeneity over a distance equivalent to the antenna spacing could be assumed. At each height gate the three averaged components were combined to produce the total wind vector. The resulting height time section of the horizontal isotachs is shown in Figure 1.7. It was the demonstrated ability to measure a vertical profile of the horizontal wind that led to the work reported here.

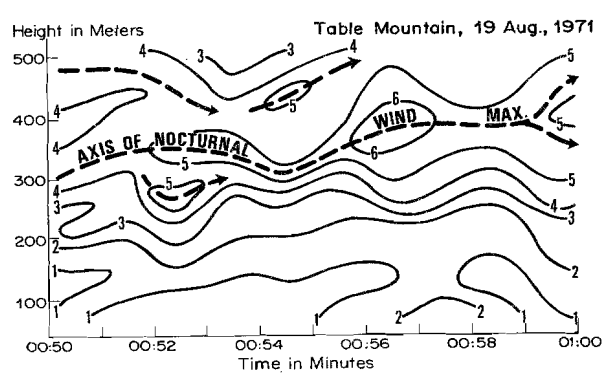

Figure 1.7 Time section of isotachs for horizontal wind m/sec under oscillating inversion. Winds were derived solely from acoustic Doppler measurements.

REFERENCES (Chapter 1)

Batchelor, G. K., 1957: Wave scattering due to turbulence. Proc. Symp. Naval Hydrodynamics, NAS-NRC Publ. 515, 409-430.

Beran, D. W., 1970a: Turbulence Detection, Ph.D. Thesis, University of Melbourne, Australia.

Beran, D. W., 1970b: Application of acoustics to meteorology, Report No. II, Project EAR, Univ. of Melbourne, Publication No. 15.

Beran, D. W., F. F. Hall, Jr., J. W. Wescott, and W. D. Neff, 1971a: Application of an acoustic sounder to air pollution monitoring, Proc. Air Pollution Turbulence & Diffusion Symp., Dec. 7-10, 1971, New Mexico Univ, Las Cruces, N. M.

Beran, D. W., C. G. Little, and B. C. Willmarth, 1971b: Acoustic Doppler measurements of vertical velocities in the atmosphere. Nature, 230, 160-162.

Beran, D. W., and S. F. Clifford, 1971: Acoustic Doppler measurements of the total wind vector. Proc. AMS Second Symp. on Meteorological Observations and Instrumentation, San Diego, Calif.

Beran, D. W., 1971: Acoustics: A new approach for monitoring the environment near airports. Jour. of Aircraft, AIAA, 8, pp. 934-936.

Beran, D. W., W. H. Hooke, and S. F. Clifford, 1972: Acoustic echo-sounding techniques and their application to gravity-wave, turbulence, and stability studies, Boundary Layer Meteorology 4, 133-153.

Delsasso, L. P., and R. W. Leonard, 1953: The attenuation of sound in the atmosphere. USAF Cont. W-28-099-AC-228.

Emmanuel, C. G., B. R. Bean, L. G. McAllister, and J. R. Pollard, 1972: Observations of Helmholtz waves in the lower atmosphere with an acoustic sounder, Jour. of Atmos. Sci., 29, No. 5, 886-892.

Georges, T. M., and S. F. Clifford, 1972: Acoustic sounding in a refracting atmosphere. Acoust. Soc. Amer, 52, No. 5 (Part 2).

Gilman, G. W., H. B. Coxhead and F. H. Willis, 1946: Reflection of sound signals in the troposphere. J. Acoust. Soc. Amer., 18, 274-283.

Hall, F. F. Jr., J. W. Wescott, and W. R. Simmons, 1971: Acoustic echo-sounding of atmospheric thermal and wind structure. Proc. Seventh Symp. on Remote Sensing of Environment. Univ. of Mich. pp. 1715-1732.

Harris, C. M., and W. Tempest, 1965: Absorption of sound in air below 1000 CPS, NASA CR-237.

Harris, C. M., 1966: Absorption of sound in air versus humidity and temperature. J. Acoust. Soc. Amer., 40, 148-159.

Harris, C. M., 1968: On the absorption of sound in humid air at reduced pressures. J. Acoust. Soc. of Amer. 43, 530-532.

Hooke, W. H., J. M. Young, and D. W. Beran, 1971: Atmospheric waves observed in the planetary boundary layer using an acoustic sounder and a microbarograph array. Boundary Layer Meteorology, 2, 371-380.

Kallistratova, M. A., 1959a: An experimental investigation into the scattering of sound in a turbulent atmosphere. Dokl. Akad. Nauk, SSSR, 125, No. 1, 69-72.

_____, 1959b: Procedure for investigating sound scattering in the atmosphere. Akust. Zh., 5, 496-498 (also Soviet Phys. Acoust. 5, 512-514).

Kelton, G., and P. Bricout, 1964: Wind velocity measurements using sonic techniques. Bull. Amer. Meteor. Soc., 45, 571-580.

Kraichnan, R. H., 1953: The scattering of sound in a turbulent medium. J. Acoust. Soc. Amer., 25, 1096-1104.

Lighthill, M. J., 1953: On the energy scattered from the interaction of turbulence with sound or shock waves. Proc. Cambridge Phil. Soc., 49, 531-555.

Little, C. G., 1969: Acoustic methods for the remote probing of the lower atmosphere. Proc. of the IEEE, 57, No. 4, 571-578.

McAllister, L. G., 1968: Acoustic sounding of the lower troposphere. J. Atmos. Terr. Phys., 30, 1439-1440.

Monin, A. S., 1961: Characteristics of the scattering of sound in a turbulent atmosphere. Akust. Zh., 7, 457-461 (also Soviet Phys. Acoust. 7, 370-373.

Tatarskii, V. I., 1961: Wave Propagation in a Turbulent Medium. New York, McGraw-Hill.

Tatarskii, V. I., 1971: The Effects of the Turbulent Atmosphere on Wave Propagation, U. S. Dept. of Commerce, Springfield, Va. 22151, 472 pp.

Tyndall, J., 1874: On the atmosphere as a vehicle of sound. Phil. Trans. Roy. Soc. London, 164, 183-244.

CHAPTER 2

WIND STUDIES

2.1 A CLIMATOLOGICAL STUDY OF WIND SHEAR IN THE LOWER LAYERS OF THE ATMOSPHERE (by R. L. Grossman)

2.1.1 Introduction. The effect of wind shear in the lower layers of the atmosphere on aircraft takeoff and landing operations is quite complex (Brown, 1961; Gera, 1971). As an example, during a landing operation, lack of correction for vertical wind shear can result in short landing, not enough thrust to compensate for fall speed, improper pitch angle, or landing long and too fast (Melvin, 1970; Neyland, 1956; Snyder, 1968). Furthermore, it is conceivable that the performance characteristics of existing aircraft and those presently under design will not be able to withstand certain extreme values of vertical wind shear no matter what corrective action is taken by the pilot (Melvin, 1970; Air France, 1963; Fichtl, 1972). The effects of vertical wind shear on automatic landing systems may be even more critical, since they may respond incorrectly or too slowly in an emergency (Burnham, 1967; Watson, 1969; St John, 1967; Burnstein, 1971).

In the charges of the CAeM/III (1964), the International Civil Aviation Commission (ICAO) member states were asked to investigate low-level wind shear conditions in the vicinity of aerodromes. As a result, since 1964 several studies having direct applicability to aircraft operations have been conducted at airfields and meteorological towers. Several of these studies are contained in Aeronautical Meteorology (1969) and Vertical Wind Shear in the Lowest Layers of the Atmosphere (1969).

The studies cited above emphasize the fact that although low-level wind profiles have been extensively studied in the U. S. (Letteau and Davidson, eds., 1957; Lumley and Panofsky, 1964; Scoggins, 1970; for example, as well as numerous studies of wind measured at the well-known U. S. meteorological towers located at Silver Hill, Md.; Round Hill, Mass.; Oak Ridge, Tenn.; Brookhaven, N. J.; Oklahoma City, Okla.; and Cedar Hill, Texas) truly climatological statistics of low-level wind shear values are lacking in the U. S.

The literature concerning the study of vertical wind profiles and associated shears derived from rawinsonde, pibal, and radiosonde balloon ascents is considerable (see Reiter, 1961). However, most of these studies were concerned with data gathered well above the planetary boundary layer. An outstanding exception is the study of boundary layer wind maxima by Blackadar (1957). It appears that no extensive stud has been made of low-level wind shear which utilized upper air balloon ascents in the Continental United States (CONUS). Further, with the exception of a few studies conducted outside of the CONUS, there are very few statistical representations of the occurrence of vertical wind shear values for relatively long periods (i.e., covering many different synoptic meso- and microclimatological situations). Notable among the exceptions is the work of Fichtl (1971).

This study, therefore, will attempt to provide a statistical background on the climatological aspects of low-level wind shear at various points in the CONUS.

2.1.2 Background.

2.1.2.1 Operational Implications and the Representation of Wind Shear. Physically, shears have the dimension, sec^{-1} and are mathematically represented by a derivative with respect to the spatial direction of interest (i.e., $\partial\bar{V}/\partial x$, $\partial\bar{V}/\partial y$, $\partial\bar{V}/\partial z$) .

Whether or not this method of representation is adequate, of course, depends upon the problem. Melvin (1970) disucsses the effect of wind shear on landing operations, and it is apparent from his discussion that the problem of ideally depicting wind shear for aircraft operations is far from the simple one of measuring gradients. As the aircraft descends along the glide path we see that if gradients were sufficient, one would need to know

$$\frac{\partial}{\partial x}\left(\frac{\partial\vec{V}}{\partial z}\right) = \frac{\partial^2\vec{V}}{\partial x\,\partial z} \quad . \qquad (2.1.1)$$

However, the principle of horizontal homogeneity is invoked so that

$$\frac{\partial^2\vec{V}}{\partial x\partial z} = 0 \quad , \qquad (2.1.2)$$

and we need only study the vertical variation of the horizontal wind. The application of this principle in practice has not been investigated, (Clodman et al., 1969). Further, we note that

$$\frac{\partial\vec{V}}{\partial z} = \left(\frac{\partial\overline{\vec{V}}}{\partial z}\right) + \left(\frac{\partial\vec{V}}{\partial z}\right)' \qquad (2.1.3)$$

where the overbar denotes some time average and the ($'$) denotes a departure from the average. The actual shear affecting the aircraft can be envisioned as a mean shear condition over a given period of time and a deviation from that mean, or a shear "gust," which can be above or below the mean value. A continuous depiction of instantaneous shear "gust," which is not possible, therefore, one must filter or chose a mean, which includes the frequencies of wind shear fluctuations which would affect the aircraft while eliminating from the representation those that do not.

Mathematically speaking this amounts to

$$\frac{\partial \vec{V}}{\partial z} \cong \overline{\frac{\partial \vec{V}}{\partial z}} \quad , \qquad (2.1.4)$$

which according to the Reynolds averaging rules can be written

$$\frac{\partial \vec{V}}{\partial z} \cong \frac{\partial \overline{\vec{V}}}{\partial z} \quad . \qquad (2.1.5)$$

Assuming that it takes a pilot about 1 sec to decide to correct for an approach problem 1 sec to act, and another 1 sec for the aircraft to respond, one notes that with a descent rate of only 3 mps and a ground speed of 85 mps, the aircraft has traversed 9 m vertically and 255 m horizontally. This gives one some limits to the vertical spacing of the shear gradient measurement (i.e. > 9 m) and the averaging time (i.e. > 3 sec) even though the aircraft may respond to a smaller spacing interval and averaging time (see for instance Duncan, 1959, p. 112). Since

$$\frac{\partial \overline{\vec{V}}}{\partial z} = \lim_{\Delta z \to 0} \frac{\Delta \overline{\vec{V}}}{\Delta z} \quad , \qquad (2.1.6)$$

it appears that from an operational point of view the quantity that affects the aircraft is $\Delta\vec{V}/\Delta z$, not $\partial\vec{V}/\partial z$. Intuitively, it can be seen that

$$\frac{\Delta \overline{\vec{V}}}{\Delta z} = f(\Delta z) \qquad (2.1.7)$$

irrespective of the averaging time (see Section 2.1.3.2).

2.1.2.2 Wind Shear and Its Effect on Aircraft Operations. As noted by Kraus (1972), wind shear has rarely been directly cited as the cause for an aircraft accident or incident. The results of failing to correct for wind shear could easily be interpreted by an investigating board as falling into the broad categories of pilot error and mechanical failure, since the influence of wind shear on aircraft control has only recently gained attention in the field of air safety. It would be interesting to see how past aircraft accidents and incidents at a particular airport correlate with past periods of extreme wind shear.

2.1.2.3 Averaging Time. Previous workers have been aware of the effect of averaging time on the value of derived wind shears. Rijkoort (1969) compared block averaged time series by investigating the ratio of the range to the standard deviation. This ratio decreased from about 5 to 4 with increasing averaging time (i.e. 6, 9, 12, and 30 sec. means). Rijkoort and Wieringa (1969) discussed the low-level shear problem as it applied to aircraft operations and suggested an averaging time for shears of less than 4 min. They stated that shears averaged for longer periods greatly underestimate the "actual" value. Muller and Mushkat (1969) report on 10 and 60 min averages of wind shear at three stations in Canada. In their discussion, they feel that the averaging time for wind shears should not exceed 15 sec. They further note the effect of vertical and horizontal spacing of the sensors and conclude that the two sensors measuring the wind at different levels be separated by a horizontal distance as well as a vertical distance. Ito (1969) investigated wind shear at Tokyo International Airport and noted the effect of averaging (he used 5 and 10 min averages). He feels that the wind shear measurement should be nearly instantaneous.

Watson (1969) saw little difference between the use of 10 min and 2 min wind shear averages. He preferred the 2 min averages because that is the approximate time the aircraft is in the approach - landing configuration. Spillane and Brook (1969) in their study of wind shear during near neutral conditions at Melbourne Airport related the variance of the shear magnitude to the 150 m mean wind speed in the following way:

$$\sigma_s\ (\Gamma,t) = h\ (\Gamma,t)\ \overline{v}_{150},\ 0 < h\ (\Gamma,t) < 1\ . \qquad (2.1.8)$$

Here Γ is the length of the time series used (often 1 hr), and t is the various averaging periods (i.e. 5 sec to 60 sec). In general, they found lower values of t were associated with high values of σ_s (see their Fig. 6 and Brook, 1968). Burnham (1970) gives a plausible argument that a pilot may not be able to distinguish between the effects of the gustiness of the horizontal wind field and a sudden wind change due his descent through a region of high vertical shear. This question can be resolved to a certain extent by comparing the spectral analysis of the horizontal wind field with a simultaneous spectral analysis of the shear field for different vertical separations and seeing which components would affect the aircraft through its response function.

2.1.2.4 Models of Wind Shear and Its Extremes. There are three basic approaches used in the modeling of wind shear; each has advantages for aircraft operations. These methods can be characterized as physical, statistical, and meteorological.

Physical Modeling. This method is largely analytical. It attempts to deduce the physical reasons for the formation of wind gradients near the ground and especially the conditions under which these gradients become extreme and break down (e.g., Schlicting, 1960; Hinze, 1959; Letteau et al., 1961; Blackadar and Panofsky, 1970; Taylor, 1969, 1970; Peterson, 1969; as well as discussions of the critical Richardson number by Goldstein, 1931; Drazin, 1958; Arya, 1972; Emmanuel, 1972).

Statistical Modeling. In this approach, the statistical properties of the wind shear population as they relate to a given area is investigated. It is assumed that the population is not universal; however, proper scaling of wind shear may reveal a universality in the wind shear population, not heretofore noticed. Due to the difficulty of measuring wind shear routinely, the amount of information available is small. In fact, as the previous discussion of averaging in

this report has indicated, the exact limits of sampling rate and size of sample for a good description of wind shear population is still unresolved.

Some methods of statistical description that could be incorporated into low-level wind shear studies have been discussed in "Vertical Wind Shear in the Lowest Layers" (1969), Scoggins (1970), and Henry and Cochrane (1964). Brook (1968) and Watson (1969) appear to model the low-level wind shear population as being normally distributed. Clodman, et al. (1969) and Essenwanger (1968) disagree with a normal distribution model, especially for the description of extreme wind shears. Among those in the USSR reporting on the statistical description of low-level wind shear are Abramovic and Glazunov (1969), Mashkova (1967), and Tsverava (1967). Kurkowski, et al. (1971) provide a nomogram for probability of wind shear exceeding 5 mps over 33 m at the White Sands Missile Range. Even though the data on the type of distribution that best fits low-level wind shear frequencies are sparse, the following general statement can be made: frequency of occurence of wind shears exceeding the ICAO criteria for extreme wind shear (see section 2.1.3.2) is not so small that shears can be neglected in the planning of aircraft operations. In the literature reviewed, extreme wind shears are generally reported to be on the order of 1% of the total number of wind shears in a given sample. The results of this investigation broadly confirm this observation.

Fichtl (1971) has investigated wind shear within the context of the similarity view of turbulent motions (Monin and Yaglom, 1971). He separates the measured wind profile according to

$$\Delta\bar{u}\,(z_1,z_2) = \bar{u}\,(z_2) - \bar{u}\,(z_1)$$

and

$$\Delta u'\,(z_1,z_2) = u'\,(z_2,t) - u'\,(z,t) \qquad (2.1.9)$$

$$\Delta u = \Delta\bar{u} + \Delta u'$$

where z_1 and z_2 are the measurement levels and $z_2 > z_1$.

In Fichtl's work, the overbar denotes a time average of 1 hr. Trends were removed from the data. He found that the standard deviation of the wind shear normalized by the friction velocity in the surface layer scaled well with three non-dimensional parameters. That is

$$\frac{\sigma}{u_*} = h\,(\eta,\epsilon,\mu) \qquad (2.1.10)$$

where $\eta = \frac{f\Delta z}{u_*}$, $\epsilon = \frac{f\bar{z}}{u_*}$, $\mu = \frac{u_*}{fL_o}$ f = Coriolis parameter, and L_o = Monin - Obukhov stability length. In a continuation of this study, Fichtl (1972) has investigated the higher moments of the wind shear distributions in the context of similarity theory.

The author feels that Fichtl's approach to the statistical modeling of shear is the most fruitful of those reviewed here. The reasons for this are as follows: (a) the question of the representation of shear as a Gaussian distribution is still open to question (this will be discussed in a later section); thus extreme value return times may well depend heavily on higher moments of the distribution; (b) it appears that higher moments of easily measured atmospheric variables may be related quite simply to the Monin - Obukhov stability length (which is normally difficult to measure) (Tillman, 1972); thus the apparent complex relationships observed by Fichtl may be simplified to a large extent by relating higher moments (thus probability of extreme values) of vertical shear to higher moments of easily measured boundary layer parameters. However, it is still an open question as to how long certain extreme values of shear persist. Kusano et al. (1967) cite some cases of extreme shear lasting up to 22 hr ! Thus, while some extreme shear occurrences may depend upon local stability (i.e. z/L_o, etc.) others may be best modeled by meso- and synoptic-scale considerations.

Meteorology. The object of this approach is to determine under what set of meteorological circumstances extremes of wind shear accur. It is probably the most useful of the three methods of modeling; even if the wind profile cannot be routinely monitored, the conditions under which extreme shears are manifest may be easily recognizable by an experienced meteorologist.

Since high wind shears in the free atmosphere are often associated with the jet stream, some workers have also noted that high low-level wind shears, appear to be linked to the low-level wind maximum (Abramovich and Glazunov, 1969; Miller, 1968; Rider and Amendariz, 1966). It appears that high wind shears are most frequently found in stable rather than unstable atmospheric stratification (Mashkova, 1967; Pettitt and Root, 1969; Rijkoort, 1969; Tsverava, 1967). In an apparent contradiction, high wind shears are often found in the cold air outflow of cumulonimbus (Goldman, 1969; Marwitz 1971; Colmer, 1971); however, the cold air outflow does provide for local stability in the boundary layer even though the atmosphere is generally unstable through a deeper layer. High wind shears are also found near frontal surfaces (Boucher, 1965; Jefferson, 1966; Sowa, 1972). In Japan Kusano et al. (1967) associate strong wind shears with the following synoptic conditions: cold fronts, outburst of winter monsoon, high pressure areas (possibly augmented by land-sea breeze circulation)*, and typhoons. They also note that low visibility is not often accompanied by high wind shear.

Summarizing, extreme wind shears have the following general characteristics, meteorologically speaking:

*The relation between high pressure and high wind shear was also found in the Denver studies (see Section 2.1.4.1).

(1) they appear to be associated with stable rather than unstable conditions, (2) they frequently seem to be caused by extreme changes in wind direction with height rather than with changes in wind speed with height (direction remaining constant), (3) extreme shears are often found in the vicinity of frontal zones which carry with them the characteristics of stable conditions and wind direction shifts noted in (1) and (2) above.

2.1.3 METHOD OF ANALYSIS

2.1.3.1 Frequency Distributions of Vector Fields: The Bivariate Frequency Table. Wind shear, like wind velocity, is a vector. It is often described by two scalar variables: either by direction and magnitude, or by x and y components. Many of the studies presented in "Vertical Wind Shear in the Lower Layers of the Atmosphere" (1969) used one-dimensional frequency distributions of each of the scalar parameters. However, such a methodology forces one to view the scalar parameters as independent of one another. While it might be true that over a very short period the x and y components of the wind might be independent (especially if the mean value is removed), this is certainly not true when dealing with component values in a climatological sense. By extension one might expect the same principle to hold for wind shear. Thus, the studies presented in "Vertical Wind Shear in the Lower Layers of the Atmosphere" would have been more informative if they had presented conditional frequency distributions rather than marginal frequency distributions. The question of the method of presenting frequency distributions of vector fields is discussed by Crutcher (1957). He proposed the use of bivariate frequency distributions as an alternative to the vector wind rose. This approach was extended by Crutcher and Baer (1962) who mathematically modeled wind distribution in the free atmosphere using climatological data. Their model was an elliptic bivariate normal distribution that can be described by relatively few statistical parameters (see also Brandt, 1970; and Lumley, 1970). In their study, Crutcher and Baer specifically state that boundary layer wind fields do not follow this model. Holland (1968) did an extensive study of low-level winds but not shear, at Round Hill Tower, Mass., using a technique similar to the one proposed here; however, he was primarily interested in turbulent structure and vertical momentum flux. He did not consider wind shear in his study. Considering the statements of Crutcher and Baer and the observations of Holland concerning the wind field, coupled with the complexity of the variation of wind with height, one would not expect the distribution of wind shear to be neatly modeled. This does not discount the bivariate frequency distribution technique for displaying the data.

The approach used in this study is described below. Vector wind is broken into x and y components as shown in Figure 2.1.1 in order to comply with the request of the CAeM/III concerning wind shear studies. The component differences are then taken. For presentation we decided to give all shear values

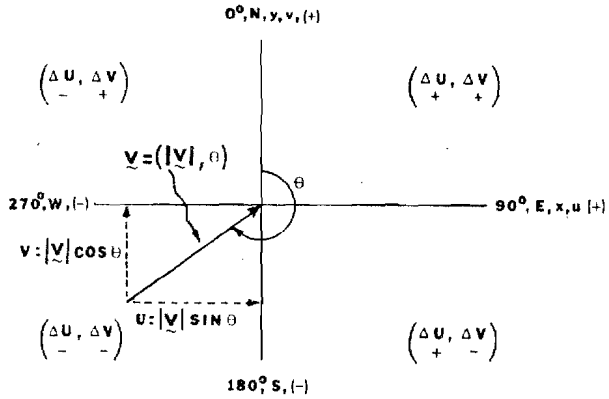

Figure 2.1.1 The wind vector and its components. Example shown is for a southwest wind. This figure is based upon NOAA, National Climatic Center, Winds Aloft Summary format.

as wind speed differences (m sec^{-1}, diff.) rather than as a differential (sec^{-1}). The vertical distance over which these shears were taken is part of the total information package (see Figure 2.1.2). A bivariate frequency table was constructed from the x and y components (Δu and Δv, respectively) as in Figure 2.1.2.

Figure 2.1.3 gives an example of a bivariate frequency table that has been contoured. The table is normalized so that

$$\iint P(x,y)\ dx\ dy = 1 \quad ,$$

where P(x,y) is the probability of occurrence for the variables x and y.

The frequency of occurrence of shear vectors originating between angles $\alpha_2 \leq \alpha \leq \alpha_1$ and having a magnitude between $|\vec{V}_2| \leq |\vec{V}| \leq |\vec{V}_1|$ is given by

$$\int_{\alpha_1}^{\alpha_2} \int_{|\vec{V}_1|}^{|\vec{V}_2|} P(\alpha,\ |\vec{V}|)\ d\alpha\ d|\vec{V}|$$

which is shown graphically in Figure 2.1.4 on a contoured bivariate table. In practice, the bivariate frequencies in each cell within the limits desired were summed without regard to contours.

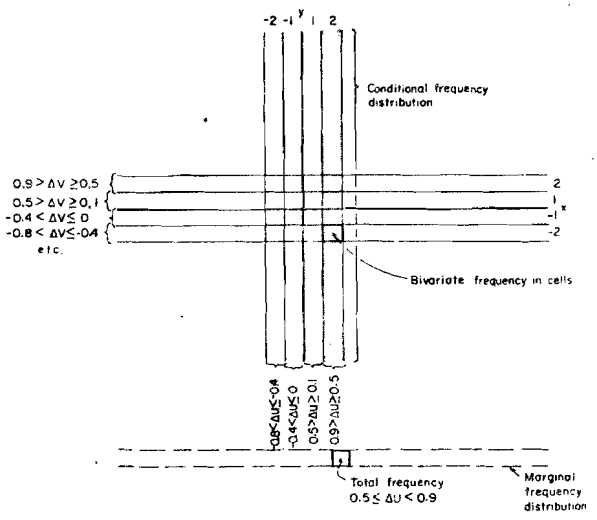

Figure 2.1.2 Format of bivariate frequency table used as basis for this study. X and Y axes are arranged to conform with Figure 2.1.1. Bivariate classes (at top and on right side of figure) form cells within which is printed bivariate frequency in percent of total occurrences. An example of a conditional frequency distribution is shown by frequencies in shaded area. Marginal frequency distributions are at bottom (for Δ u) and on left side (for Δv). Other information includes station, month, period of observation, sample number, log of methods of observation, number of calms, layer considered, and mean shear vector in component form. Computed at NOAA, National Climatic Center.

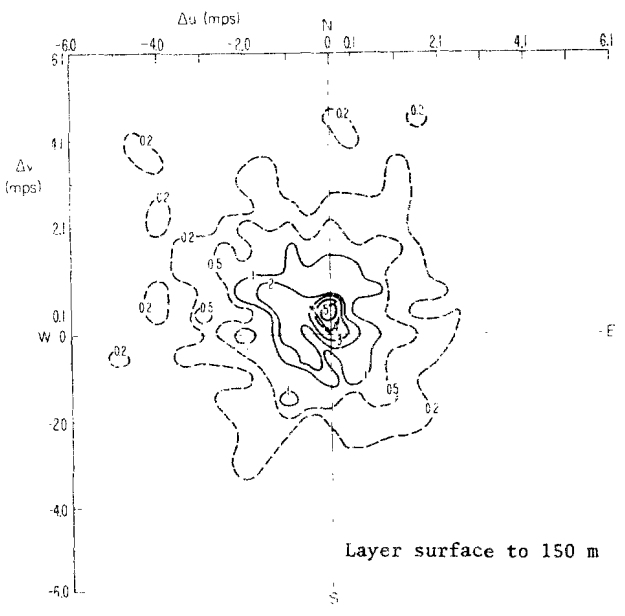

Figure 2.1.3 An example of a contoured bivariate frequency table. Contours are in percent of total occurrence. Arrow shows mean wind shear vector. Example is for Denver, Colo. for January.

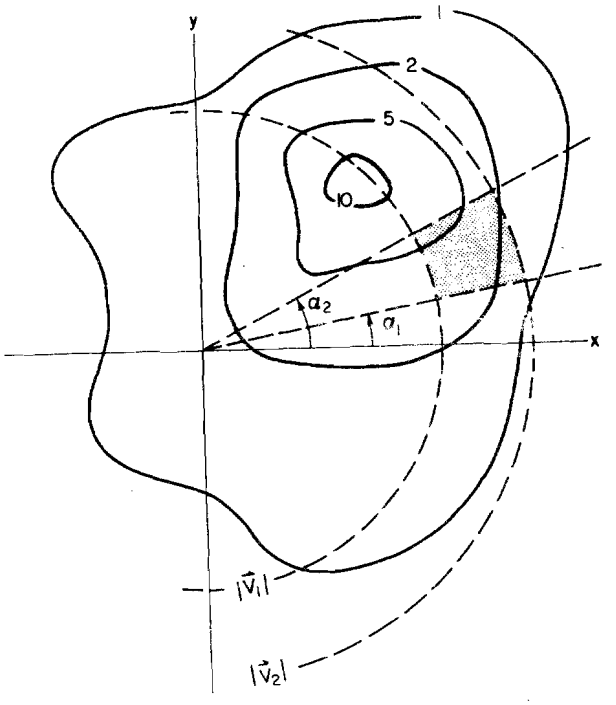

Figure 2.1.4 Graphical depiction of integration limits for finding frequency of occurrence (sum of cell frequencies within shaded area) of wind shear vectors whose magnitude was between $|\vec{V}_1|$ and $|\vec{V}_2|$ and which originated between angles α_1 and α_2.

Some authors (see e.g. Brook, 1968) argue that the shear should be related to the active runway as alongwind and crosswind components. However, at some large international aerodromes situated in a complex meteorological environment (for example Kennedy International and O'Hare International Airports) the runway layout is so complex that such a representation would be highly confusing. The bivariate frequency table satisfies both the CAeM/III's desire for consistency and the aircraft personnel's desire for simplicity. Simple overlay placed upon the frequency table gives the percentage occurrence of alongwind and crosswind shears for any given runway direction (see Figure 2.1.5).

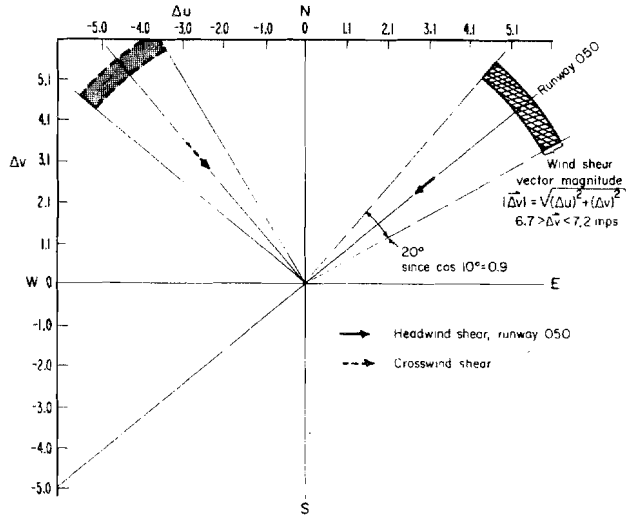

Figure 2.1.5 Overlay scheme to be used with bivariate frequency tables to obtain percentage occurrence of wind shear along and perpendicular to a given runway. Δu and Δv are given in mps. To obtain percent occurrence add all values in shaded areas.

In addition to the bivariate frequency the table also provides the marginal frequency distributions for the two variables. Note that the sum of the frequencies in these distributions will often be very close, but not equal to 100%. This is due to round-off errors introduced by the computer analysis.

2.1.3.2 Criteria for Extreme Wind Shear. The CAeM/III, as well as numerous authors (e.g. Synder, 1968; Roberts, 1969; St. John, 1967; Clodman et al., 1969, Burman, 1967), suggests that the most critical height range is the last 33 m of vertical height before landing.* However, frequent references of from 100 m to 700 m appear in the literature (Sowa, 1972 Burnham, 1970 and others). The CAeM/III set an extreme shear criteria of 5 mps vector wind difference magnitude over the first 33 m above the ground.

In the data set used in this investigation, the first measurement level above the surface value is 150 m. Thus, a method must be found which relates the extreme shear criteria over a 33 m depth to that measured over a 150 m depth. A simple linear extrapolation gives an absurd result (i.e. ~25 mps vector wind difference magnitude). Essenwanger (1963) and Essenwanger and Billions (1965) have investigated the relationship between shear magnitude and the interval over which the magnitude of the vector wind difference is taken. The proposed relationship by Essenwanger is a power law given by

$$\Delta V = a_o \, (\Delta z)^b \qquad (2.1.11)$$

where $\Delta V = (\overline{V}_2 - \overline{V}_1)$, $\Delta z = (z_2 - z_1)$, a_o is a constant and b is a constant. He arrived at a value of $b = 1/3$ for "extreme" wind shears and $b = 1/2$ for "mean" wind shears. These values were tentatively confirmed by Essenwanger and Billions. Further confirmation of the power law hypothesized by Essenwanger was made by Amendariz and Rider (1966) and the dependence of shear on interval is alluded to by Crossely (1962). Essenwanger and Reiter (1969) relate the power law to the structure function. Reiter and Lester (1967) discuss its applicability to critical values of the Richardson's number, an indicator of atmospheric stability. Adelfang (1971) also confirmed the power law hypothesis but indicated the values of b may have a climatological variation. Eckhardt and Newell (1964) attempted to relate extreme shears to a wind profile modeled by

$$\frac{V_2}{V_1} = \left(\frac{z_2}{z_1}\right)^n \qquad 0.1 \le n \le 1 \qquad (2.1.12)$$

V_2 = wind speed at level z_2, and V_1 = wind speed at level z_1. They report extreme shear conditions for military aircraft for $n \cong .3$.

All of the above workers except Eckhardt and Newell were dealing with shear layers in the free atmosphere, often at relatively high altitudes (6 - 20 km). However, many of their extreme shear conditions were associated with the tropopause - jet stream system where one boundary condition to the flow was a strong inversion. The applicability of Essenwanger's hypothesis may well be questioned for boundary layer wind profiles. The following discussion attempts to show that, for a reasonable model of the surface layer, the Essenwanger power law relationship holds.

Consider Equation (2.1.12) and expand it to give

$$V_2 - V_1 = V_1 \left(\frac{z_2}{z_1}\right)^n - V_1 \qquad (2.1.13)$$

*The landing condition is more delicate since it is performed at below maximum power settings. Brunstein (1971) notes that 20% of all U.S. carrier aircraft turbulence related accidents from 1964 to 1969 occurred on the approach-descent pattern.

since $\Delta V \equiv V_2 - V_1$,

manipulation of (2.1.13) gives

$$\Delta V = V_1 \left[\left[\frac{\Delta Z}{Z_1} + 1 \right]^n - 1 \right] . \qquad (2.1.14)$$

Expanding (2.1.14) in accordance to the binomial expansion yields

$$\Delta V = V_1 \left[\left[\left(\frac{\Delta Z}{Z_1} \right)^n + n \left(\frac{\Delta Z}{Z_1} \right)^{n-1} + n(n-1) \left(\frac{\Delta Z}{Z} \right)^{n-2} + \ldots \right] - 1 \right] \qquad (2.1.15)$$

If Z is small (i.e. 5 m) and ΔZ relatively large (i.e. greater than 25 m) then (2.1.15) becomes

$$\Delta V \approx V_1 \left[\left(\frac{\Delta Z}{Z_1} \right)^n - 1 \right] \qquad (2.1.16)$$

which is only slightly more complex than that proposed by Essenwanger.

To investigate the ratio of wind speed differences taken with a ΔZ of 31 m and 148 m, respectively, one obtains

$$\frac{\Delta V_b}{\Delta V_a} = \frac{\left(\frac{\Delta Z_b}{Z_1} \right)^n - 1}{\left(\frac{\Delta Z_a}{Z_1} \right)^n - 1} \qquad (2.1.17)$$

where $\Delta Z_b = 150$ m

$\Delta Z_a = 33$ m

$Z_1 = 2$ m

$n = 0.3$.

The value of n refers to extreme shear profiles. Performing the indicated operations yields

$$\Delta V_b / \Delta V_a \cong 2$$

Thus, a theoretical approach to the extreme shear criteria gives an extreme shear wind difference with a 150 m separation of 10 mps when the 33 m difference is given as 5 mps.

A similar expression for the logarithmic wind profile is*

$$\frac{\Delta V_b}{\Delta V_a} = \frac{\ln \left[\Delta z_b \, (z_1 - z_o)/z_1^{\,2} + 1 \right]}{\ln \left[\Delta z_a \, (z_1 - z_o)/z_1^{\,2} + 1 \right]} \qquad (2.1.18)$$

where Z_o is the so-called roughness height. This expression gives $\Delta V_b / \Delta V_a \approx 1.5$ for the data used in (2.1.17), use of (2.1.18) yields $\Delta V = 7.7$ mps for the 150 m separation extreme shear wind difference.

Equation (2.1.18) refers to the rare case of neutral stability in the surface layer. Including the effects of stability in (2.1.18) would complicate the expression further.

Taking Essenwanger's work into account, the results of the use of Equations (2.1.17) and (2.1.18), as well as a pilot study of the wind shear environment of Denver, Colorado, we have set the extreme shear criteria for this study at 6.5 mps difference over 150 m interval.

2.1.3.3 Data Set and Its Limitations. Although this study will not be specifically directed to applying the results to aircraft design criteria, it may be used as an input for the solution to aircraft operations problems. This factor was considered when the representative stations were selected for analysis. (FAA) has compiled a list of 41 major airports in the CONUS. Among the criteria resulting in a classification of "major" is the amount of commercial air traffic and its economic importance to a given region (Kraus, 1972). Table 2.1.1 lists the upper air stations chosen.

TABLE 2.1.1

Stations Selected for Low Level Wind Shear Analysis

Station	Major Airport
Tatoosh Is., Wash.	No
Oakland, Calif.	Yes
Salt Lake City, Ut.	Yes
Carswell AFB, Tex.	No
Denver, Colo.	Yes
Topeka, Kan.	No
Athens, Ga.	No
Dayton, Ohio	Yes
Green Bay, Wisc.	No
Nantucket, Mass.	No

*The logarithmic profile is strictly applied to the constant flux layer, or surface layer, which in most cases is less then 33 m deep. It would be a very rare occurrence to have the log profile extending to 150 m Thus, (2.1.18) should be interpreted with caution.

The rawinsonde data made available by the National Climatic Center, NOAA (NCC) were obtained by standard procedures during 1956-1964, providing a maximum of 108 months of data. Three levels above the surface were used, providing three layers over which a shear could be measured. NCC data storage formats required the use of the following levels: surface, 150 m, 300 m, and the first level above sea level which was greater than 300 m. Therefore, the spacing of the first two layers is 150 m, while the spacing of the last layer varies from station to station. Calm winds were not included in the computation of shear (the number of calms at each level is noted) at any level, since a vector difference could not be taken. When this situation was encountered the shear value was not included in the statistical population.

The data set that we are investigating is subject to error. Because of the infrequent use of low-level wind data, the NCC did not audit much of the data here presented. Thus, one source of error in extreme values is due to improper coding and key punching. Another source of error is due to the difficulty in locking on the tracking radar soon enough to give reasonable results in the lowest layers of a radiosonde or rawinsonde ascent. This is especially difficult in built up areas under strong wind conditions. Thus, the data must be interpreted with the caution that it is not likely that all extreme values are valid and that two very significant error sources exist. This point will be explored further for Denver. It is hoped, however, that certain qualitative features will be apparent in the compilation of extreme shear statistics. This is certainly true of Denver

2.1.4 RESULTS OF INVESTIGATION

2.1.4.1 Denver Case Study. It was beyond the scope of this initial investigation to examine in detail the data from each of the 10 stations. Since Denver was selected as the site of an extensive field program to determine the applicability of acoustic Doppler wind measuring techniques, it was chosen for closer examination to provide background information for the field program.

Error Analysis. As was mentioned before, it was likely that the extreme wind data did contain errors. To investigate this aspect, we plotted all wind profiles having $|\Delta\vec{V}| >> 6.5$ mps between any two levels on a hodograph. These profiles were then screened, and out of 176 extreme profiles obtained over the 9 year period, 41 were judged to be suspect. These 41 profiles were then audited at NCC; it was determined that four profiles were mispunched and 10 logged improperly. Of the 27 remaining profiles the main comment from the NCC auditor was "questionable surface winds." However, as will be discussed, the local flows at Denver may effect extreme shear conditions, thus such questionable profiles may genuinely reflect the situation. One could not say for sure how many of the 27 remaining cases were subject to lock-on errors. However, of these 27, 13 had surface wind speeds under 5 mps, 13 had surface wind speeds between 5 to 7 mps and only one had a surface wind speed greater than 7 mps suggesting lock-on errors were unlikely. Even if as many as 10 had lock-on errors, that number represents only about 5% of the total number of extreme wind shears. It seems reasonable to conclude that the Denver statistics are relatively error free.

Marginal Distribution Analysis. The marginal distributions of the Δu and Δv for each layer and each month were plotted on probability paper to check the normality of the distributions. The marginal distributions appear to be very nearly normal. There is distortion at the extremes, which is to be expected from a finite (and in this case relatively small) data sample, but overall the relationships between cumulative probability and class were linear irrespective of layer or month. This leads to the conclusion that the possibility does exist for mathematically modeling the low-level wind shear at Denver in terms of an elliptical bivariate distribution (Crutcher and Baer).

2.1.4.2 Meteorological Conditions During Extreme Wind Shear; Synopsis of Results. Extreme shear cases were investigated from a synoptic point of view. The five highest shears in Denver for the 9 year period were studied. Daily weather maps produced by the Department of Commerce for the day preceding, during, and after the shear occurred were studied as well as temperature-humidity soundings near the time of occurrence. Table 2.1.2 presents the pertinent information about the shear occurrence. Of the five cases, two had the extreme shear in surface to 150 m layer, and in three the shear occurred between 150 m and 300 m.

A recurring pattern was apparent in the synoptic situations and soundings associated with the cases listed above. First, in every case the extreme shear was due to a rapid shift in wind direction rather than speed differences between the two levels. The synoptic pattern was generally one of a weak ridge or shallow

high in the Denver area; skies were, for the most part, clear; visibility was well above minimum for aircraft landing (for the map time analyzed); the 500 mb wind field generally showed strong westerly winds either directly over Denver or to the north of Denver over southern Wyoming. All cases were associated with very strong radiation inversions with the directional wind shift occuring across the inversion surface. Below the inversion surface the flow appeared to be local (for a description of local flows in the Denver area see Riehl and Herkhof, 1972) with the wind having some easterly component. Most of the shifts were backing rather than veering.

TABLE 2.1.2

Extreme Wind Shear Cases Chosen For Synoptic Analysis

DATE	$\lvert\Delta\vec{V}/\Delta z\rvert$	LAYER
1 Feb 61 1200	11.1	SFC - 150m
12 Oct 62 0600	12.0	150m - 300m
20 Nov 62 1800	11.0	150m - 300m
28 Nov 62 0600	12.0	150m - 300m
13 May 63 0600	11.1	SFC - 150m

2.1.4.3 Conclusions Using All Stations. One of the primary purposes of this study was to provide some background on the occurrence of extreme wind shear conditions in the lower layers of the atmosphere at different points within the CONUS. Using an overlay constructed as in Figure 2.1.6, percentage of occurrence was summed within an area bounded by $|\Delta\vec{V}| > 6.5$ mps and $\pm 45^{\circ}$ about local north, south, east and west. The results of this are given in tabular and graphical form in Appendix A.

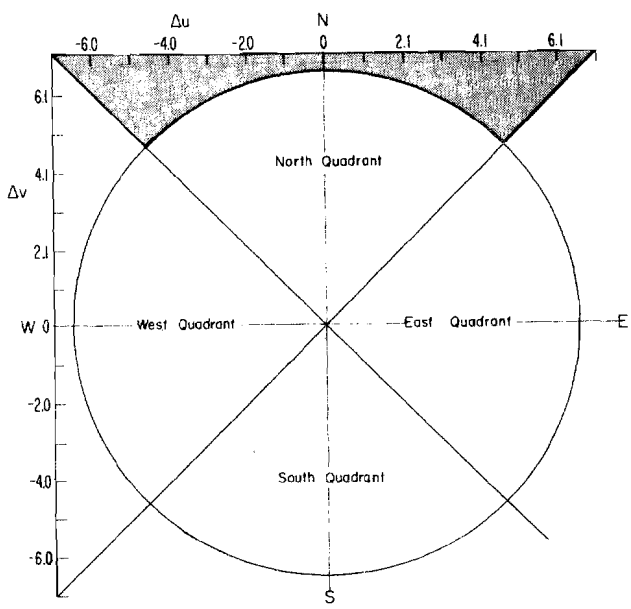

Figure 2.1.6 Schematic of overlay used in extreme wind shear analysis. Circle defines $|\Delta\vec{V}| \geq 6.5$ mps. For example, north quadrant percentage extreme wind shear is found by summing all cell percentages in shaded area.

Some general characteristic of all 10 stations can be discussed. With few exceptions, extreme wind shears depend upon season; the greater percentage of extreme shears occuring in the late fall through early spring and the smallest percentage occuring from late spring through late summer. For four out of the 10 stations investigated there was little significant difference between the percentage of extreme shear occurrence in the surface to 150 m layer and the 150 m to 300 m layer. At one station, a higher percentage of extreme shear was found in the 150 m - 300 m layer when compared to the surface - 150 m layer. These observations are unusual, since classical boundary layer concepts would predict a higher percentage of strong shears in the layer nearest the ground (this was the case for five of the 10 stations). The highest frequency of extreme shear occurrence was shared by Athens, Ga., and Nantucket, Mass., in the eastern U. S., while the lowest was Oakland, California, in the west.

The results of the literature review, the seasonal march of extreme wind shear occurrence and the fact that extreme shears are not especially confined to the lowest layer, allow one to speculate that the major portion of extreme wind shears are closely tied to synoptic conditions, especially baroclinic situations during which present boundary concepts break down. To further investigate this speculation, Figure 2.1.7a and 2.1.7b present the total percentage of extreme wind shear occurrences for each of the 10 stations (see Table 2.1.3) with the major mean cyclone tracks over the CONUS superimposed. The correlation between high incidence of extreme wind shear and passage of cyclonic storms is evident in both the SFC-150 m layer and the 150 m - 300 m layer. This observation would encourage the examination of meteorological conditions attending extreme wind shear occurrences.

TABLE 2.1.3

Total Percentage of Occurrence of Extreme Wind Shear

STATION	SFC-150m LAYER	150m-300m LAYER
Oakland, Calif.	.35	.28
Tatoosh, Wash.	2.07	1.37
Greenbay, Wisc.	2.30	2.29
Nantucket, Mass.	4.65	2.32
Salt Lake City, Utah	.89	.55
Denver, Colo.	.83	.89
Topeka, Kansas	3.55	3.38
Ft. Worth, Texas	3.05	.76
Dayton, Ohio	2.05	3.09
Athens, Ga.	4.64	2.11

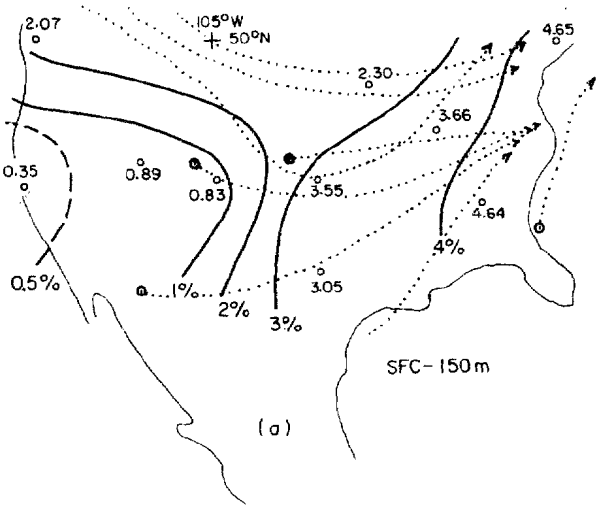

Figure 2.1.7a Total annual percentage of extreme wind shears for the 10 stations analyzed. Dotted arrows are mean cyclone tracks (circle denotes origin of cyclone track) for CONUS. Layer considered is surface to 150 m.

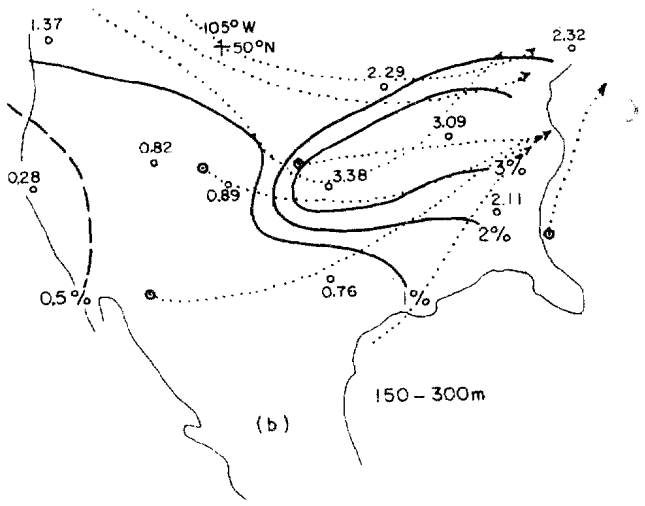

Figure 2.1.7b As above except for layer 150 m to 300 m

Acknowledgments. The author wishes to acknowledge fruitful discussions with Drs. Harold Crutcher and Donald Beran. The bivariate frequency tables were constructed by the Applied Climatology Division, National Climatic Center. Ms. Pam Sedillo and Mr. Mike Sanchez were helpful in the construction of Tables A1 and A2, as well as Figures A1 through A10.

REFERENCES (Chapter 2, Section 1)

Abramovich K. G., and V. G. Glazunov, 1969: Wind shear in the lower atmosphere, WMO Tech. Note No. 93, 195-202.

Adelfang, S. I., 1971: On the relations between wind shears over various altitude intervals, J. Appl. Meteor. 10(1), 156-159.

Aeronautical Meteorology, 1969, WMO Tech. Note, No. 95.

Air France, 1963: Effects of wind vertical gradient during final approach, Int. Air Transport Assn. Proc. 15th Tech. Conf., Agenda Item 2.2, 9 pp.

Arya, S.P.S., 1972: The critical condition for the maintenance of turbulence in stratified flows. QJRMA (Quarterly J. Roy. Met. Soc.), 98 (416), 264-273.

Blackadar, A. K., 1957: Boundary layer wind maxima and their significance for the growth of the nocturnal inversion, Bull. Am. Met. Soc., 38(5), 283-290.

Blackadar, A. K. and H. Panofsky, 1970: Effects of a change in terrain on wind profiles, Penn. St. Univ. AFC Final Report, Contract AT(30-1) - 3562, 83 pp.

Boucher, R. J., R. Wexler, D. Atlas, and R. Lhermitte, 1965: Mesoscale wind structure revealed by Doppler radar. J. Appl. Meteorol., 4(5), 590-597.

Brandt, S., 1970: Statistical and Computational Methods in Data Analysis, American Elsevier, New York, 61-67 61-67.

Brook, R. R., 1968: Estimation of maximum wind shear in the boundary layer. Australian Met. Mag., 16(2), 47-55.

Brown, J. A., 1961: Wind shear effects on air speed, TWA, Met. Dept., Tech. Bull. 61-3, 18 pp.

Brunstein, A. I., 1971: Lessons to be learned from accidents attributed to turbulence, Proc. Int. Conf. on Atmospheric Turbulence (18-21 May 1971), Roy. Aeronautical Soc. (London).

Burnham, J., 1967: A note on turbulence problems associated with takeoff and landing. Roy. Aircraft Est. (UK), Tech. Rept. 67240, 10 pp.

Burnham, J., 1970: A brief review of R.A.E. research on wind and gust effects relevant to landing and takeoff, Roy. Aircraft Est. Tech. Memo. Aero 1201, 12 p.

CAeM/III (abridged), 1964, WMO Report 157, Vol I.

Clodman, J., F. B. Muller, and E. G. Morrissey, 1969: Wind regime in the lowest 100 m as related to aircraft takeoffs and landings. WMO Tech. Note No. 95, 29-43.

Colmer, M. J., 1971: On the character of thunderstorm gust fronts, Proc. Int. Conf. on Atmos. Turbulence (18-21 May, 1971), Roy. Aeronautical Soc. (London).

Crossely, A. F., 1962: Extremes of wind shear. Met. Office (U.K.), Scientific Report No. 17, 23 p.

Crutcher, H., 1957: On the standard vector-deviation wind rose, J. Meteor., 14, 28-33.

Crutcher, H., and L. Baer, 1962: Computations from elliptical wind distribution statistics, J.A.M., 1(4), 522-530.

Drazin, P. G., 1958: The stability of a shear layer in an unbounded heterogeneous inviscid fluid, J. Fl. Mech., 4, 214-224.

Duncan, W. J., 1959: The Principles of the Control and Stability of Aircraft, Cambridge Univ. Press 391 p.

Eckhardt, H. D. and J. S. Newell, 1964: Study of tactical army aircraft landing systems. R.C.A. Corp., Tech. Rept. DDC, AD433632, 52 p.

Emmanuel, C. B., 1972: Observations of Helmholtz waves in the lower atmosphere with an acoustic sounder. Colorado State University, Dept. of Civil Engr. Ph. D. dissertation, 94 pp.

Essenwanger, O., 1963: On the derivation of frequency distributions of vector wind shear valves for small shear intervals. Geofisica pura e applicata. 56(3), 216-224.

Essenwanger, O. and N. Billions, 1965: On wind shear distributions for smaller shear intervals. U. S. Army Missile Command, Directorate of Research and Development, Report No. RR-TR-65-4, 23 p.

Essenwanger, O., 1968: On deriving 90-99% wind and wind shear thresholds from statistical parameters, Proc. 3rd Nat. Conf. on Aerospace Met., Amer. Met. Soc. (Boston), 145-153.

Essenwanger, O., and E. R. Reiter, 1969: Power spectrum, structure function, vertical wind shear and turbulence in the troposphere and stratosphere, Arch. Met. Geoph. Biokl., Ser. A., 18, 17-24.

Fichtl, G., 1971: Standard deviation of vertical two point longitudinal velocity differences in the atmospheric boundary layer, Boundary Layer Met., 2, 137-151.

Fichtl, G., 1972: Third and fourth moments of vertical two-point differences of turbulent velocity fluctuations in the atmospheric boundary layer. Proc. of Int. Conf. on Aerospace and Aeronautical Meteor., American Met. Soc. (Boston).

Gera, J., 1971: The influence of vertical wind gradients on the longitudinal motion of airplanes. NASA-TN-D-6430, 17 pp.

Goldman, J. L., 1969: Analysis of wind field conditions adversely affecting vehicle operations. NASA Contractor Report CR 61286. 96 p.

Goldstein, S., 1931: On the stability of superposed streams of fluids of different densities, Proc. Roy. Soc. London (A), 132, 524-548.

Henry, R. M. and J. A. Cochrane, 1964: Geographical variations of wind loads on vertically rising vehicles, J.A.M., 3(6), 734-743.

Hinze, J. O., 1959: Turbulence, McGraw-Hill, New York, 586 p.

Holland, J. Z., 1968: An application of some statistical techniques to the study of eddy structure, AEC Tech. Report, TID-24585, 378 pp.

Ito, H., 1969: Time and space variation in meteorological elements in the aerodrome (Tokyo) and its vicinity. WMO Tech. Note No. 95, 142-157.

Jefferson, G. J., 1966: An incident of severe low-level turbulence. Met. Magazine (London), 95 (1130), 279-285.

Kraus, K., 1972a, Aspects of the influence of low-level wind shear on aviation operations. Proc. Int. Conf. on Aerospace and Aeronautical Met. American Met. Soc. (Boston), 332-333.

Kurkowski, R. L., G. H Fichtl, and J. Gera, 1971: Development of turbulence and wind shear models for simulator application. NASA Aircraft Safety and Operating Problems, Vol. 1, NASA SP-270, 291-306. 291-306.

Kusano, K., Y. Suzuki, and H. Tasori, 1967: Vertical wind shear in the lower layers at the Tokyo Int. Airport, Geophysical Mag. (Tokyo), 33(3), 239-256.

Letteau, H., and B. Davidson (eds.). 1957: Exploring the Atmosphere's First Mile, Vols. I & II, Pergamon, New York.

Letteau, H., J. Dutton, H. Hamilton, Jr., W. Johnson, Jr., D. Lenschow, J. Sparkman,Jr., C. Stearns, and A. Super, (1962): Studies of the three-dimensional structure of the planetary boundary layer. Univ. Wis., Dept. Meteor. Ann. Rpt. on Contract DA-36-039-SC-80282, 176 p.

Lumley, J. L., and H. Panofsky, 1964: The Structure of Atmospheric Turbulence, Interscience, J. Wiley, N. Y., 239 pp.

Lumley, J. L., 1970: Stochastic Tools in Turbulence, Academic Press, New York, p. 23-24.

Marwitz, J. D., 1971: Severe storm types in relation to wind shear. Proc. 7th Conf. on Severe Local Storms, American Met. Soc. (Boston), 240-243.

Mashkova, G. B., 1967: Wind profiles during low cloudiness at a height of less than 300 m. Akademia Nauk, SSSR, Institut Prikladnoi Geofiziki, Trudy., 10, 39-43 (In Russian).

Melvin, W. W., 1970: Wind shear on the approach, Shell Aviation News, 393, 16-20.

Miller, A., 1968: Wind profiles in west coast temperature inversions. San Jose State College, Dept. Meteorology Land-Sea Boundary Effects on Small Scale Circulations: Rept. No. 4. 57 p.

Monin, A. S., and A. M. Yaglom, 1971: Statistical Fluid Mechanics, Vol. 1, MIT Press, 769 p.

Muller, F. B., and C. M. Mushkat, 1969: Preliminary analysis of Canadian wind shear data. WMO Tech. Note No. 93, 31-36.

Neyland, F. J., 1956: Change without notice. Flying Safety, April 16-20.

Peterson, E., 1969: Modification of mean flow and turbulent energy by change in surface roughness under conditions of neutral stability. QJRMS, 95(405), 561-576.

Pettitt, R. B., and R. G. Root, 1969: Vertical wind shear in the boundary layer, WMO Tech. Note 93, 1-30.

Reiter, E. R., 1961: Jet Stream Meteorology, Univ. Chicago Press, 515 pp.

Reiter, E. R. and P. F. Lester, 1967: The dependence of the Richardson number of scale length, Colo. State Univ., Dept. of Atmos. Sci. Atmos. Sci. paper No. 111., 39 p.

Rider, L. J. and M. Armendariz, 1966: Low-level jet winds at Green River, Utah. J. Appl. Meteor. 5(5), 733-736.

Riehl, H. and D. Herkhof, 1972: Some aspects of Denver air pollution, J. Appl. Meteor., 11(7), 1040-1047.

Rijkoort, P. J., 1969: Dependence of observed low level wind shear on averaging period and lapse rate. WMO Tech. Note No. 93, 185-194.

Rijkoort, P. J., and J. Wieringa, 1969: Wind information for landing and takeoff and setting of instruments. WMO Tech. Note No. 95, 158-166.

Roberts, C. F., 1969: A preliminary analysis of some observations of wind shear in the lowest 100 ft of the atmosphere for application to the problem of the control of aircraft on approach. WMO Tech. Note 93, 203-218.

Schlicting, H., 1960: Boundary Layer Theory, (4th ed) McGraw-Hill, New York, 647 p.

Scoggins, J. R., 1970: The wind field, in Wind Effects on Launch Vehicles (ed. E. Geissler), AGARograph #115, Technivision, Slough (UK).

Sowa, D. F., 1972: Turbulence plot program, Shell Aviation News, April, 16-19.

Spillane, K. T., and R. R. Brook, 1969: Vertical wind shear in the boundary layer at Melbourne airport, WMO Tech. Note 95, 44-60.

St. John, O. B., 1967: Implications of all weather landing in the UK., Roy. Arcft. Est. Tech. Rpt. 67032, 19 p.

Synder, C. T., 1968: Analog study of the longitudinal response of a swept-wing transport airplane to wind shear and sustained gust during landing approach. NASA, Tech. Note D-4477, 18 p.

Taylor, P. A., 1969: On wind and shear stress profiles above a change in surface roughness. Quarter J. Roy. Met. Soc., 77-91.

_____, 1970: A model of airflow above changes in surface heating flux, temperature and roughness. Boundary Layer Meteor., 1(1), 18-39.

Tillman, J. E., 1972: The indirect determination of stability, heat and momentum fluxes in the atmospheric boundary layer from simple scalar variables during dry unstable conditions. J. Appl. Meteor., 11(5), 783-792.

Tsverava, V. G., 1967: Investigation of vertical wind vector shears based on observations on a 300 m meteorological tower, Meteorologira Gidrologiia (Moscow) (In Russian) 2, 82-84.

Vertical Wind Shear in the Lowest Layers of the Atmosphere, 1969, WMO Tech. Note No. 93, 250 pp.

Watson, I. A., 1969: Report of an investigation into low-altitude wind structure for automatic landing. WMO Tech. Note No. 95, 61-78.

APPENDIX A

Tabular Results. Table A-1 presents the percentage of all vector wind differences whose magnitude was greater than or equal to 6.5 m/sec. These are given for each station as a function of quadrant and climatological month. Values given are in percent so that 0.64, for example, is 0.64% not 64%. The values in the layer "300 m to next highest reported level" are often large because the interval is often much greater than 150 m and the 6.5 m/sec criteria did not apply. The height separations for this layer are given in the far right column of the tables.

Graphical Results. Figures A1-A10 are the tabular values for the first two layers presented in graphical form. The circles in the upper right side of each figure are the percent occurrence of extreme wind shear over the entire year for the different quadrants. The figure in brackets below each circle is the total percent occurrence for the year.

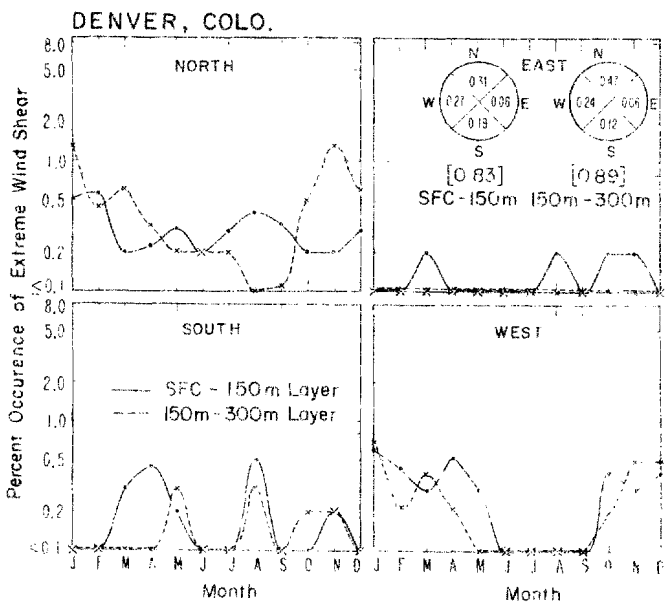

Figure A1

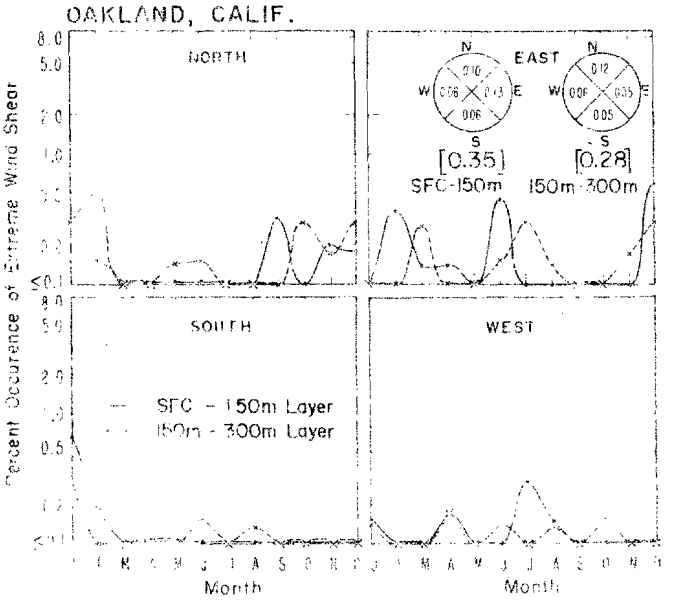

Figure A3

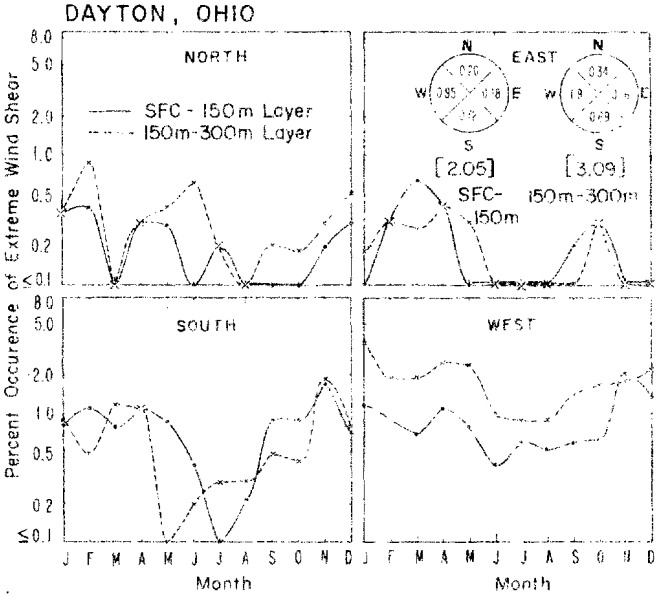

Figure A2

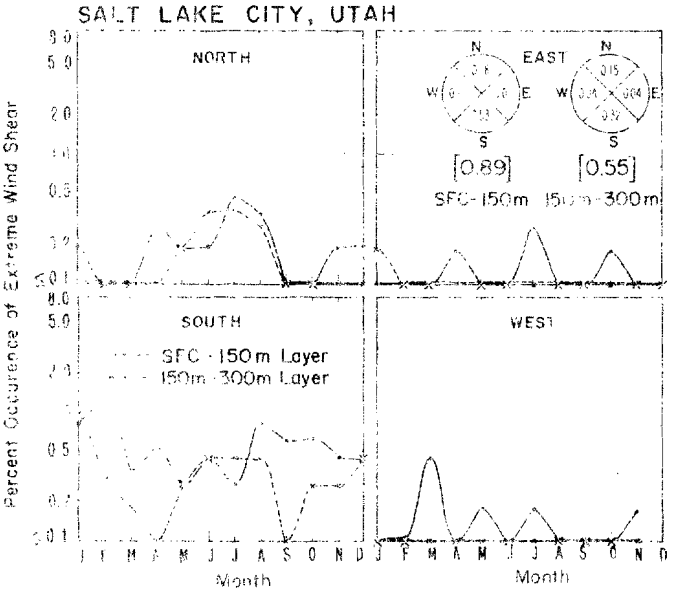

Figure A4

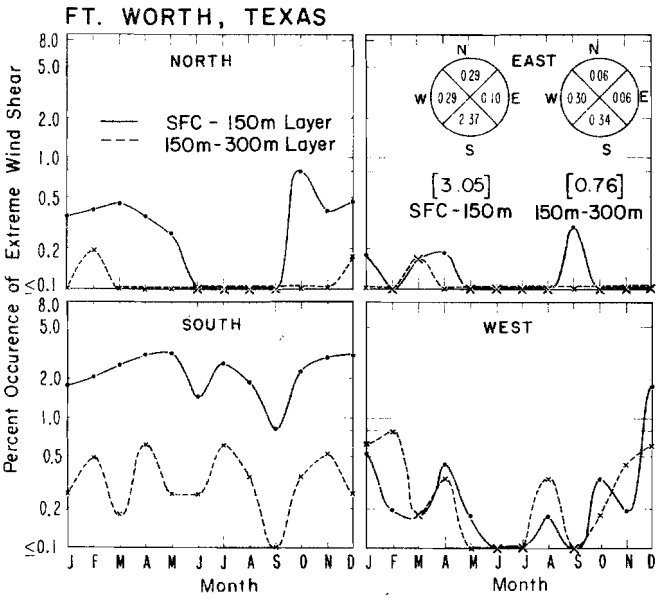

Figure A5

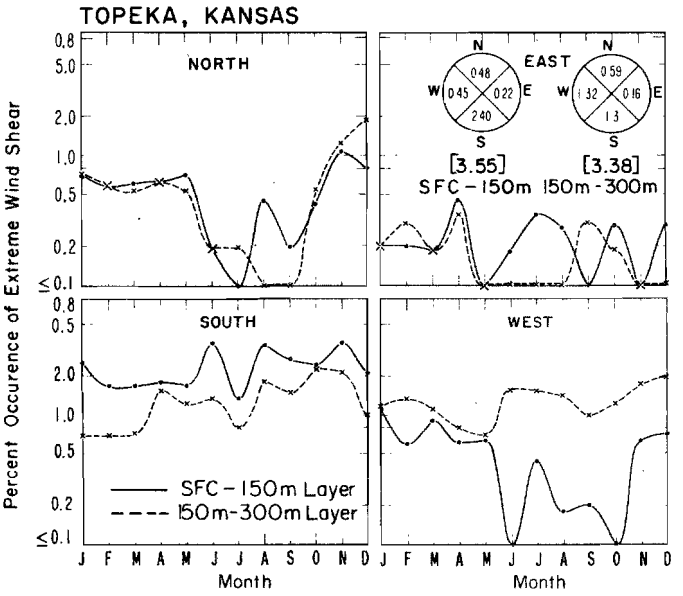

Figure A7

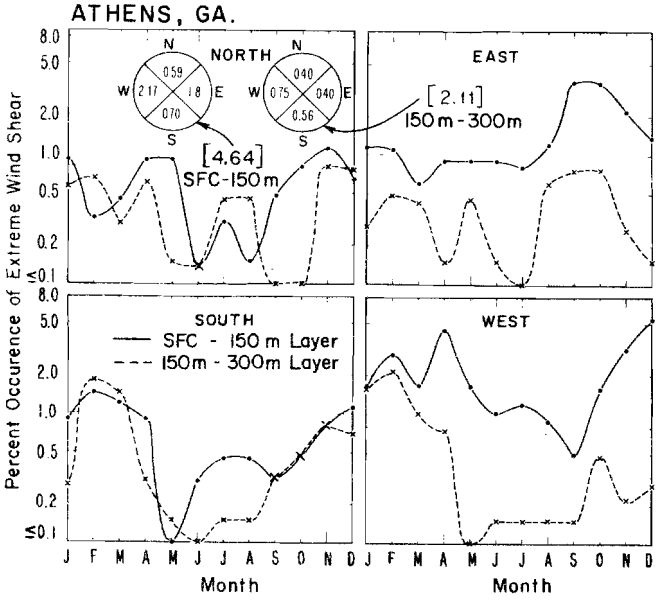

Figure A6

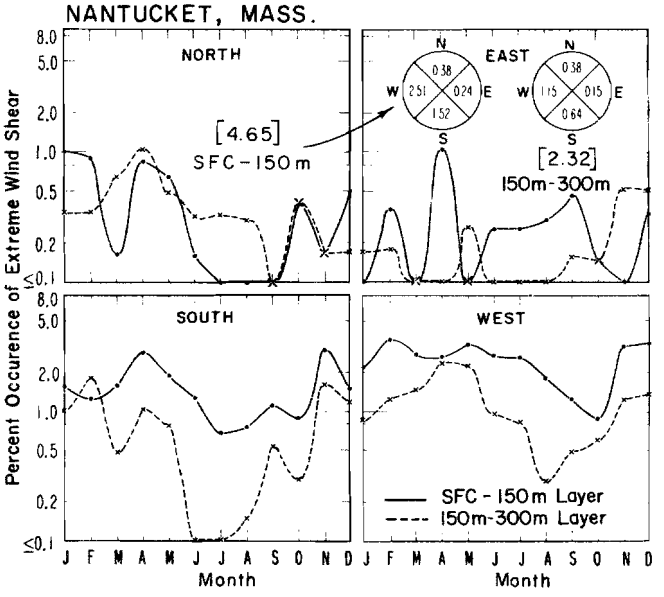

Figure A8

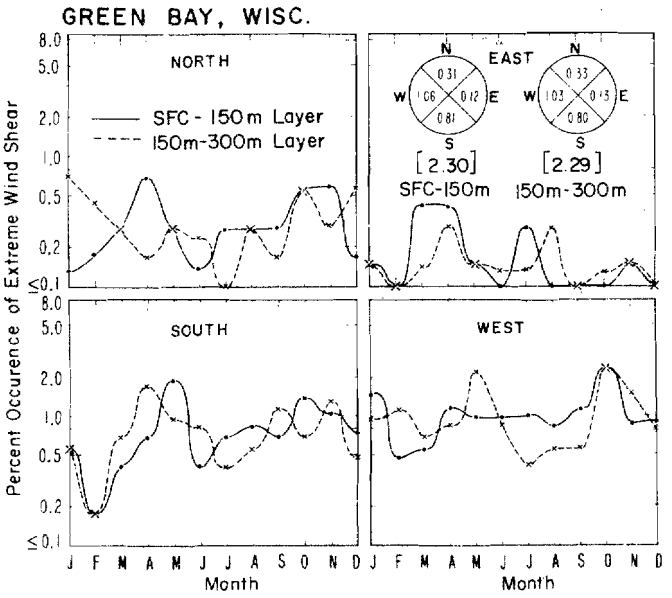

Figure A9

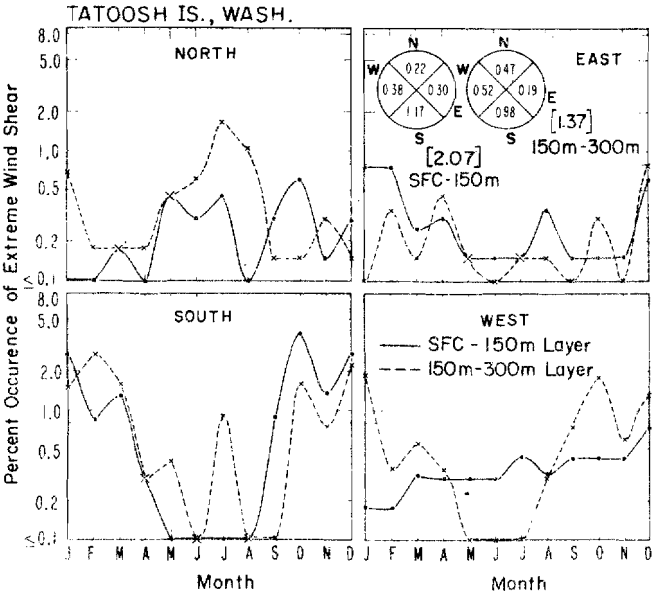

Figure A10

TABLE A-1

Percentage Occurrence of Extreme Wind Shear by Month For Ten Selected Stations in Conus
(see text for explanation of Table)

JANUARY

	SURFACE - 150M, ΔZ = 150M					150M - 300M, ΔZ = 150M					300M - Next Highest Level Reported					
Station	Sample No	N	E	S	W	Sample No	N	E	S	W	Sample No	N	E	S	W	ΔZ(m)
DENVER	988	.5	0	.1	.6	992	1.3	.1	.1	.7	991	.2	0	.2	0	89.
DAYTON	1055	.36	.09	.82	1.37	1079	.36	.18	.90	4.08	1092	3.25	.36	2.62	12.95	396.
OAKLAND	633	.16	0	.64	.16	724	.28	0	.28	.14	766	.26	0	.39	0	198.
SALT LAKE CITY	1069	.09	.09	.82	0	1068	.18	.18	.91	.09	1061	1.84	.18	5.14	2.22	419.
FT. WORTH	1055	.36	.18	1.86	.54	1079	0	.09	.27	.63	1085	4.53	2.44	7.70	13.33	526.
ATHENS	687	.89	1.05	.90	1.60	695	.56	.28	.28	1.55	695	4.20	3.84	7.01	8.11	454.
TOPEKA	1030	.69	.20	2.53	1.08	1036	.70	.20	.69	1.18	1035	6.75	2.64	6.80	7.77	432.
NANTUCKET	598	1.01	0	1.53	2.20	598	.34	.17	1.02	.85	594	.34	.17	.51	.51	196.
GREEN BAY	699	.14	.14	.57	1.45	700	.70	.14	.56	.98	677	6.29	2.40	2.69	5.36	487.
TATOOSH	598	0	.68	2.71	.17	604	.68	0	1.53	1.87	602	.34	0	.50	1.68	169.

FEBRUARY

	SURFACE - 150M, ΔZ - 150M					150M - 300M, ΔZ = 150M					300M - Next Highest Level Reported					
Station	Sample No	N	E	S	W	Sample No	N	E	S	W	Sample No	N	E	S	W	ΔZ(m)
DENVER	898	.55	0	.11	.44	894	.44	0	.11	.11	896	.22	0	.11	0	89.
DAYTON	986	.40	.30	1.30	.90	1003	.90	.30	.50	1.90	1013	1.80	.70	2.99	2.89	396.
OAKLAND	562	.16	.36	.18	0	613	.48	0	0	0	635	.16	.32	0	.16	198.
SALT LAKE CITY	970	.10	0	1.23	0	971	.1	0	.30	0	971	2.36	.10	2.04	2.44	419.
FT. WORTH	1002	.4	.1	2.1	.2	1012	.2	.1	.5	.8	1014	3.50	2.30	8.81	10.9	526.
ATHENS	642	.32	.96	1.44	2.87	645	.64	.48	1.77	2.09	642	4.17	1.44	5.04	9.80	454.
TOPEKA	983	.60	.20	1.70	.60	990	.60	.30	.70	1.30	988	4.20	1.60	6.22	7.95	432.
NANTUCKET	568	.90	.36	1.25	3.55	568	.36	.18	1.80	1.24	568	.90	.18	.36	1.08	196.
GREEN BAY	639	.16	0	.16	.48	639	.48	0	.16	1.11	628	5.76	1.76	4.16	4.64	487.
TATOOSH	599	0	.68	.85	.17	601	.17	.33	2.70	.34	599	0	0	.50	.84	169.

MARCH

	SURFACE - 150M, ΔZ - 150M					150M - 300M, ΔZ = 150M					300M - Next Highest Level Reported					
Station	Sample No	N	E	S	W	Sample No	N	E	S	W	Sample No	N	E	S	W	ΔZ(m)
DENVER	982	.2	.2	.3	.3	985	.6	.1	.1	.4	986	.1	.1	.1	.1	
DAYTON	1067	0	.63	.81	.72	1080	.09	.27	1.20	1.94	1091	1.35	1.08	3.86	9.77	
OAKLAND	661	0	.15	0	0	700	0	.28	0	0	718	0	.28	0	.28	
SALT LAKE CITY	1098	0	.09	.36	.45	1102	.09	.09	.18	.09	1098	1.71	.45	.72	1.53	
FT. WORTH	1102	.45	.18	2.61	.18	1109	.09	.18	.18	.18	1110	2.43	1.17	7.83	9.18	
ATHENS	659	.45	.60	1.20	1.65	664	.30	.45	1.50	1.00	658	2.70	.15	7.69	6.61	
TOPEKA	1096	.63	.18	1.71	.90	1100	.54	.18	.72	1.17	1100	3.78	2.16	7.13	8.96	
NANTUCKET	627	.16	0	1.60	2.72	627	.64	0	.48	1.44	623	.48	0	.32	.96	
GREEN BAY	691	.28	.42	.42	.56	693	.28	.14	.70	.70	683	2.69	1.95	4.59	4.28	
TATOOSH	707	.14	.28	1.26	.42	709	.14	.14	1.54	.56	700	0	.14	.42	.42	

APRIL

Station	SURFACE - 150M, ΔZ = 150M Sample No	N	E	S	W	150M - 300M, ΔZ = 150M Sample No	N	E	S	W	300M - Next Highest Level Reported Sample No	N	E	S	W	ΔZ(m)
DENVER	946	.22	0	.44	.55	946	.33	.11	0	.11	948	0	.11	0	0	89.
DAYTON	1010	.30	.40	1.10	1.30	1023	.30	.40	1.19	2.48	1044	1.49	.20	4.09	9.35	396.
OAKLAND	639	0	.16	0	.16	675	0	0	0	.15	689	.30	0	0	0	198.
SALT LAKE CITY	1059	.27	.18	.54	.09	1059	.09	0	.09	0	1060	1.28	.09	1.46	1.73	419.
FT. WORTH	1072	.36	.18	3.14	.45	1078	.09	.09	.63	.36	1080	2.34	.45	5.70	11.78	526.
ATHENS	676	.90	.90	.90	4.49	679	.60	.15	.30	.75	684	2.25	.60	4.53	5.92	454.
TOPEKA	1053	.63	.45	1.84	.64	1061	.63	.36	1.55	.81	1061	2.09	.91	4.52	7.27	432.
NANTUCKET	598	.85	1.02	2.88	2.69	596	1.02	0	1.02	2.38	593	.85	.51	.34	.85	196.
GREEN BAY	695	.70	.42	.71	1.13	694	.14	.28	1.68	.85	683	3.13	.88	5.31	6.07	487.
TATOOSH	649	0	.30	.30	.30	653	.15	.45	.30	.30	652	0	0	.30	.15	169.

MAY

Station	SURFACE - 150M, ΔZ = 150M Sample No	N	E	S	W	150M - 300M, ΔZ = 150M Sample No	N	E	S	W	300M - Next Highest Level Reported Sample No	N	E	S	W	ΔZ(m)
DENVER	973	.3	0	.2	.3	976	.2	0	.3	.1	981	.1	0	0	.1	89.
DAYTON	1030	.29	.10	.89	.8	1051	.40	.30	0	2.39	1080	1.98	.54	.99	6.22	396.
OAKLAND	682	0	0	0	0	708	.14	0	0	0	721	.14	0	.28	0	198.
SALT LAKE CITY	1099	.18	.09	.27	.18	1098	.18	.09	.27	0	1094	.90	.36	1.26	.45	419.
FT. WORTH	1122	.27	.09	3.23	.18	1131	0	.09	.27	.09	1135	.81	.45	6.74	5.26	526.
ATHENS	682	.90	.90	.15	1.64	681	.15	.45	.15	0	693	0	1.12	3.54	1.26	454.
TOPEKA	1120	.72	.09	1.71	.63	1120	.54	.09	1.26	.90	1121	1.71	1.26	5.49	9.78	432.
NANTUCKET	638	.64	0	1.91	3.32	638	.48	.16	.79	2.22	638	.48	0	.32	.48	196.
GREEN BAY	730	.28	.14	1.94	.97	730	.28	.14	.97	2.22	715	3.08	1.12	3.78	9.10	487.
TATOOSH	687	.45	.15	.15	.30	689	.45	.15	.5	0	685	0	.15	0	.30	169.

JUNE

Station	SURFACE - 150M, ΔZ = 150M Sample No	N	E	S	W	150M - 300M, ΔZ = 150M Sample No	N	E	S	W	300M - Next Highest Level Reported Sample No	N	E	S	W	ΔZ(m)
DENVER	953	.2	0	.1	0	953	.2	.1	0	0	956	0	0	.1	.1	89.
DAYTON	963	.1	0	.4	.41	1003	.6	.1	.2	1.0	1041	1.19	0	.59	3.91	396.
OAKLAND	658	0	.45	0	0	678	.15	.15	.15	.15	692	.28	.14	.14	.28	198.
SALT LAKE CITY	1057	.18	.09	.45	.09	1057	.36	0	.45	0	1057	.72	.27	1.46	.90	419.
FT. WORTH	1066	0	.09	1.53	0	1076	0	0	.27	0	1079	.36	.18	2.57	2.49	526.
ATHENS	661	.15	.90	.30	1.05	667	.15	.15	0	.15	678	.45	.45	1.35	2.23	454.
TOPEKA	1067	.18	.18	3.63	0	1076	.18	.09	1.34	1.52	1076	1.18	.36	3.29	5.68	432.
NANTUCKET	619	.16	.16	1.28	2.73	621	.32	0	0	.96	620	.16	0	0	.32	196.
GREEN BAY	706	.14	0	.42	.98	708	.28	.14	.84	.84	701	1.83	.42	1.40	5.41	487.
TATOOSH	655	.30	.15	.15	.30	659	.60	0	0	0	666	.15	0	.15	0	169.

JULY

Station	SURFACE - 150M, ΔZ = 150M Sample No	N	E	S	W	150M - 300M, ΔZ = 150M Sample No	N	E	S	W	300M - Next Highest Level Reported Sample No	N	E	S	W	ΔZ(m)
DENVER	985	.3	0	.1	0	983	.2	.1	0	0	987	0	0	.1	.1	89.
DAYTON	999	.2	0	0	.6	1024	.2	.1	.3	.90	1068	1.18	.36	.36	2.09	396.
OAKLAND	666	0	0	0	.30	682	0	.30	0	0	697	0	0	.14	0	198.
SALT LAKE CITY	1107	.45	.27	.27	0	1106	.36	0	.45	0	1103	1.35	0	.54	.81	419.
FT. WORTH	1082	.09	0	2.73	.09	1099	0	0	.63	0	1106	.72	.27	1.37	1.62	526.
ATHENS	647	.30	.77	.45	1.20	655	.45	0	.15	.15	685	.45	.15	1.33	1.19	454
TOPEKA	1086	0	.36	1.35	.45	1089	.18	.09	.81	1.53	1088	.54	.27	1.44	7.30	432.
NANTUCKET	602	0	.17	.68	2.69	602	.34	0	0	.85	599	.17	0	.51	.17	196.
GREEN BAY	699	.28	.28	.70	1.00	703	0	.14	.42	.42	699	1.82	.28	1.41	4.42	487.
TATOOSH	665	.45	.15	0	.45	672	1.65	.15	.90	0	672	.90	0	0	0	169.

AUGUST

Station	SURFACE - 150M, ΔZ = 150M Sample No	N	E	S	W	150M - 300M, ΔZ = 150M Sample No	N	E	S	W	300 - Next Highest Level Reported Sample No	N	E	S	W	ΔZ(m)
DENVER	985	.4	0	.5	0	986	0	0	.03	.1	985	0	.2	.2	0	89.
DAYTON	943	.11	0	.22	.54	975	.1	0	.31	.91	1021	1.3	.1	.6	2.48	396.
OAKLAND	685	0	0	0	.15	707	0	.14	.14	.14	715	.14	.14	0	.14	198.
SALT LAKE CITY	1108	.36	.09	.81	.18	1106	.27	0	.36	.09	1106	.90	.09	1.35	.63	419.
FT. WORTH	1091	0	0	1.92	.18	1105	0	0	.36	.36	1112	.90	.27	1.71	1.62	526.
ATHENS	661	.15	1.20	.45	.90	673	.45	.60	.15	.15	692	.70	.70	1.18	.56	454.
TOPEKA	1085	.45	.27	3.55	.18	1092	.09	.09	1.80	1.44	1091	1.26	.45	1.98	5.67	432.
NANTUCKET	652	0	.30	.76	1.81	655	.30	0	.15	.30	658	.45	.30	0	0	196.
GREEN BAY	723	.28	0	.84	.84	723	.28	.28	.56	.56	714	2.52	.14	1.82	4.90	487.
TATOOSH	641	0	.32	0	.32	655	1.05	.15	.15	.30	650	0	0	.15	.15	169.

SEPTEMBER

Station	SURFACE - 150M, ΔZ = 150M Sample No	N	E	S	W	150M - 300M, ΔZ = 150M Sample No	N	E	S	W	300 - Next Highest Level Reported Sample No	N	E	S	W	ΔZ(m)
DENVER	948	.33	.11	.11	0	946	.11	0	.11	0	949	0	0	0	.11	89.
DAYTON	1000	.1	.2	.90	.6	1019	.20	0	.50	1.40	1041	.99	.3	1.00	3.88	396.
OAKLAND	633	.32	0	0	0	662	0	0	0	0	693	0	0	0	0	198.
SALT LAKE CITY	1005	.1	0	.60	0	1005	.1	.1	.1	0	1002	1.10	.30	1.10	.70	419.
FT. WORTH	1052	0	.30	.87	0	1067	.09	0	0	0	1074	.45	.72	2.73	1.76	526.
ATHENS	633	.48	3.53	.32	.48	639	0	.95	.32	.16	660	.75	1.20	3.00	1.65	454.
TOPEKA	981	.20	.10	2.71	.20	985	.10	.30	1.50	1.00	985	1.40	.60	5.26	5.66	432.
NANTUCKET	636	0	.47	1.11	1.27	636	0	.16	.64	.48	634	0	0	0	0	196.
GREEN BAY	691	.28	0	.71	1.12	691	.14	0	1.13	.56	680	1.79	.30	1.64	6.80	487.
TATOOSH	650	.30	.15	.90	.45	662	.15	0	.15	.75	664	.15	0	.30	.30	169.

OCTOBER

Station	SURFACE - 150M, ΔZ = 150M Sample No	N	E	S	W	150M - 300M, ΔZ = 150M Sample No	N	E	S	W	300M - Next Highest Level Reported Sample No	N	E	S	W	ΔZ(m)
DENVER	984	.2	.2	.1	.4	984	.5	.1	.2	.2	986	0	.1	0	.2	89.
DAYTON	1059	0	.27	.90	.63	1079	.18	.27	.45	1.64	1105	1.44	.45	1.62	3.87	396.
OAKLAND	596	0	0	0	0	665	.30	0	0	.15	711	.14	.14	0	0	198.
SALT LAKE CITY	1106	0	.18	.63	0	1107	.09	0	.27	.09	1105	1.26	.36	1.53	1.08	419.
FT. WORTH	1090	.8	0	2.35	.36	1106	0	.09	.27	.18	1109	1.44	.27	2.7	3.69	526.
ATHENS	609	.80	3.55	.48	1.61	622	0	.96	.48	.48	643	.96	1.28	3.02	2.70	454.
TOPEKA	1093	.54	.27	2.43	.09	1102	.54	.18	2.25	1.26	1102	1.89	.36	2.52	7.02	432.
NANTUCKET	658	.45	.15	.90	.90	659	.45	.15	.30	.60	660	0	.30	.15	.30	196.
GREEN BAY	710	.56	0	1.40	2.38	710	.56	.14	.70	1.82	700	4.00	.99	2.53	7.28	487.
TATOOSH	660	.60	.15	3.90	.45	672	.15	.30	1.65	1.95	675	.15	.15	0	.75	169.

NOVEMBER

Station	SURFACE - 150M, ΔZ = 150M Sample No	N	E	S	W	150M - 300M, ΔZ = 150M Sample No	N	E	S	W	300M - Next Highest Level Reported Sample No	N	E	S	W	ΔZ(m)
DENVER	956	.2	.2	.2	.3	956	1.1	.1	.2	.5	955	0	.1	0	0	89.
DAYTON	1029	.2	0	1.70	2.07	1042	.3	0	1.87	1.77	1060	1.64	0	1.86	11.99	396.
OAKLAND	509	.20	0	0	0	588	.17	.17	0	0	633	.32	0	0	0	198.
SALT LAKE CITY	1054	.18	0	.45	.09	1059	0	.09	.27	.09	1065	1.63	.18	3.15	1.74	419.
FT. WORTH	1049	.40	.10	3.01	.20	1063	.09	.09	.54	.45	1068	4.77	.92	6.86	7.18	526.
ATHENS	618	1.12	2.05	.80	3.20	628	.80	.32	.80	1.28	646	3.01	2.26	5.51	5.64	454.
TOPEKA	1060	1.09	.09	3.61	.63	1064	1.27	.09	2.12	1.72	1060	5.51	1.18	2.85	9.78	432.
NANTUCKET	563	.18	0	3.08	3.23	565	.18	.54	1.62	1.26	565	.72	0	.72	.54	196.
GREEN BAY	661	.60	.15	1.05	.90	660	.30	.15	1.50	1.50	632	5.27	1.76	3.04	7.97	487.
TATOOSH	676	.15	.15	1.35	.45	673	.30	0	.75	.60	672	.30	0	0	1.05	169.

DECEMBER

Station	SURFACE - 150M, ΔZ = 150M Sample No	N	E	S	W	150M - 300M, ΔZ = 150M Sample No	N	E	S	W	300M - Next Highest Level Reported Sample No	N	E	S	W	ΔZ(m)
DENVER	981	.3	0	0	.4	983	.6	0	0	.6	985	.2	0	0	0	89.
DAYTON	1010	.3	.1	.7	1.40	1023	.5	.1	.8	2.19	1042	4.71	.2	2.06	11.92	396.
OAKLAND	552	.18	.54	0	0	665	.30	.30	0	0	702	.14	.28	0	0	198.
SALT LAKE CITY	1070	.18	0	.45	.18	1082	0	.09	.45	0	1088	1.63	.09	3.38	2.98	419.
FT. WORTH	1100	.54	0	3.06	1.17	1111	.18	.09	.27	.63	1111	4.68	2.61	7.29	9.63	526.
ATHENS	640	.64	1.43	1.12	5.43	648	.75	.15	.90	1.35	667	4.20	2.25	4.80	8.10	454.
TOPEKA	1092	.81	.27	2.16	.72	1094	1.72	0	.99	1.89	1089	5.93	.99	3.71	9.44	432.
NANTUCKET	588	.51	.34	1.53	3.40	588	.17	.51	1.19	1.36	588	.17	.34	.17	.51	196.
GREEN BAY	689	.15	0	.75	.90	690	.56	0	.49	.85	669	7.95	1.65	2.55	6.45	487.
TATOOSH	664	.30	.60	2.55	.75	644	.15	.75	2.25	1.35	600	.30	0	.60	1.95	169.

YEARS AVERAGE

	SURFACE - 150M, ΔZ = 150M					150M - 300M, ΔZ = 150M					300M - Next Highest Level Reported					
Station	Sample No	N	E	S	W	SAMPLE No	N	E	S	W	Sample No	N	E	S	W	ΔZ(m)
DENVER	11579	.31	.06	.19	.27	11584	.47	.06	.12	.24	11605	.07	.05	.07	.06	89.
DAYTON	12151	.42	.18	1.50	1.56	12401	.34	.16	.69	1.9	12698	1.77	.36	1.89	5.70	396.
OAKLAND	7476	.10	.13	.06	.06	8067	.12	.05	.05	.06	8372	.16	.10	.06	.07	198.
SALT LAKE CITY	12802	.18	.07	.53	.11	11762	.15	.26	.37	.04	12810	1.4	.20	1.92	1.43	419.
FT.WORTH	12883	.29	.10	2.37	.29	13036	.06	.06	.34	.30	13083	2.16	.99	5.14	6.49	526.
ATHENS	7815	.59	1.18	.70	2.17	7896	.40	.40	.56	.75	8043	1.97	1.28	3.98	4.45	454.
TOPEKA	12746	.48	.22	2.40	.45	12809	.59	.16	1.31	1.32	12796	3.00	1.05	4.24	7.70	432.
NANTUCKET	7347	.38	.24	1.52	2.51	7353	.38	.15	.64	1.15	7340	.38	.14	.27	0.46	196.
GREEN BAY	8333	.31	.12	.81	1.06	8341	.33	.13	.80	1.03	8181	3.79	1.11	2.89	4.37	487.
TATOOSH	7857	.22	.30	1.17	.38	7893	.47	.19	.98	.52	7889	1.00	.03	.21	.61	169.

APPENDIX B

RECOMMENDATIONS

Recommendation No. 1: Decrease Sampling Period. This study was preliminary. The data set imposed certain limitations upon the analysis as set forth in the agreement governing this study. First of all, nothing could be said about the short-term duration of occurrence of extreme wind shears, since the sampling period of the data was only several hours. The most likely periods (minutes to hours) were not sampled. This leads to the first recommendation. The sampling period of wind shear data should be decreased to periods on the order of minutes. This would greatly increase the confidence of the bivariate statistics of the extreme values and help to quantitatively define return times and duration of wind shear. Since extreme wind shears are of primary concern, it may be advisable to record only those periods during which the wind shear is high, and then from these data derive extreme value distributions and durations. Acoustic Doppler systems seem to be the best blend of safety, accuracy, and economy to routinely measure extreme wind shears. To satisfy other areas of interest, during times of extreme shear recording, data channels may be provided for logging temperature profiles as well as transmissometer and ceilometer output.

Recommendation No. 2: Increase Vertical Resolution. The data used for this study dictated a 150 m separation in the lower two layers, the layers of most interest when relating wind shear to aircraft operations. As pointed out earlier, wind shears occuring over a vertical spacing on the order of tens of meters appear to be important in the maintenance of control of the aircraft in an extreme shear condition, thus the vertical resolution of wind profiles at aerodromes should be increased to a spacing of from 30 to 50 m. Again, the most suitable instrument for such measurements is an acoustic Doppler system. However, it may be entirely possible, with the cooperation of the air transport industry to utilize on board inertial guidance platforms to derive approach wind profiles for comparison with *in situ* measurements. This could be done by deriving the slope $\Delta u/\Delta z$ of a linear regression of the mean of the head or tail wind component, $\bar{u}$, against the height of the aircraft, z where,

$$u = TAS - GS + \int_{t_1}^{t_2} a_\ell \, dt, \text{ head or tail wind component} \qquad (B.1)$$

$$z = \int_{t_1}^{t_2} \int_{t_1'}^{t_2'} a_z \, dt dt' \quad , \qquad (B.2)$$

and TAS = true air speed

GS = ground speed

a_ℓ = longitudinal acceleration of aircraft at C.G.

a_z = vertical acceleration of aircraft at C.G.

t = time

This technique would not necessitate absolute calibration, since only relative values are used. The length of time used for computation of the means would determine smallest distance over which the shear could be determined.

Recommendation No. 3: Test Horizontal Homogeneity Assumption. In an earlier discussion, it was mentioned that the wind shear quantity actually affecting the aircraft was $\partial/\partial x(\partial\vec{V}/\partial z)$, but that horizontal homogeneity must be assumed to give only $\partial\vec{V}/\partial z$ at one spot. It is suggested that this assumption be tested in at least two ways. The first could be part of the investigation described in the latter part of Recommendation No. 2 (i.e. utilization of inertial platforms on aircraft compared with *in situ* measurements of wind shear). The second method would be to correlate the output of wind profiles derived from boundary layer sampling of acoustic Doppler systems at different distances and azimuths from a stationary acoustic Doppler system as in Figure B.1. From this test the dependence of homogeneity upon averaging time of the profiles could be determined. It will not be surprising to find horizontal homogeneity also a function of stability.

Recommendation No. 4: Closer Examination of Individual Stations. Due to limitations of time and funding, the nine stations other than Denver , could not receive the same intensive investigation. It is suggested that these nine stations be individually examined using our analysis of Denver as a model. Of particular interest would be the investigation of synoptic situations which were contemporaneous with very extreme shear conditions; such an investigation for Denver proved quite fruitful. Further investigation of the normality of the marginal distributions of the other stations would be in order. If these distributions do appear normal, as was the case for Denver, then the possibility of mathematically modeling the bivariate distribution of vertical wind shear exists.

The bivariate frequency table gives a great deal of information about the low level shear conditions at a

given station; however, it does not answer a basic question: is a given shear vector produced by speed variations with direction remaining constant or is it primarily directional in nature? This can be answered by considering the vector diagram as in Figure B-2. The angle between the wind vectors is

$$\alpha = \cos^{-1}\left\{\frac{u_2^2 + v_2^2 + u_1^2 + v_1^2 - ((\Delta u)^2 + (\Delta v)^2)}{2\left(u_2^2 + v_2^2\right)^{1/2}\left(u_1^2 + v_1^2\right)^{1/2}}\right\} \quad (B.3)$$

and the magnitude of the shear vector is

$$|\Delta\vec{V}| = \left(\Delta u^2 + \Delta v^2\right)^{1/2} .$$

There are now two basic options in the presentation of this data. The first would be to plot α - vs - $|\Delta\vec{V}|$ and see if a relationship exists between shear magnitude and the angle between the two wind vectors. This could be done for the three layers considered in this study. A further refinement would be to plot α and $|\Delta\vec{V}|$ as functions of the wind direction at the highest level thus relating the two to a gross synoptic indicator (i.e. geostrophic wind direction).

Recommendation No. 5: Initiation of Work Similar to That of Fichtl's (see Section 2.1.2.3) for different areas of CONUS and utilizing acoustic Doppler systems to gather shear information.

Recommendation No. 6: Use of Extreme Shear Information to Re-Evaluate Aircraft Accidents and Incidents. As noted in the literature review the relationship of shear to the control of aircraft has only recently gained attention in aircraft operations. It is entirely possible that the influence of wind shear in an aircraft accident or incident was not considered in the overall accident or incident evaluation but was unknowingly included in either aircraft malfunction or pilot error categories of possible causes. It is suggested that at the four FAA major airports (and with the cooperation of the USAF, Carswell AFB, Ft. Worth) the dates and times of the extreme wind shears be reviewed in conjunction with aircraft accidents or incidents $\pm$ 6 hr about the extreme shear time to see if any correlation does exist between extreme shear conditions and aircraft accidents or incidents. The years of this study generally ran from 1956 to 1964. Such a study would be relatively easy and might shed valuable light upon the ability of aircraft to cope with extreme shear conditions.

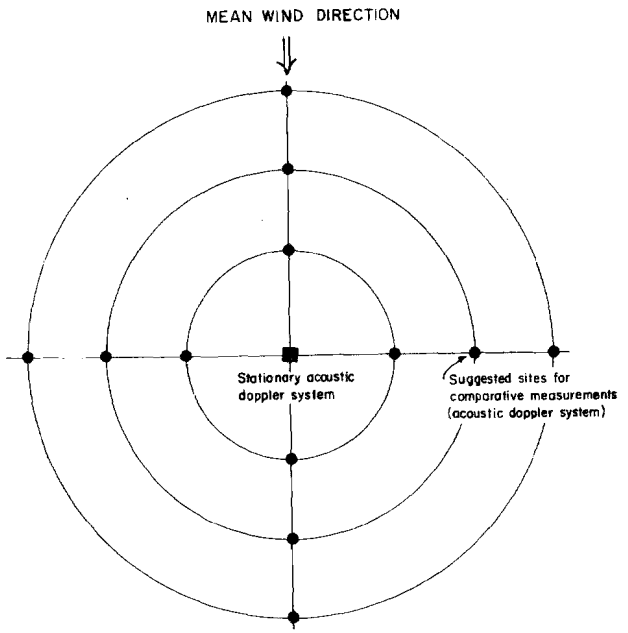

Figure B1. Schematic view of site for testing horizontal homogeneity assumption. Spacing of sites along any axis should be on the order of 0.5 km to 2 km.

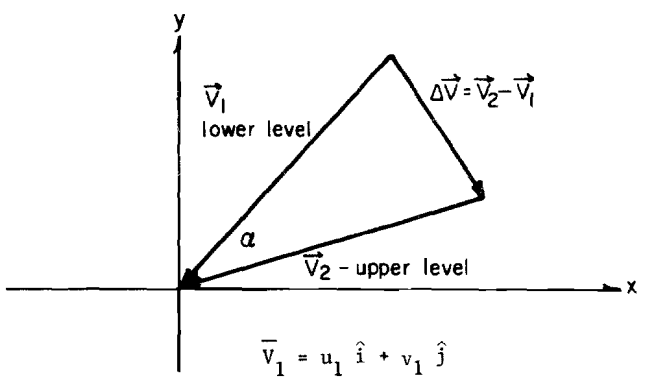

$$\overline{V}_1 = u_1\,\hat{i} + v_1\,\hat{j}$$

$$\overline{V}_2 = u_2\,\hat{i} + v_2\,\hat{j}$$

$$\Delta\overline{V} = \Delta u\,\hat{i} + \Delta v\,\hat{j}$$

where $\Delta u = u_2 - u_1$

$\Delta v = v_2 - v_1$

Figure B2. Vector diagram showing notation for recommendation No. 4.

SECTION 2.2 OPTIMUM AVERAGING TIMES FOR SHORT TERM PREDICTION OF WINDS IN THE BOUNDARY LAYER (by J. E. Gaynor)

2.2.1 INTRODUCTION

The importance of wind information along both the flight approach path and runway has become increasingly important with stricter requirements for low visibility precision approaches and the increased demand for maximum use of aircraft and facilities. More necessary than real-time data is the ability to predict winds accurately, of the order of a few minutes ahead, in time for aircraft landings. Such predicted winds allow the pilot to anticipate the wind speed and direction in the vicinity of the touchdown while he is still on his approach and to make adjustments which will insure a safer landing.

The International Civil Aviation Organization (ICAO) Fifth Air Navigation Conference (1967) defined the surface wind given to the pilot as a 2 min mean wind direction (reported to the nearest 10 degrees) and a 2 min mean wind speed (reported to the nearest knot). This information is given to a pilot a few minutes prior to his actual touchdown. It would be more desirable if a prediction of the conditions at touch down (a few minutes later) could be given. The hardware for on-line digital averaging exists (Koren, 1972), and it remains to find the best predictor of the 2 min averaged wind and azimuth.

Root mean square (RMS) statistics for evaluating a prediction scheme have been used to test relatively long-term forecast schemes (Thompson, 1961). As the base comparison, these studies used a simple persistence value, a technique adapted for the work reported here.

Rachele and Armendariz (1967) used meteorological tower data for prediction criteria for a 4 sec mean wind and azimuth 4.2 m above the surface at a horizontal distance separation of 30 and 45 m to predict winds for rocket launches. They found, using root mean square error (RMSE) statistics, that the longer averaged winds and azimuths (of the order of 360 sec) measured within 60 sec and preferably around 10 to 15 sec before launch to be the best predictors for both stable and unstable cases.

Armendariz and Lang (1968) separated free convection, forced convection, and neutral cases depending on the Richardson's number. They found little difference in RMS variability between the cases. The researchers discovered that a single point measurement yielded less dispersion, which can be measured by the slope of the RMS curves, for lag times less than 60 sec and a wind average of less than 60 sec. Using an array of three towers 275 m from one another and wind and azimuth data all at the 19 m level, they found that zero lag was not necessarily the best correlation between towers in agreement with Taylor (1938). For the two towers most nearly horizontal to the average wind direction, they discovered that a 60 sec wind and azimuth average provides a better predictor up to a lag of 60 sec. Beyond that, the 240 or 300 sec average is preferable. For the towers aligned nearly perpendicular to the mean wind, they found the wind variability much more dependent on space than time.

In this study no attempt will be made to analyze the effect of physical distance on the predictability of wind or azimuth. Only single point measurements will be analyzed.

Assuming Taylor's hypothesis of frozen turbulence, Sparks and Keddie (1971) used anemoneter data 10 m above the ground for calculating RMS errors for wind during a 300 m run of a descending airplane (or about a 4 or 5 sec mean wind relative to the moving airplane). Their results showed that to predict this mean wind 10 min ahead, a 4 or 5 min averaged wind should be used. In general, the longer averaging times (over 4 min) were the best predictors of short (4 or 5 sec) averages at all lag times. They made no attempt to separate stable and unstable regimes.

In the current work, an effort is made to separate the two regimes using the variance of the wind. Singer and Smith (1953) have shown that the wind variance can be a good indicator of the stability of the atmosphere. The larger magnitude variance can indicate more instability. However, Singer and Smith also mentioned that a large variance of the wind also occurs in neutral, strong wind, regimes. This means that the variance is not an unambiguous indicator of stable and unstable regimes. Another very basic and important difference between the above mentioned studies and the current one is the use of running averages as opposed to block averages.

This work is an investigation and analysis of the least error from the observed mean wind to the actual wind at a time difference of 0 to 10 min later at 1 min increments. The data will be analyzed to determine the optimum sampling mean time for each of these increments. Also, the problem of the optimum location for the wind and wind shear sensors at an airport will be discussed.

2.2.2 OPTIMUM SENSOR LOCATION

We can gain some insight into the optimum location of a wind sensor at an airport runway by considering the work of Armendariz and Lang (1968). Using the three tower array, they found maximum time dependency of the wind for the towers aligned most nearly horizontal to the mean wind direction. If we use Taylor's hypothesis of frozen turbulence we can compute the maximum lag correlation for an upwind location of the sensor by the simple relation

$$\Delta t = \frac{\chi}{V} \quad , \qquad (2.2.1)$$

where χ is the distance to the prediction location and V is the mean wind speed (for about an hour). When only one sensor is used, it should be located at some average upwind location from the prediction point, an impossible situation for a multiple runway airport.

To indicate how the winds vary with horizontal distance at an airport, Ito (1968) conducted a study using two sensors at a height of 3 m and a few kilometers horizontal distance apart at Tokyo Airport and found that 95% of the wind direction differences between the sensors were within 20° and 1.6% exceeded 34°. However, within this 1.6% were a few cases of large wind shifts and speed differences perhaps associated with frontal passages lasting for many minutes and occurring with moderate wind speeds.

Rijkoort and Wieringa (1968) recommend a wind sensor at the 10 m level at each end of the runway with another sensor at one end at about 40 m for the surface wind shear measurement. They would interpolate between the two 10 m sensors to reduce the distance uncertainty. The difference between the two measurements gives a knowledge of the distance uncertainty, which may be combined with the single-point wind variability to give the information of the variation about the mean wind using sigma or a multiple. The effect of mesoscale nonstationary activity, like sea breeze fronts or small squalls can perhaps be reduced by averaging, but averaging over a time which would not greatly reduce the gust information. They found the 2 min average to be optimum.

We can make the reasonable assumption that the atmosphere is locally horizontally homogeneous with respect to wind shear. The large problem is the great horizontal inhomogeneity of point measurements of the winds themselves at a particular level near the surface. This problem cannot be solved using a single sensor and, from the above discussion, only partially solved using two or more sensors. A possible suggestion to avoid this problem would be to use the optical laser line-of-sight method developed by Lawrence (1972) which can measure a spacial average of the wind across a runway.

2.2.3 METHOD OF ANALYSIS

The approach of this study was to separate the data into high and low variance regimes using 5 min running variances, updated every second. These running variances were averaged for each sample hour so that each hour is tagged with a representative variance. The equation used for the variance was

$$S^2 = \frac{1}{n-1} \sum_{i=1}^{n} (\chi_i - \bar{\chi})^2 \quad , \qquad (2.2.2)$$

where n is the number of observations in 5 min, χ_i the particular data point, and $\bar{\chi}$ is the average of the data over the 5 min. The variance of only the horizontal winds and not those of the azimuths were calculated. Since the winds and azimuths are for the same period, the high variance winds were associated with the azimuths of the same period, and these azimuths were assumed high variance also. The running variance is a parameter which can be easily monitored with an on-line computer.

The actual predictability conditions were represented using an RMSE approach normalized by the standard deviation (the square root of the variance) of the 2 min running average. The equation is given by

$$r_n = \frac{\sqrt{\sum(\chi_2 - \chi_t)^2 / N}}{\sigma_2} \quad , \qquad (2.2.3)$$

where χ_2 is the 2 min running average of the wind or azimuth which is the variable we wish to predict. The χ_t value is the running average (1/2, 1, 2, 3, 4, 5 min.) of the wind or azimuth, and σ_2 is the standard deviation of the 2 min running average. Using the above equation and lagging χ_2 from χ_t for times of 0-10 min at 1 min increments we collect a total of 11 RMS errors for each of the six running averages. Rather than call it a "lag" we will often use the more descriptive phrase of "forecast interval." With t = 2 min the RMSE values for the various forecast intervals represent the "persistence" values. In other words, they represent the error between the actual 2 min average of the wind or azimuth and the 2 min mean simply extrapolated ahead in time.

Remember that Equation 2.2.3 is the prediction criteria of the 2 min mean a number of minutes ahead. The forecast interval is from the end of the period of the current average to the beginning of the period of the 2 min mean (see Figure 2.2.1).

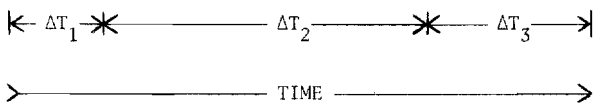

ΔT_1: BASE AVERAGE

ΔT_2: FORECAST INTERVAL

ΔT_3: 2 MIN. MEAN

Figure 2.2.1 Visual schematic of the forecasting problem.

To test whether a running average can be used as a forecast of the two minute mean wind, it remains to show that the RMSE value of the running average in question is significantly less than the persistence value for a particular forecast interval. To help in testing the significance of the data, standard deviations from the average of all the sample RMSE values in each of the two variance classifications were calculated for the persistence value, and for all the other running averages.

The significance of the forecast criteria was tested using the standard one-sided t-test. The equation used was

$$t = \frac{\bar{r}_2 - \bar{r}_t}{\sqrt{\frac{S_2^2 + S_t^2}{n}}} , \qquad (2.2.4)$$

where $\bar{r}_2$ is the sample average of the RMSE statistics from Equation 2.2.3 for persistence at a particular forecast interval. The quantity r_t is the sample average of the RMSE statistics which fall below persistence for the same forecast interval. S_2^2 and S_t^2 are the variances and n is the number of samples. The test assumes a normal distribution of the RMSE values. The hypothesis that the persistence was not equal to the particular average was tested at the 90% confidence level.

The technique used in this study obviously cannot predict sudden shifts in wind and azimuth due to cumulus activity or small-scale squall lines. These sudden changes are some unknown function of the local pressure changes with time which are not included in our purely statistical approach.

2.2.4 DATA PROCESSING

The data for this study came from digital tapes containing wind speed, elevation and azimuth angles generated during 1972 Haswell Experiment conducted by the Wave Propagation Laboratory of NOAA from mid-July to the end of August. The Haswell site is located in southeast Colorado, and includes a 152 m meteorological tower equipped with five equally spaced Gill Anemometer Bivanes, the lowest at 30 m. The anemometers have a theoretical damped natural wave length of 5.8 m, a distance constant of 0.74 m, and measure wind direction fluctuations up to 1/2 Hz at wind speeds above 2.7 m/sec.

The data used in this study were samples of high and low variance cases chosen from the period between the first and 13th of August. Eight high variance cases and 11 low variance cases, each an hour long, were selected by visual inspection of strip chart records. The data rate on the digital tapes was one sample per second. Three levels were included for analysis - 30, 91, and 152 m.

The base data consisted of horizontal winds (The vertical component was taken out.) and azimuths, 3600 points per sample hour, seperated into high and low variance cases at three levels.

2.2.5 RESULTS

Table 2.2.1 shows the hourly averaged 5 min running wind variance, averaged over the respective sample numbers for the high and low variance cases and separated by level.

TABLE 2.2.1 Sample Averaged High and Low 5 min Running Variances Separated by Level

LEVEL (m)	LOW VARIANCE (11 Samples)	HIGH VARIANCE (8) Samples)
30	.034 m^2/sec^2	1.187 m^2/sec^2
91	.053	.507
152	.032	.707

It can be seen that the low and high variances are separated by nearly an order of magnitude or more. The averages of the high variances show a marked decrease in magnitude above the 30 m level. This is reasonable if we understand that much of the time thermal plumes do not penetrate above the 30 m level in an unstable atmosphere.

Figure 2.2.2 is a scatter diagram of the RMSE of the wind versus the averaged 5 min running variance of the wind for each of the sample hours. A typical example of the 30 m level, 1 min running average at the 5 min forecast interval was chosen to depict the increase in the RMSE with variance. Due to the large scatter and the lack of points between the extreme high and low variance cases, the exact cut-off between high and low variance is difficult to locate.

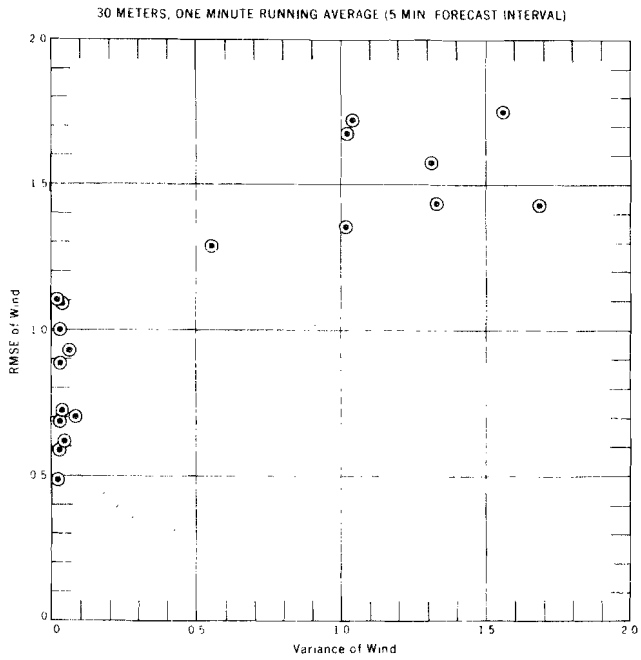

Figure 2.2.2 An example of the scatter diagram of the RMSE of the wind versus the averaged 5 min running variance for each sample hour for the 30 m level. 1 min running average at the 5 min forecast interval.

The 12 cases are summarized as follows:

1) Three levels (30, 91, 152 m).
2) Wind and azimuth.
3) High and low variance.

The RMSE statistics were computed using Equation 2.2.3 for each of the above cases for six running averages (1/2, 1, 2, 3, 4, 5 min) and at forecast intervals from 0 to 10 min at 1 min intervals.

The data are presented in a series of 12 graphs, one graph for each of the 12 cases with each containing six curves for the six running averages. These graphs are the averages for the 11 low variance samples and eight high variance samples. They contain standard deviation bars on the persistence (2 min running average) curve and also bars drawn on most of the 1/2 and 1 min running average curves at the 1 min forecast interval, only, at which point the bars overlap very little, if at all. The standard deviation bars for the 1/2 min average have been off-set slightly to the left to avoid confusion.

The first six graphs are taken from the predominantly unstable, high variance cases. The first three graphs for wind speed are followed by three graphs for azimuth, one graph for each of the three levels.

Figure 2.2.3 of the high variance, 30 m level wind shows that the 1/2 and 1 min running averages seem to be better predictors of the 2 min mean wind out to about the 2 min forecast interval. After this interval, the curves cross and the 3 to 5 min averages drop below persistence and appear to be the better predictors out to the 10 min forecast interval. The standard deviation bars for all cases are fairly large, an aspect which is probably caused by the relatively small number of samples used.

Figures 2.2.4 and 2.2.5 depict the 91 and 152 m level high variance winds, respectively. The graphs look similar to the 30 m level, differing only at the point where the various running averages cross the persistence curve. At both these upper levels, it is noticed that there is a gap in the forecast interval (about 2 to 4 min at 91 m and about 2 to 5 and 1/2 min at 152 m) in which all curves are above persistence. At any forecast interval where the curves are above persistence, we can conclude, while ignoring the significance of the results, that persistence is the best predictor.

Figures 2.2.6, 2.2.7 and 2.2.8 show azimuth data for the high variance case at the three levels. They are very similar to the wind graphs except for the exact location at which the various curves cross the persistence line. Except for the 152 m level, they tend to cross at higher forecast intervals than the wind curves. Also, in general, the RMSE values are lower than for the wind cases.

The following six graphs, Figures 2.2.9 through 2.2.14 are for the low variance (early morning, stable) cases. In each of these six graphs for both the winds and azimuths, the 1/2 and 1 min averages remain below persistence from about 1/2 min forecast interval on, and approach the persistence curve toward the 10 min forecast interval. The 3 to 5 min average curves remain above persistence throughout and show no signs of approaching persistence. In general, the RMSE values for the winds and azimuths in the low variance cases do not show a significant difference in their magnitudes.

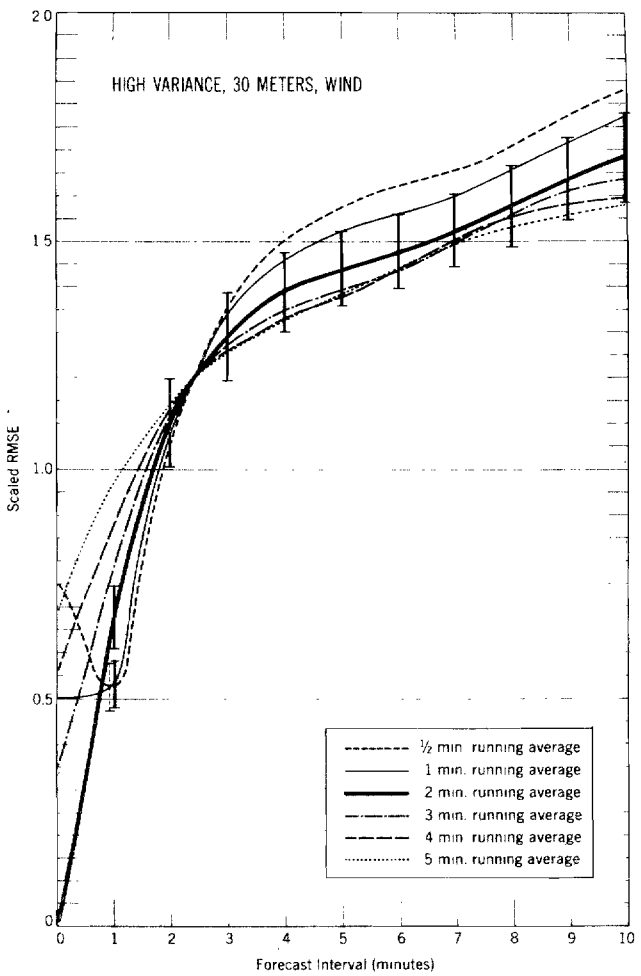

Figure 2.2.3 Normalized RMSE of the wind for each forecast interval at the 30 m level (averaged over the eight high variance samples).

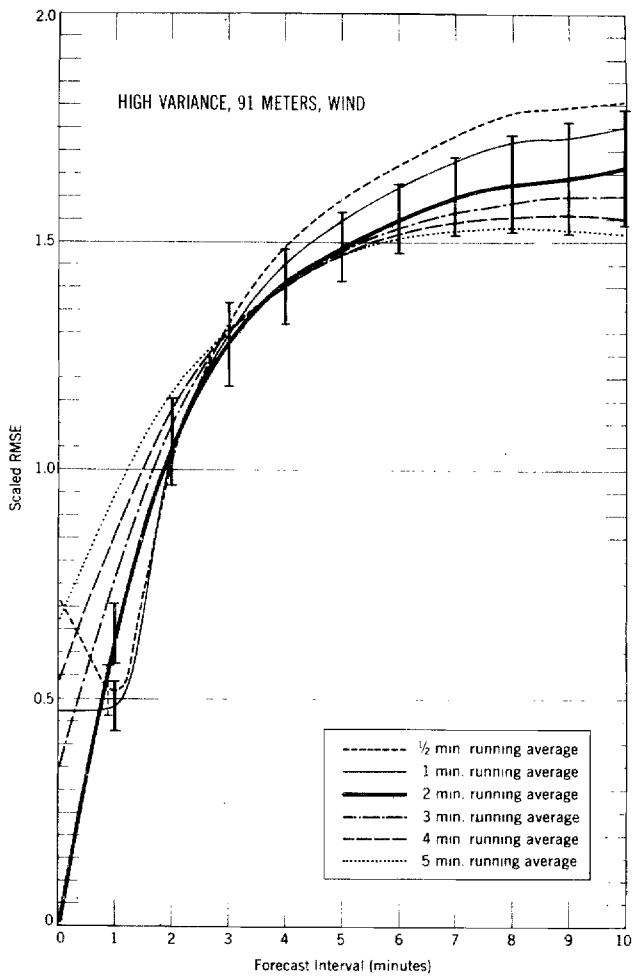

Figure 2.2.4 Normalized RMSE of the wind for each forecast interval at the 91 m level (averaged over the eight high variance samples).

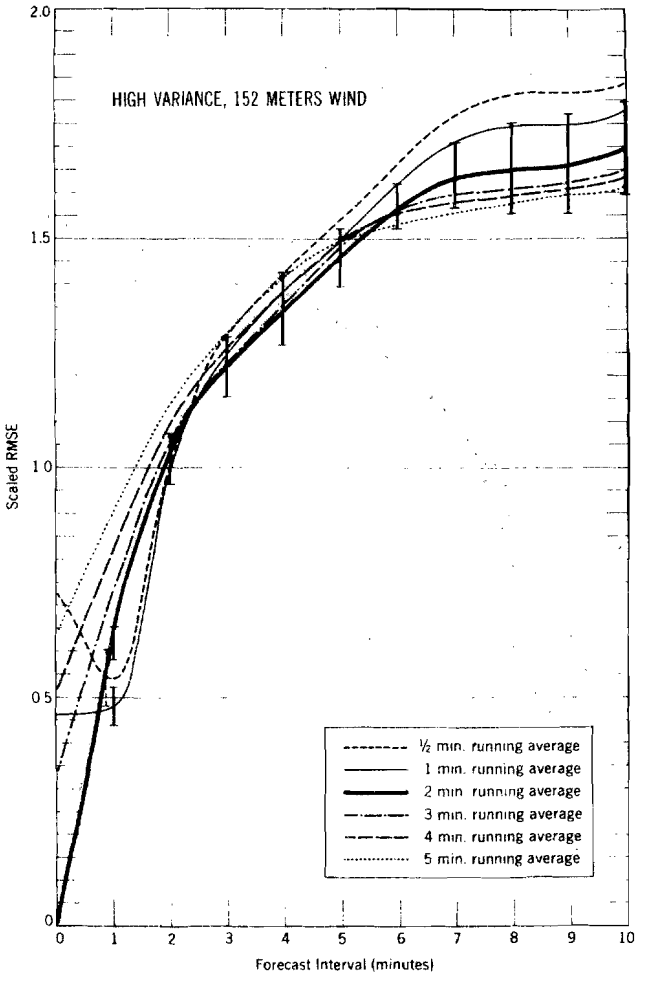

Figure 2.2.5 Normalized RMSE of the wind for each forecast interval at the 152 m level (averaged over the eight high variance samples).

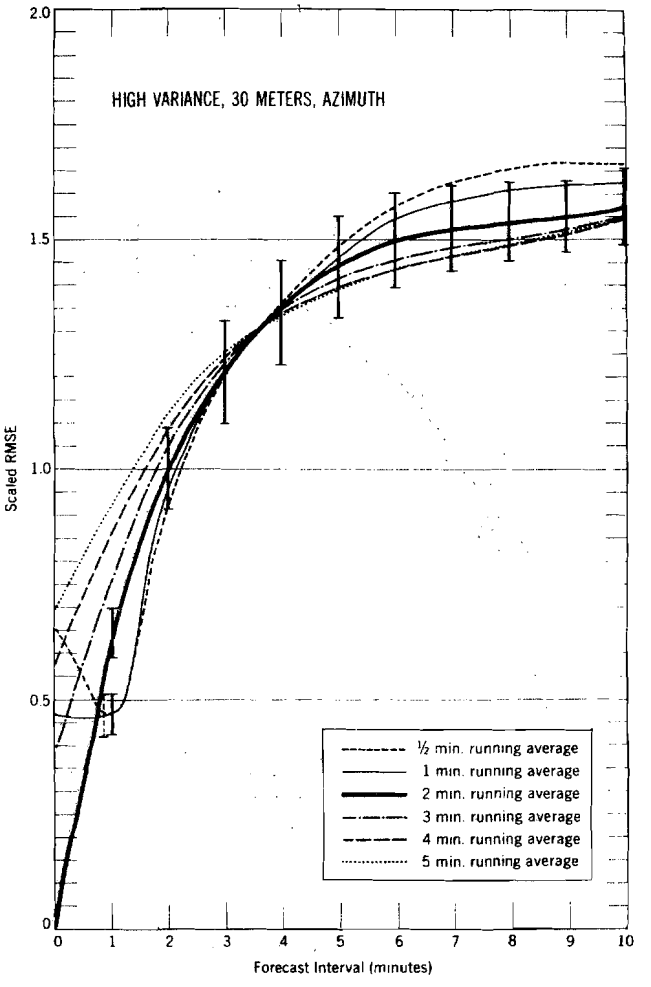

Figure 2.2.6 Normalized RMSE of the azimuth for each forecast interval at the 30 m level (averaged over the eight high variance samples).

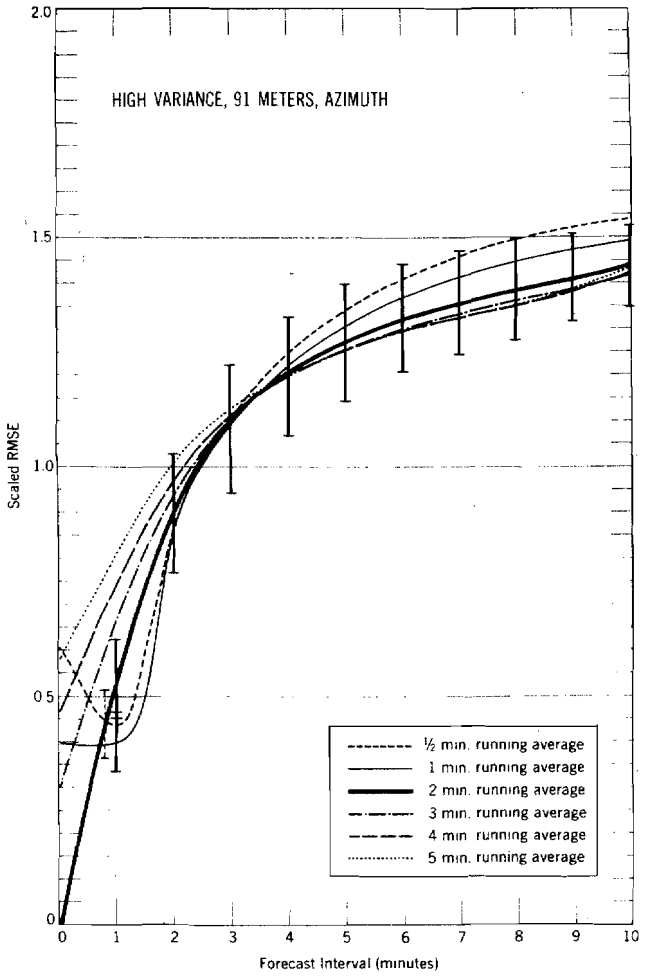

Figure 2.2.7 Normalized RMSE of the azimuth for each forecast interval at the 91 m level (averaged over the eight high variance samples).

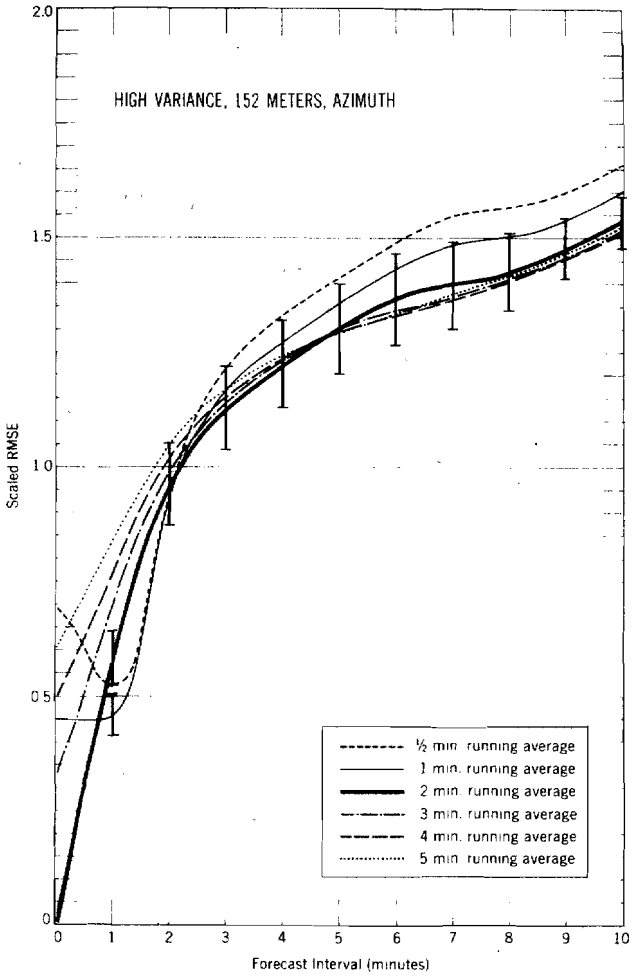

Figure 2.2.8 Normalized RMSE of the azimuth for each forecast interval at the 152 m level (averaged over the eight high variance samples).

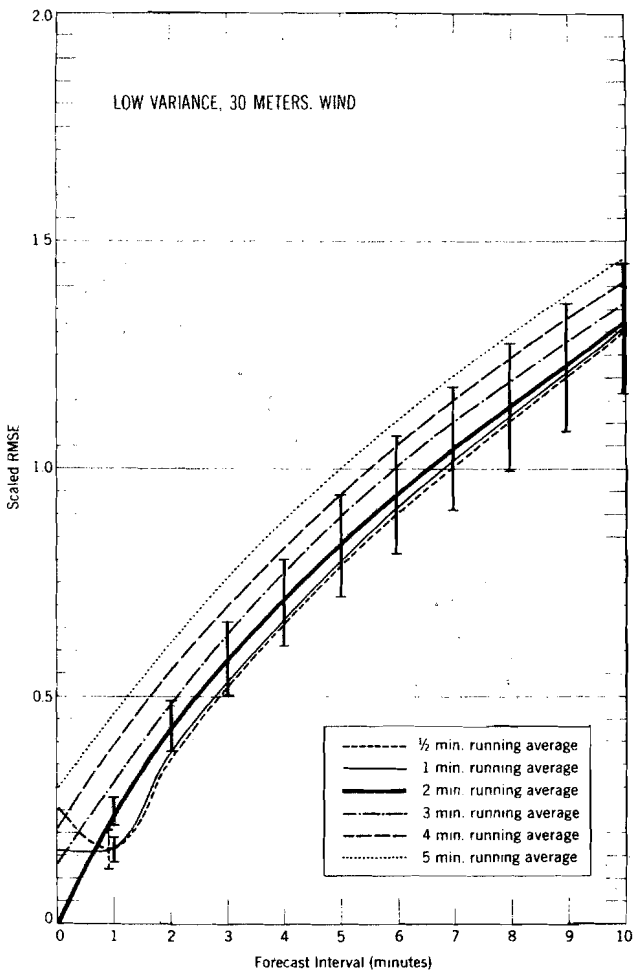

Figure 2.2.9 Normalized RMSE of the wind for each forecast interval at the 30 m level (averaged over the 11 low variance samples).

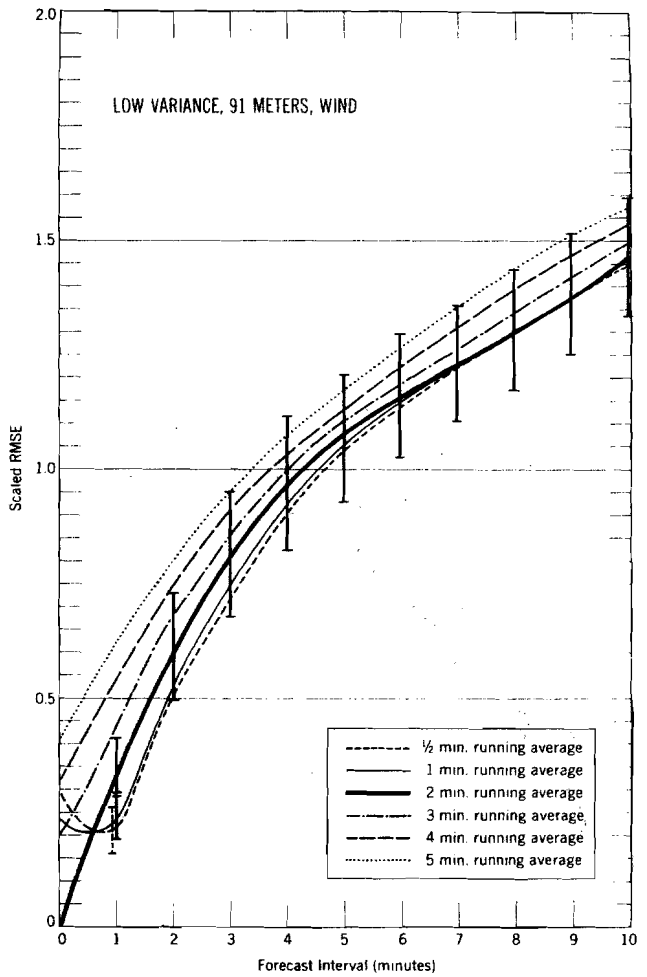

Figure 2.2.10 Normalized RMSE of the wind for each forecast interval at the 91 m level (averaged over the 11 low variance samples).

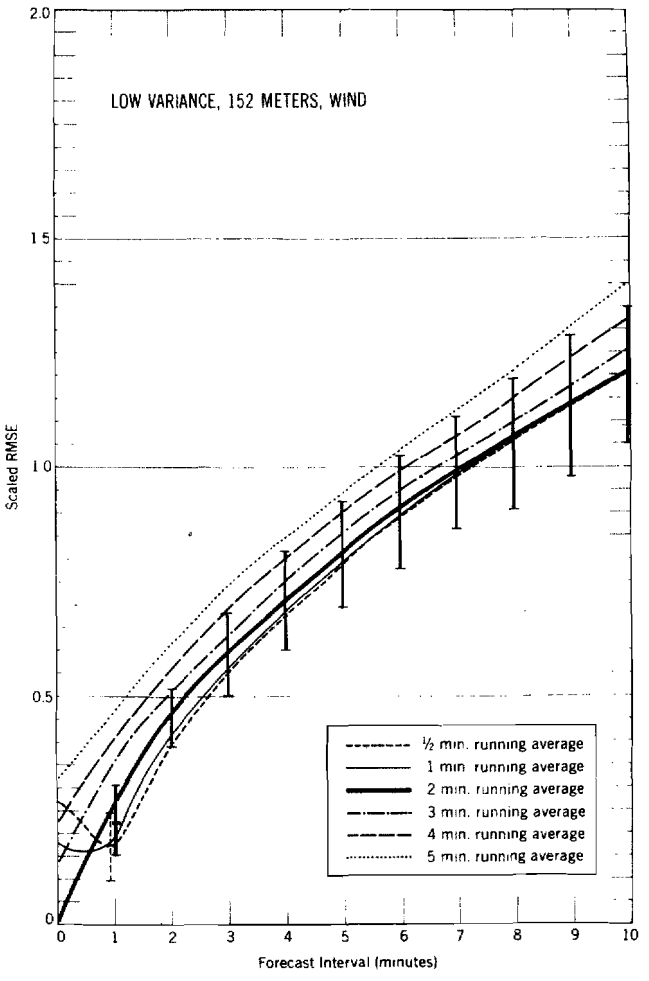

Figure 2.2.11 Normalized RMSE of the wind for each forecast interval at the 152 m level (averaged over the 11 low variance samples).

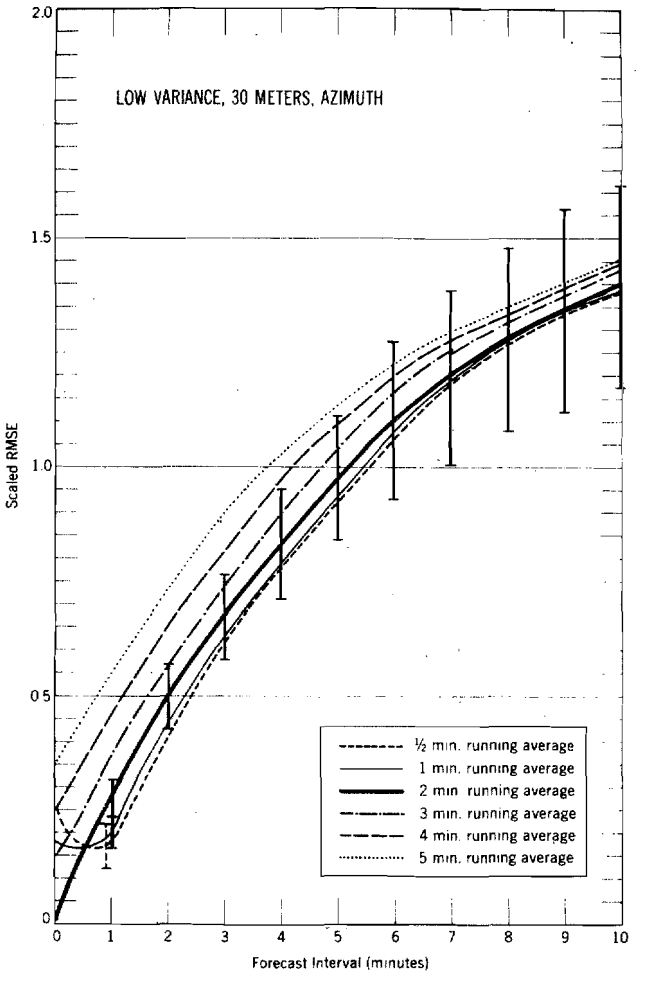

Figure 2.2.12 Normalized RMSE of the azimuth for each forecast interval at the 30 m level (averaged over the 11 low variance samples).

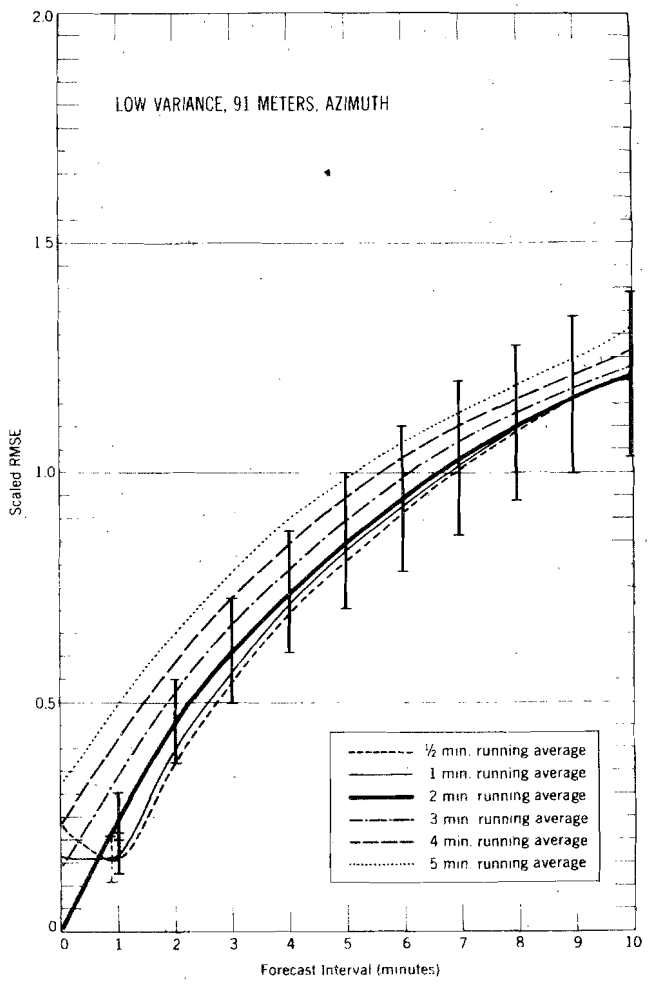

Figure 2.2.13 Normalized RMSE of the azimuth for each forecast interval at the 91 m level (averaged over the 11 low variance samples).

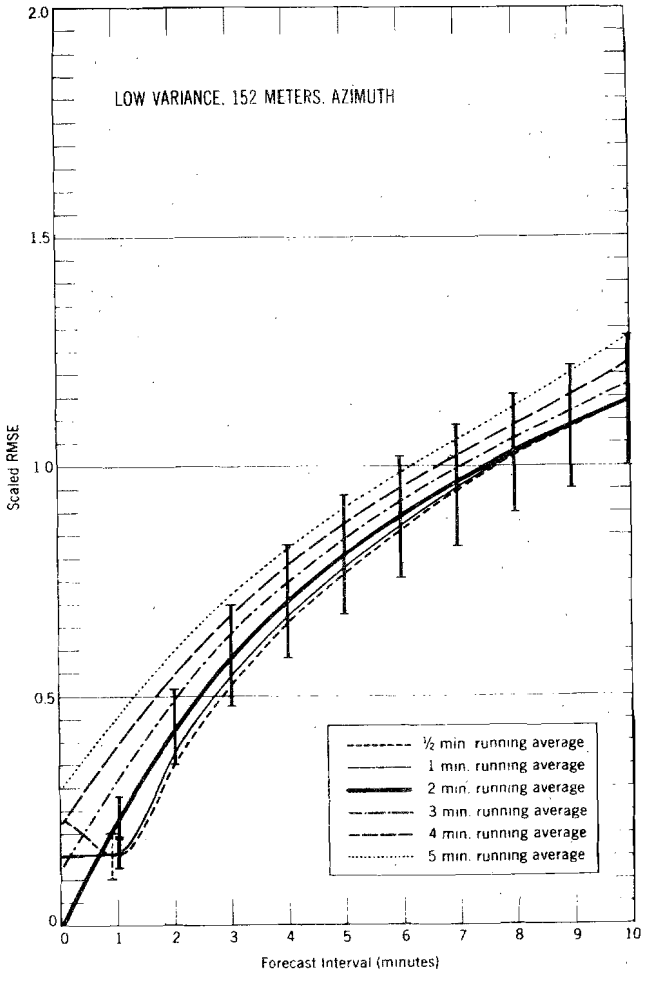

Figure 2.2.14 Normalized RMSE of the azimuth for each forecast interval at the 152 m level (averaged over the 11 low variance samples).

The departure in the high and low variance cases can be explained by the difference in the frequency distribution of the atmospheric wave structure between the stable and unstable boundary layer. Generally, the stable boundary layer contains gravity waves with periods of the order of 4 to 10 min (Hooke et al., 1972) with superimposed higher frequency oscillations containing relatively little energy also present. When comparing the 2 min persistence with the 1/2 and 1 min running averages, the comparison is good because these longer period undulations are not filtered out. The gravity waves have not been filtered from the persistence time series. However, much or perhaps most of the gravity wave energy has been filtered out of the 3 to 5 min running averages. For this reason the comparison between persistence and these longer averages may not be good at the various forecast intervals and therefore these curves appear above the persistence curves on the low variance graphs.

The high variance curves crossing the persistence curves is a more difficult feature to explain. In the unstable boundary layer, most of the energy is in the small scale oscillations, certainly of the order of, or less than, 2 min periods. According to a hypothesis raised by Businger (1972), these small scale oscillations are superimposed on a much larger scale oscillation induced by convective activity with periods of many minutes, which may not be filtered out even by our longest averaging periods. For small forecast intervals, comparing the 1/2 and 1 min averages with the persistence, it may be hypothesized that the RMSE may be relatively low since the small scale oscillations have not been completely filtered out and the lag is such that the correlation is good. However, if we assume that the small scale oscillations are not periodic, then at longer forecast intervals, the lag correlation of these oscillations becomes low for the shorter averages. For this reason the curves eventually cross above the persistence curve. The small scale oscillations have been filtered out by the 3 to 5 min running averages. At these shorter forecast intervals, the RMSE comparison of these longer averages with persistence is not particularly good. At longer forecast intervals, the longer period oscillations are the dominant lag correlation factor. With the shorter oscillations filtered out by the longer averages, the comparison with persistence becomes relatively good and the curves eventually cross below persistence.

Another basic difference between the high and low variance curves is the greater slope through the first few minutes of the forecast interval and then a leveling off for the high variance cases. The low variance cases have a smaller slope and do not level off by the 10 min forecase interval. The slopes of the RMSE curves are a rough measure of the rate of dispersion. The slopes indicate that there is a fairly rapid dispersion rate for the high variance cases in the first few minutes and then a slower dispersion rate (possibly of the longer period waves) occurring later. The low variance cases indicate a slower dispersion rate with a slowly decreasing rate with time. These results agree well with what generally occurs for the unstable and stably boundary layer, respectively.

We would expect that the high variance persistence curves would have higher standard deviations when compared with the low variance curves. However, this is generally not true. The relatively small number of samples may be the explanation for this apparent discrepancy.

As mentioned in the introduction, Sparks and Keddie (1971) found that to predict a 300 m run of wind 10 min ahead, a 4 or 5 min average should be used. The author calculated the one sigma standard deviations on their results and found that the "dip" in their RMSE curve which indicated the 4 or 5 min mean gives the best forecast, did not look significant, since a straight line could be drawn within the standard deviation bars.

As a comparison with their results, the approach of Sparks and Keddie was used on an hour-long sample of a 30 m, fairly strong wind case chosen from our data. It was concluded that, at least for this one sample hour, the shortest averaging times (certainly less than 4 or 5 min) are the best predictors of this 300 m run of wind 10 min ahead in time. However, note that the results of Sparks and Keddie were based on 6 hours of data at the 10 m level and block averages taken. Our data were only an hour's sample at a 30 m level, but with running averages used. Also, their data contained a slightly higher average wind speed for their sample and what looked like a generally higher variation of wind speed than for our data sample.

Since this 300 m run of wind turns out to be about a 1/2 min average when we use Taylor's hypothesis, an outgrowth of the above study was a predictability condition on this 1/2 min mean wind. Drawing a graph of the RMSE values versus the forecast intervals, we conclude that persistence is the much better predictor of the 1/2 min mean wind for all forecast intervals for this sample hour.

2.2.6 CONCLUSIONS AND SUMMARY

Tables 2.2.2 and 2.2.3 show the significance of the data for the predictability conditions on the 2 min mean wind and azimuth using the t-test discussed previously. The tables are for the high and low variance cases respectively. We can say with 90% configence that the 1/2 or 1 min averages are better predictors than persistence of the 2 min averaged wind and azimuth 1 min ahead. The exception is the 91

and 152 m high variance azimuth where the confidence of the 1/2 min average drops below 90%. In general, the 1 min averaged wind and azimuth gives us slightly better confidence of prediction than the 1/2 min average. For the 30 m low variance wind, the 1/2 min average proved to be a better predictor of the 2 min mean wind 2 min ahead. However, with this one exception, the confidence drops greatly after the 1 min forecast interval. Therefore, from this study we conclude that after 1 min, persistence is the best predictor of the 2 min mean wind and azimuth at the three levels.

It has been found that there is little or no difference between wind and azimuth and between the levels with respect to the predictability conditions. As indicated in the previous section, although the variance criterion separated the stable and unstable atmospheric cases quite well, there again is little or no significant difference in the predictability conditions between the two cases, even though the RMSE curves appear quite different. For aviation applications the 2 min wind is optimum for predicting the winds a few minutes in advance.

TABLE 2.2.2

Accepted data from the t-test for the running average less than persistence at the 90% confidence level for the high variance case containing eight samples (cut-off at t = 1.415).

WIND

LEVEL (m)	FORECAST INTERVAL (min)	RUNNING AVE. (min)	t
30	1	1/2	2.527
	1	1	2.967
91	1	1/2	1.844
	1	1	2.609
152	1	1/2	1.727
	1	1	3.819

AZIMUTH

LEVEL (m)	FORECAST INTERVAL (min)	RUNNING AVE. (min)	t
30	1	1/2	3.537
	1	1	3.491
91	1	1	1.898
152	1	1	2.537

TABLE 2.2.3

Accepted data from the t-test for the running average less than persistence at the 90% confidence level for the low variance case containing 11 samples (cut-off at t = 1.372).

WIND

LEVEL (m)	FORECAST INTERVAL (min)	RUNNING AVE. (min)	t
30	1	1/2	2.736
	1	1	3.305
	2	1/2	1.543
91	1	1/2	2.477
	1	1	2.300
152	1	1/2	1.830
	1	1	2.119

AZIMUTH

LEVEL (m)	FORECAST INTERVAL (min)	RUNNING AVE. (min)	t
30	1	1/2	2.464
	1	1	2.795
91	1	1/2	2.105
	1	1	2.050
152	1	1/2	2.317
	1	1	2.340

REFERENCES (Chapter 2, Section 2)

Armendariz, M. and V. D. Lang, 1968: Wind correlation and variability in time and space. Atmos. Sci. Lab., White Sands Missile Range, New Mexico, Report ECOM-5201, 26p.

Businger, J. A., 1972: The atmospheric boundary layer. Remote Sensing of the Troposphere, WPL/ERL, Dept. of Engineering, C.U., Boulder, Colorado, Ch. 6.

Hooke, W. H., J. M. Young and D. W. Beran, 1972: Atmospheric waves observed in the planetary boundary layer using an acoustic sounder and a microbarograph array. Boundary Layer Meteorology, 2, D. Reidel Publishing Co., 371-380.

ICAO, 1967: Report of the Fifth Air Navigation Conf., Montreal, Nov. 14 - Dec. 15, Doc 8720, AN-CONF/5.

(References Continued) Chapter 2, Section 2

Ito, H., 1968: Time and space variation in meteorological elements in the aerodrome and its vicinity. Aeronautical Meteorology, WPL Tech. Note No. 95, 142-157.

Koren, O., 1972: Second Symposium on Meteorological Observations and Instrumentation. AMS, San Diego, Calif., March 27-30, 262-266.

Lawrence, R. S., 1972: Remote sensing by optical line-of-sight propagation. Remote Sensing of the Troposphere, WPL/ERL, Dept. of Engineering, C.U., Boulder, Colo., Ch. 25.

Rachele, H. and M. Armendariz, 1967: Surface wind sampling for unguided rocket impact prediction. J. Appl. Meteor., Vol. 6, 516-518.

Rijkoort, P. J. and J. Wieringa, 1968: Wind information for landing and take-off and siting of instruments. Aeronautical Meteorology, WMO Tech. Note No. 95, 135-166.

Singer, I. A. and M. E. Smith, 1953: Relation of gustiness to other meteorological parameters. J. of Meteor., Vol. 10, No. 2, 121-126.

Sparks, W. R. and B. Keddie, 1971: A note on the optimum averaging time of wind information for conventional aircraft landings. Meteorological Mag., Vol. 100, No. 1186, and 129-143.

Taylor, G. I., 1938: The spectrum of turbulence. Proc. Roy. Soc., A164, 476p.

Thompson, P. D., 1961: Numerical Weather Analysis and Prediction. The Macmillan Co., N.Y., 170p.

CHAPTER 3

A COMPARISON OF METHODS FOR THE REMOTE DETECTION OF WINDS IN THE AIRPORT ENVIRONMENT

3.1 FOREWORD AND SUMMARY

3.1.1 INTRODUCTION

In this Chapter a relative appraisal of several different methods of remotely detecting winds within the first 1 km of the earth's atmosphere is given. Each method selected for discussion represents a unique area of contemporary remote sensing research. For this reason, highly qualified individuals in each of the fields have been called upon to prepare a section relating to their particular expertise. The methods covered and the authors are as follows:

Section 3.2	Doppler Radar	R. G. Strauch (WPL)
3.3	Laser Radar	R. Schwiesow (WPL)
3.4	Laser-Eddy Correlations	V. E. Derr, R. E. Cupp, & N. A. Abshire (WPL)
3.5	Passive Pressure Sensors	T. Priestley (WPL)
3.6	Acoustic Angle of Arrival	A. Mahoney (WRE Australia)

Each of the following sections is purposely confined to a discussion of only one technique, with no attempt being made within it to judge the relative merits and future potential in relation to the overall field of remote wind sensing. Such a value judgment, while essential for planning, is difficult to make and may prove to have a rather short "shelf life." A breakthrough in either the basic theory or hardware technology can alter the entire picture, permitting a currently less desirable technique to become the apparent optimum.

With this caution in mind, Table 3.1 attempts to compare the eight different remote sensing techniques, on the basis of eight criteria chosen to reflect the desirability of a given system for the specific application of wind sensing at an airport. The purpose of the table is to summarize. It should not take precedence over the summary discussions presented in the following sections of this chapter, or the detailed presentations made in the remainder of this report. A brief explanation of the categories used in Table 3.1 follows.

Stage of Development. Given the goal of placing a wind sensing device into full operation at an airport with a minimum of delay, this category is of prime importance. The comments ranging from theory to prototype give an indication of the present phase of development for each device. A projected rate of future development is not attempted as this would depend on such unknown factors as the future interest and financial support that might become available.

Relative Cost. This category represents a subjective estimate of the relative cost to produce a prototype of each device. The comments are based on experience gained during the development phases and with similar types of equipment. The word "relative" should be emphasized as it is clear that the cost for any of the units would go down after they reach production.

Potential For Continuous, All-Weather Operation. Various factors affect the full-time operation of each of the techniques considered. For example, the microwave radar requires some form of tracer, either natural or artificial, which may not always be present; the laser on the other hand may not be able to operate during intense storms when the density of hydrometeors might severely attenuate the signal.

Availability of Tracer. This category is partially reflected in the above comments; however, there are important differences such as in the case of the acoustic technique. Acoustic tracers are abundant, but high background noise could affect the continuous operation capability.

Total Range. Here, an attempt is made to rate the systems on their ability to detect winds out to the range required for airport operation. A classification of "medium" indicates that the system should give winds to heights of 1 km.

Spatial or Range Resolution. A basic FAA requirement is to measure a wind profile, at 30 m increments, up to 1 km. Various range gating and scanning techniques are used to separate the winds at these height increments. The comments here simply reflect the ability of each device to achieve this goal.

Time or Velocity Resolution. Most of the techniques require that the returned signal be integrated for a certain period before providing a readout of the wind. Here, a classification of "medium" suggests something less than 1 min averaging times.

Accuracy. The accuracy of each method is dependent on several factors including the wavelength and speed of the carrier, the beamwidth, and the relationship between the velocity of the tracer and the wind. As most of the devices have not been fully tested, the comments given in the table are necessarily subjective and reflect only best estimates.

Acceptability. All of the systems mentioned in Table 3.1, except the passive pressure sensor, transmit an active wave into the medium to be interrogated. This category gives an indication of the potential hazard to personnel or the possible interference with other equipment that may result from these active waves.

TABLE 3.1

Relative Ratings for Remote Wind Sensing Techniques

Technique \ Category	Stage of Development	Relative Cost	Potential for Continual, all Weather Operation	Availability of Tracer	Total Range Potential	Spatial or Range Resolution	Time or Velocity Resolution	Accuracy	Acceptability
ACOUSTIC DOPPLER	Near Prototype	Low	Medium	High	Medium	Medium	Medium	Medium	High
ACOUSTIC ANGLE OF ARRIVAL	Experimental	Low	Medium	Medium	Low	Low	Low	Medium	High
MICROWAVE PULSED DOPPLER RADAR	Prototype	High	Low	Low	High	Medium	High	High	High
MICROWAVE CODED MODULATION RADAR	Early Experimental	High	Low	Medium	Medium	High	High	High	High
LASER DOPPLER	Early Experimental	Medium	Medium	Medium	Medium	High	High	High	Medium
LASER EDDY CORRELATION	Experimental	Medium	Medium	Medium	Medium	High	Medium	Medium	Medium
PASSIVE PRESSURE SENSING	Theory	Low	Medium	Medium	Medium	Low	Low	Low	High

3.1.2 MAJOR ADVANTAGES AND DISADVANTAGES

Further amplification and justification of the reasons for some of the ratings given in Table 3.1 is required. This section explains the reasoning and states the strong and weak points for each of the techniques considered:

Acoustic Doppler. The combination of low cost, high availability of tracers and advanced stages of development make this system the present leader of the field. This does not overlook the potentially serious shortcoming of only a moderate potential for continuous all-weather operation. It is expected that the high ambient background noise at an airport will cause intermittent loss of the signal. Provision has been made for this potential problem, and it is expected that aircraft noise during periods of heavy traffic will cause signal loss for only a few tens of seconds during each landing or takeoff. Sufficient valid data should be available during the intervening quiet periods to insure a good representation of the wind profile. A second potentially limiting condition may exist when strong surface winds are present. The solution to this problem is to isolate the receiver from the direct effects of turbulent eddies by burying and shielding the antenna-transducer system. Finally, it is anticipated that heavy rain impinging on the face of the antenna will be a limiting condition. The degree to which these factors affect the continuous operation of the system can only be determined by the extensive tests that are planned for the late phases of the project.

Acoustic Angle of Arrival. The relative simplicity of the equipment, reflected in the low relative cost, is the most favorable characteristic of this technique. It suffers in comparison with the acoustic Doppler technique because of its "low rating" in range potential, spatial and time resolution, and its early stage of development.

Microwave Pulsed Doppler Radar. The advanced stage of development of this sensor would make possible early installation of a prototype. The high cost factor should be considered a definite drawback for an operational system installed at a large number of airports. More critical, however, is the low rating under the category of availability of tracer, a factor that would severely limit its use on a continual basis.

Microwave Coded Modulation Radar. Tracer availability for this system can be considered somewhat better than for the pulsed radar, in that, it would have a higher sensitivity and therefore sometimes detect tracers in

the clean air as well as hydrometers. While this increased sensitivity may overcome the earlier objections to the use of a radar system, the cost factor is still high. A greater problem, in terms of achieving early operation, is the "early experimental" stage of development, moving the point at which a prototype might be available well into the future.

Laser Doppler. This system has the potential of becoming a very good wind sensing device. Its high accuracy and resolution should produce wind profiles of a quality that are somewhat better than would be required for aircraft operational use. This would imply that its real future may lie more in the areas of research where greater accuracy and resolution are essential. Alternatively, a less costly system may be developed for operational use.

Hardware development has advanced to the stage where experimental models have actually measured winds that compare well with those measured by standard instrumentation. Before a prototype is developed, however, it will be necessary to collect more information on the availability of tracers, to determine if continuous operation is feasible.

Laser Eddy Correlation. The characteristics of this system are similar to the laser Doppler technique. Because the method is dependent on a correlation of eddies, the accuracy and resolution may be less, but are still high enough for the application. Some very preliminary experimental results indicate that a CO_2 laser has successfully penetrated nearly 1 km through a cumulonimbus cloud. This is impressive and suggests that the all-weather potential of a Doppler or eddy correlation system using a CO_2 laser may be better than had been previously anticipated.

Passive Pressure Sensing. This is the most unique of the methods considered. Its very early stages of development suggests that there is still much to learn and that it is not ready for a large-scale development program. However, its simplicity and the possibility that it would measure winds best when strong shear is present should be considered when future developments are planned.

3.1.3 Combined Sensor Approach. The previous sections and Table 3.1 indicate that none of the systems considered have a high potential for continuous, all-weather operation. It is encouraging to note, however, that the conditions that limit one system (i.e. heavy rain may interfere with the acoustic Doppler) are exactly those under which another system would operate best. (Doppler radar would work well during heavy rain.) This same argument would hold true for a combined laser-radar sensor, where again dense hydrometers might limit the laser, but would provide the needed tracer for the radar.

If early tests indicate that a combined system approach is required to achieve continual operation, it should not prove difficult to add a second type of sensor to the present system of sensor-computer-display. This approach would significantly reduce the total cost of the final system by sharing the computer and display portions.

SECTION 3.2 SHORT RANGE RADAR FOR WIND MEASUREMENTS AT AN AIRPORT (by R. G. Strauch) submitted December 1972.

3.2.1 INTRODUCTION

The purpose of this report is to examine the potential capability of microwave Doppler radar to obtain wind field measurements in an airport environment under a wide variety of meteorological conditions. Low altitude wind profiles (up to 1 km altitude) are of particular interest. Microwave radar systems are examined and compared for their ability to obtain velocity measurements to a range of 5 km. Radar detection of hydrometeors, atmospheric particulates, and clear air turbulent structure are considered. A method of obtaining the wind field from radial Doppler velocity measurements of a single monostatic radar is described. Finally, conclusions regarding the microwave Doppler potential are summarized and recommendations based on these conclusions are made.

The meteorological radar equation, using the approximation of a Gaussian radar antenna pattern illuminating a volume of uniform reflectivity, is given by (Probert-Jones, 1962)

$$\overline{P}_r = \left(\frac{1}{512\pi^2 \ln 2}\right)\left(\frac{P_t\lambda^2 G_o^2\,\theta\phi\Delta\eta L^2}{r^2}\right) \qquad (3.2.1)$$

$\overline{P}_r$ is the power received (watts) from the scattering volume averaged over a large number of observations,

- P_t is the transmitted power (W),
- λ is the radar wavelength (m),
- G_o is the on-axis antenna gain,
- θ and ϕ are the horizontal and vertical beamwidths,
- Δ is the length (m) of the radar range resolution,
- r is the range (m) from the radar to the scattering region,
- η is the reflectivity (m^{-1}) of the scattering process, and
- L is the one-way transmission loss of the atmosphere.

In this report the attenuation factor will be neglected. Only short ranges are of interest, so the attenuation is not a principal consideration for this application, although the short wavelength radars will have significant attenuation in heavy rain.

The range of interest is taken to be 5 km. If a single monostatic radar is used to obtain wind field information, the velocity azimuth display scan (discussed in section 3) will enable wind profiles to be obtained to 1 km with an 11.5° elevation angle. A 150 m range resolution with an 11.5° elevation angle gives a height resolution of 30 m. 150-m range resolution is easily achieved by pulsed radars, and the radars now being developed for boundary layer studies have much greater resolution. The range resolution for a pulsed radar is given by

$$\Delta = c\tau/2 \qquad (3.2.2)$$

where c is the velocity of propagation and τ is the pulse width. The range resolution is dependent only on the bandwidth of the transmitted signal and is given by

$$\Delta = \frac{c}{2F} \qquad (3.2.3)$$

for an FM/CW radar where F is the frequency excursion,

$$\Delta = \frac{c}{2B} \qquad (3.2.4)$$

for a random noise radar, where B is the rf bandwidth, and

$$\Delta = \frac{c}{2f_c} \qquad (3.2.5)$$

for a digitally coded pseudorandom radar, where f_c is the digital clock rate.

Equation (3.2.1) can be used to evaluate the intensity of refractive index fluctuations from radar measurements using a relationship derived by Ottersten (1969a,b)

$$\eta = 0.38\, C_n^2 \lambda^{-1/3} \qquad (3.2.6)$$

where C_n^2, usually given in units of $cm^{-2/3}$, is the structure constant for the refractive index field. The radar detects refractive index irregularities at a spatial size of about $\lambda/2$ since these spatial sizes contribute additive phases in the backscatter to the receiver.

Scattering by particles small compared with λ (Rayleigh approximation) can be described using a reflectivity factor (Z) to characterize the scattering particles.

$$\eta = \frac{\pi^5 |K|^2}{\lambda^4} Z \qquad (3.2.7)$$

and

$$Z = \sum_{\substack{\text{Unit} \\ \text{Vol}}} D^6 \qquad (3.2.8)$$

where

$$K = \frac{m^2 - 1}{m^2 + 2} \qquad (3.2.9)$$

and m is the complex refractive index of the scatterers. D is the particle diameter, and Z is commonly expressed in mm^6/m^3. If the scatters are too large for the Rayleigh approximation, an equivalent reflectivity factor, Ze, can be used.

The sensitivity of a meteorological radar can be expressed as the minimum detectable reflectivity or reflectivity factor that the radar can detect at a given range and range resolution.

For particle scattering,

$$Z_{min} = \frac{512 \ln(2)}{\pi^3} \frac{\left(\overline{P}_r\right)_{min} \lambda^2}{P_t G_o^2 \theta \phi |K|^2 L^2} \frac{r^2}{\Delta} \qquad (3.2.10)$$

and for scattering from turbulent eddies,

$$\eta_{min} = \frac{512 \pi^2 \ln(2) \left(\overline{P}_r\right)_{min}}{P_t \lambda^2 G_o^2 \theta \phi L^2} \frac{r^2}{\Delta} . \qquad (3.2.11)$$

A microwave radar can measure wind fields if detectable scatterers that can be assumed to be moving with the wind are found in many radar resolution cells and the radar is capable of recovering Doppler velocity. Radial velocity data must be measured throughout a region of space if the wind field is to be recovered from a single monostatic radar. The most widely used microwave Doppler radar for meteorological applications utilizes the coherent pulsed technique. A CW radar measures a frequency shift from a single moving target given by

$$f_D = \frac{2 V_r}{\lambda} \qquad (3.2.12)$$

where f_D is the Doppler frequency (sec^{-1}) and V_r is the radial velocity (m/sec) of the target. The CW radar provides no range information. Measurements from meteorological (incoherent) scatterers show the velocity of the individual scatterers weighted by their reflectivity coefficient. This Doppler velocity spectrum contains information about the mean particle motion and the variability of the motion.

The pulsed Doppler radar maintains the phase coherence of a sinusoidal oscillator from pulse-to-pulse and is therefore able to sample the Doppler velocity at the radar repetition rate. The pulse Doppler radar has range resolution, Δ, equivalent to ordinary pulsed radars and a maximum unambiguous range given by

$$R_{max} = \frac{c T}{2} \qquad (3.2.13)$$

where T is the pulse repetition period. The maximum unambiguous velocity, determined by Equation (3.2.12) and the sampling theorem, is given by

$$V_{max} = \pm \frac{\lambda}{4 T} . \qquad (3.2.14)$$

Range and velocity can be obtained by other types of radar systems. The FM/CW radar can obtain velocity from point targets (Chadwick and Warner, 1971), but velocity data have not been obtained from distributed targets. The random noise radar has excellent range and velocity measurement capability (McGillem, et al., 1969) as does the pseudorandom coded radar (Reid, 1969). Various types of radars potentially suited for airport wind measurements will be discussed in Section 3.2.4.

3.2.2 RADAR REFLECTIVITY VALUES

Radar reflectivity values for meteorological scatterers can be computed from 3.2.6 if the structure constant is known or from 3.2.7 if the distribution of scattering sizes is known. Empirical values will be used whenever possible for this report.

3.2.2.1 Reflectivity Factor of Rain. The reflectivity factors of typical rainfall are summarized by Atlas (1964). An expression sufficient for use here is the Marshall-Palmer (1948) relationship,

$$Z\ (mm^6/m^3) = 200\ R^{1.6} , \qquad (3.2.15)$$

where R is the rainfall rate in mm/hour. Typical values of reflectivity are shown below:

	R	Z
mist	0.05	1.6
drizzle	0.25	21.7
light rain	1.0	200
moderate rain	4.0	1.8×10^3
heavy rain	16	1.7×10^4

3.2.2.2 Reflectivity Factors for Clouds and Fog. The reflectivity factor can be related to the total liquid water content as given by Atlas (1964)

$$Z = 0.048\ M^2 \qquad (3.2.16)$$

where M is the liquid water content in grams per m^3. Typical liquid water content for fogs range from 0.05

to 0.2 gm/m^3 and for clouds from 0.05 to 3 gm/m^3 (Mason, 1957). Thus, the reflectivity factor for fog is typically 10^{-4} to 10^{-3} mm^6/m^3 and the cloud reflectivity can vary from 10^{-4} to 10^{-0}. Advection fogs, using the results of Donaldson (1955), have higher reflectivities given by

$$Z = 8.2\,M^2 \qquad (3.2.17)$$

or typical values of 10^{-1} to 10^{-2} mm^6/m^3.

3.2.2.3 Uniform Water Drops. The reflectivity factor, ΣD^6, for uniform drops is simply

$$Z = ND^6 \qquad (3.2.18)$$

where N is the density of drops (m^{-3}), or equivalently,

$$Z = \frac{6\times10^3}{\pi} MD^3 \qquad (3.2.19)$$

for D in millimeters and M in gm/m^3 of liquid water. Values for 20, 40 and 80 micron drops are shown in Table 3.2.1

TABLE 3.2.1

Reflectivity of Uniform Droplets

D(microns)	$M(gm/m^3)$	$N(m^{-3})$	Zmm^6/m^3
20	10^{-3}	2.5×10^5	1.5×10^{-5}
"	10^{-4}	2.5×10^4	1.5×10^{-6}
"	10^{-5}	2.5×10^3	1.5×10^{-7}
40 μ	10^{-3}	3×10^4	1.22×10^{-4}
"	10^{-4}	3×10^3	1.22×10^{-5}
"	10^{-5}	3×10^2	1.22×10^{-6}
80 μ	10^{-3}	3.7×10^3	9.8×10^{-4}
"	10^{-4}	3.7×10^2	9.8×10^{-5}
"	10^{-5}	37	9.8×10^{-6}

3.2.2.4 Reflectivity Factor for Atmospheric Aerosols. The size and number distributions of aerosol particles varies widely in time and space. Observations by Junge (1964) led to a formulation

$$dn(r) = cr^{-v}\, d\log(r) \qquad (3.2.20)$$

or

$$N(r) = \frac{dn(r)}{dr} = 0.434\,cr^{-(v+1)} \qquad (3.2.21)$$

for naturally occurring aerosols. The constant, c, depends on the particle density, $v\approx3$ for typical aerosols, and dn(r) is the number of particles with radii between r and r+dr.

Using the results of a general survey (Bullrich, 1964),

$$\frac{d\,n(r)}{d\log(r)} = 10^7\ m^{-3}$$

$$\frac{d\,n(r)}{dr} = 4.34\times10^6\ r^{-(v+1)} \qquad (3.2.22)$$

$$= 4.34\times10^6\ r^4\,dr$$

for typical aerosols. Thus,

$$N(D) = \frac{d\,n(D)}{dD} = 3.47\times10^7\ D^{-4}\ . \qquad (3.2.23)$$

Since the reflectivity factor varies as the sixth power of the particle diameter, the few large particles will primarily determine Z.

Using 3.2.22 and 3.2.9,

$$Z = \int_{D_{min}}^{D_{max}} D^6\ N(D)\,dD$$

$$\approx 1.16\times10^7\ D^3_{max}\left(\text{microns}^6/m^3\right)$$

or $$1.16\times10^{-11}\ D^3_{max}\left(mm^6/m^3\right) \text{ for D in}$$

microns. This result was obtained by Mitchell (1966). Most measured values of aerosol distribution (Blifford, 1971) indicate the Junge distribution should be valid to at least 10 microns, giving a contribution to the reflectivity factor for aerosols of $Z\approx10^{-8}$ mm^6/m^3 for particles up to 10 microns in diameter. If the Junge distribution is valid up to particle sizes of 50 microns, then the reflectivity factor would be $\approx10^{-6}$ mm^6/m^3. The density and size distribution of "giant particles" greater than 10 microns in diameter is not well known and can also be expected to be highly variable.

3.2.2.5 Reflectivity Values for Refractive Index Fluctuations. The theory of clear air radar returns is summarized by Hardy (1972). Equation (3.2.6) relates the radar reflectivity, a measurable quantity, to the atmospheric fluctuations of refractive index. The refractivity, given by Bean and Dutton (1966), is

$$N = 77.6\,\frac{P}{T} + 3.73\times10^5\,\frac{e}{T^2} \qquad (3.2.24)$$

where $N = (n-1) \times 10^6$, n is the refractive index, T is the absolute temperature in degrees Kelvin, e is the partial pressure of water vapor (mb) and P is the total air pressure (mb). Temperature and water vapor fluctuations result in refractive index fluctuations which in turn give rise to radio wave scatter. The refractive index fluctuations are described by the structure constant through the relationship

$$\overline{\Delta n(r)^2} = \langle | n(x) - n(x+r) |^2 \rangle = C_n^2 r^{2/3} , \quad (3.2.25)$$

assumed to hold for the inertial subrange. $\overline{\Delta n(r)^2}$ is the mean square difference of refractive index between two points separated by a distance r.

Values calculated by Bean et al. (1971) from tower measurements indicate values of η using (3.2.24) and (3.2.6) of 0.7×10^{-13} to 1.1×10^{-15} (m^{-1}) during times when clear air echoes were received by a 10-cm FM/CW radar. Values of η computed from airborne refractometer measurements were compared with measured radar reflectivity values of the Wallops Island 10-cm radar by Kropfli et al. (1968). Values of 10^{-12} to 10^{-14} m^{-1} were measured. Radar reflectivity in moderate clear air turbulence for a 10-cm radar is estimated to be about 3×10^{-15} m^{-1} (Hardy, 1972). Since the values reported are those taken when clear air returns are measured by the radar, these values are probably typical of the maximum values expected.

3.2.3 WIND FIELD MEASUREMENTS FROM DOPPLER RADAR

As noted in the introduction, a single monostatic radar can only measure the radial component of the motion of the scatterers. Nevertheless, extensive information about the wind field can be deduced from single radar Doppler measurements.

3.2.3.1 Vertical Velocity. Many experiments have been performed with vertical looking pulsed Doppler radars in various meteorological conditions. The major problem in data interpretation has been the separation of vertical air motion from the particle fall velocity. If the size distribution of the particle scatterers is known, the fall velocity can be calculated and the vertical air motion can be deduced from the radar measurements. Alternatively, if the vertical air motion is known or is small, the size distribution of scatterers can be calculated. (Probert-Jones, 1960; Rogers and Pile, 1962; Caton, 1963, Rogers, 1966).

3.2.3.2 Horizontal Velocity. If there are detectable radar targets covering a wide area above the radar, the VAD (velocity azimuth display) can be employed. The VAD technique is illustrated in Figure 3.2.1. Examples of data for two different heights are shown. The h_1 trace indicates variability in the mean velocity measurement, and at h_2 a uniform wind is illustrated. Turbulent eddies smaller than the pulse volume will cause an increased variance of the Doppler spectrum which will increase the uncertainty (noise) in the measurement of the mean velocity.

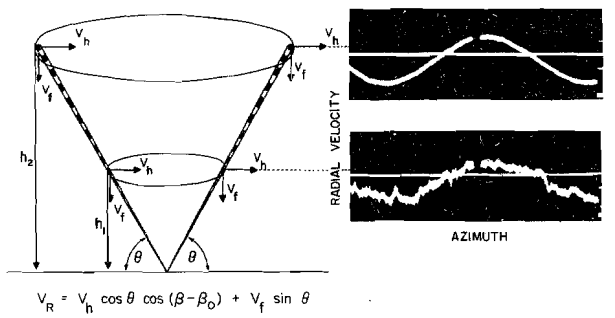

Figure 3.2.1 Velocity azimuth display (VAD) scanning for wind field measurements.

Other irregularities in the record will be caused by turbulent eddies large compared with the pulse volume, horizontal gradients of the mean wind, or horizontal gradients of the vertical velocity. The mean radial velocity is given by Lhermitte and Atlas (1961).

$$V_R = V_h \cos\theta \cos(\beta-\beta_o) + V_f \sin\theta \quad (3.2.26)$$

where

- V_R is the measured radial velocity
- V_h is the mean horizontal wind velocity
- θ is the elevation angle of the radar antenna
- β is the azimuth angle of the radar antenna
- β_o is the wind direction and
- V_f is the vertical velocity, fall velocity plus vertical air motion.

For a constant elevation angle, $V_R(\beta)$ consists of a sinusoidal term related to the horizontal wind and a dc term given by the vertical motion. The amplitude of the sinusoid determines the horizontal velocity and the phase determines the direction. There is, however, an ambiguity (Caton, 1963) in the vertical motion term when convergent or divergent wind fields are being scanned. A method of deducing the wind field from VAD records is given by Browning and Wexler (1968), using a Fourier analysis of the record to obtain the mean wind components, the horizontal divergence, and the stretching and shearing deformations. In addition, the variance of the velocity obtained in a VAD scan can be Fourier analyzed to obtain information about the turbulent energy and momentum fluxes (Wilson, 1970).

The VAD technique can obtain mean wind profiles in snow or rain with excellent velocity accuracy and resolution. The technique is applicable to any scanning radar capable of measuring range and Doppler velocity during a fixed elevation scan where targets are detected at all azimuth angles.

Multiple Doppler Radar. The wind measurement capability of Doppler radar can be increased if independent radial velocity measurements of the same scatterers can be made by several separated radars. Lhermitte (1968) introduced the concept to observe circulation in thunderstorms and Miller (1972), using computer analysis of data taken in snow with two 3-cm Doppler radars, showed the potential power of the multi-Doppler concept. Measurements of the total wind field have been obtained with dual Doppler radars at the Wave Propagation Laboratory at Boulder, Colorado. If the mean flow is removed from the horizontal wind field, the eddy flow field shown in Figure 3.2.2 is obtained. If the flow had been uniform, the eddy field would have been composed of random vectors indicative of the uncertainty of the mean velocity measurements. This data, obtained in snow, reveals the detailed structure of the wind field and illustrates the ability of Doppler radar to obtain accurate radial velocity measurements.

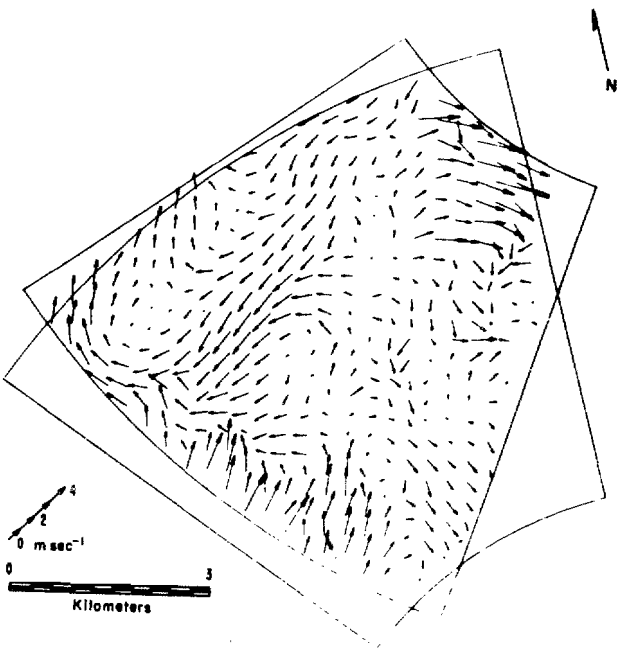

Figure 3.2.2 Eddy flow field of wind field obtained from Doppler wind measurements. The mean flow was from 14.8° at 5.5 m/sec.

3.2.4 RADAR SYSTEM FOR AIRPORT WIND MEASUREMENTS

A single microwave radar with Doppler capability, operating in a VAD scan, can measure velocity fields whenever detectable radar targets occur throughout the volume of space surrounding the radar. In this section, various possible types of radars are examined for their ability to detect targets up to a range of 5 km and measure their radial velocity. Existing radar systems and potential radar systems are discussed. At a range of 5 km, the VAD scan technique at 11.5° elevation gives a 1 km altitude. Reasonable estimates of the horizontal wind field can be made at this elevation angle. A 150-m range resolution results in a 30-m resolution. Vertical velocity measurements can be made at higher elevation angles, but with degraded altitude resolution.

3.2.4.1 Pulse Doppler Radar. Existing pulse Doppler radar systems have demonstrated their ability to measure wind fields whenever hydrometeor targets are present. The pulse Doppler method has also been used with artificial targets (chaff) in experiments at Haswell, Colorado, by the Wave Propagation Laboratory. Wind fields similar to those shown in Figure 3.2.2 have been obtained in preliminary data analysis. An ultra-sensitive 10-cm radar has also operated in a Doppler mode (Browning, 1972) and obtained measurements from clear air refractive index fluctuations. However, the systematic use of chaff at an airport is not considered in this report and the operational use of ultrasensitive radar at an airport is also not envisioned since these radars utilize large and costly components. Therefore, the pulse Doppler consideration is given to detection of natural particle scatterers using short wavelength radar.

The pulse Doppler radar measures the Doppler velocity by measuring the phase of the return signal from pulse-to-pulse. Data from 50 to 500 pulse samples are typically used to measure the Doppler spectrum. Signal dwell time, that is the length of time required to obtain the data, is about 0.25 sec. The Doppler velocity can be obtained in real time using either Fourier analysis or coherent filter methods. The velocity can be obtained for all range cells simultaneously, so that if detectable targets occur, the data required to measure a wind field can be obtained in less than 3 min.

Table 3.2.2 lists the parameter of three pulse Doppler radar systems. The 3.2-cm system parameters are approximately those of existing WPL Doppler radars, and the 8.6 mm and 3.2-mm systems are potential systems using parameters that could be achieved with the present technology. The maximum unambiguous velocities are not sufficient for all meteorological cases, but the ambiguity can be resolved using spatial continuity and ground measurements. The maximum range becomes troublesome when low angle scanning is used and the scatterers extend to large altitudes. Variable pulse repetition rate can be used to resolve the range ambiguity. (Several methods are potentially available to overcome the maximum range-maximum velocity product of $\pm c\lambda/8$ given by Equations 3.2.13 and 3.2.14. These methods are not presently in use but could be implemented if needed.)

The minimum detectable reflectivities are calculated

for a range of 5 km and a signal-to-noise ratio of 6 dB. Signal-to-noise ratio of the Doppler spectrum will be greater than this because the noise will be broadband and the Doppler signal narrowband. The values listed for minimum detectable signal are therefore very conservative and allow determination of the mean velocity to a fraction of the spectral width (Lhermitte and Miller, 1970).

TABLE 3.2.2

Pulse Doppler Radar Parameters

λ	3.2 cm	8.6 mm	3.2 mm
$\|K\|^2$	0.93	0.91	0.80
τ	10^{-6}sec	10^{-6}sec	10^{-6} sec
P_t	20 kW	5 kW	1 kW
Antenna Diameter	3 m	2 m	1 m
Noise Figure	6 dB	12 dB	18 dB
Unambiguous Range	77 km	20 km	10 km
Unambiguous Velocity	±15.7m/sec	±16.1m/sec	±12m/sec
Range Resolution	150 m	150 m	150 m
Velocity Resolution	0.06m/sec	0.1m/sec	0.3m/sec
$(Z_{min})^*$ (mm^6/m^3)	1.67×10^{-2}	3.93×10^{-3}	1.23×10^{-3}

* 5 km range
6 dB S/N ratio in time domain

3.2.4.2 The FM/CW Radar. The FM/CW radar has been utilized as a boundary layer probe for clear air returns (Richter, 1969; Bean et al., 1971). These radars operate at a wavelength of 10 cm and could also be used for particle scatterers. Strong radar returns from insects are reported by Bean et al. (1971). This radar utilizes separate transmitting and receiving antennas that require isolation to prevent receiver saturation. A scanning antenna system has been devised (Richter, 1972).

The Doppler velocity of isolated point targets can be measured, but implementation of Doppler capability for meteorological targets has not been achieved (Chadwick and Warner, 1971).

Figure 3.2.3 shows results of wind profiles obtained from clear air returns with an ultra-sensitive pulsed Doppler radar (Browning, 1972). A radar designed for boundary layer measurements, using CW transmission should also be able to obtain these profiles. Figure 3.2.4 shows an example of clear air returns obtained with an FM/CW radar. The radar returns are usually obtained in layers as shown in the figure. Signals returned from different ranges occur at different frequencies in the FM/CW radar. The data are analyzed

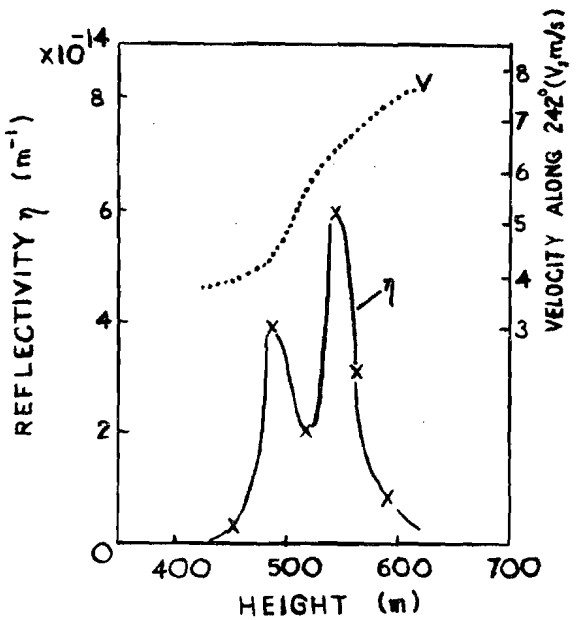

Figure 3.2.3 Velocity measurements of clear air returns using pulsed Doppler radar.

with a spectrum analyzer, with the signal return from each range resolution cell appear in a separate spectrum analyzer channel. Data for all channels is typically acquired and frequency analyzed in 100 msec. The parameters for an FM/CW radar that has operated on clear air return (Richter, 1969) are listed in Table 3.2.3.

A short wavelength FM/CW radar could provide high sensitivity for small particle scatterers. (Note that the wavelength dependence for scattering for Rayleigh particles is λ^{-4} whereas for refractive index scattering it is $\lambda^{-1/3}$.)

Table 3.2.4 lists the parameter for potential FM/CW radars operating at shorter wavelengths. The FM/CW radar requires a linear frequency sweep to obtain good range resolution, especially at longer ranges (Richter, 1972), and the linear frequency control of the shorter wavelength transmitters would present a problem. (Minimum detectable powers are based on the value given by Richter (1969) for the 10-cm FM/CW. The range resolution listed in Table 3.2.4 is much less than the FM/CW radar so the required excursion of the frequency sweep is much less. The sweep duration and the equivalent receiver bandwidth are assumed to be the same as the 10-cm radar.)

3.2.4.3 The Pseudorandom Coded Radar. The FM/CW radar is a sensitive radar for detecting small particles, but the extraction of Doppler velocity for

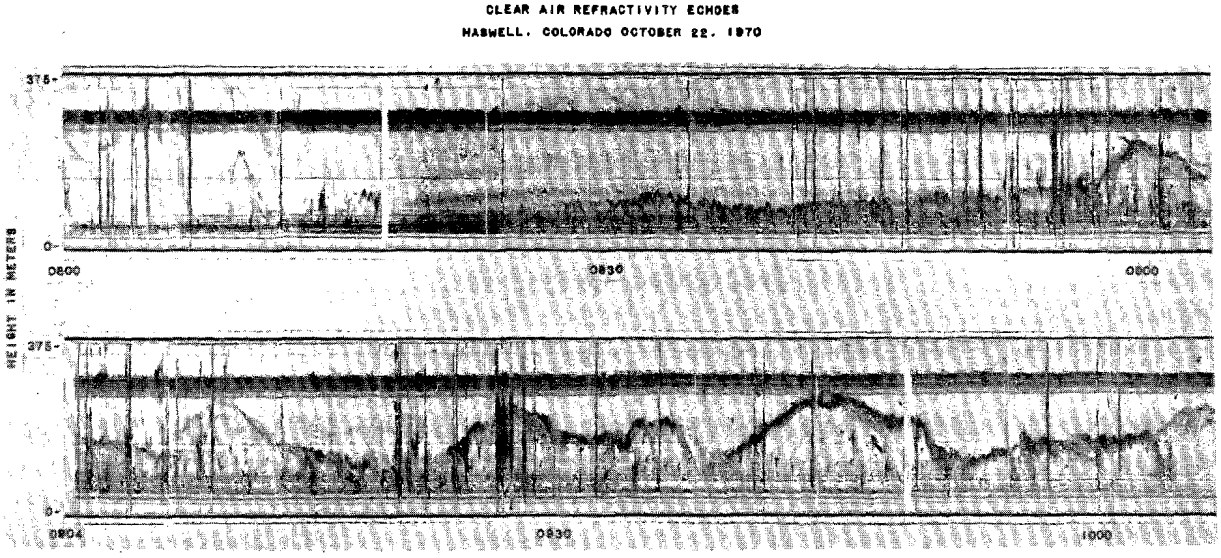

Figure 3.2.4 Radar record of clear air returns from FM/CW radar

TABLE 3.2.3

FM/CW Radar Parameters (Richter, 1969)

λ	$\approx$ 10cm (2.8-3.1 GHz)
P_t	= 150 W
Antenna Gain	= 35 dB
η_{min} at 1 km	= 4.2×10^{-15} cm^{-1}
$(P_r)_{min}$	= - 150 dBm
Sweep Duration	= 50 msec
Using Richter's value of η min for R=5 km and h=150 m, η min	= 7×10^{-14} m^{-1}
and using 1:7, Z_{min}	= 2.5×10^{-6} mm/m^6 .

TABLE 3.2.4

Potential FM/CW Radar

λ	3.2 cm	8.6 mm	3.2 mm
P_t	1 kW	1 kW	1 kW
Noise Figure	6 dB	12 dB	18 dB
$(\overline{P}r)$ min	-142 dBm	-136 dBm	-130 dBm
Δ	150 m	150 m	150 m
Antenna Diameter	1 m	1 m	1 m
Z_{min}*	2.8×10^{-4}	5.9×10^{-6}	5×10^{-7}

*S/N = 6 dB r = 5 km

distributed targets may prove to be a formidable task. The pseudorandom coded radar (Reid, 1969) can provide the Doppler information easily, but at the expense of utilizing a correlation receiver that does not lend itself to rapid scanning. The pseudorandom coded radar transmits a phase-modulated CW signal and therefore requires separate transmitting and receiving antennas. The phase modulation is coded and the time delay required to correlate a stored sample of the code with the received signal determines the range.

The code is generated digitally and versatile codes can be used to match the range and velocity requirements. The maximum unambiguous range is determined by the time required for the code to repeat; it is given by

$$R_{max} = \frac{cN}{2f_c} \qquad (3.2.27)$$

where N is the bit length of the code, and f_c is the digital clock frequency. The maximum unambiguous velocity is determined by the code rate and the sampling theorem and is given by

$$V_{max} = \pm \frac{\lambda f_c}{4N} \quad . \qquad (3.2.28)$$

The range resolution, determined by the bit length, is $\frac{c}{2f_c}$. Although $(V_{max})(R_{max}) = \pm \frac{c\lambda}{8}$ as in the pulsed Doppler, the advantage of the pseudorandom coded radar lies in the high average power transmitted, the ease with which very good range resolution can be obtained and the versatility of the trade-off between V_{max} and R_{max}.

Table 3.2.5 uses Reid's data and extends it to 150 m range resolution. A 8.6 mm pseudorandom radar has been constructed and first results are now being reported (Pasqualucci, 1972).

TABLE 3.2.5

Pseudorandom Radar*

λ	3 cm	8.6 mm	3.2 mm
Antenna Diameter	1 m	1 m	1 m
P_t	1 kW	1 kW	1 kW
Noise Figure	8 dB	14 dB	17 dB
Δ	49 m	15 m	5.9 m
Z_{min}	1.73×10^{-1}	1.57×10^{-2}	1.52×10^{-3}
R_{max}	50 km	15 km	6 km
V_{max}	20 m/sec	20 m/sec	20 m/sec
Velocity Resolution	0.06 m/sec	0.1 m/sec	0.3 m/sec

where Z_{min} is for 5 km range and the range resolution given. If the range resolution is extended to 150 m, the corresponding values of Z will be (keeping the same bandwidth):

(Z_{min})	5.6×10^{-2}	1.57×10^{-3}	5.9×10^{-5}

5 km range

150 m range resolution

*Reid, 1969

3.2.5 CONCLUSIONS

Figure 3.2.5 summarizes the potential of microwave radar for detecting atmospheric scatter for wind measurements at short range. The figure shows the present and potential capability of radar to detect particle scatters and clear air refractive index fluctuations.

There exists at present, with pulse Doppler radar, the technology for wind profile measurements in most conditions of poor visibility. Existing 3-cm radars, using the VAD method, could obtain wind profiles with precipitation targets in real time with 50 m altitude resolution and 0.25 m/sec velocity resolution. An 8.6-mm pulse Doppler radar could be built that would extend the measurement capability to include fog and clouds. Shorter wavelength pulse Doppler radars do not offer significant sensitivity increases with the present status of millimeter wave technology.

Clear air scattering from aerosol particles is clearly beyond the capability of microwave radar. Under some clear air conditions, the 10-cm ultrasensitive radar and 10-cm FM/CW radar can detect clear air refractive index fluctuations. The wind profile can be measured at the altitudes where the refractive index fluctuations are detected by the radar. Although the FM/CW radar has not been used to measure velocity and the ultrasensitive radar is not envisioned for operational uses, Doppler measurement of refractive index fluctuations is potentially available from the pseudorandom radar. The 10-cm pseudorandom radar could also operate in precipitation. The FM/CW radar has already proved its capability in clear air studies, and if Doppler velocity can be obtained it would be a versatile boundary layer radar.

An interesting possibility is raised regarding the use of large particles or droplets as radar tracers near an airport. A short wavelength FM/CW radar should detect relatively few 20 to 80 micron diameter water droplets per cubic meter. Little information is available on the size distribution and density of these types of particles, especially at airports near industrial complexes, or near the ocean. This information needs to be determined if a short wavelength CW radar is to be considered.

Although the wind profile can presently be obtained using microwave radar for only a relatively small fraction of the total time, the cases included are important and are not available from other remote sensors.

Two points raised in this report are recommended for further investigation:

1) A 10-cm FM/CW radar should be operated at an airport to determine if sufficient clear air return cases exist to warrant developing a 10-cm boundary layer radar with Doppler capability. The detection of clear air fluctuations induced by jet aircraft should be investigated. The FM/CW radar should be utilized with long integration to determine if clear air scattering can be detected between the radar and the typically observed layers.

2) The natural distribution of liquid droplets in an airport environment should be determined for droplet diameters of 10 to 1000 microns. This will readily determine if short wavelength radar can be envisioned for this application.

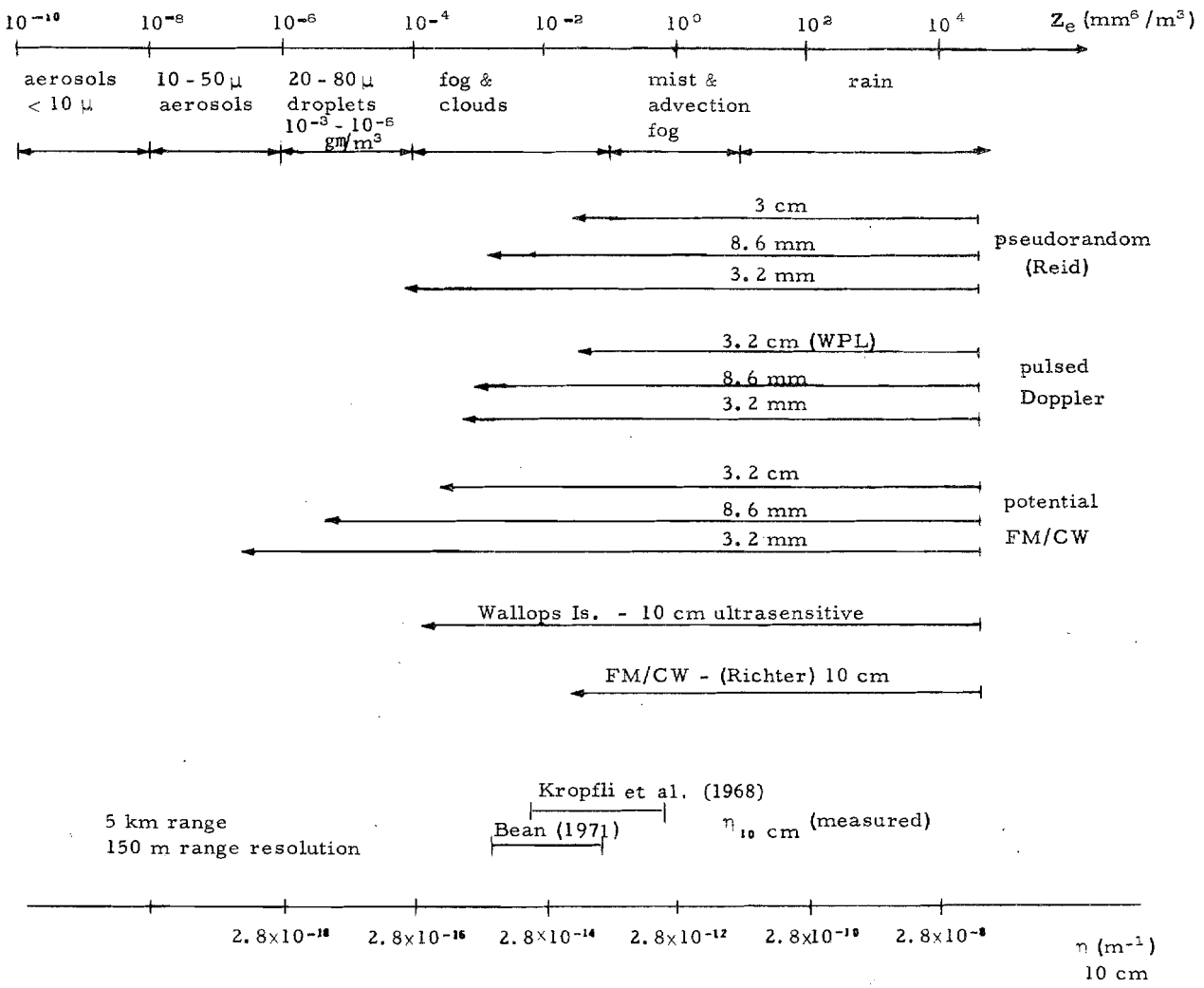

Figure 3.2.5 Radar reflectivity factors and minimum detectable values for existing and potential radar.

REFERENCES (Chapter 3, Section 2)

Atlas, D. (1964), Advances in radar meteorology, Advan. Geophys., 10, 317-478.

Bean, B. and E. Dutton (1966), Radio Meteorology, New York: Dover.

Bean, B., R. McGavin, R. Chadwick, and B. Warner (1971), Preliminary results of utilizing the FM radar as a boundary layer probe, Boundary Layer Meteorol. 1, 466-473.

Blifford, I. (1971), Global aerosol models - NCAR Tech. Note - NCAR - TN/PROC 68.

Browning, K. A. (1972), Atmosphere research using the Defford radar facility, Weather 27, No. 1, pp 1-66.

Browning, K. A. and R. Wexler (1968), A determination of kinematic properties of a wind field using Doppler radar, J. Appl. Meteorol. 7, 105-113.

Bullrich, K. (1964), Scattered radiation in the atmosphere and the natural aerosol, Advan. Geophys., 10, 99-260.

Caton, P.G.F. (1963), The measurement of wind and convergence by Doppler radar, Proc. 10th Weather Radar Conf., Boston, Am. Meteorol. Soc., 190-196.

Chadwick, R. and B. Warner (1971), Frequency modulated continuous-wave radar, NOAA Tech. Report, ERL-227-WPL-20.

Donaldson, R. (1955), Drop-size distribution, liquid water content, optical transmission, and radar reflectivity in fog and drizzle, Proc. 5th Weather Radar Conf., Asbury Park, N. J., 275-280.

REFERENCES (Continued) Chapter 3, Section 2

Hardy, K. (1972), Studies of the clear atmosphere using high power radar, Remote Sensing of the Troposphere, NOAA/Univ. of Colo.

Junge, C. (1964), Air Chemistry and Radio Activity, New York: Academic Press.

Kropfli, R. A., I. Katz, T. G. Konrad, and E. B. E. B. Dobson (1968), Simultaneous radar reflectivity measurements and refractive index spectra in the clear atmosphere, Radio Sci., 3, 991-994.

Lhermitte, R. M. (1968), Atmospheric probing by Doppler radar, Proc. Tech. Sessions Remote Atmospheric Probing Panel of the Natl. Acad. Sci. Committee on Atmospheric Science (NAS-CAS), Chicago, 253-285.

Lhermitte, R. M. and D. Atlas (1961), Precipitation motion by pulse Doppler radar, Proc. 9th Weather Radar Conf., Boston, Am. Meteorol. Soc., 218-223.

Lhermitte, R. M. and L. J. Miller (1970), Doppler radar methodology for the observation of convective storms, Preprints 14th Radar Meteorol., Conf., Boston, Am. Meteorol. Soc., 133-138.

Marshall, J. and W. Palmer (1948), The distribution of raindrops with size, J. Meteorol. 5 (4), 165-166.

Mason, B. J. (1957), The Physics of Clouds, New York, Oxford.

McGillen, C. D., G. R. Cooper and W. B. Waltman (1969), Use of wideband stochastic signals for measuring range and velocity EASCON Record, IEEE Electronics and Aerospace Convention, 305-311.

Miller, L. J. (1972), Dual Doppler radar observations of circulation in snow conditions, Preprints 15th Radar Meteorology Conf., Champaign-Urbana, Am. Met. Soc. 309-314.

Mitchell, R. (1966), Radar meteorology at millimeter wavelengths, Air Force Report, SSD-TR-66-117.

Ottersten, H. (1969), Atmospheric structure and radar backscattering in clear air, Radio Sci., 4, 1179-1193.

Ottersten, H. (1969), Radar backscattering from the turbulent clear atmosphere,Radio Sci., 4, 1251-1255.

Pasqualucci, F. (1972), Measurements of drop size distribution using a 35 GHz radar, Preprints 15th Radar Meteorol. Conf., Champaign-Urbana, Am. Met. Soc., 309-314.

Probert-Jones, P. R. (1960), The analysis of Doppler radar echoes from precipitation, Proc. 8th Weather Radar Conf., Boston, Am. Meteorol. Soc., 377-385.

Probert-Jones, P. R. (1962), The radar equation in meteorology, Quart. J. Roy. Meteorol. Soc. 88, 485-495.

Reid, M. (1969), A millimeter wave pseudorandom coded meteorological radar, IEEE Trans. Geosci. Elec. 7, (3), 146-156.

Richter, J. H. (1969), High resolution tropospheric radar sounding, Radio Sci. 4, (12), 1261-1268.

Richter, J. H. (1972), New developments in FM-CW radar sounding, Boundary Layer Meteorology (to be published).

Rogers, R. R. and R. J. Pilie (1962), Radar measurements of drop size distribution, J. Atmos. Sci. 19, 503-506.

Rogers, R. R. (1966), Doppler radar investigation of Hawaiian rain, Proc. 12th Weather Radar Conf., Boston, Am. Meteorol. Soc., 128-134.

Wilson, D. A. (1970), Doppler radar studies of boundary layer wind profile and turbulence in snow conditions, Preprints 14th Radar Meteorol. Conf., Boston, Am. Meteorol. Soc., 191-196.

SECTION 3.3 WIND PROFILES BY LASER SCATTERING
(by Ronald L. Schwiesow)
submitted December 1972

3.3.1 INTRODUCTION

Natural aerosols in the atmosphere serve as flow markers for laser scattering wind measurement techniques. The velocity of the particulates is actually measured, but for small particles the aerosol velocity is identical to the wind velocity. Although flow velocities in artificially seeded laboratory flows have been measured by laser scattering techniques for some time (for example see Yeh and Cummins, 1964), the application of optical techniques to atmospheric wind measurement at long ranges (10 to 1000 m) is a comparatively new research field.

It is the purpose of this report to analyze in comparative terms the various types of laser scattering wind measurement systems that are useful for remotely determining wind shear. Researchers at FAA are undoubtedly aware of the NASA, Huntsville work on CO_2 homodyne systems (Lawrence et al., 1972, Huffaker 1970) and studies on two beam interference fringe systems at the Air Force Arnold Engineering Development Center (Farmer and Brayton, 1971) and in England (Bourke and Brown, 1971). Valuable long range work is also being done in Italy under Fiocco's direction (Benedetti-Michelangeli et al., 1972). We will not attempt to treat all the literature related to the problem, but instead cite representative publication which illustrate various aspects of laser Doppler wind velocity measurements.

In particular, our analysis is designed to treat the various types of Doppler techniques in a unified, fundamental fashion so that the suitability of the measurement methods to the wind shear problem can be intelligently assessed. While we will present conclusions and recommendations, we have no particular system to promote and can discuss the various techniques fairly objectively. Only qualitative comments of the signal-to-noise of the various Doppler methods can be made at this stage of knowledge. Various authors have come to widely different numerical conclusions (compare for example Owens (1969) and Farmer and Brayton (1971)) simply because Doppler system parameters are not yet well enough understood. The demonstrated performance of practical systems provides one useful form of comparison.

We will first discuss basic principles common to all laser scattering velocity measurement techniques, and then apply these principles to various operational implementations of the methods for wind shear determination. The possible practical systems can then be compared to nonoptical wind sensing techniques. Comparison between practical systems is possible by considering some experimental results of laser wind velocity sensors. We conclude by mentioning various unsolved research problems and some tentative conclusions and recommendations.

3.3.2 LASER SCATTERING FUNDAMENTALS

3.3.2.1 Doppler frequency shifts. Aerosol velocities in the troposphere are small with respect to the speed of light so that we may neglect relativistic Doppler effects and apply the classical formalisms. The wave vector of the incident and scattered light has the propagation direction, and has a magnitude given by

$$|\vec{k}| = 2\pi\nu/c = 2\pi/\lambda = 2\pi\tilde{\nu} \qquad (3.3.1)$$

where ν is the optical frequency, λ the optical wavelength in vacuum, $\tilde{\nu}$ the optical wave number in vacuum (approximately 6×10^{14}Hz, 0.50 μm and 20,000 cm^{-1} respectively for green light), and c is the speed of light. If the propagation medium is not a vacuum, but has a refrective index n, c is replaced by c/n in the above expression. Let the scatterer move with velocity $\vec{v}$. Considering the shift of the incident radiation ($\vec{k}_o$) with respect to the scatterer and of the scattered radiation ($\vec{k}_s$) with respect to a stationary detector, the Doppler frequency shift is

$$\Delta\nu_D = \nu_s - \nu_o = (n/2\pi)\vec{v}\,(\vec{k}_s - \vec{k}_o) \quad . \qquad (3.3.2)$$

In particular, for the case of backscatter $\vec{k}_o = -\vec{k}_s$ and $\Delta\nu_D$ is negative for velocity components away from the detector. As an example of typical frequency shifts, a velocity of 1 m/sec along the laser beam for green light in backscatter results in a shift of 4 MHz.

These Doppler shifted optical signals may be detected directly by high resolution (Fabry-Perot interferometric) spectroscopy. This detection method is incoherent in the sense that the measured frequency is not affected by atmospheric-induced phase fluctuations. Coherent heterodyne or homodyne detection,

where two optical signals are mixed in a nonlinear detector to produce the difference frequency, is also possible. Either the scattered signal may be mixed with an optical local oscillator at the detector, or the scattered signals from a single scatterer at the intersection of two illuminating beams may interfere with each other at the detector to produce beat frequencies after both scattered signals have returned along the same atmospheric-optical path.

Incoherent detection methods favor shorter wavelengths, say 0.515 μm, over 10.6 μm, simply because the required optical elements are smaller. For local oscillator coherent detection, atmospheric-induced phase fluctuations on the return beam become an overriding factor and longer wavelengths should result in a stronger heterodyne signal (better signal to noise) because atmospheric refractive index fluctuations are much weaker in the 10.6 μm spectral region. The two illuminating beam or two (collinear) scattered beam system (sometimes called differential Doppler) is less susceptible to phase fluctuations than the local oscillator method since both scattered beams are acted on by the same elements of the atmosphere. For **differential** Doppler coherent detection, shorter wavelengths are preferred for compact apparatus and for sensitive, low-noise detectors.

3.3.2.2 Aerosol scattering intensity. For the scattering of optical radiation by dielectric particulates, Mie scattering theory is useful. The scattering formulations are usually in terms of a size parameter α where

$$\alpha = 2\pi a/\lambda = 2\pi a\tilde{\nu} \quad . \qquad (3.3.3)$$

Wavelength λ is the optical radiation wavelength as before and a is the radius of the scattering particle. Particle radius a for real aerosols varies widely, but typical aerosols are in the range 0.1 to 10 μm. A Junge distribution of particle sizes in the form

$$f(r) = \frac{dn}{dr} = cr^{-(j+1)} \qquad (3.3.4)$$

with j in the range 2.2 to 4.0 is representative of natural silicate aerosols in some instances. The number of particles with radii between r and r plus dr is given by dn to within the constant scaling coefficient c. The important point is that smaller particulates greatly outnumber the larger, so that the choice of an optimum wavelength for maximum scatter is influenced principally by the smaller particulates of radius 1.0 μm or less.

Calculations of the absolute scattered return from an idealized atmosphere are not particularly useful and, in fact, may be responsible for some of the divergent systems analyses published from time to time. Measurements discussed later are more reliable. Useful comparative results come from the Mie theory, however. Scattered intensity at a fixed angle increases strongly with α, with approximately an α^4 dependence for small α. The intensity reaches a maximum at $\alpha \approx 1$. For larger α the scattered intensity function $I(\alpha)$ exhibits a long series of irregular maxima and minima oscillating about a value typically one half that of the peak intensity $I(1)$. The angular dependence of the scattered intensity also depends on α. At $\alpha \approx 0.01$ forward and backward scatter are approximately equal, with weaker scatter at right angles to the incident beam similar to a classical dipole radiation pattern At $\alpha \approx 1.0$, forward scatter for typical dielectric spheres is almost two orders of magnitude stronger than backscatter. As α increases further, the forward scattering maximum breaks into a number of smaller subsidiary maxima. In terms of an extinction cross section, diffraction effects cause the extinction (scattering plus absorption) cross section of a large α, opaque particle to be twice its geometrical cross section, while the extinction cross section of a small α particle may be many times the geometrical cross section.

We conclude that for maximum total scattered intensity based on the assumption of a Junge size distribution over the range 0.1 to 10 μm, $2\pi a\tilde{\nu} \gtrsim 1$; or setting $a \approx 0.1$ for the larger number of particles

$$\tilde{\nu} \gtrsim 16{,}000 \text{ cm}^{-1}. \qquad (3.3.5a)$$

That is, light in the visible region is likely to be scattered much more strongly than light in the near or middle infrared for the assumed aerosol size distribution. This distribution is more typical of a nominally clear or slightly hazy atmosphere than it is of a foggy or misty situation. Forward scatter will be strongest, backscatter less strong by approximately an order of magnitude and the scattered light at right angles to the incident beam will be at least two orders of magnitude weaker than forward scatter.

For a backscatter system, the conclusion (3.3.5a) is not as obvious. Although maximum scatter occurs for $\alpha \gtrsim 1$, maximum backscatter favors smaller size parameters because of the higher back-to-front scatter ratio at small α. Quantitative estimates for best α for various atmospheric conditions will depend on future experimentarion. It may be that for backscatter,

$$\tilde{\nu} \lesssim 16{,}000 \text{ cm}^{-1} \qquad (3.3.5b)$$

is a better working criteria than (3.2.5a). This would favor powerful infrared lasers.

3.3.2.3 Two beam interference. Two coherent intersecting laser beams will interfere in their common intersection volume. One can show (Auth, 1970) that the intensity distribution in the intersection region is

$$I(\vec{r}) = 2A^2(1 + \cos(\Delta\vec{k}\cdot\vec{r})) \qquad (3.3.6)$$

where $\Delta\vec{k} = \vec{k}_2 - \vec{k}_1$, the vector difference of the two incident wavevectors, A is the wave amplitude of each of the beams, and $\vec{r}$ is a general position vector. That is, if the two beams intersect at some angle 2θ, the interference fringes will be planes parallel to the beam angle bisector and perpendicular to the plane containing the beams. Since $|\Delta\vec{k}| = 2k\sin\theta$ for $|\vec{k}_1| = |\vec{k}_2|$, the perpendicular spacing between the planes will be

$$d = 2\pi/2k\sin\theta = (2\tilde{\nu}\sin\theta)^{-1} \qquad (3.3.7)$$

where θ is the half angle between the beams.

Consider a scattering particle traversing the intersection region perpendicular to the planes of maximum (interference) intensity. Light scattered from both beams is observed along the bisector of the incident beams, in the plane of the intersection. From a vector diagram appropriate to the figure, setting $|k_1| = k_o = |k_2|$ and recalling $k_o = 2\pi\tilde{\nu}_o$, it is clear that

$$\vec{v} \cdot (\vec{k}_s - \vec{k}_1) = (-1)\vec{v} \cdot (\vec{k}_s - \vec{k}_2) = vk_o \sin \theta. \quad (3.3.8)$$

Setting the atmospheric refractive index n equal to 1, the Doppler shift frequencies from Equation 3.3.2 are

$$\Delta\nu_{D1} = v\tilde{\nu}_o \sin \theta; \quad \Delta\nu_{D2} = -v\tilde{\nu}_o \sin \theta. \quad (3.3.9)$$

Because of the spatial variation in intensity (interference fringes), the return signals are intensity modulated as well as Doppler shifted. From Equation 3.3.7, the modulation frequency for the postulated geometry is

$$F = v/d = 2v\tilde{\nu}_o \sin \theta. \quad (3.3.10)$$

If one observes at a detector the heterodyne differential Doppler beat frequency of Equation 3.3.9, these Doppler beats are equal to the fringe intensity modulation frequency for this special geometry.

If the particle velocity makes some ϕ with the incident beam bisector, it can be shown that the generalized form of Equation 3.3.9 is

$$\Delta\nu_{D1} = 2v\tilde{\nu}_o \cos \theta/2 \cos (\phi - \theta/2) \quad (3.3.11)$$
$$\Delta\nu_{D1} = 2v\tilde{\nu}_o \cos \theta/2 \cos (\phi + \theta/2),$$

which gives rise to beat frequencies

$$\Delta\nu_{D1} - \Delta\nu_{D2} = 2v\tilde{\nu}_o \sin \phi \sin \theta \quad (3.3.12)$$

These expressions reduce to the previous results for $\phi = \pi/2$. For the single beam backscatter case, $\theta = 0$ and Equation 3.3.11 reduces to an alternative expression of Equation 3.3.2 for the backscatter case.

Of course in addition to the beat frequencies mentioned here, the strong optical fundamental at $\nu_D + \Delta\nu_1$ and $\nu_D + \Delta\nu_2$ can be observed directly at the detector by the Fabry-Perot (incoherent) detection technique. A local oscillator mixed with each return beam is also a possible alternative configuration.

3.3.3 OPERATIONAL IMPLEMENTATION

3.3.3.1 Wind Shear Measurement Limitations. For the measurement of wind shear at airports, we assume that the desired information is a vertical profile of wind velocity (speed and direction) essentially continuous in time. Wind velocity information along, or slightly offset from, the glide path would be even more desirable. Wind components in a plane perpendicular to the vertical profiling direction are most important, with components along the probing beam also useful if additional cost and complexity are not too great.

From the geometry of the situation it is obvious that some sort of a backscatter or single-ended laser scattering system is required. Laser Doppler systems using forward scatter require detectors out along the path, which is an impossible configuration for the airport wind shear problem. The low intensity of right angle scattering was mentioned in a previous section. Because the system is restricted to backscatter, higher optical frequencies in the visible or near visible region are more likely to give a useful scattering intensity for natural aerosols (see Equation 3.3.5). Although the visible vs. infrared signal-to-noise tradeoff has not yet been resolved.

The range of a useful wind shear measurement system should cover distances from 10 to approximately 1000 m. A 10 m range resolution element is assumed adequate for the desired system, although for some special purposes a two or three times finer resolution would be beneficial. If one uses a pulsed optical lidar (laser radar) system, pulses 60 nsec long correspond to a 10 m range resolution. For an AM-FM-CW system (discussed later), a 10 m range resolution requires a 15 MHz modulation sweep.

3.3.3.2 Safety Considerations. With lidar systems, the question of laser eye safety must be considered. A useful operational technique, used by NASA and others, is to mount an inexpensive, narrow beam radar on the laser transmitter. The radar may be very low power and need not even be range gated. When a target enters the radar beam pattern, which is wider than the laser transmitter beamwidth, the laser system is automatically shuttered. A redundant radar system assures reliability. Proper orientation of the wind shear lidar system with the airport traffic pattern will limit the percentage of time the laser needs to be shuttered.

An alternative safety approach is to use infrared (say CO_2 at 10.6 μm wavelength) lasers, which operate in a spectral region where the eye is opaque. Safe power thresholds are at least 10 times higher for IR lasers compared to visible, and may be as much as 10^2 or 10^7 times higher with further research.

3.3.3.3 Possible Systems. A direct approach to wind velocity determination by optical Doppler techniques is to use the optical analog of existing three-axis acoustic Doppler sensors. The purely longitudinal component of the wind is measured in direct or near backscatter as discussed with Equation 3.3.2. The apparatus would take the form of a single, vertically pointing laser beam with three spatially separated receivers. One receiver could be collocated with the transmitter and measure only the vertical wind component. The other two receivers would look upward at an angle toward the transmitted beam. Ranging along the beam requires the mechanical or optical angular scan of the two separated receivers. Three separate ground locations are required for this system, as for acoustic and microwave Doppler wind measurements.

The longitudinal Doppler shift can be measured by several methods. Lawrence et al. (1972) use an optical homodyne method where the laser transmitter is used as a sensitive preamplifier and mixer element, with the homodyne beat frequency measured on the laser

output itself. This requires a laser at each of the three ground locations. Alternatively, the Doppler shifted optical frequencies may be measured directly by high resolution spectroscopy, as has been done by Benedetti-Michelangeli et al. (1972). This technique is probably the most direct and simple. The laser carrier may also be modulated at microwave frequencies. Each microwave modulated pulse is then handled as in the case of Doppler radar (see Section 3.2). Essentially this system is identical to Doppler radar except that an optical carrier is used. Three transmitters are needed, as in the case of the homodyne system.

A velocity measurement using the differential Doppler technique (discussed previously) is uniquely suited to optical frequencies. Operationally, the system could take the form of a single-point ground-based unit. The laser source is split into three transmitted beams located around a 1.2 m diameter circle with the receiving telescope centered in the circle. A 2 mrad beam intersection angle (θ = 1 mrad in Equation 3.3.12) has been useful in field trials (Bourke and Brown, 1971) and is consistent at 500 m with the 1.2 m circular transmitter spacing. Full beam intersection over the 10 to 1000 m range requires angular scanning of the transmitter mirrors. For this close transmitter spacing, accurate ranging demands some sort of pulse time of flight or FM-CW gating.

Differential Doppler without range gating is possible, with a slight degradation in range resolution beyond 500 m, by separating the transmitter elements by 5 m. A single laser may be split into three beams with a mutual separation of 5 m, and with a beam full width at 1/2 intensity of 0.1 mrad by the use of suitable beam expanders. Range is determined by the mutual beam intersection volume, which typically has a height of less than 10 m at a range of 500 m. Scanning the range is accomplished by coupled angle scanning of the transmitted beams. Only one collecting telescope is required by the system.

This kind of differential Doppler geometry may be used with either visible or infrared lasers. Sufficient velocity accuracy for transverse wind components requires a coherent frequency measuring system.

3.3.4 COMPARISON WITH OTHER WIND SHEAR SENSORS

A precise, quantitative comparison of laser Doppler with acoustic Doppler, Doppler radar, passive infrasound, cross beam correlation, or other methods is not possible, given the present state of experimental knowledge. The host of unsupported assumptions needed for a numerical comparison makes the effort an exercise in algebraic virtuosity rather than a demonstration of useful results. Some very useful qualitative comparisons are possible. In addition, experimental results already obtained allow extrapolation for the performance of proposed systems.

A principal difference between optical Doppler and acoustic and radar systems is the extremely short wavelengths associated with optical systems. This allows small transmitter antennas (5 cm aperture) with narrow beamwidths (0.1 to 1 mrad). Optical photons scatter from normal atmospheric aerosols much more strongly than do microwave radar signals. Thus, optical Doppler is preferred for usable signals in a nominally clear atmosphere, but microwaves are indicated in low visibility conditions of fog, heavy rain and the like. Because of the narrow beamwidth, optical systems offer much higher spatial resolution at close range than do acoustic or microwave systems. For currently available components, optical Doppler systems are limited to approximately 1 km range, while microwave Doppler radars have much longer ranges.

The immunity of optical systems to noise, in contrast to acoustic systems, is an obvious advantage in an airport environment. However, optical systems must be protected from high ambient light levels. The background light level problem is common to both the optical Doppler and optical crossed beam correlation methods. Any aerosol distribution provides a usable target for Doppler techniques, but the crossed beam method relies on significant fluctuations in aerosol density. The crossed beam measurements therefore depend on a second order aerosol distribution property while the Doppler uses a first order property.

Infrared systems are not subject to high background radiation levels from an ambient environment.

3.3.5 PERFORMANCE OF PRACTICAL LASER DOPPLER SYSTEMS

3.3.5.1 Existing Systems. Some of the most successful existing Doppler lidar systems were mentioned in the introduction. A group at NASA, Huntsville (Huffaker, 1970 and Lawrence et al., 1972) has studied the CO_2 laser homodyne system over horizontal atmospheric paths. The apparatus involves a 25 W CO_2 laser operating at a wavelength of 10.6 μm and a 30 cm diameter collecting telescope. A single longitudinal component of the wind was measured successfully at a range of 33 m in a "normal" (unseeded) atmosphere and the instrument is expected to give useful data to 100 m. The correlation between Doppler and anemometer data was good. A calculated range resolution of 30 cm at 33 m total range applies to the system.

Operating in a different spectral range, a group under Fiocco's direction (Benedetti-Michelangeli et al., 1972) at ESRIM in Italy has measured the longitudinal (along the beam) wind component using interferometric (inconherent) spectral analysis of the Doppler return. Their equipment includes a single mode Ar^+ laser with 0.2 W output at a wavelength of 488 nm and a beam divergence of 0.1 mrad. The detector consists of a 50 cm telescope, scanning spherical Fabry-Perot interferometer, and photon counting photodetector. Useful returns were observed at night from a few hundred meters range resolution element, centered at a range of approximately 750 m. The range resolution was limited principally by the simple mechanical chopper used. The range of greater than 750 m is especially noteworthy. Results compared favorably with rawinsonde data and showed a typical error of ± 0.5 m/sec which may have been an instrumental effect or the natural variability of the wind. This interferometer experiment has demonstrated more useful range than any other reported Doppler lidar measurement, although the current limitation to night operation should be noted.

Bourke and Brown (1971) in England, and Farmer and Brayton (1971) in the United States, have tested two beam systems such as analyzed in Section 3.3.2.3. Although these authors prefer to think in terms of an interference fringe analysis, our more general

differential Doppler formalism applies exactly and expresses the results in a fundamental form, which is consistent with the analysis of longitudinal (pure backscatter) Doppler systems. Only Bourke and Brown report atmospheric scattering returns with enough detailed information to be useful for performance evaluation. These authors use two 20 mW intersecting laser beams with a wavelength of 632.8 nm. The collecting optics for backscatter detection subtended a solid angle of 3×10^{-2} steradian for a better than 10 to 1 signal-to-noise ratio. This collection system corresponds to a range of only 2.5 m for a 50 cm telescope aperture. Based on these results, Bourke and Brown estimate that a range of 152 m in backscatter would require an argon ion laser of 10 W power operating at 488.0 nm or 514.5 nm wavelength and 60 cm diameter telescope. A geometrically defined range resolution element is expected to be 2 m at 152 m range. Subsequent informal information reports successful measurement of wind at 50 m with a 1 W argon laser and a 20 cm telescope. Farmer and Brayton in informal reports suggest that a range of 150 m has been observed with an 85 W pulsed argon laser and a 61 cm collecting telescope.

3.3.5.2 Comparison of Possible Systems. A comparison of operational requirements for wind shear determination with the performance of existing systems seems to indicate that a three axis longitudinal component (pure backscatter) velocity sensor using a single mode argon laser and interferometric spectral analysis is most likely to be quickly successful. Such a visible light incoherent detection system has demonstrated a greater operational range than any other optical Doppler system. The optical and electronic components are relatively simple and well developed.

A differential Doppler system offers a much more compact and elegant method of wind measurement than does the three axis system. However, current examples of the technique have not demonstrated as good a range as the longitudinal component, incoherent detection systems. We are unaware of any fundamental reasons for the poorer performance of the differential Doppler other than the possible serious effect of atmospheric turbulence on the coherent detection system and the alignment difficulties inherent in such a system. Further study on differential Doppler is indicated.

It is possible, in principle, to combine some features of both the interferometer detection and differential Doppler systems. Three fairly closely spaced transmitted laser beams from a single laser are arranged at the periphary of a 6 m diameter circle, surrounding a centrally located 100 cm receiving telescope in the projected system. Returns from each of the three incident beams are distinguished by applying a distinctive frequency offset to each beam as discussed by Farmer and Brayton (1971). Ranging is achieved by coordinated angular scanning of the transmitted beams. A single incoherent (Fabry-Perot rapid-scan interferometer) detector determines the frequency shift for each beam in a natural multiplex fashion. The direct Doppler-shifted frequency is measured in the sense of Equation 3.3.11.

The combination system has a number of advantages over both the three-axis and differential Doppler techniques. By using a single laser receiver rather than three separated ones, as for the three-axis technique, the combination achieves an economy of apparatus and space, since only a single telescope and interferometer are required. Pointing and angular alignment problems are also reduced. Some of the spatial economy may need to be sacrificed for a wider transmitter separation in order to reduce the variance in the transverse wind. If the apparatus can be aligned more along the prevailing wind (say nearly parallel to the glide slope) in a suitable mount, the significant wind shear will be principally longitudinal and little variance in the significant wind is expected even for closely spaced transmitter beams. The combination system, when using incoherent detection, is much more immune to atmospheric turbulence induced phase fluctuations than is the differential Doppler, which in turn is less sensitive (for the same optical wavelength) to refractive index fluctuations than is a visible homodyne system.

Even more advantages accrue to the combination geometry when used with a coherent infrared laser system. Although the backscatter return from a "typical" atmosphere at 10.6 μm incident wavelength is unknown, the infrared system offers the advantages of: 1) comparative eye safety (perhaps making the safety radar unnecessary), 2) freedom from background radiation interference effects, which limit the best visible-spectrum systems to night operation, 3) relative immunity from turbulent refractive index effects (because of 20x larger wavelength, aperture averaging, and flatter index vs. temperature curve), which allows 4) successful implementation of narrow band, low noise, coherent detection techniques, with 5) rugged, efficient layers, which are 6) easily FM-CW modulated.

If one assumes a horizontally stratified atmosphere over the few kilometer region of interest for the airport wind shear problem, the problem is much simplified. In this case a single axis, scanning, longitudinal component velocity sensor is adequate. The system described by Benedetti-Michelangeli et al. (1972), with an improved range gating system, is then directly and immediately applicable, as is an infrared coherent system.

3.3.6 RESEARCH RECOMMENDATIONS

We think that this analysis shows the exciting potential of optical Doppler for the airport wind shear sensing problem. It seems wise to apply the simplest system to the airport environment to gain operating experience and to determine if more sophisticated data are required. A single-axis, incoherent detection, scanning Doppler lidar with coaxial safety radar is the least complex, best proved system of those reported or proposed in the literature or this report. Such a system can be set up and tested comparatively quickly and inexpensively.

Slightly more development effort would be required to implement the CO_2 (infrared) lidar systems. The significant advantages of the infrared approach justify the effort.

3.3.6.1 Ranging. Reported systems for backscatter incoherent Doppler lidar have not demonstrated adequate range resolution. Research on pulse time of flight and AM-FM-CW ranging methods should be pursued. Doppler systems require highly monochromatic laser light, which in turn practically requires a CW gas

laser. Cavity dump modulators which provide 15 nsec pulses from a CW argon ion laser are commercially available and should be applicable to the pulse ranging method. Frequency sidebands from the pulse length are above expected Doppler frequency shifts, and sidebands from the repetition rate can be arranged to be less than the interferometer linewidth.

The AM-FM-CW ranging method involves the (sinusoidal) amplitude modulation of a continuous wave gas laser, where the frequency of the amplitude modulation is swept in a sawtooth fashion. The frequency difference between the instantaneous transmitted and received modulation frequencies determines the range. The principal advantage of such a system for scattering is the inherently high average power involved, making for usefully strong scattering returns. More research is required to determine the suitability of AM-FM-CW ranging for Doppler lidar applications.

A CO_2 laser, by modulating the cavity length, becomes a simple direct FM-CW transmitter, exactly analogous to FM-CW radar discussed elsewhere in this report. Only a low frequency cavity length modulator (not optical modulator) is required.

3.3.6.2 Atmospheric Turbulence Effects. Coherent methods (mixing and beating) of detecting Doppler shifted frequencies depend on a coherent phase relationship between the incident and reference signals. In the differential Doppler system, the interfering optical signals travel nearly the same paths. The question of fringe stability and contrast (in the interference fringe representation) is nevertheless a serious one, because of the problems of laser beam scintillation, well known from laser communications work. The homodyne frequency difference measurement method is even more sensitive to variations in the atmospheric refractive index in the visible spectrum. Because the scattered and reference beams do not travel the same path or even the same distance, it is easy for the interfering beams to develop random phase relationships. First, the laser must have a coherence length equal to at least twice the range of the systems. Second, the effect of atmospheric refractive index variations must average to a constant over the path length. These criteria are easily satisfied in the infrared.

Atmospheric effects on the differential Doppler or coherent combination setup can be studied experimentally and theoretically. Such research is necessary to evaluate the operational suitability of differential Doppler for wind shear determination. Turbulence effects on refractive index for the homodyne case can be determined from existing work on atmospheric scintillation. Laser communications research is directly applicable to the local oscillator Doppler lidar analysis, given similar transmitter wavelengths.

3.3.7 CONCLUSIONS

Optical Doppler methods for determining wind shear in the vicinity of airports show much promise. While the Doppler scattering fundamentals are obvious, a number of different applications of the principles are possible. The general distinction between techniques depends on the method used to determine the Doppler frequency shift and on the wavelength of the transmitter laser (visible or infrared). A high resolution Fabry-Perot interferometer is used to measure optical frequencies directly. This method relies on laser monochromaticity, but is independent of phase and therefore is an incoherent detection scheme. The scattered optical signal may be homodyned with the laser transmitter frequency and the resulting beat frequency used to determine the Doppler shift. Homodyning is a coherent method which relies on the phase coherence of the returned and local oscillator signals. A third method, which also relies on coherent detection, examines the beat frequency between the scattered signals coming from two coherent, intersecting incident beams. The choice of laser frequency depends on the frequency dependence of backscatter intensity from typical aerosols and on the magnitude of atmospheric refractive index fluctuation effects.

Incoherent detection of backscattered argon ion laser light has shown the most reported success in determining wind velocity by optical Doppler techniques. The reported success involves a range the order of 800 m, good correlation with other wind data, and fairly simple, well-developed apparatus. We recommend implementing such a system, with improved laser pulse ranging, safety radar, and rapid interferometer scanning, at a representative airport for the purpose of system evaluation and improvement. Expansion of the system to include three-axis sensing can be done if operational tests show that this is desirable.

Alternatively, the coherent infrared (CO_2 laser) system shows exciting promise. Advantages of freedom from background light, eye safety, relative insensitivity to atmospheric turbulence, ruggedness, and efficiency must be balanced against the uncertain signal-to-noise of a 10.6 μm wavelength system. Risk and payoff are somewhat higher for coherent methods.

Field tests in a real atmospheric environment are the only dependable way of evaluating the potential of Doppler lidar, given our present state of knowledge.

REFERENCES (Chapter 3, Section 3)

Auth, D. C., Appl. Phys. Letters 16, 521 (1970).

Benedetti-Michelangeli, F. Congeduti, and Fiocco, J. Atmos. Sciences 29, 906 (1972).

Bourke, P. J. and C. G. Brown, Optics and Laser Technology 3, 23 (1971).

Farmer, W. M. and D. B. Brayton, Appl. Optics 10, 2319 (1971).

Huffaker, R. M., Appl. Optics 9, 1026 (1970).

Lawrence, T. R., D. J. Wilson, C. E. Craven, I. P. Jones, Jones, R. M. Huffaker and J. A. L. Thomson, Rev. Sci. Inst. 43, 512 (1972).

Owens, J. C., Proc. IEEE 57, 520 (1969).

Yeh, Y. and H. Z. Cummins, Appl. Phys. Letters 4, 176 (1964).

SECTION 3.4 MEASUREMENT OF WIND VELOCITY BY EDDY CORRELATION METHODS

(by V. E. Derr, R. E. Cupp, and N. A. Abshire) submitted December 1972

3.4.1 INTRODUCTION AND SUMMARY

This section presents the results of a first phase of study on a method of remote measurement of transverse wind velocity. This technique, called the eddy correlation method, depends on following the motion of the air by observing radiation from atmospheric constituents. Passive systems, depending on natural radiation from the atmosphere (thermal or scattered), are compared with active systems using artificial illumination, and it is concluded that the greater signal-to-noise (S/N) ratio available with active systems favors their use over the simpler passive systems for most applications. From the results of field measurements the conclusion can be drawn that under most meteorological situations the wind velocity can be determined as a function of altitude by active eddy correlation methods. However, the experiments performed have been limited in several important characteristics. They demonstrated the method only in short range (up to 150 ft) and for time constants greater than 0.3 sec. In addition, the success of the measurement depended on the relatively large fluctuations that occur in the received signals. The significance of these limitations is discussed and methods of minimizing them are proposed. The potential of this method, its ultimate limitations, and its application to the measurement of wind shear are considered in Section 3.4.7. Presently available data are shown to be insufficient for a final determination of the usefulness of the method, and further atmospheric experiments are recommended. However, extrapolation from the successful experiments leads to the conclusion that the method can be extended to 1 km, using modified commercially available equipment.

Summary of the report. The principle results of the report are summarized below. The detailed discussion on which the conclusions are based will be found in the following sections.

Statement of the problem. Devise a system to measure horizontal wind direction and speed along a vertical line through the atmosphere to 1000 m, with a spatial resolution of 10% of the altitude. The system may use integration times up to 3 min.

Description of the eddy correlation method. The eddy correlation method uses multiple laser beams or a single rapidly scanning beam to measure the passage time of aerosol inhomogeneities between known points by means of backscattered laser radiation.

What are its all-weather capabilities? Range is limited by heavy clouds, rain, or fog. The use of a CO_2 laser will minimize the limitation (Chu and Hogg, 1968). Insufficient data are available on the attenuation of CO_2 laser radiation (10.591 μm) in clouds, but Huffaker (NASA, Huntsville) has reported backscatter observed from greater ranges than 1 km in cumulus clouds. McClatchey et al. (1971) show the effect of haze at 10.591 μm to be substantially less than at other spectral regions where useful lasers exist. Further experiments are needed here to determine ultimate all-weather range. A combination of microwave radar (for inclement weather) and optical laser methods (for relatively clear weather) should be considered.

What has been accomplished in wind measurement by the eddy correlation method? (a) Passive systems have measured wind to 30 m altitude with poor S/N ratio under atmospheric conditions when large inhomogeneities exist. Extrapolation to greater altitudes is doubtful. (b) With low-power pulse and continuous wave (CW) lasers, wind velocity has been measured and compared with anemometer measurements to 50 m altitude. Equipment was not optimum. Extrapolation to 1,000 m is promising.

Based on these results what may be done? Using commercial equipment and adding special design features for stability and reliability, 0.2% fluctuations of aerosol content can be detected with a laser-ranging system up to 1000 m. Strong wind shears could be detected by this system whenever the fluctuations in aerosol content are as high as 0.2%. The chief uncertainty results from the lack of statistical data on the distribution and scattering cross sections of aerosols and on the aerosol content fluctuations above 50 m.

What specific systems are recommended? Two systems contend. Since it is recommended that the Doppler described below (see 3.3) and eddy correlation methods be simultaneously developed, the CO_2 laser system is given priority over the N_2 laser system. Because important statistical data on the atmospheric aerosol fluctuations are needed, a low-cost interim CW CO_2 laser system should be developed.

System 1 - CO_2 pulse laser system.

Power (peak)	400 kW
Energy per pulse	0.2 J
Pulse repetition frequency	200 pps
Wavelength	10.6 μm
Beam divergence	4 mrad
Filter width	20.0 nm
Filter transmission	50%
Scattering cross section	5×10^{-9} $cm^2 sr^{-1}$/particle
Telescope area	1 m^2
Telescope beam width	2 mrad

System 2 - N_2 pulse laser system.

Power (peak)	10 MW
Pulse width	10^{-8} sec
Energy per pulse	0.1 J
Pulse repetition frequency	100 pps
Wavelength	337.1 nm
Beam divergence	12.5 mrad
Filter width	3.0 nm
Filter transmission	30%
Scattering cross section	1.5×10^{-14} $cm^2 sr^{-1}$/particle
Telescope area	1 m^2
Telescope beam width	12.5 mrad

The S/N ratio as a function of range is presented for each system in Section 3.4.1.3.2.

3.4.1.1 Principle of operation. When the atmosphere is inhomogeneously loaded with fine material visible to the eye, such as rain, snow, dust, fog, smoke, or haze, the motion of the air may be apparent to the unaided observer. The random, inhomogeneous aerosols or hydrometeors form patterns that persist sufficiently and they have almost the same velocity as the air. We may use the motion of the recognizable features of eddies to determine the wind velocity. Fundamentally, the method described in this report consists of measuring the passage time of a recognizable pattern or eddy in the atmosphere between two points separated by a known distance. The points must be sufficiently close so that the eddy is recognizable after its passage between them. (See Sections 3.4.2 and 3.4.3.) Among methods of pattern recognition, the cross-correlation function between signals obtained from observation of the eddy passage across each of the two separated regions is preferred because of its simplicity and relative ease of calculation.

The eddies followed in this measurement may be marked by other than aerosols or hydrometeors. Inhomogeneitites in temperature, density, carbon dioxide content, or any other traces may be used if there is a method available for observation. Thus, for example, water vapor content is observable by means of infrared radiometry and by choosing the wavelength so as to be sensitive to thermal emission of water vapor. (This method is discussed in Section 3.4.1.2, while the use of aerosols as a tracer is presented in Section 3.4.1.3.)

The cross-correlation function used is

$$R(\tau) = \frac{1}{T}\int_{-T/2}^{T/2} f_1(t) f_2(t+\tau)\,dt \Big/ \left\langle f_1^2(t)\right\rangle^{1/2} \left\langle f_2^2(t)\right\rangle^{1/2} \qquad 1.1:1$$

where $f_1(t)$ is the signal received from the first "point" and $f_2(t)$ is that from the second. (The "points" are volumes, of course, and are herein referred to as cells.) The function is normalized by dividing by the product of the root-mean-square (RMS) values of the two functions. As in any meteorological data, the averaging interval must be chosen with care. Longer averaging times smooth noise; they must not be long in comparison with the time of significant change of the meteorological variable or else those changes are not observed. The problem of trending in random variables is discussed by Krause et al. (1969) and will not be considered in this report. For a selected value of T, the value of τ for which $R(\tau)$ is a maximum is the measure of the delay in the passage of eddies. The maximum value of $R(\tau)$ is a measure of the confidence which can be placed in τ.

3.4.1.2 Passive techniques. Because passive eddy correlation techniques have been discussed by Krause et al. (1969) and Little et al. (1970), they will be reviewed only briefly here. Passive systems, where applicable, have advantages of simplicity and economy. As will be seen below, they are severely limited by background noise and by lack of range information.

Passive techniques use receivers sensitive to natural radiation from the atmosphere, either thermal or scattered sunlight. Thermal radiation from the atmosphere has a spectral maximum in the infrared, and often infrared radiometers are used. Scattered sunlight may be used in the visible or ultraviolet in the daytime. In the infrared spectral region, inhomogeneities in water vapor emission or carbon dioxide emission may be observed, while in the visible, Mie scattering of sunlight from irregular aerosol content is the most important source of observed radiation. In the visible spectral region, background noise from clouds is very troublesome. This noise may be eliminated by operating at an infrared wavelength where water absorption is large and observation of emission from distant sources is prevented. A tunable spectral filter gives greatest flexibility. If such a filter could be of variable width, additional flexibility could be obtained. The large variation with wavelength of the absorption coefficient of water vapor in the infrared spectral range, typically from 10^{-6} to $10^{-3}(m^{-1})$, calculated for a typical water vapor content of 7.5 gm/m^3, gives a wide choice of operating conditions and observation of clouds may be prevented by proper choice of operating frequency.

Experimental results have been obtained for both infrared and optical passive systems (Krause et al., 1969; Sanborn, 1969). The conclusion from this work is that passive systems are capable of measuring wind velocity at short ranges with long integration times. However, range information must be obtained from the geometry of at least two receivers. A specific atmospheric cell can be observed by crossing the fields of view of two telescopes at the cell. The correlated part of the signal received is then the signal common to each receiver from the cell. The extraction of these signals is often not practical because of the background noise.

The noise component of the radiation received arises from all of the remainder of the telescope pattern, aside from the cell of interest. Under most conditions, this noise will be larger than the signal. Thus a tremendous disadvantage of passive signals is that the S/N ratio is often less than one.

The signal of interest results from the fluctuation of the observed constituent of the air, not its mean value, in the eddy correlation technique. The passive technique is thus at a great disadvantage when the atmospheric fluctuations are large in other regions of the receiver field of view than the cell of interest. Under the special circumstance that the fluctuations are large in the cell of interest and absent in the rest of the beam, the S/N ratio will be larger than one. These circumstances decrease in frequency as the range to the cell of interest is increased, but have been observed to occur sufficiently often at heights less than 50 m so that wind velocity can be sampled several times, on the average, over tens of minutes. The time required for a measurement of wind velocity approximates the time in which wind variations often occur, hence the measurement is not valuable when an up-to-date record of wind or wind shear is required.

These disabilities of passive systems make them unattractive for the measurement of wind profiles, and we turn now to active systems which are, with added expense, capable of greater range and accuracy and of higher data rates.

3.4.1.3 Active techniques. Active eddy correlation systems use an artificial source of radiation rather than scattered sunlight or thermal emission. Because background noise from the atmosphere causes a low S/N ratio in passive systems, as shown above, active systems are preferred. Although preferred for this reason, it should be recognized that active systems have a disadvantage of $1/R^2$ losses from the scattering element and require greater expense and complication. However, by using sufficiently powerful sources, the range of operation can be longer than the range of passive systems.

Elimination of background noise can be accomplished by the use of monochromatic sources and narrow band receivers. Both requirements clearly indicate laser use. Other sources, searchlights for example, have been only marginally successful.

Active systems depend on the aerosol content of the atmosphere for backscattering the projected laser beam. Backscatter from molecules (Rayleigh scatter) is comparatively weak (typically by a factor of 10^{-15}), and the observation of fluctuations of Rayleigh scattering is usually prevented by the radiation scattered by aerosols. We may estimate from the perfect gas law that a change of $1^{\circ}K$ at $300^{\circ}K$ at one atmosphere pressure, produces a change in density by a factor of 1.0003. Thus, temperature fluctuations are not likely candidates for use as tracers of air motion. The fluctuations of aerosol content are typically several percent of the total backscatter and may be used as tracers.

Many system configurations are possible, depending on the specific task. As a prototype, we will consider a simple configuration of two vertical receiver beams separated by a distance D, with a laser transmitter halfway between (Figure 3.4.1). The laser beam is steerable, can be split into two parts, and illuminates the receiver beams at an altitude z, as shown. This system measures only the horizontal wind component in the plane of the receiver beams. The beams might be made steerable for optimum geometry under a changing wind, or three or more beams could be used with multiple correlation between them to separate the vector wind components. Balance between complexity of data processing and field complexity must be considered in any practical systems. The parameters of interest in this report can be calculated from the simple configuration described. The parameters are the signal power at the receiver, the noise power at the receiver, and their ratio. The absolute signal power is important if the system is limited by detector noise. Considering the case where the noise N results from only background noise, we see that the laser illuminator gives a considerable advantage because the cell of interest is illuminated, but the rest of the receiver beam is not. Thus, the background noise falling upon the receiver from the atmosphere has a different spectral character than the signal produced by the scatter of the laser beam. In this case, it is useful to narrow the receiver (optical) bandwidth to eliminate noise.

At present, pulse or CW laser systems can be most easily obtained. Other modes of operation, such as frequency chirping a Q-switched dye laser, are possible, but they will not be considered here.

Advantages of the active system over the passive are:

(a) Narrower spectral bandwidth lowers background noise. The background noise resulting from reflected sunlight can be minimized by narrowband filters or eliminated by operation below 2900 Å for short ranges.

(b) The active system can operate night or day; it depends neither on sunlight nor as thermal emission.

(c) The geometry allows illumination of the cell of interest only. Nearby unillumiated turbulence does not produce an input to the receiver. The rest of the receiver beam contributes no signal. If the receiver and transmitter are coaxial, the receiver time gate discriminates against all other portions of the beam.

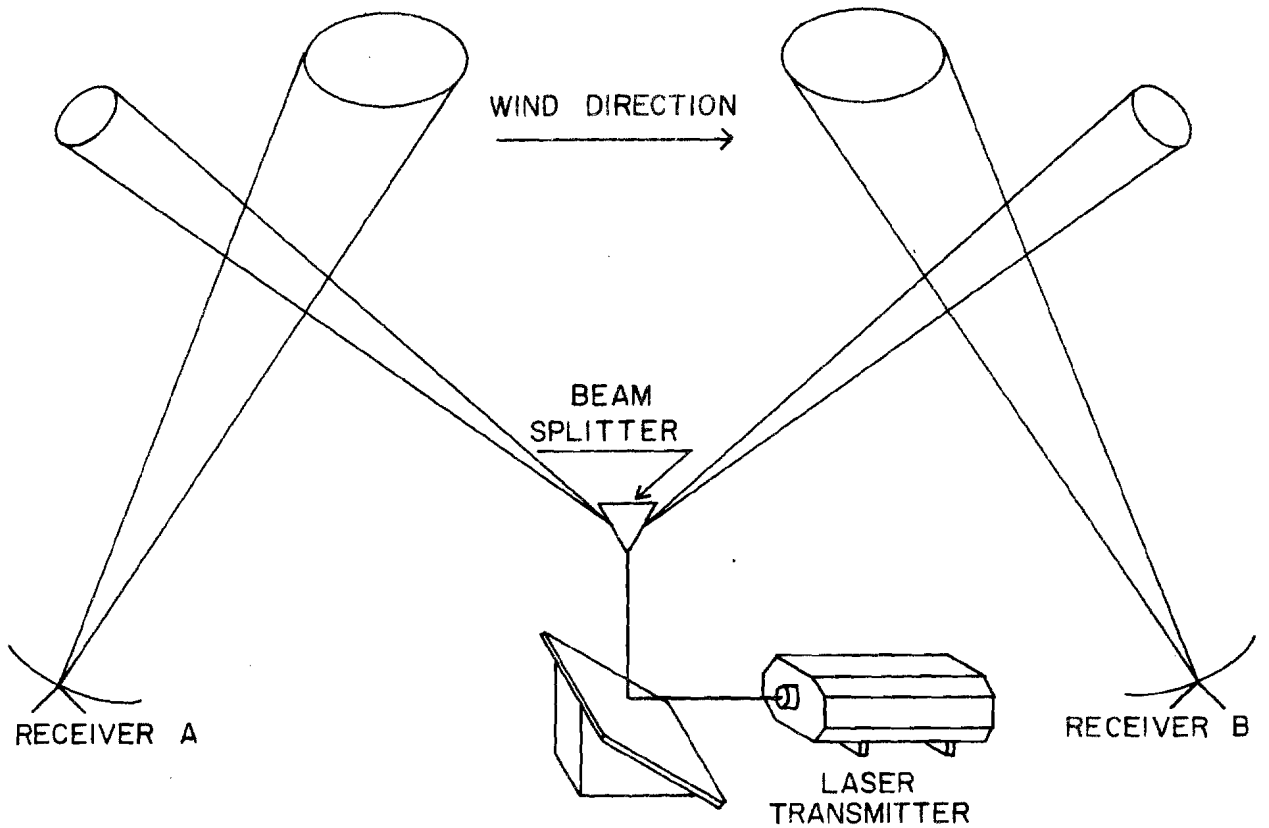

Figure 3.4.1 Configuration for eddy correlation measurements.

Difficulties that may arise in the active illuminator system include:

(a) The laser's stability must be sufficiently high so that the fluctuating return caused by atmospheric eddies is not masked.

(b) The laser beam in illuminating the cell of interest must pass through the intervening fluctuating atmosphere on its way to the receiver. Scintillations along the path from laser to cell of interest may cause the illumination to fluctuate.

(c) The signal on the cell of interest may vary because of the varying attenuation of the intervening atmosphere.

(d) The active system depends on the presence of an atmospheric tracer: aerosols are the most likely candidate.

(Difficulties similar to those in (a), (b), and (c) also arise in passive systems. The sunlight illuminating the cell of interest is filtered through the turbulent atmosphere, and the signal from the cell to the receiver is affected by the intervening atmosphere.)

The laser stability problem mentioned in (a) above has been found to be the limiting noise for low altitude experiments. If we accept as typical a fluctuation of the signal from aerosol backscattering of 4%, we would require the laser fluctuations to be perferably less than one-tenth of this value. Such regulation has been achieved in readily available lasers. If sufficient stability is not available, the laser output must be constantly monitored and the signal appropriately adjusted. This adjustment is imperfect to some degree, and probably a combination of a highly regulated laser output and monitoring is the best solution.

If the laser signal is initially perfectly stable, the random character of the medium lying between the

correlation cell and the laser will introduce variations, as mentioned under (b) above. These random variations will produce noise on the signal illuminating the cell. If they are equal to or larger than those arising in the cell, we must account for them in calculating the S/N. We next estimate the magnitude of the scintillation effect.

Suppose the illuminated volume is a cube of side S, the illuminating wavelength is λ, and the length of path from laser to correlation volume is L. Then the correlation distance of scintillations in the illuminated volume is $r = \sqrt{\pi\lambda L}$. Thus, each independently illuminated region has an approximate area of $r^2 = \pi\lambda L$. Because the entire illuminated area is S^2, the number of independently illuminated areas is $N = S^2/r^2$. Letting S = 10 m, for example, and letting L = 1,000 m and λ = 337.1 nm (one of the laser system wavelengths discussed in section 1.3.2), we have $N = 9.44 \times 10^6$. The log amplitude of the intensity ratio, defined as $\chi = \frac{1}{2} \log_e \frac{I}{I_o}$, is used to measure the effect of scintillation. Here I is the irradiance on the scattering volume, and I_o is the average of I. Many observations indicate that the maximum possible variance of χ in the scattering volume is $\sigma_\chi^2 = 0.6$; the limit is the result of saturation of scintillation. The variance is reduced by the factor N when the entire volume is received, that is,

$$\sigma^2_\chi(\text{for } S^2) = \frac{\sigma^2_\chi(\text{for } r^2)}{N} = \frac{0.6}{9.44 \times 10^4} = 6.3 \times 10^{-6} \quad (3.4.1)$$

The corresponding variance for the irradiance I is

$$\sigma^2_I = I^2_o \left[\exp\left(4\sigma^2_\chi\right) - 1 \right] = 25.2 \times 10^{-6} \times I^2_o . \quad (3.4.2)$$

Then the maximum possible relative fluctuation of the irradiance is

$$\frac{\sigma_I}{I_o} = \sqrt{25.2 \times 10^{-6}} = 5 \times 10^{-3} = 0.5\%. \quad (3.4.3)$$

In practice, turbulent conditions rarely permit observation of this maximum, except for paths close to the ground (within a few m). One effect is that turbulence generally diminishes with altitude, hence, the relative fluctuation will be lessened. The second effect is that in winds with velocity in the range of interest, the fading rate of the scintillation will be on the order of $V_T/\sqrt{L\lambda}$ where V_T = transverse wind velocity, that is, it will be on the order of 50 to a few hundred Hz. Because most turbulent fluctuations observed in eddy correlation experiments lie in the frequency range below 10 Hz, a large percentage of scintillation-caused noise can be removed by electronic filtering. The exact decrease depends on experimental conditions, but we can expect for most meteorological situations that the fluctuations of the illuminating intensity on the cell of interest will be lowered by a factor of 10^3 or will have a value of $\sigma_I/I = 5 \times 10^{-6}$. Thus, scintillation of the illumination can be expected to add only insignificant noise.

In the above calculation, the effect of the scintillation on the return signal was neglected. If we assume direct backscatter, however, the effect will be negligible for areas as large as S = 10 m.

In addition to the ultraviolet wavelength considered above, it is of interest to look at the calculation from the point of view of a system using a CO^2 laser at 10.6 µm. In this case, r^2 is some 30 times larger, and the fluctuations of the irradiance will be increased by a factor of five. The variance is reduced somewhat, however, by the wavelength dependence, because $\sigma_I^2 = 1.23\, C^2 \left(\frac{2\pi}{\lambda}\right)^{7/6} L^{11/6}$. Thus again we can expect negligible effect of scintillations (Tatarski, 1967).

The effect of the attenuation mentioned in (c) above is negligible for a 1-km path at 337.1 nm. At 10.6 µm, the attenuation per km at high humidity may amount to 30%. The power available in CO_2 lasers is quite adequate to compensate for this loss. Information is not available to determine whether fluctuations of water vapor content will be a problem.

3.4.1.3.1 Calculation of maximum lidar range. If the laser emits N_o photons per pulse, the number of photons at range R is

$$N_o e^{-\alpha R} , \quad (3.4.4)$$

which is equal to $(N_o e^{-\alpha R}/\Omega_T R^2)$ photons per unit area, where α is an atmospheric attenuation coefficient and Ω_T is the solid angle of the laser beam. The number of photons scattered from the beam back into a solid angle Ω_R by a single particle through a process represented by a differential cross section $\sigma(\Omega)$ is

$$\frac{N_o \sigma(\Omega) \Omega_R e^{-\alpha R}}{\Omega_T R^2} . \quad (3.4.5)$$

The number of particles at a density $\rho(R)$ in the volume defined by the laser beam and a range increment ΔR is

$$\rho(R) \Delta R \Omega_T R^2 , \quad (3.4.6)$$

so that the number of photons scattered back into a telescope of area A from the particles in the range increment ΔR is

$$\frac{N_o \sigma(\Omega) \rho(R) \Delta R A e^{-2\alpha R}}{R^2} . \quad (3.4.7)$$

The signal S is taken to be the number of photoelectrons generated by n laser pulses, transmitted through an optical system of transmission β to a photocathode of quantum efficiency. Thus,

$$S = \frac{\beta \eta n N_o \sigma(\Omega) \rho(R) \Delta R A e^{-2\alpha R}}{R^2} . \quad (3.4.8)$$

The detector photocathode current is composed primarily of three components:

(a) Signal current i_s (the information carrier).

(b) Dark current i_d (the current present with no light on the detector), and

(c) Background current i_b (the current generated by sunlight scattered from the earth's atmosphere into the detector).

The relative magnitude of these components, along with their spectral and temporal characteristics, and the type of signal processing performed determine the S/N ratio at the output of the signal processor.

The DC component of background and dark current can be rejected or subtracted from the total current so that the receiver sensitivity is ultimately limited by the magnitude of the statistical fluctuations in the photocathode current. Assuming Poisson statistics, this limitation may be represented by an effective noise current at the photocathode which generates N electrons in time $n\tau$ according to the equation

$$N = \sqrt{\frac{n\tau}{e}(i_s + i_d + i_b)}, \qquad (3.4.9)$$

with e being the electron charge. The quantity $n\tau i_s/e$ is just the signal S. It is usually more convenient to represent i_d by

$$i_d = I_d/G, \qquad (3.4.10)$$

where I_d is the anode dark current and G is the detector current gain. The background photocathode current i_b can be obtained from the background radiant flux through the relation

$$i_b = \frac{\beta\eta B_\lambda A\Omega_R \Delta\lambda e}{hc} \qquad (3.4.11)$$

where

B_λ = background radiant flux ($W - cm^{-2}\text{-}sr^{-1}\text{-}Å^{-1}$),

λ = wavelength (cm),

$\Delta\lambda$ = filter optical bandwidth (Å),

h = Planck's constant (6.63×10^{-34} J/sec),

and

c = velocity of light (3×10^{10} cm/sec).

Substituting this into the equation for N produces an effective noise of

$$N = \sqrt{S + n\tau\left(\frac{\beta\eta B_\lambda A\Omega_R \lambda\Delta\lambda}{hc} + \frac{I_d}{eG}\right)} \qquad (3.4.12)$$

The following expressions relate some of the system parameters to more readily available quantities:

$N_o = \frac{J\lambda_o}{hc}$ where J is the energy per laser pulse,

n = (PRF) x T where (PRF) is the pulse repetition rate and T is the observation time,

$\tau = \frac{2\Delta R}{c}$ (assuming the receiver is closed except when returns from the range increment ΔR arrive),

$\Omega_R \cong \frac{\pi\Phi^2}{4}$ where Φ is the receiver telescope beamwidth (FWHM), and

$A = \frac{\pi D^2}{4}$ where D is the diameter of the receiver telescope.

Combining these quantities and substituting the values of the constants generates the following expression for the system S/N ratio:

$$\frac{S}{N} = \frac{3.95 \times 10^{10} J\lambda_o \sigma(\Omega)\rho(R)\Delta R\beta\eta D^2 (PRF) T e^{-2\alpha R}}{R^2\sqrt{S + 0.667(PRF)T\Delta R\left(3.1\beta\eta B_\lambda D^2\Phi^2\lambda\Delta\lambda + \frac{6.25 \times 10^{10} Id}{G}\right)}} \qquad (3.4.13)$$

where

J = laser energy (J)

λ_o = laser wavelength (Å)

$\sigma(\Omega)$ = interaction cross section (cm^2/sr)

(R) = particle density (cm^{-3})

ΔR = range increment (m)

β = transmission of receiver optics

η = detector quantum efficiency

D = receiver telescope diameter (m)

PRF = laser pulse repetition frequency (sec^{-1})

T = observation time (sec)

α = extinction coefficient (km^{-1})

R = range (km)

$B\lambda$ = background flux ($W\text{-}cm^{-2}\text{-}sr^{-1}\text{-}Å^{-1}$)

Φ = receiver telescope beamwidth (mrad)

λ = wavelength of maximum receiver transmission (Å)

$\Delta\lambda$ = receiver optical bandwidth (Å)

I_d = detector anode dark current (A)

G = detector current gain.

3.4.1.3.2 Performance characteristics of two specific systems. Using the formulas of section 3.4.1.3.1, the performance characteristics of two systems were calculated. The two systems were chosen to present contrasts in power and wavelength. Without a detailed evaluation of all laser systems, it cannot be asserted that one of these systems is optimum. However, experience indicates that better choices of laser types are not very probable. The first system described uses a pulsed CO_2 laser at 10.6 μm, and the second uses a pulsed N_2 laser at a wavelength of 337.1 nm. Each system is capable of sufficiently high pulse rate (several hundred per second) so that the fluctuations of the atmosphere can be followed. However, the limitation on bandwidth is imposed by the integration time. The high pulse rate also contributes usefully to the average power. Because of the narrow pulse width and low duty cycle of the N_2 laser, it can discriminate against daytime background noise. The N_2 laser has the additional capability of measuring temperature and humidity profiles simultaneously with wind measurements. The CO_2 laser has the advantage that it is unaffected by scattered sunlight (day and night are not distinguishable), and its output can be made sufficiently coherent so that a Doppler velocimeter can be developed simultaneously. In addition, it promises much better penetration of fog and haze than an ultraviolet system.

The CO_2 laser system was assumed to have the following characteristics:

Energy per pulse	0.2 J
Pulse repetition frequency	200 pps
Telescope area*	1 m^2

* Because energy collection, not accurate imaging, is needed, low-cost spun-metal mirrors may be used. Searchlight mirrors have been used efficiently.

Telescope main lobe angular width	2 mrad
Telescope reflectivity	50%
Filter bandwidth	0.2 μm
Filter transmission	50%
Integration times	1.0, 0.5, 0.1 sec
Detector sensitivity	20-60 V/W
Detector noise equivalent current (100 Ω load)	4×10^{-9} A
Detector D^*	5×10^{9} cm $Hz^{1/2} W^{-1}$
Detector NEP	1.02×10^{-8} W
Detector quantum efficiency	50%

As will be seen, this system must be improved to attain the desired range.

The background sky radiance was obtained from Kuhn (NOAA, APCL) from his direct measurements.* The radiance used was 1.46×10^{-3} W cm^{-2} sr^{-1} (or 2.08×10^{-4} W m^{-2} sr^{-1} $Å^{-1}$) in the interval from 8-15 μm.

Determination of the correct scattering cross section of the atmospheric aerosols at 10.6 μm is difficult because few, if any, accurate measurement of scattering cross sections at this wavelength have been made. The scattering cross sections depend on the distribution of particle sizes as a function of altitude. Rosenberg (1967) has shown that most aerosols have water coatings at humidity above 35%, and this coating governs the refractive index. Therefore, in most climates, except the very driest, we may neglect the material (or the refractive index). A number of estimates and extrapolations have been made from existing data and, for the purposes of the calculation of system performance, the following assumptions have been made:

(a) Scattering is observed (at 10.6 μm) mainly from particles with diameters greater than 1 μm.

(b) The density of particles is 8×10^{-2} cm^{-3} at the ground (R = 0). It decreases as $e^{-0.921 R}$, where R is in km. Thus we assume density of particles of greater diameter than 1 μm is $8 \times 10^{-2} e^{-.921R}$ cm^{-3}.

(c) The backscatter cross section was determined from measurements made by C. M. Sonnenschein** (private communication to R. Schwiesow):
σ (per particle) = 5×10^{-9} $cm^2 sr^{-1}$.

*This is somewhat lower than most of the values for $\lambda = 10\ \mu$ given in the Handbook of Military Infrared Technology, which range from about 1.00 to 10.0 x 10^{-4} W $m^{-2} sr^{-1} Å^{-1}$.

**Raytheon Corp., Sudbury, Mass.

Because accurate quantitative values for aerosol backscatter cross section at 10.6 μm wavelength are not available, the value assumed is pessimistic. The value for number density of particles of 1 μm or larger may vary greatly from one locale to another and thus change the maximum range of lidar systems used.

Figure 3.4.2 shows maximum range versus S/N for the CO_2 system described. The range of this system is limited. The system paramaters were chosen to correspond to an existing system that is not the best available. Using a filter bandwidth of 0.024 μm and an increase in energy per pulse to 0.4 J, we obtain the curves shown in Figure 3.4.3. These results show the second system is still too low in S/N for a range of 3,000 ft.

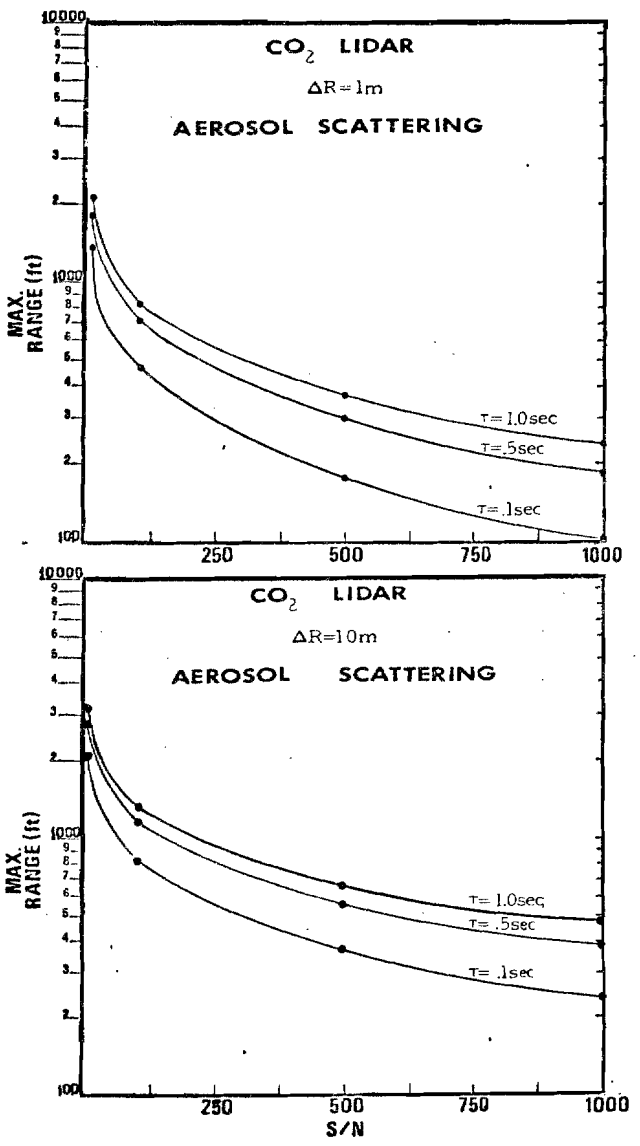

Figure 3.4.2 Maximum range vs. S/N, low-power CO_2 laser system (τ = integration time)

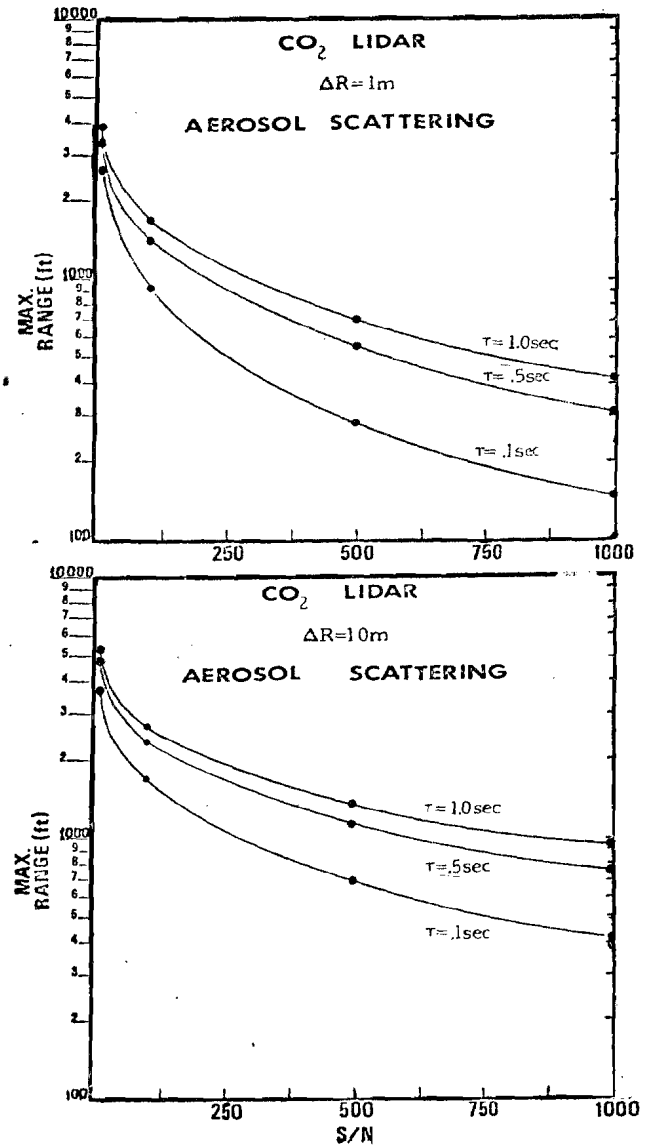

Figure 3.4.3 Maximum range vs. S/N, CO_2 laser system power doubled, receiver narrowed.

To determine the characteristics of a laser system which would give S/N = 1,000 at 3,000 ft, the S/N was fixed and the maximum range computed as a function of the energy per pulse, as shown in Figure 3.4.4. We see that between 150 and 200 mJ per pulse are necessary to give adequate range. Laser engineers consulted believe that the larger system can be constructed, but the cost is uncertain. The lower power system curves of Figures 3.4.2, 3.4.3 indicate what performance compromise would be necessary if lower costs are required.

Although further analysis has not been performed, it is clear that the system can be improved by narrowing the receiver bandwidth and decreasing the range resolution from ΔR = 10 m (applied uniformly

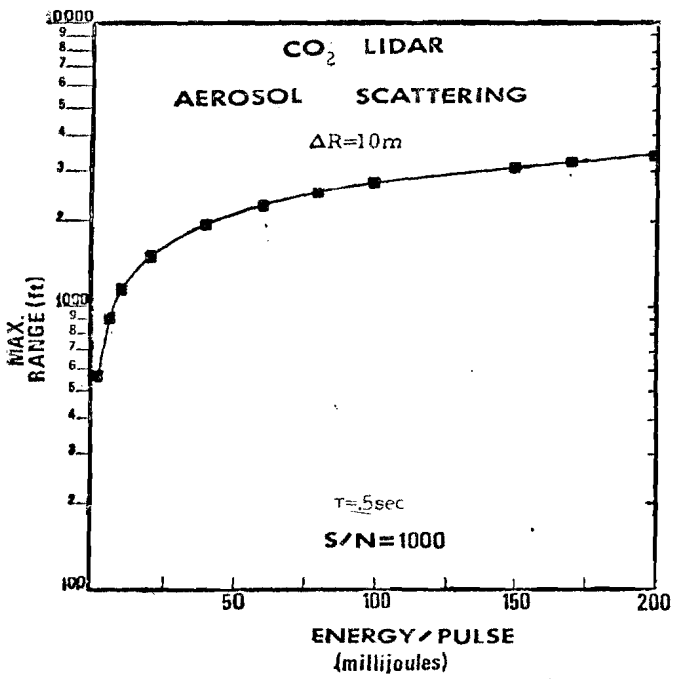

Figure 3.4.4 Maximum range vs. energy per pulse, CO_2 laser system.

throughout the range) to ΔR = 0.1R. Specially selected detectors and larger telescopes can be considered. Thus, the required power may be reduced.

Optimizing the data processing step might permit the system to be effectively used at lower S/N ratio. This might most easily be done by recording the data which could later be analyzed using analog and/or digital processing methods.

The pulsed N_2 laser system was assumed to have the following characteristics:

Energy per pulse	100 mJ
Power peak	10 MW
Pulse width	10^{-8} sec
Pulse repetition frequency	200 pps
Telescope area	1 m^2
Telescope main lobe angular width	125 mrad
Filter band width	3.0 nm
Filter transmission	30%
Integration times	1.0, 0.5, 0.1 sec
Detector quantum efficiency	17%

The scattering cross section was assumed to be $1.5 \times 10^{-14} cm^2/sr/$(average) particle. Particle densities appropriate to the Denver altitude and climate were assumed (Handbook, 1957 and Handbook, 1965 and private communication from A. Cohen.) This cross section differs greatly from that chosen for 10.6 μm because this quantity was averaged over all particle sizes; the former was chosen for only large particles. This lack of symmetry in treatment was necessitated by the differing forms in which data were available

In Figure 3.4.5, the results of the calculation are shown for two range increments. (The range increment is the length of the region from which signals are accepted through the receiver range gate.) In this figure, the integration time (τ) assumed are shown with their respective curves. Experience has shown that τ = 0.1 s is an adequately short integration time to avoid loss of information. We may estimate the minimum S/N ratio by observing from field data taken at low altitude that typical fluctuations from the Mie scattering are on the order of 0.5 to 1 percent. Conservatively, let us assume that we must measure the fluctuations to 5 parts in one thousand. Then S/N = 5,000 is adequate. Under these circumstances, ranges of several thousand feet are possible. By increasing the range increment and by increasing the integration time, we can achieve greater ranges All the curves shown are for daylight operation.

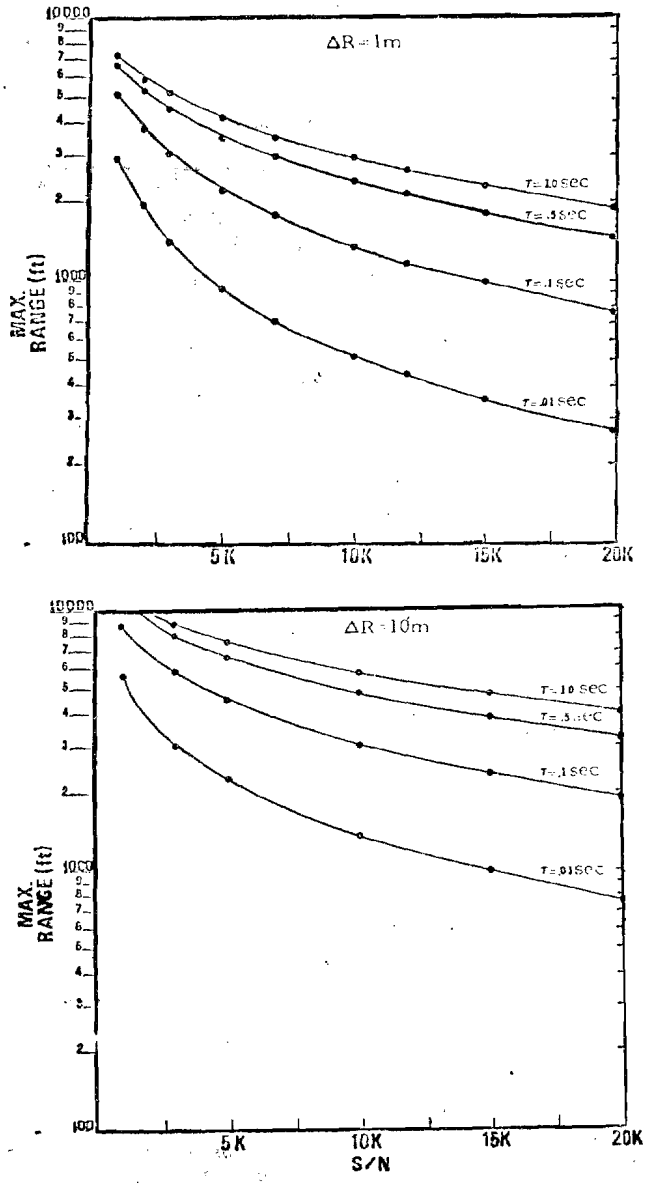

Figure 3.4.5 Maximum range vs. S/N, N_2 laser system.

3.4.2 THE STATISTICAL CHARACTER OF ATMOSPHERIC EDDIES

The eddy correlation technique depends on persistence of configurations of eddies as they pass between two detectors. More precisely, the wind moves the aerosol-loaded atmosphere past two laser-illuminated regions. If the inhomogeneities are large enough to be detected and if their identities are not destroyed in the passage between the cells of interest, the energy scattered from them can be used as a measure of a component of the wind velocity. The signal may be considered as made up of an average value and of the fluctuations about that average.

In clear Colorado air, measurements of aerosol backscatter have shown that at low wind velocity (a few meters per second), the signal fluctuation is often approximately 4 percent of the average signal. It has been observed at times to reach between 15 and 20 percent in high wind conditions. In general, a system designed for Colorado would work most of the time in other areas of the United States because it is assumed that the aerosol content would usually be higher. Information on the geographical distribution of aerosol inhomogeneities is not available.

Sufficiently small aerosols act as passive additives (Tatarski, 1967). The decay time ("lifetime") of inhomogeneities of aerosols is proportional to their size. Larger, longer lifetime inhomogeneities are fewer in number. Although the larger eddies give stronger signals often observable on strip charts, their lower frequency of occurrences makes it necessary to use the smaller ubiquitous and shorter lifetime inhomogeneities. For the smaller eddies, the cells of interest must be closer together, and the S/N ratio is smaller. A discussion of the effect of these qualitative considerations on the accuracy of the measurement is given in Section 3.

Figure 3.4.6 shows the change of correlation (covariance) as a function of separation of two point-temperature sensors aligned with the wind stream. (The data and curve are from Ochs, NOAA, WPL.) It shows normalized covariance curves for separations of 0.1, 0.3, 1.0, and 3.0 m. The data were obtained a few meters above the ground in a wind of nearly 1 m/sec. We may deduce from these curves that under like conditions the peak of the correlation function is broadened, hence accuracy in velocity determination is lowered for separations beyond 3 m, on the average.

If measurements are not required at short intervals but may be obtained over a few minutes, the intermittently large signals may be used. Although definitive statistical data are unavailable for this geographic area, intermittent characteristics are frequently observed. In this situation, even when very low signals are received (the atmospheric aerosols are well mixed), occasionally large inhomogeneities are observed that are often separated by a few minutes. Such intermittently large signals allow a wind velocity measurement. These conditions are usually obtained when the wind is low. The observations on which these remarks are based were obtained below 50 m altitude.

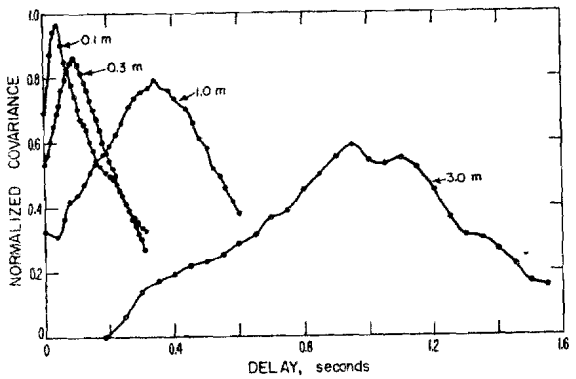

Figure 3.4.6 Covariance vs. delay for separated temperature sensors. Separation between sensors is referred to each curve.

The observation of strong wind shears by the eddy correlation method would probably be aided by the differences in aerosol content of atmospheric layers aloft. However, this plausible argument requires extensive observations for verification. Indeed, the chief difficulty in evaluating the feasibility of the eddy correlation method lies in the lack of knowledge of the statistical properties of aerosol inhomogeneities as a function of altitude.

3.4.3 ACCURACY

Any direct velocity determination requires the measurement of the time interval required to move between two points separated by a known distance. The error is dependent on the spacing and the elapsed time (τ). The change in measured v (i.e., dv) as a result of the change or the error in measured time (dt) is

$$dv = \frac{D}{t^2}\, dt \qquad (3.3.14)$$

where D is the separation. (The algebraic sign is omitted.) If dt is the uncertainty of the measurement of time, then dv is the velocity uncertainty and

$$\frac{dv}{v} = \frac{dt}{t} \quad . \qquad (3.4.15)$$

We consider first the case where the uncertainty τ results from the integration time τ. We assume here that the observing apertures are small compared with the separation distance. We also assume that two events are indistinguishable in our system unless separated by a time greater than the integration time. Then,

$$\frac{dv}{v} = \frac{\tau}{t} \quad . \qquad (3.4.16)$$

Thus, we require that the integration time be short compared with τ in order to have a small fractional error dv/v.

The time t depends on D and v. If we choose a permissible error $\frac{\tau}{t} < f$, then $t > \tau/f$. Because $D = vt$, $D > \frac{v\tau}{f}$ is required to maintain a fractional error less than f. On the other hand, if D is too large, the eddies do not maintain their individuality. Thus, D is constrained to be less than the eddy decay distance and greater than $v\tau/f$. The eddy decay distance is a function of eddy size, mean wind, and mixing conditions, thus equipment must be flexible in choice operating conditions such as cell spacing.

3.4.4 GEOMETRICAL CONFIGURATIONS FOR FIELD APPLICATIONS

Although the two separated beams shown in Figure 3.4.1 are most convenient to visualize for the principle of eddy correlation methods and also for the feasibility experiments, the configuration is awkward for operational use because of the necessity that the wind velocity vector lie in or near the vertical plane containing the two cells of interest. This necessity arises from the variation of transit times occurring when the wind vector is much more than 30° from the line connecting the cells. Many of the inhomogeneities are tilted with respect to the wind vector, and some will produce a lengthened and some a shortened time of transit. Thus, experience shows that the variation of transit times for a steady off-angle wind often becomes excessive.

The problem may be considerably reduced when three or more beams are used. Then, the wind direction cannot be farther than 30° from one of the lines connecting the two cells. Cross correlation between the cells will determine wind speed and direction. Correlation between the pair showing the least time delay would be eliminated from the computation of the vector wind.

An effective separation into three or more beams may be achieved optically by dividing the telescope field of view into sectors, each with its own detector, and by filling the telescope field of view with laser light. However, an additional problem arises because the optimum separation of the cells of interest depends on the wind speed. The dependence is a weak one and arises because the size of inhomogeneities generally increases as the wind near the ground increases and the passage time then decreases. As shown in the previous section, if the passage time is too small, the accuracy of the measurement suffers. This problem can be avoided by providing for a method of widening the field of view of the telescope or by dividing the field of view into rings.

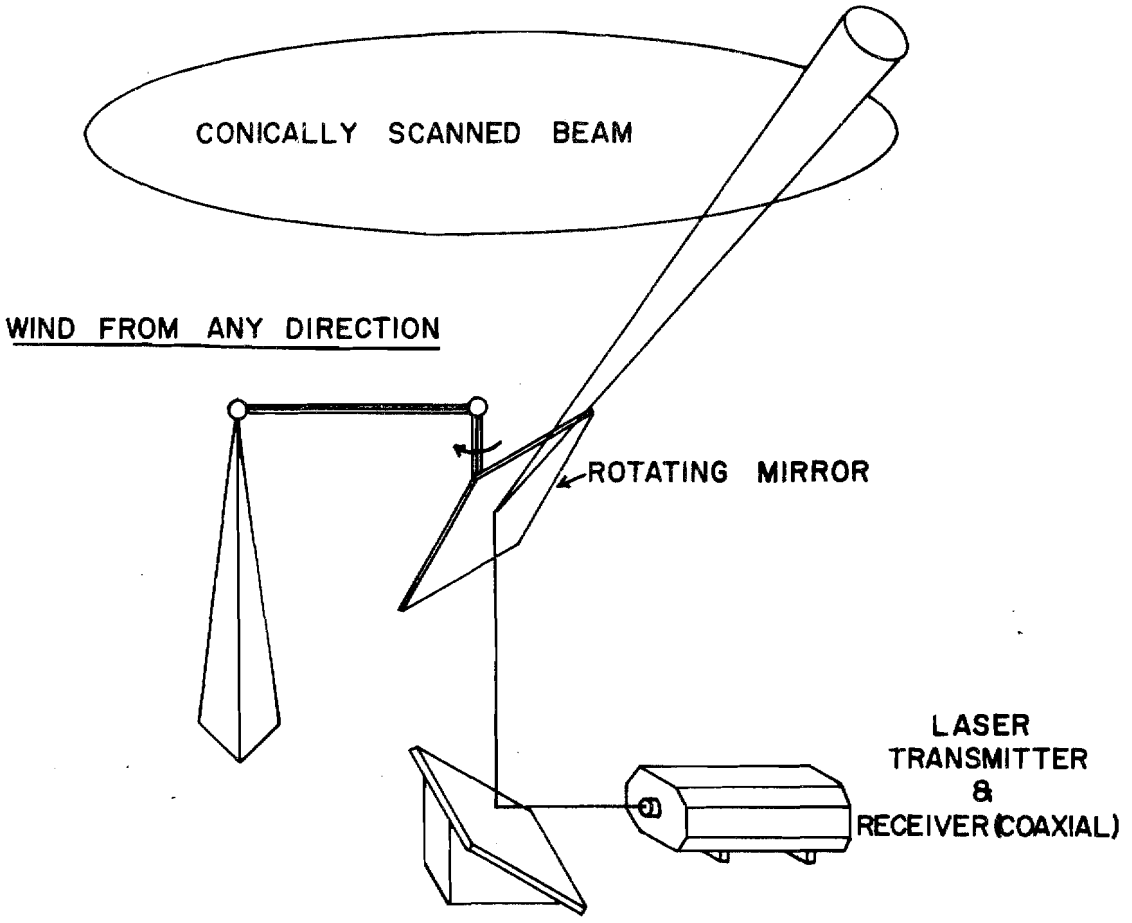

Figure 3.4.7 Conical scan wind-measuring configuration.

An alternative configuration has been proposed as in Figure 3.4.7. In this system, the laser beam and receiver are coaxial and rotate in a cone with vertical axis. The cross correlation is calculated between opposite elements of the cone.

3.4.5 EXPERIMENTAL RESULTS

Two groups of experiments have been performed at WPL on eddy correlation wind-measuring techniques. The first set of experiments in 1970 concentrated on the comparison between passive and active methods. The more recent set in the fall of 1972 was aimed at developing computer methods of processing the data rather than relying on visual examination. In this section, we review briefly both sets of experiments. All experiments used the configuration of Figure 3.4.1.

Under conditions of large-scale inhomogeneities, passive systems will show good correlation between separated receiver beams. Figure 3.4.8 shows the signals received in two passive vertical parallel beams, with 8 ft separation. (The voltage scale of the lower trace is reversed.) The signals were received on two infrared radiometers with filters of 0.2 μm, the edge of a major water absorption band. Emission from large-scale fluctuations in water vapor moved by a 15 mph x m/sec wind is responsible for the signals shown. The chart speed of 0.25 mm/sc used here does not allow the delay to be seen. This large S/N ratio is unusual for passive systems; most of the other data taken earlier in that group of experiments show very little correlation between signals measured by separated beams.

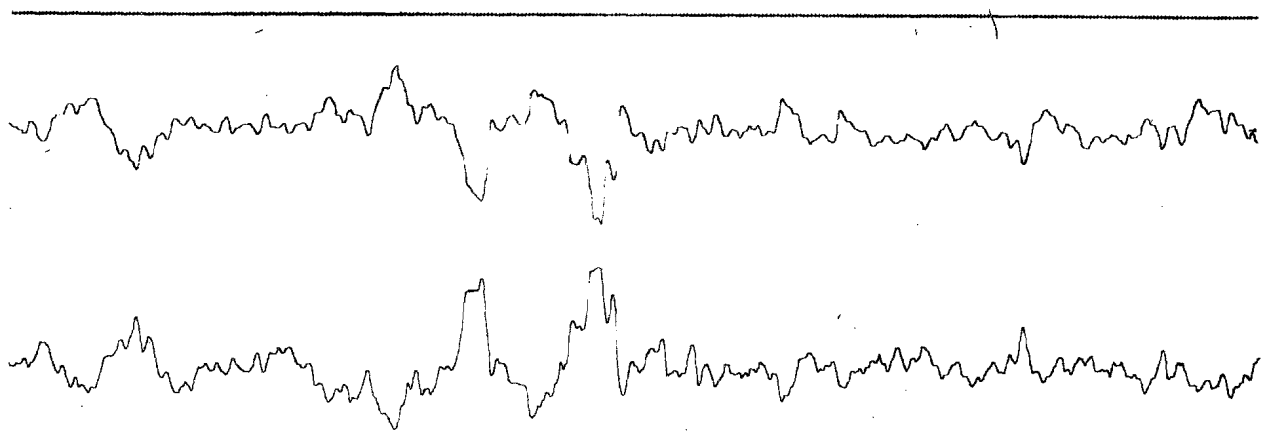

PASSIVE VERTICAL PARALLEL BEAMS

(8-foot separation)

0.3 sec. integration time
5.4 ± .1 micron

10:00 PM
15 September 1970

Figure 3.4.8 Passive vertical parallel beams-eddy correlation.

Two kinds of lasers were used in the study of active eddy correlation methods. The first of these was a 1-W argon ion laser 488 nm, continuously operating. The beam was split into two parts, and Figure 3.4.9 shows the delays observed using a 12 ft separation between beams. The telescopes' field of view crossed the beams at 30 ft above the ground. The 5 nm/sec chart speed here allows the delays of approximately 1 sec to be observed easily and the wind speed to be estimated from the chart. This record is typical of many records observed in that it alternates from good correlation and large S/N to little correlation and poor S/N. The right and left portions of the chart have good signals, the center portions less so.

To demonstrate that a pulsed laser can be used, a N_2-pulsed laser at 337.1 nm was employed. Its peak power is 100 kW, the pulse width is 10 nsec. The pulse repetition frequency is 100 pps. It is necessary to have a sufficiently high pulse repetition frequency rate so that the atmospheric fluctuations may be followed. Most fluctuations are below 30 Hz; because sampling theory would require a 50 Hz sampling rate, 100 pps is a sufficiently high rate. Figure 3.4.10 shows in the upper two traces that the signals received from atmospheric cells are separated by 5.2 m. The lower traces show wind direction and velocity registered by an anemometer. Light variable winds of this kind (1-2 m/sec) are not easily measured by this method. In this case, because the system was not optimized, a long (3 sec) integration time was chosen that obfuscated the delays. This experiment proved that a pulsed laser could be efficiently used. The pulsed laser, paired with a gated receiver, is effective in eliminating daytime background noise.

In Figure 3.4.11 data are shown from a CW argon laser, split into two beams, with approximately 0.5 W in each beam. A typical section of data is shown, with a smaller section expanded. The cross correlation was performed over 6.5 sec of data. At that time, the wind speed measured by an anemometer showed an average value of 10.9 mph. Calculating the wind speed from the delay at the maximum value of the correlation function gave approximately 10.6 mph. The anemometer and the illuminated cells were approximately 40 ft above the ground. The data were taken at night to avoid the background of scattered sunlight.

The most recent experiments are typified in Figure 3.4.12. Two cells are separated by 3 m at a 20 m altitude, lying in an east-west plane. The telescopes' fields of view subtend 41 cm of the argon laser beam. Approximately 0.4 W per beam was used. The experiments were at night to avoid sky background noise. The top trace is the wind direction (in this case from the west), the second trace is the wind speed, and the third trace is the wind component on the east-west line (here equal to the wind velocity). The laser

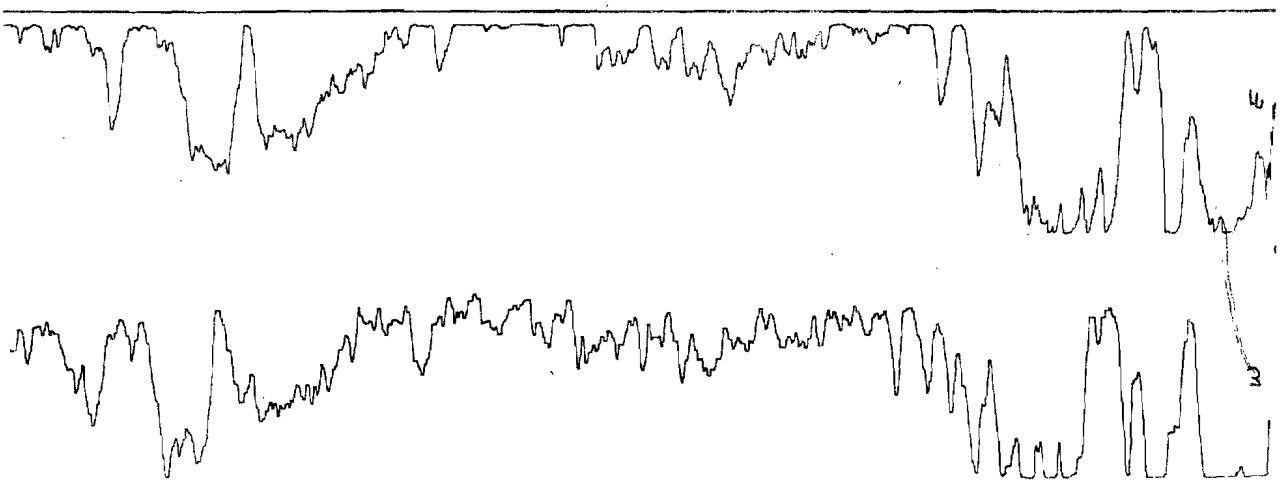

26 February 1970

Wind - 5-10 mph from West

10:55 PM

CW Argon Laser

.3 sec integration time

5 mm/sec chart speed

12-foot delay, altitude = 30 feet
range = 100

Figure 3.4.9 Active laser-illuminated eddy-correlation observation.

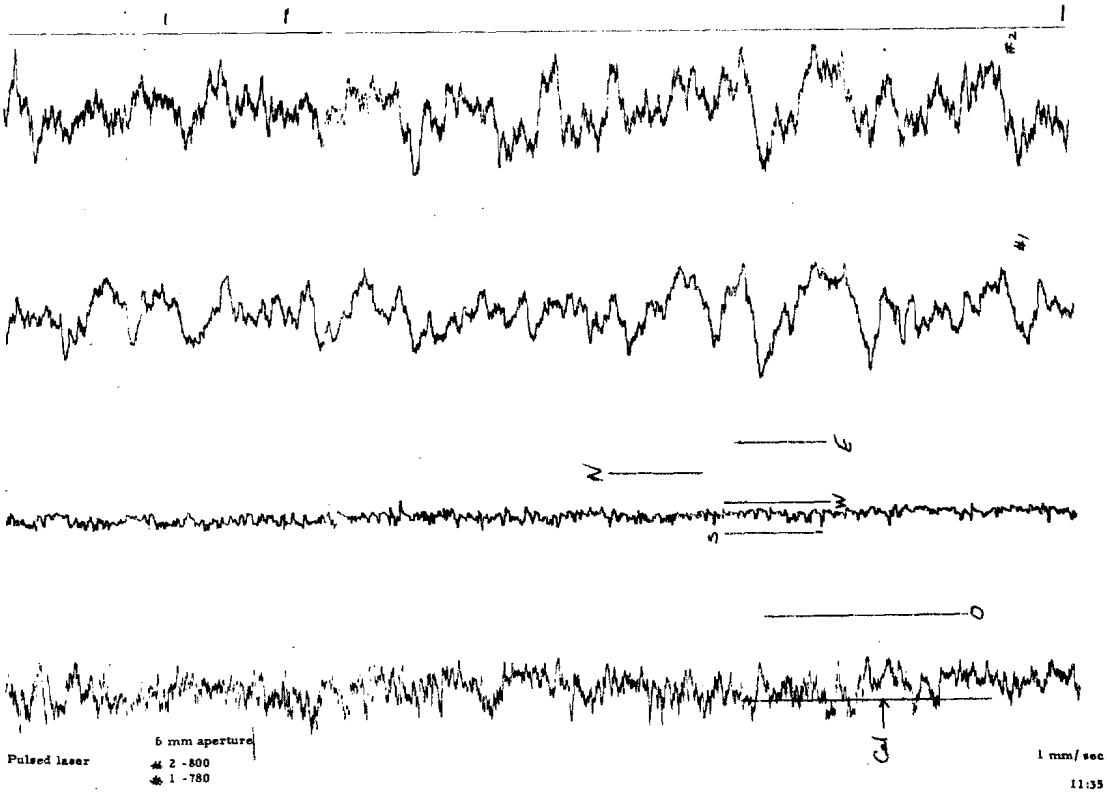

Figure 3.4.10 Eddy-correlation observation using pulsed laser.

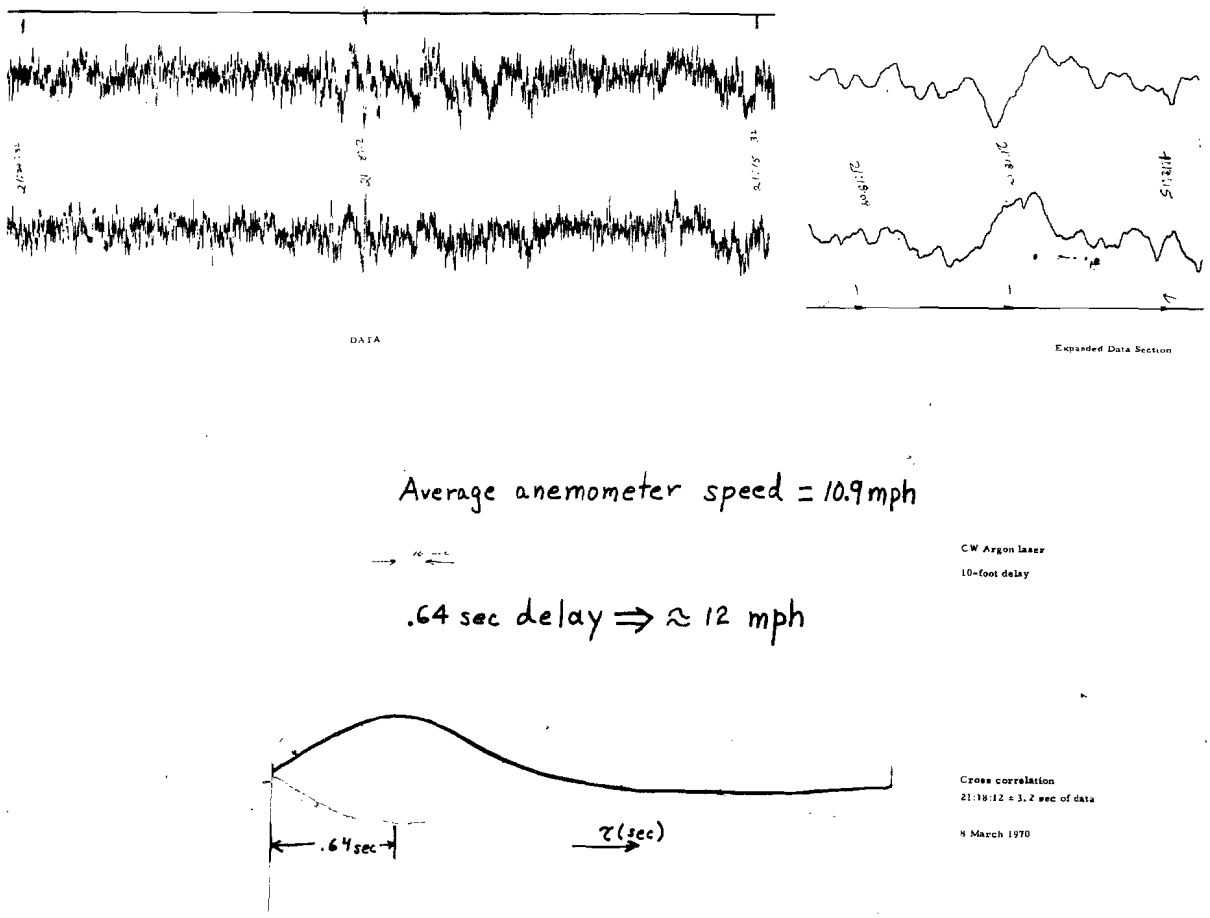

Figure 3.4.11 Measurement of wind velocity by eddy correlation.

power is monitored in the next trace, with an expanded scale that shows fluctuations of nearly 2 percent. (The laser fluctuations are the chief limitation in this experiment.) The next two traces show the west and east detector outputs. A 0.3 sec integration time was used. The data presented in this figure are typical excellent S/N situations. They do not always occur. Experience has shown that lower wind speeds and light and variable winds produce poorer signals. During the time covered by this trace, the wind direction and speed remained quite constant, and the laser power did not drift.

The lowest trace of Figure 3.4.12 shows the wind speed calculated from the delay at the maximum of the correlation function (1.1:1), as previously described in Section 3.4.1.1. The analog data were digitized at 10 points per second. The correlation function and the delay at maximum were computed over a 20 sec integration time, every 2 sec. The velocity obtained by dividing the separation by the delay is plotted. The results are accurate within the limitations discussed earlier. The accuracy deteriorates when fluctuations decrease as between 22:50:20 and 22:58:40. On this chart, the delay and hence the velocity may be measured by eye in many places. However, the smoothing imposed by the correlation calculation increases accuracy. Insufficient study has been made of the optimum averaging times and of other parameters in the calculation to determine optimum procedures.

3.4.6 SAFETY CONSIDERATIONS

Laser systems are inherently dangerous to human eyes, and they must be operated so that no possible injury can occur. A primary safety step is to restrict the area where the equipment operates, but to be useful in wind measurement, the laser beam must project into the atmosphere where it could be intercepted by aircraft. Two methods of preventing eye damage to aircraft personnel are: (a) to lower the power density by defocusing, or (b) to choose a wavelength

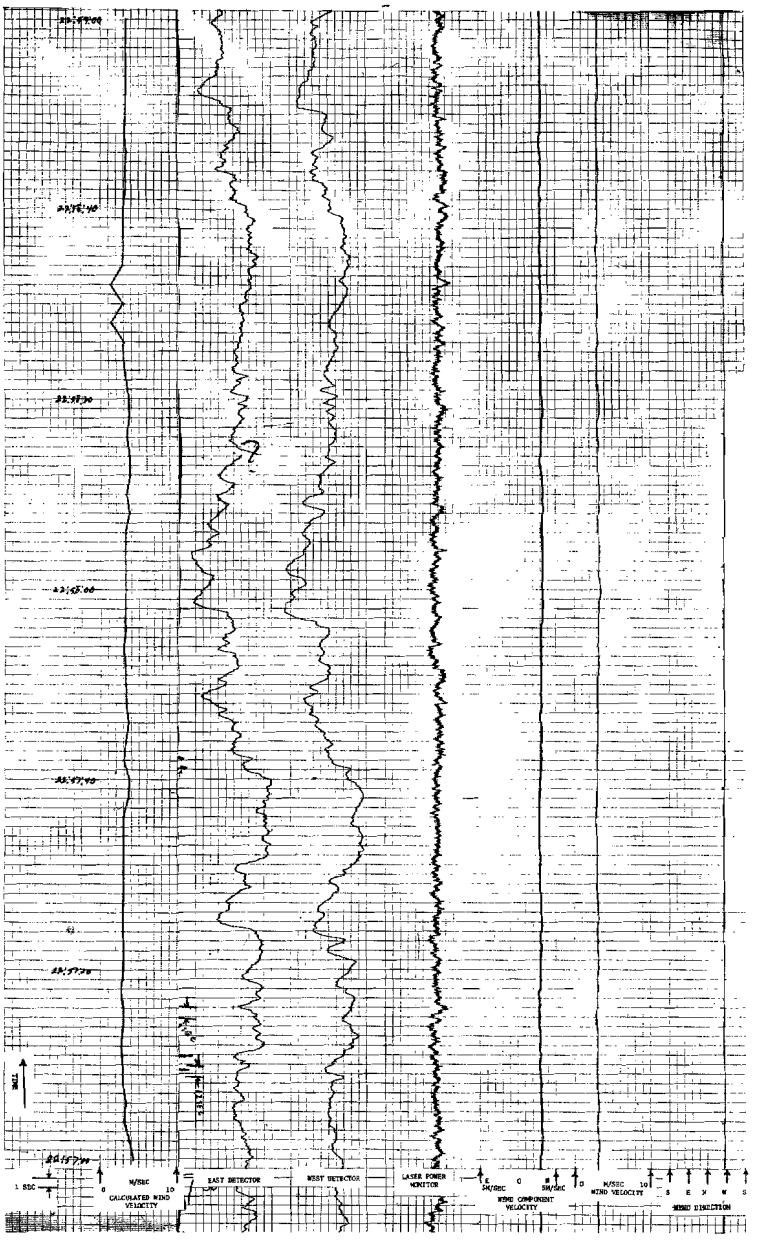

Figure 3.4.12 Calculation of wind velocity from eddy correlation measurements.

that is absorbed by aircraft windows. Some wavelengths do not penetrate the human eye to the retina where damage is irreversible. Lasers at these wavelengths could be defocused so that the power density will not burn the cornea.

The infrared CO_2 laser considered in this proposal is probably the safest high-power laser that can be used near aircraft. The radiation does not penetrate the cornea at any foreseeable power level. The cornea is relatively resistant to damage. If the exposure is less than $0.56\ t^{-3/4} J\ cm^{-2}$ where t is the time of exposure (on the order of microseconds), then the cornea is safe. Further, the CO_2 laser radiation will not penetrate the windows of aircraft, either glass or plastic. Based on estimates given in Laser Focus (May 1972), this laser is completely safe around airports.

The ultraviolet N_2 laser can also be made completely safe by defocusing. Most aircraft windows will absorb the major portion of the radiation.

Further, it should be realized that the probability of the human eye intercepting a laser beam in space is exceedingly low because the speed of the aircraft carries the eye through the beam very quickly. Due care must be given to laser safety problems, but they can be solved without excessive costs.

3.4.7 CONCLUSIONS

The experimental results given in Section 3.4.5 were carefully selected to illustrate various points. However, the careful examination of more than 20 hours of data shows that signals are received with adequate S/N, sufficiently often to measure wind velocity with the nonoptimum equipment employed. Using equipment analyzed in Section 3.4.1.3.2, we can expand the technique to greater range. The chief uncertainty lies in our ignorance of the mean aerosol distributions and of the fluctuations from those averages as functions of altitude. The best data on mean aerosols presently available are those given in Section 3.4.1.3.2. The density of aerosols at 1 km is not reduced as much as an order of magnitude from that at ground level. The determination of these statistics would be an important preliminary to a final evaluation of the feasibility of the method.

If we may assume that the fluctuations of aerosol content at 1 km altitude are not so much less than at 50 m so that the signals become unobservable, we conclude that the laser systems described in subsection 1.3.2 will allow the determination of wind profiles with a few tens of meters resolution up to 1 km within periods of a few minutes, on the average.

ACKNOWLEDGEMENTS

The authors thank R. Slusher for calculations, G. T. McNice for the development of the equations of Section 1.3.1 and F. Hall and R. Schwiesow for discussions on scattering.

REFERENCES (Chapter 3, Section 4)

Chu, T. S. and D. C. Hogg (1968), Effects of precipitation on propagation at 0.63, 3.5, and 10.6 microns, BSTS, 47, pp. 223-759.

Harris, F. S., Jr. (1969), Changes in polarization and angular distribution of scattered radiation during cloud formation, Appl. Opt. 8, No. 1, pp. 143-145.

Krause, F. R., V. E. Derr, N. L. Abshire, R. G. Strauch (1969), Remote probing of wind and turbulence through cross-correlation of passive signals, Proc. 6th Int. Symp. on Remote Sensing of Environment, University of Michigan, Ann Arbor, pp. 327-359.

Little, C. G., V. E. Derr, R. H. Klein, R. S. Lawrence, R. Lhermitte, J. C. Owens, J. D. Thayer (1970), Remote sensing of wind profiles in the boundary layer, ESSA Technical Report ERL 168-WPL 12, Boulder, CO.

McClatchey, R. M., R. W. Fenn, J.E.A. Selby, F. V. Volz, J. S. Garing, (1971), Optical properties of the atmosphere, (revised), Env. Res. Paper No. 354, AFCRL-71-02279.

Rosenberg, G. V. (1967), The properties of an atmospheric aerosol from optical data, Izv. Atmos. and Ocean. Phys. 3, No. 9, pp. 936-949.

Sanborn, V. (1969), A Atmospheric exploration by remote research probes, National Academy of Science -National Research Council, Washington, D.C., -pp.589-594.

Tatarski, V. E. (1967), Wave Propagation in a Turbulent Medium, Dover, N.Y.

Handbook of Geophysics for Air Force Designers (1957), United States Air Force.

Handbook of Geophysics and Space Environments (1965) McGraw-Hill Book Co., Inc., N.Y.

SECTION 3.5 PASSIVE DETECTION OF WIND PROFILES WITH GROUND BASED PRESSURE SENSORS

(by J. Tant Priestley and Earl E. Gossard)
submitted December 1972

3.5.1 INTRODUCTION

In this section, we examine the possibility of deducing winds aloft, and their height gradients, from passive measurements made at the ground. Specifically, we consider the use of spaced pressure sensors at the ground to continually monitor wind structure, and we estimate the accuracy and height resolution to be expected from such a system of moderate cost.

The principle behind this approach rests on the hydrodynamic filtering effect of the atmosphere which causes high frequency (or small-scale) pressure fluctuations to die out a short distance from the source, while larger scale features can be sensed at greater distances. Thus, a pressure sensor at the ground will sense small-scale fluctuations only from turbulent wind fluctuations near the ground, but larger scales can be sensed from higher in the atmosphere. Therefore, if the large-scale frequency components in the spectrum are moving over the sensor array more rapidly than the small-scale components, it is safe to conclude that the winds aloft are carrying the turbulent features past the sensors more rapidly than are the winds near the surface and the wind apparently increases with height. Conversely, if the larger scales move past the pressure sensors more slowly than the smaller scales, we would conclude that the wind speed decreases with height.

The method can be made quantitative by carrying out full cross spectrum analyses between multiple sensors, and in principle it can provide the kind of height resolution required by the FAA in the present application. The phase cross spectrum yields velocity as a function of frequency and therefore provides the velocity vs. scale information needed.

A complete experimental evaluation should be conducted; but within the funding limitations of the present study we have used data available in the literature, along with theoretical analysis to arrive at a judgment of its feasibility.

3.5.2 THEORY

In order to relate wind fluctuation to pressure fluctuations we use the Navier-Stokes equation and the equation of continuity for an incompressible fluid to obtain the Poisson equation

$$\nabla^2 p = -\rho \frac{\partial^2 (u_i u_j)}{\partial x_i \, \partial x_j} \qquad (3.5.1)$$

where p is the pressure perturbation, $\underset{\sim}{u}$ is the velocity field perturbation, and $\underset{\sim}{x}$ is the position vector of the sensor. If we locate the pressure sensor at the bounding surface (of the earth), say $x_3 = 0$ we can by means of Green's Function write

$$p = \frac{\rho}{4\pi} \int \frac{d\underset{\sim}{y}}{|\underset{\sim}{x}-\underset{\sim}{y}|} \frac{\partial^2}{\partial y_i \partial y_j} \left[u_i(\underset{\sim}{y})\, u_j(\underset{\sim}{y}) \right] \qquad (3.5.2)$$

where $\underset{\sim}{y}$ is the location (say the height) of the velocity perturbation contributing to the pressure perturbation. The integral is over y. Although the evaluation of this integral would have to be done numerically for an arbitrary function $u_i(\underset{\sim}{y})\, u_j(\underset{\sim}{y})$, some features are clear. The influence on the pressure perturbation dies off quickly with separation $|\underset{\sim}{x} - \underset{\sim}{y}|$ of the pressure sensor and the contributing velocity perturbation (i.e., it dies off with height). Also it is clear that the perturbation of pressure depends on the magnitude of the product $\overline{u_i u_j}$, in other words on the velocity correlation function. For large-scale features, the correlation is high between elements separated by large distances, but for small scale features the correlation is low over large distances. Therefore, only large-scale features will influence the pressure sensor if the feature is high in the atmosphere. If, instead of the cross covariance function $\overline{u_i u_j}$, we use the cross spectrum, we can sort out the velocity of each frequency component across the array and map this information into a plot of velocity vs. height. The modulus of the cross spectrum is the square root of the narrowband coherence ($\mathrm{coh}^{1/2}$). The cross spectrum is obtained by Fourier transforming the cross correlation into the frequency domain. In addition to the coherence spectrum, the Fourier analysis yields the phase spectrum which is the phase lag between sensors for each frequency resolved by the analysis. From the phase spectrum the velocity and direction across the array of each frequency and each wavenumber in the spectrum can be determined.

3.5.3 SPECTRUM OF WALL PRESSURE IN TURBULENT FLOW

Little experimental data on wall pressure fluctuation spectra exist except from wind tunnel measurements. However, measurements in the atmosphere near the earth's surface have been reported by Gossard (1960),

(Herron et al., 1969; Kimball and Lemon, 1970). The only extensive analysis of cross spectra of pressure fluctuations in the real atmosphere was done by Priestley (1966). Analysis of the theoretical problem has been attempted by Obukov (1949) and White (1964). Laboratory measurements have been made by Bull et al. (1963) and by Corcos (1963,1964). White finds the theoretical relationship between spectral power density and frequency of pressure fluctuations at a wall sensor in a boundary layer of finite thickness, δ, to be as shown in Figure 3.5.1. In this figure ϕ_ω is power, u_∞ is the velocity of the flow outside the boundary layer, and ρ is density. Priestley's measurements in the real atmosphere are shown in Figure 3.5.2 and the general agreement with White's calculation is impressive. Priestley's real atmosphere measurements are perhaps more in accord with a ω^{-2} law as found by others (i.e., Gossard, 1960) than the form indicated by the finite boundary layer theory, but the agreement seems adequate. Thus, the form of the pressure spectrum in the atmospheric boundary layer appears to be fairly well understood.

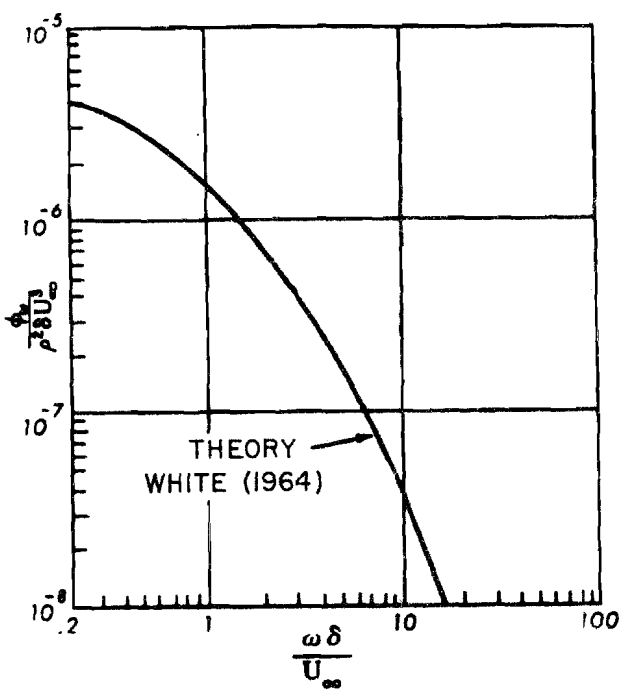

Figure 3.5.1 The theoretical wall pressure power spectrum of White (1964).

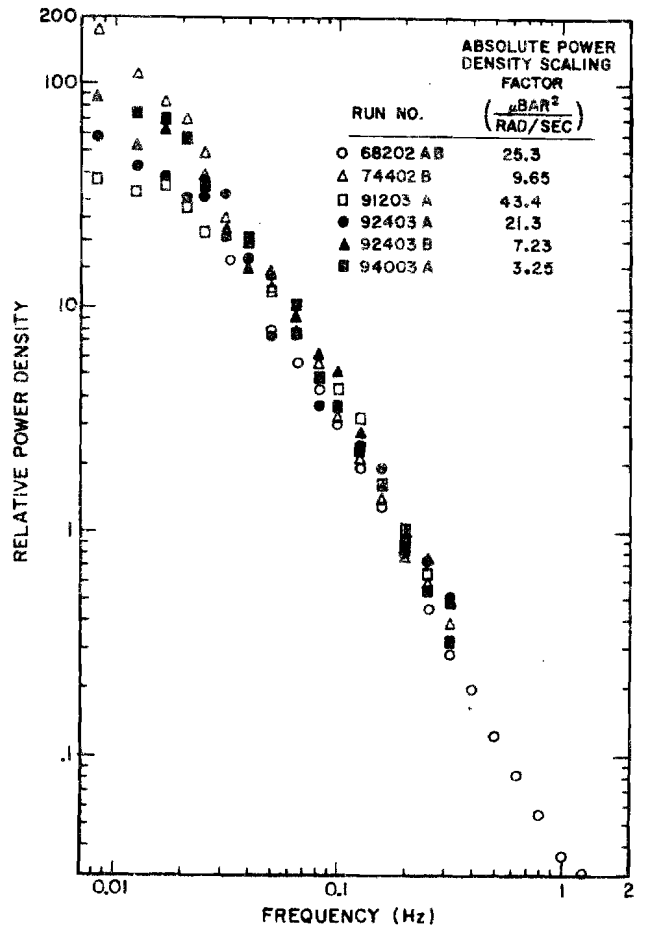

Figure 3.5.2 Composite plot of normalized power spectra for the more typical data.

Formally, the cross correlation between temporal records at stations separated by a distance ξ can be expressed as the Fourier transform of the cross power spectrum, i.e.,

$$R(\tau, \xi) = \int_{-\infty}^{\infty} |E(\omega, \xi)| \, e^{i\omega\tau} \, d\omega \qquad (3.5.3)$$

where τ is the time lag in the correlation analysis. In general E is complex, so if we have two time series

$$E(\omega) = C(\omega) + i\, Q(\omega) \qquad (3.5.4)$$

where the cospectrum $C(\omega)$ is the spectrum of the in-phase components in the (two) records and $Q(\omega)$ is the quadrature spectrum, or the spectrum of the out-of-phase components. If there is no "lag" between the records, or if the time lag has been artificially adjusted to zero, the cross spectrum $E(\omega)$ is just the cospectrum, $C(\omega)$ and is real. For a single frequency component we might then write the correlation R_ω as

$$R_\omega(\xi) = A_\omega(\xi) \cos(k\xi) \qquad (3.5.5)$$

where A is a monotonically decreasing function of ξ which approaches zero asymtotically, and k is the wave number.

Both Priestley (1966) (in the atmosphere), Willmarth and Wooldridge, 1962 (in a wind tunnel) found that experimentally $A_\omega(\xi)$ falls off exponentially with separation, so that

$$A_\omega(\xi) = e^{-\alpha\xi} \quad . \qquad (3.5.6)$$

The situation is summarized in Figure 3.5.3 in which theoretical curves from White (1964) for various values of the dimensionless wavenumber $\frac{\omega\delta}{u_\infty}$, are shown plotted against the data of Willmarth and Wooldridge.

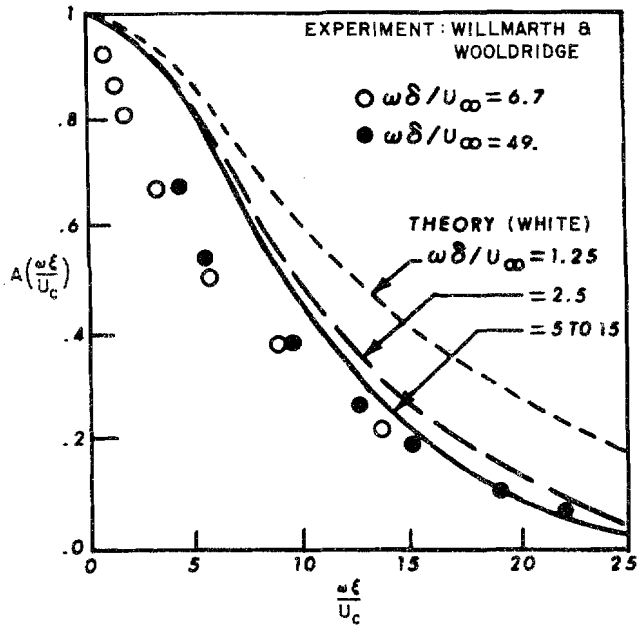

Figure 3.5.3 Optimized longitudinal correlation coefficient (White, 1964, from Figure 6).

It is evident that the data approach the origin in a sharp cusp as in an exponential function rather than approaching it with zero slope as the theory of White would predict. The rate at which A_ω (or $\mathrm{coh}^{1/2}$) falls off with distance is, of course, determined by α. The behavior of α was explored by Priestley (Figure 3.5.4) and found empirically to be

$$\alpha = 0.33\ k^{1.28} \qquad (3.5.7)$$

where α and k are expressed in reciprocal meters. For small scales (i.e., large k) $A(\xi)$ will become unmeasurably small unless we use small sensor separations. It is recommended that a logarithmic spacing of pressure elements on the ground be chosen to satisfy the requirement for detailed small-scale wind structure near the ground, and the need for grosser structure to higher elevations.

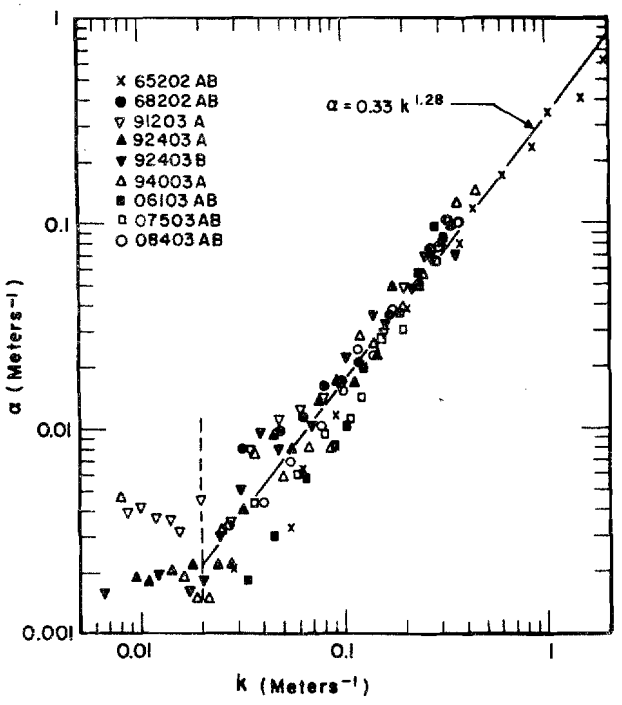

Figure 3.5.4 Reciprocal longitudinal scale α versus wave number k.

3.5.4 PHASE SPECTRUM AND CONVECTION VELOCITY

We have so far only discussed the coherence spectrum, but the primary measurable for our present purposes is the phase cross spectrum between spaced sensors. This provides the phase lag between any pair of sensors for each frequency component in the spectrum. Thus, if we know the separation of the sensors, the phase lag for each frequency gives us the velocity across the array (convection velocity) for each frequency and therefore each wavenumber also.

If the records from two recorders have a time lag for best matching (best cross correlation), the cross power spectrum will be complex unless the time lag is artificially removed. The quadrature spectrum is then no longer zero and

$$E(\omega) = \sqrt{C^2 + Q^2}\ e^{i\theta(\omega)} \qquad (3.5.8)$$

where

$$\theta(\omega) = \omega\tau = \tan^{-1}\frac{Q}{C} \quad . \qquad (3.5.9)$$

The phase spectrum is $\theta(\omega)$ and τ is the time lag between the records at the frequency, ω. The coherence,

$$\text{coh} = C^2 + Q^2 \quad , \qquad (3.5.10)$$

is the $(\text{magnitude})^2$ of the cross spectrum and has already been discussed.

The phase spectrum is the primary measurable for our present purpose since it provides the basic velocity vs. frequency information needed to map velocity into a height profile of wind. With modern computers of moderate capacity the spectral computations can be carried out in real time for several sensors. The required height resolution determines the number of pressure sensors needed and therefore the number of pairs of sensors that must be analyzed. This in turn, determines the capacity and speed of the computer needed. The form of weighting function needed to translate velocity vs. k information to velocity vs. height is provided by Equation (3.5.2). The necessary relationship of "correlation scale" $1/\alpha$ to wavenumber needed in Equation (3.5.2) can be estimated from Equation (3.5.7). However, the best approach will probably be an empirical determination of the relationship between scale size and height, using theory for guidance in the appropriate measurements and scaling.

Actual measurements are scarce for verifying the validity of this approach to velocity profile determination. In fact the only data available are those of Priestley (1966) shown in Figure 3.5.5. Although only two levels of in situ anemometer measurements were available for comparison, the agreement is certainly impressive. It is also obvious that the profile obtained is reasonable in the sense that a more or less logarithmic profile is to be expected under uniform conditions of flow over flat terrain. Clearly more measurements are urgently needed.

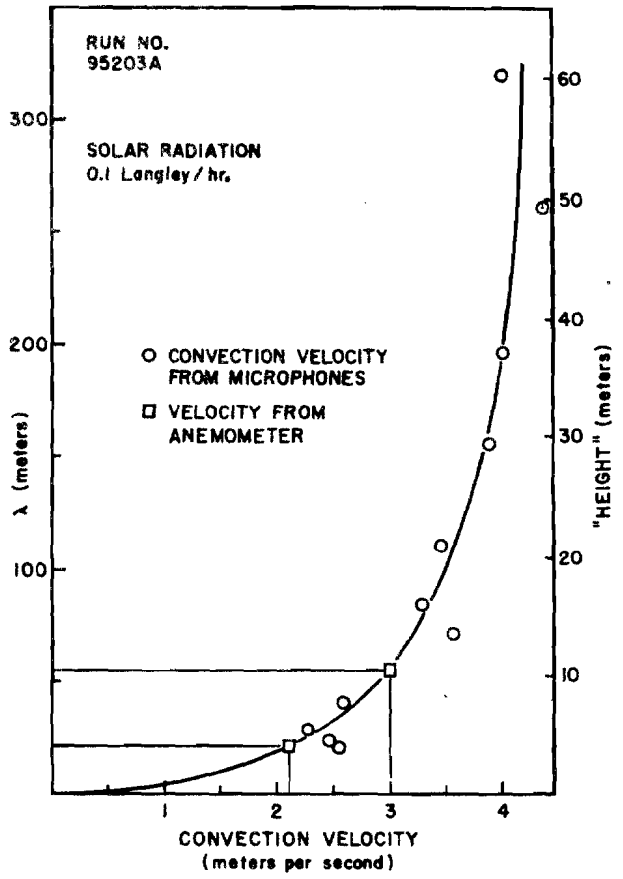

Figure 3.5.5 Relation between convection velocity and wavelength for run 92403A

3.5.5 PROPOSED CONFIGURATION OF SYSTEM

We suggest a configuration of spaced pressure sensors consisting of two lines of sensors at right angles to each other so that the direction as well as speed of the horizontal wind can be obtained. The spacing of the sensors in each line should be more or less logarithmic. We suggest that the array be aimed at resolving winds at the following heights: 30', 50', 75', 112', 170', 255', 380', 570', 1140' and 2280'. For this height range it would be desirable to have sensor spacings on the surface at separations of approximately 20', 60', 100', 150', 224', 340; 510', 760', 1140', 2280' and 4560'. We suggest an arrangement something like that shown in Figure 3.5.6.

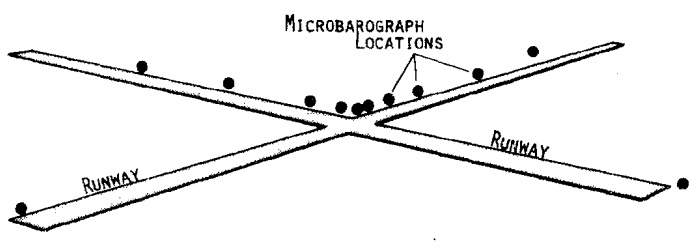

Figure 3.5.6 Suggested airport arrangement

3.5.6 CONCLUSIONS

We conclude that a passive system of surface pressure sensors can come close to satisfying the FAA requirements as stated. However, the system is basically not well-suited for measuring thin regions of large shear to great heights. Consequently, the array would have to be larger than would be necessary for other applications, and the computer processing system would be sophisticated and expensive. To obtain adequate statistical confidence for the large scales of the upper levels, long integration time (about 20 min running time sample) would be required. Lower in the atmosphere much shorter samples could provide better time resolution.

The advantages of the system are: (1) It is passive. (2) It requires very little attendance. (3) Maintenance should be minimal.

The disadvantages are as follows: (1) The initial cost would be high because of the on-line, dedicated computer required. (2) Many sensors are needed in the array to obtain the required height resolution and statistical confidence. This increases cost and complexity. (3) The winds obtained would be horizontally averaged over the array as a whole. This may be an advantage in some applications. (4) A large amount of initial software would be required and some R&D would be needed to optimize the mathematical profile inversion methods to be used. (5) Since the technique depends upon velocity induced pressure fluctuations, it will probably not give reliable information at altitudes above the turbulent boundary layer. Typically, this might vary between 1000 and 5000 feet.

REFERENCES (Chapter 3, Section 5)

Bull, M. K., Wilby, J. F., Blackman, D. R. (1963), Wall pressure fluctuations in boundary layer flow and response of simple structures to random pressure fields. University of Southampton A.A.S.U. Report No. 243.

Corcos, G. M. (1963), Resolution of pressure in turbulence. J. Acoust. Soc. Am. 35, No. 2, 192-199.

Corcos, G. M. (1964), The structure of the turbulent pressure field in boundary layer flows., J. Fluid Mech, 18, 353-378.

Gossard, Earl E. (1960), Spectra of atmospheric scalars, J. Geophys. Res., 65, No. 10, 3339-3351.

Herron, T. J., Tolstoy, I., Kraft, D. W. (1969), Atmospheric pressure background fluctuations in the mesoscale range, J. Geophys, Res., 74, No. 6, 1321-1329.

Kimball, B. A., Lemon, E. R. (1970), Spectra of air pressure fluctuations at the soul surface, J. Geophys. Res., 75, No. 33, 6771-6777.

Obukov, A. M. (1949), Pulsations of pressure in turbulent streams. Doklady ANSSSR, 66, p. 17.

Priestley, Joseph Tant (1966), Correlation studies of pressure fluctuations on the ground beneath a turbulent boundary layer, NBS Report 8942.

White, Frank M. (1964), A unified theory of turbulent wall fluctuations. U. S. Navy Underwater Sound Laboratory Report, No. 629.

Willmarth, W. W., and C. G. Wooldridge (1962), Measurement of the fluctuating pressure at the wall beneath a thick turbulent boundary layer, J. Fluid Mech., 14, 187-210.

SECTION 3.6 ACOUSTIC ANGLE OF ARRIVAL WIND SENSING TECHNIQUE (by A. Mahoney) submitted December 1972

3.6.1 INTRODUCTION

In the initial acoustic sounding experiments conducted at the Weapons Research Establishment during the period, 1966 to 1967, a concrete, parabolic antenna, 15 m in diameter, was employed in a vertical monostatic mode. The operating frequency was about 750 Hz, the beamwidth, 2°, and a peak radiated power of about 20 W was obtained using an exponential horn at the focal point of the antenna. Using this system we obtained good records (particularly during relatively stable, anticyclonic conditions) of turbulent layers associated with both elevated subsidence inversions and airflow over a nearby range of hills. With the introduction of much smaller acoustic arrays in 1967, the magnitude of the signals received using these arrays was found, in many cases, to be comparable with or to exceed the signal levels received with the larger parabola. The degradation of the performance of the large antenna was subsequently found to be due to the horizontal transport of pulses of sound by horizontal airflow in the region between the ground and the height of the scattering volume. The scattered acoustic radiation was returning to the antenna at angles to the vertical which, in many circumstances, exceeded the narrow beamwidth of the large parabola, with a subsequent reduction in the "effective collecting area" (i.e. all of the incoming power was not being focused into the collecting area of the exponential horn at the focal point). The smaller acoustic arrays with larger beamwidths, typically 10°-14°, were not as sensitive to these angle-of-arrival effects.

3.6.2 THEORY

A simple theoretical study of this effect showed that the angle of arrival, θ, of the incoming radiation was, to a first approximation, directly proportional to the mean of the horizontal wind speed in the region between the antenna on the ground and the height of the scattering volume. Experiments were subsequently commenced to determine the feasibility of measuring this angle of arrival to give information on the "mean wind speed" in the lower troposphere ("mean wind speed" is to be taken as the mean of the horizontal wind speed up to the height of a scattering layer). In practice, short pulses of sound are transmitted vertically into the lower troposphere using a monostatic acoustic sounder. In traveling vertically to the height of a scattering layer, the pulse is transported horizontally by the horizontal flow and scattering occurs directly above a point downwind from the antenna. The phase center of the scattered wave also drifts downwind as the wave returns to the antenna, and the measured angle of arrival, θ, becomes

$$\theta \approx 2\,\overline{U}(z)/c \qquad (3.6.1)$$

where c is the velocity of sound and $\overline{U}(z)$ is the mean of the horizontal wind speed, U(z), between the surface and the height, z. In the current system, the angle of arrival from the vertical is determined by measuring the difference in phase, ψ, between the voltages induced (by the incoming wave) in two antennas with phase centers separated by a distance, D.

The angle of arrival, θ, and therefore the "mean wind speed" is obtained from the relationship

$$\psi = (2\pi D/\lambda)\sin\theta \approx (2\pi D/\lambda)\theta \qquad (3.6.2)$$

where λ is the wavelength of the incoming wave and θ is assumed small. Measurements are made along two orthogonal axes, using, for example, three or four antennas in a triangular or square configuration respectively, to give the mean wind speed and direction up to the height of a scattering layer. Where possible, null sensing and analogue feedback techniques are employed to obtain the best estimate of the angle of arrival. Range gating techniques are also used to give values of the mean wind speed and direction at a number of different levels.

In practice, errors are introduced into angle-of-arrival measurements by factors such as phase and amplitude scintillations, the effect of a finite antenna beamwidth, ambient noise, etc. The magnitude of phase and amplitude fluctuations may be estimated from a knowledge of the intensity of the turbulence in the region between the surface and the scattering volume (Tatarskii, 1961). Amplitude scintillations are generally important only at very low signal-to-noise ratios. Phase fluctuations (on the incoming acoustic wave) over a separation, D, between the antenna phase centers are directly proportional to frequency, f, and vary with separation as $D^{5/6}$ and with with propagation distance L, as $L^{1/2}$. Typical values of the corresponding standard deviation, σ_s, for D = 1 m and strong turbulence over a path, L = 100 m, may be $\sigma_s \sim 45^{o}$ at f = 3000 Hz falling to $\sigma \sim 15^{o}$ at f = 1000 Hz. When a finite antenna beamwidth is employed, a distribution of angles of arrival about a most probable angle will be measured. For example, we may be attempting to measure an angle-of-arrival of $\theta \sim 2^{o}$, when $\overline{U}(z)$ = 5 m/sec, using an antenna with a beamwidth of 10°. This source of error may be minimized by using the minimum antenna beamwidth

necessary to maintain adequate collecting area. A desirable system would steer a narrow beam into the direction of the incoming radiation from a particular range gate interval to maintain maximum antanna gain. Ambient noise errors may be minimized by accepting angle of arrival information only during periods of strong signal-to-ncise ratio.

3.6.3 CONCLUSIONS

Two of the advantages of the angle-of-arrival technique are that a single, vertically pointing antenna system may be employed and that vertical Doppler measurements may be conducted simultaneously. Angle-of-arrival and vertical Doppler information are also obtained from the same scattering volume and not, as for inclined monostatic Doppler measurements, along different paths (although, given sufficient averaging periods, for example, 3 to 5 min, this difference may be unimportant). The major disadvantage is that estimates of the "mean wind speed" up to the height of a scattering layer and not (as with Doppler measurements) the wind speed at that height are obtained. If some technique can be derived to give the profile of horizontal wind velocity from angle-of-arrival measurements at a number of levels, the three-dimensional wind field in a common scattering volume (averaged over a period of say 3 to 5 min) may be determined. A method that is now being investigated is as follows: The "mean wind speed", $\overline{U}(z_1)$ up to a height, z_1, is given by

$$z_1\overline{U}(z_1) = \int_0^{z_1} U(z)\, dz \qquad (3.6.3)$$

where $U(z)$ is the horizontal wind velocity at a height, z. By measuring the "mean wind speed," $\overline{U}(z_i)$, at a number of heights, z_i, and fitting a curve $P(z)$ (for example, a least-square polynomial) through the periods $z_i\overline{U}(z_i)$, the profile of the horizontal wind speed, $U(z)$, could theoretically be obtained from the derivative of $P(z)$. An accurate knowledge of the vertical variation of "mean wind speed" $\overline{U}(z)$ would be necessary, since derivatives are involved. The accuracy with which this technique can predict the profile of horizontal wind speed is not known at present. Considerable averaging times (for example, up to five min) and pulse compression techniques (good spatial resolution with long integration periods) may be necessary. At present, experimental results at one or two fixed levels show good correlation, at least between measurements of the mean wind speed up to the height of a scattering layer and the Doppler velocity measured at the layer. Experiments designed to compare angle-of-arrival and Doppler wind velocity measurements are planned.

REFERENCES (Chapter 3, Section 6)

Tatarskii, V. I. (1961), Wave Propagation in a Turbulent Medium (trans by R. A. Silverman) McGraw-Hill.

CHAPTER 4

ACOUSTIC DOPPLER SYSTEM DEVELOPMENT

Doppler wind measurements can be made in any one of several ways, the main variable being the arrangement of the transmitting and receiving antennas, and the sequence in which they are activated. In this chapter we first consider some of the possible antenna configurations and the evolution of tests which led to the experimental configuration used at Stapleton. We then discuss the hardware which was used with this configuration and give details of the final experimental system.

4.1 ANTENNA CONFIGURATION STUDIES

A variety of antenna configurations have been used to measure winds with the acoustic Doppler system. The exact layout of the antennas is critical for achieving optimum range, resolution and noise rejection. In selecting an optimum configuration, one must also consider the nature of sound scattering and the angle which the Doppler vector makes with the horizon (if horizontal winds are to be measured). The intensity of the sound scattered from a given volume of the atmosphere is a function of the scattering angle, defined as the angle measured from the direction of the transmitted ray to the direction of the scattered ray (see Section 1.2.1). Monostatic systems, where the transmitter and receiver are located at the same point, receive only backscattered signals ($\theta = 180^{\circ}$), and these signals are a function of temperature fluctuations only. Bistatic systems, where the transmitter and receiver are separated, but aimed at a common volume, receive signals which are a function of both wind and temperature fluctuations, significantly increasing the signal strength. The intensity of bistatic returns are, further, a function of the scattering angle, peaking at a value near 135°.

A second consideration in selection of an optimum antenna configuration is the angle between the Doppler resolution vector and the horizontal. As was shown in Section 1.2.3, the direction of the Doppler shift for a monostatic system is along the antenna beam. For the bistatic configuration the direction of the Doppler shift is along the bisector of the angle made by the intersection of the transmitted and received beams. For example, a monostatic system tilted at an elevation angle of 45° from the horizontal would measure a Doppler shift or wind component only 45° from the horizontal; however, a bistatic system with a vertically pointed transmitter and a receiver similarly tilted to an elevation angle of 45° would measure a wind component 67.5° from the horizontal. Clearly, as the angle between the total horizontal wind and the component being measured increases it becomes more and more difficult to resolve the horizontal wind. The dilemma then becomes, whether it is more important to consider the high signal strength of a bistatic system with its associated poor Doppler resolution angle, or to improve the Doppler resolution angle with a tilted monostatic system at the expense of stronger signals.

Preliminary tests (see Section 1.3) showed that winds, during selected periods, could be measured successfully by either the monostatic or bistatic system. Additional tests of both systems and combinations of the two systems were carried out during Phase I and II; these tests and their results are summarized below.

4.1.1 Monostatic, Spaced Antennas. This configuration consisted of three separate monostatic antennas similar to that shown in Figure 1.5 with one pointed vertically and the other two separated from the first, pointed upward in two orthogonal vertical planes. The two separate antennas were tilted at elevation angles ranging from 30° to 60°.

The tests of this configuration indicated that very accurate wind speeds could be measured if and when sufficient signal strength was present. The loss of signal during thermally quiet periods and the lack of range (the height of acceptable signals rarely exceeded 200 m during these tests) were much worse than originally anticipated. It was concluded that since the signal strength was a function of highly variable thermal structure in the lower atmosphere a reliable operational system could not be based on this configuration.

4.1.2 Monostatic, Clustered Antennas. This concept was similar to the spaced antenna configuration except the three antennas were clustered together with the tilted beams pointing out from a central point along the orthogonal planes. The results were similar and the conclusion the same as given above.

4.1.3 Bistatic, Fanned or Wide Beam. This configuration was designed to take full advantage of the increased signal strength gained from scattering induced by wind fluctuations. The test configuration was similar to that shown in Figures 4.1 and 5.1, with a single vertically pointing transmitter (A) and two receivers (B_1, B_2) spaced along one of the orthogonal lines intersecting at the transmitter. The distance from A to B_1, was 400 m and from A to B_2, was 700 m. Tests indicated that horn reflector antennas commonly used by WPL had at low frequencies, beamwidths wide enough to cover the ranges indicated in Figure 4.1

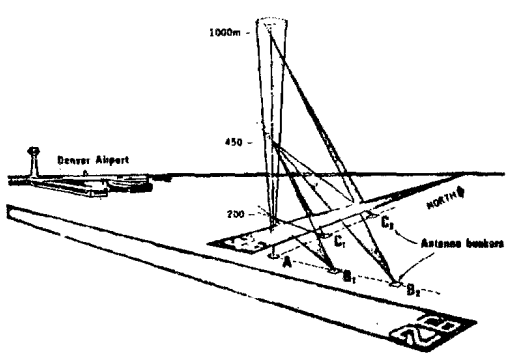

Figure 4.1 Bistatic antenna configuration.

Signal strengths, as expected, were generally adequate throughout most of the range. During these tests it was discovered that the signal strength did, however, fall off rapidly above strong inversion layers. This weak signal region was not anticipated when the 1000 m range requirement was requested in the interagency agreement. It was possible, however, to produce wind profiles at the higher levels which compared well with those from a GMD-1 tracked radiosonde. A second weakness of this configuration was its inability to measure the winds between the ground and 200 m. No sound is scattered at scattering angles of 90°, and only at much reduced intensities at angles near 90° This factor precluded the measurement of low-level winds.

4.1.4 Monostatic-Bistatic Configuration. In an attempt to fill in the lower portion of the measured wind profile, the antennas at locations B_2 and C_2 were activated and operated in a monostatic mode for a brief period of each pulse cycle. In this way it was hoped that the lower winds could be measured in the monostatic mode while the winds aloft could continue to be sensed in the bistatic mode. Tests of this concept were only partially successful. The problem again was continuity of signals, even over short ranges, on the monostatic portion of the system.

4.1.5 Bistatic, Multiple Transmitter. It was apparent that high reliability at all levels could be achieved only with a purely bistatic system. To do this the configuration shown in Figure 4.2 was devised. Here, the powerful transmitter at location A is retained, and in addition, satellite transmitters, generating less acoustic power, are located at A′ and A″ some 50 m in front of the receivers at B and C. The satellite transmitters are tilted to an elevation angle of 70°. Bistatic returns are received at all heights, increasing the probability of receiving continuous strong signals. This configuration was designed to reach altitudes of only 500 or 600 m. If more acoustic power were generated, the second bistatic receiver could be re-introduced (as in the configuration shown in Figure 4.1) and greater ranges might be possible. The reliability at these ranges must remain an unknown quantity, even with higher powers, until more is understood about the scattering properties above certain temperature inversions.

4.1.6 Conclusions. The bistatic multiple transmitter configuration described above was used at Stapleton Airport. Results indicate that the configuration was successful, but certain modifications would still be desirable. The intersections of the beams from antennas A′ and B, and from A″ and C are still not low enough to obtain good wind readings in the first 30 m. This problem might be solved by adjusting the distance between the satellite transmitters and the receivers, but the solution is more likely to lie in the use of different receiving antennas with improved beam patterns. Note that the carrier frequency during the early bistatic tests at Table Mountain was 1000 Hz. This frequency was too low for use at the airport because of the higher ambient background noise, so the carrier frequency was raised. This resulted in the expected narrowing of the antenna beam patterns, a factor which affects the optimum configuration. Again, this aspect of the problem is more readily treated by antenna redesign. The remainder of this Chapter is devoted to the equipment used with the configurations described above.

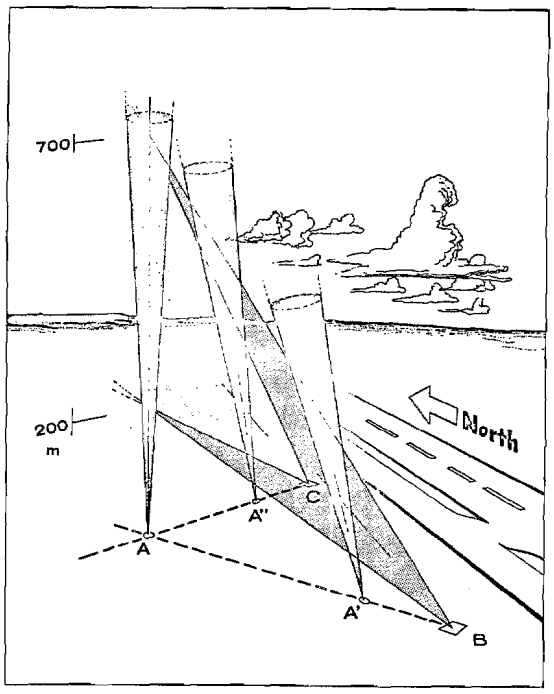

Figure 4.2 Multi-transmitter bistatic antenna configuration.

4.2 BASIC COMPONENTS REQUIRED

The Acoustic Doppler Wind Measuring System can be thought of as a collection of sub-systems interfaced to produce the operating unit. These sub-systems are (a) the transducers, preamps, and antennas, (b) the basic acoustic sounder, (c) a computer, and (d) a display. A block diagram of the entire system is shown in Figure 4.3. The acoustic sounder provides the basic control and timing for the entire system be generating and amplifying tone bursts for the transducers, receiving and amplifying the signal picked up by the antennas, extracting the Doppler shift, and then sending the signals to an analog-to-digital (A/D) converter for use in the computer. The antenna sub-system includes the transducers which convert electrical power into acoustic power and vice versa, the antennas which reflect and focus the acoustic waves, and the preamplifiers which amplify the weak received signal from the transducer for transmission to the acoustic sounder sub-system. The computer collects and processes data from the sounder, tests for validity, and converts the Doppler information into wind values. The display sub-system presents the computer output to the user.

The following sections give details on each of the four sub-systems which make up the Doppler wind measuring unit. Where several techniques or devices were tested for a specific purpose they will be mentioned, but the main emphasis will be on the equipment that was used in the final experimental model at the airport site.

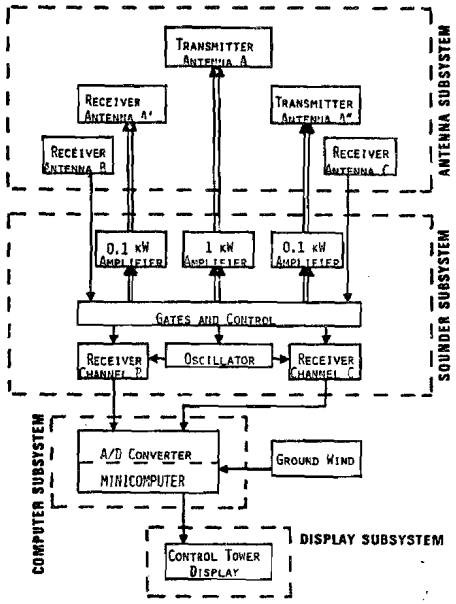

Figure 4.3 Block diagram of Acoustic Doppler Wind System.

4.2.1 Antenna Sub-System. The components of the antenna sub-system are shown in Figure 4.4. The main transmitting antenna, labeled A, was an aluminum parabolic dish 3 m in diameter. The antenna was fed by four 100 W capacity, commercial drivers (more commonly used as theater speakers) wired in series. These four drivers were connected to an acoustic manifold with a common outlet into a single exponential horn at the focal point of the parabolic dish. During each cycle of the system, 800 W of electrical power, in a tone burst that could be varied in duration from 100 to 600 msec, was delivered to the transducers. The power delivered to each driver was twice their design rating; however, the duty cycle was low enough that any excess heat was dissipated and they were not damaged by this momentary overloading. Transducer failure from other causes was a problem and must be corrected by improved engineering in later models. For example, the air gap provided for the voice coil is not always symmetrical, an apparent failure of the manufacturers quality control, and the coil may drag causing shorting and failure of the transducer.

The transmitters shown at A′ and A′′ are identical 1.5 m diameter parabolic dishes, modified from surplus military searchlights. The arc light was removed and replaced with single 100 W transducers and exponential horns. These antennas were acoustically damped and fitted with extended cuffs which reduced the sidelobes and helped to protect the driver from wind eddies, making them suitable for use as receivers or transmitters. Beam patterns for the searchlight antennas, without cuffs, are shown in Figure 4.5.

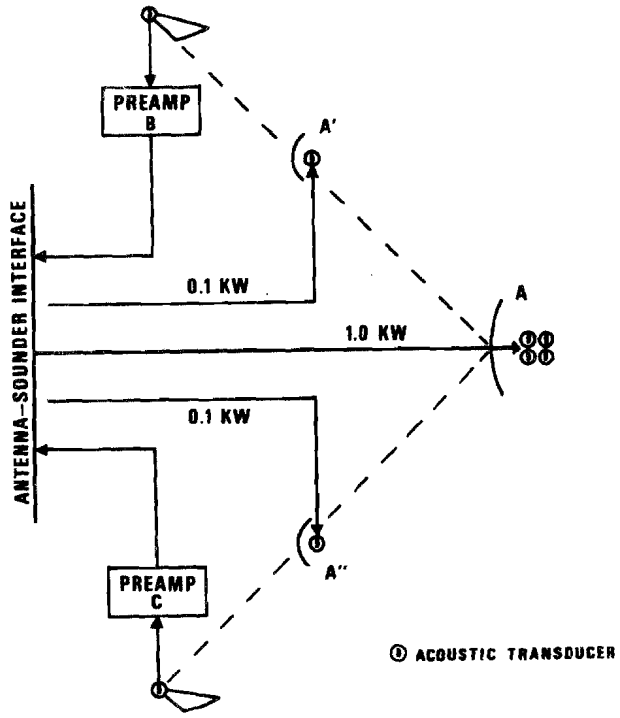

Figure 4.4 Components of antenna sub-system.

The receiving antennas located at points B and C in Figure 4.4 were off-axis parabolic horns; an example of which is shown in Figure 4.6

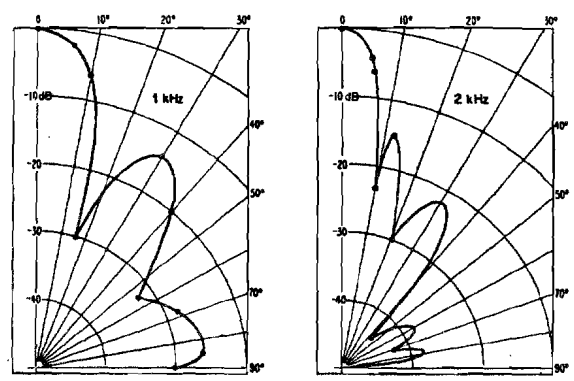

Figure 4.5 Searchlight antenna beam patterns.

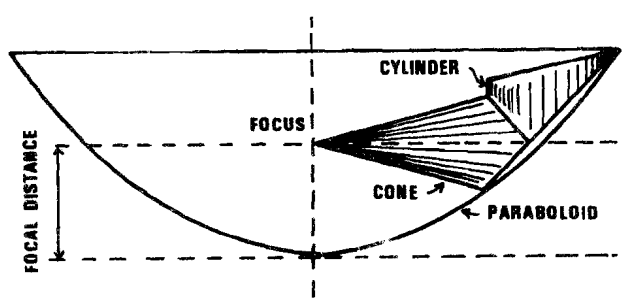

Figure 4.6 Off axis parabolic horn shown with the parabolic shape from which it is derived.

These antennas have excellent sidelobe rejection and at low (1.0 kHz) frequencies produce a half beamwidth of about 15° between the -10 dB points (see Figure 4.7) If it had been possible to use the 1.0 kHz frequency at the airport this antenna would have been more suitable. Unfortunately, it was necessary to use an operating frequency of 1.4 kHz to achieve an acceptable S/N in the airport noise environment. Interpolating between the beam patterns for 1.0 kHz and 2.0 kHz (see Figure 4.7) shows that the beam pattern at 1.4 kHz was too narrow.

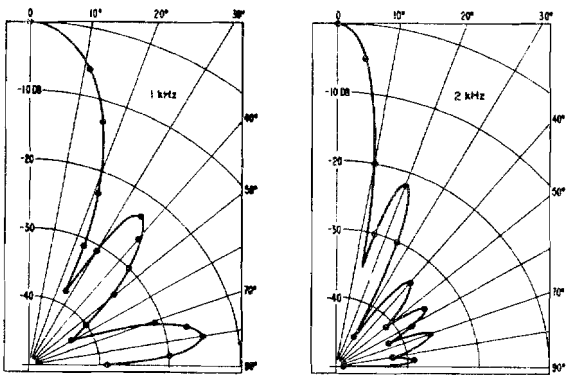

Figure 4.7 Beam patterns for off axis parabolic horn shown in Fig. 4.6.

The complex configurations used for wind profile measurements require special antenna beam patterns to achieve optimum efficiency. The final experimental configuration should use narrow beamwidth (on the order of 10°) transmitting antennas (A, A´, A´´). The receiving antennas (B and C) should ideally have a fan shaped beam which is narrow ($\approx 10^{\circ}$) in the horizontal plane, wide (30° to 40°) in the vertical plane, but with at least 60 dB rejection of horizon noise. The less than optimum beam patterns used at the airport degraded the performance of the system in two ways: first, the wider than necessary horizontal axis of the beam collected unwanted noise, adding to the problem of poor S/N; second, because the vertical dimension of the beam was too small, the wind measurements along the center axis of the beam had high reliability while those near the upper and lower edge were at best marginal.

This problem was recognized early in the work, and both new and modified designs were tested during Phase I and II. One attempted solution used an array of randomly spaced transducers, to produce a theoretical fan beam with a 60° vertical axis and $\approx 20^{\circ}$ horizontal axis. Tests of this antenna at the Haswell, Colorado, field site indicated that the beam shape was near the theoretical prediction; however, the very wide vertical extent of the beam was also a highly efficient collector of ambient background noise. The resulting poor S/N characteristics led to the abandonment of this design.

A second attempt was made to produce a "fan beam" by aperture masking of a 1.5 m diameter parabolic reflector. This produced some changes in the beam shape, but also reduced the collecting area, hence, the efficiency of the antenna. Any loss of efficiency with present antennas was not tolerable and this modification was abondoned in favor of using a lower operating frequency to achieve a wider beam pattern. As pointed out above, this solution was also not optimum.

A second antenna design factor, equally as important as the beam shape, was the method used for shielding the antenna from noise collected in sidelobes, and from strong winds and rain. Satisfactory sidelobe noise rejection can be achieved by surrounding the antenna aperture with sound absorbing cuffs of materials such as lead, convoluted foam, and plywood.

The most successful solution yet found for reducing all of these affects was to place the antenna in an underground bunker. Because the receiving antenna beam is tilted at an angle of 45° to the horizontal, the bunker opening could be located in such a way that the roof of the installation was directly over the face of the antenna, (see Figure 4.8) protecting it from the disastrous noise effect of direct hits by raindrops. In addition, the bunker could be designed to produce minimum change in the local terrain, reducing the potential for the creation of wind eddies. Combined antenna-bunker installations could produce a further variation in the resulting beam shapes, a factor that must be considered when designing the installations.

We feel the problems associated with the present design can be solved; however, further design and testing effort will be required. Among the approaches that should be tested are; (a) a fanned beam produced by aperture masking and increased pulse length or power to maintain received signal strength, (b) a pencil-beam cluster made up of several elements pointed at increasing angles, (c) a phased array of transducers having a narrow beam which can be steered by computer control, and (d) a fanned beam antenna designed to have maximum gain at high elevations.

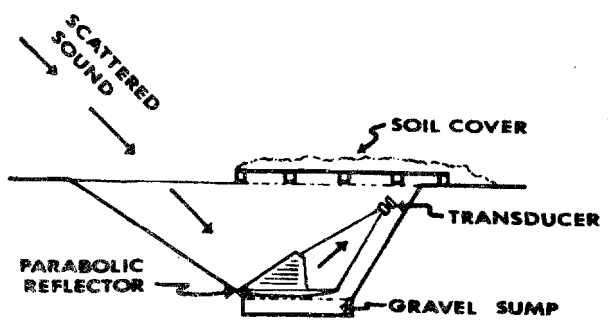

Figure 4.8 Bunker installation with a horn reflector antenna.

The antenna sub-system also included low noise preamplifiers, physically located in the antenna bunkers at points B and C. Cabling, the final part of this sub-system, was extensive and the source of some problems. The very long cable runs (up to 1000 m) acted as RF antennas, and unacceptable oscillations occurred in the preamp circuitry. The addition of hum-bucking circuits, filters, and better grounding eliminated these problems; however, the cabling is an area which will require more design effort in the future.

4.2.2 Acoustic Sounder Sub-Systems. The block diagram shown in Figure 4.9 gives the essential details of the acoustic sounders used to generate the transmit tone bursts and to receive the signals. Except for the single 1.0 kW power amplifier and the central timing generator, the system was comprised of two parallel acoustic sounders, one for each of the receiver legs.

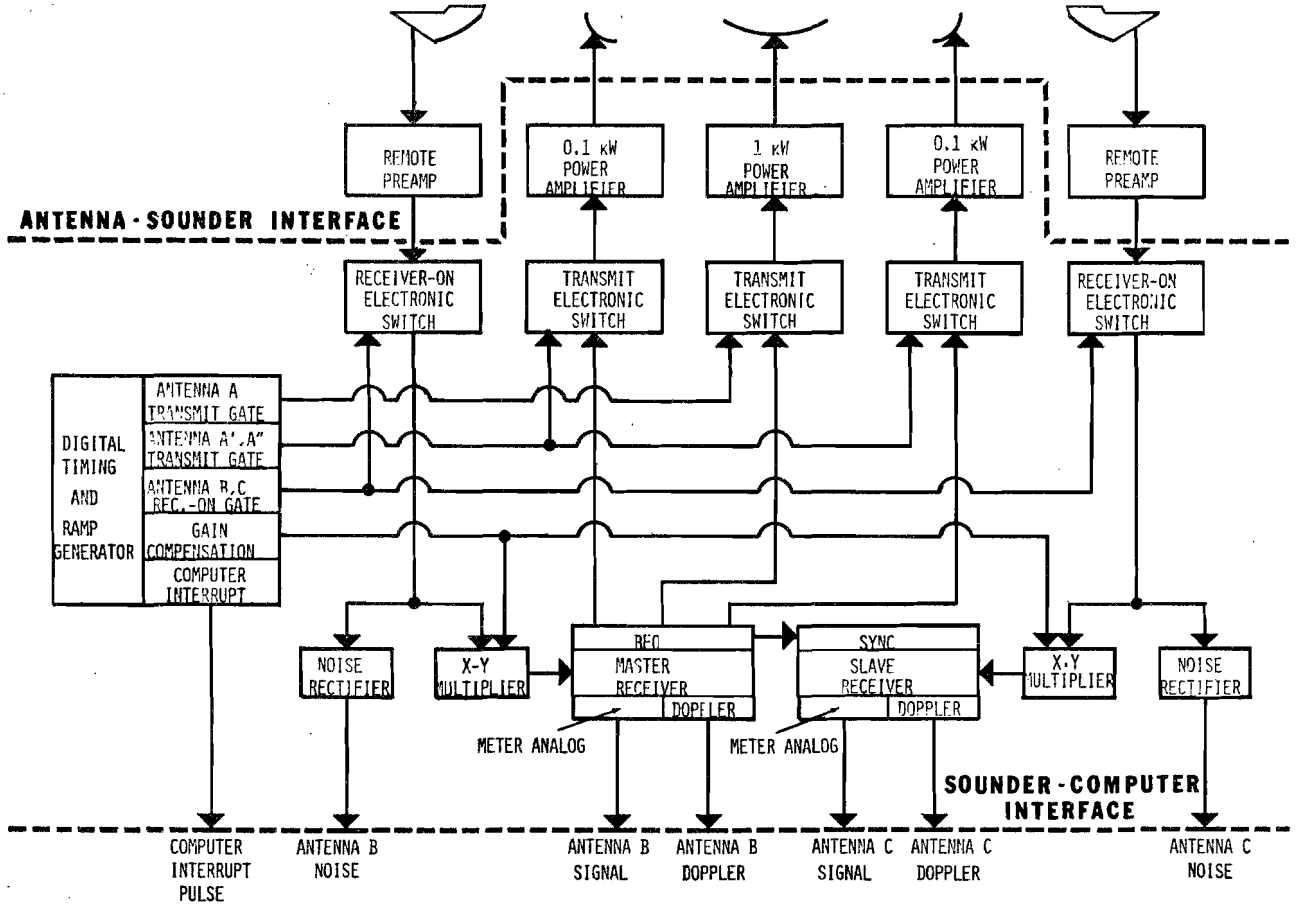

Figure 4.9 Block diagram of acoustic sounder sub-system.

The operation of the acoustic sounder sub-system can be followed from the block diagram in Figure 4.9 and the timing diagram in Figure 4.10. The digital timing and ramp generator provided; (a) the three 0 to + 5V d-c control voltages used to enable the transmit and receive electronic switches, (b) the 0 to + 10V d-c control voltage used as the gain function to one input of the X·Y multipliers in the receive circuits, and (c) the + 5V d-c trigger pulse which was used by the computer to start the processor cycle. The above-listed functions could be varied by thumbwheel switches. The BFO signal coming from the Master Receiver was used both as an input to the transmit electronic switches (then applied to the audio power amplifiers as the transmit tone burst), and to the phase lock input circuits of the slave receiver to insure that both receivers were tuned to the carrier frequency which was transmitted into the atmosphere. The receiver electronic switches in turn coupled the outputs of the remote preamps to the noise rectifier and X·Y multiplier of receiver antennas B and C. These receiver switches were disabled during the actual transmitted tone burst to protect the sensitive receivers from overloading by leak-through signals in the remote preamp electronics. The outputs of the noise rectifiers were available to the computer, along with the meter analog and Doppler analog signals from the receivers through the X·Y multipliers.

The meter analog voltage is a signal that is proportional to the received signal intensity. The Doppler analog voltage is a signal that automatically tunes a voltage-controlled local oscillator (VCO) in the receiver so as to cause the receiver tuning to track the frequency of a received echo. The voltage is developed by a phase detector that senses the departure in phase of the heterodyned echo signal from an IF reference frequency. This error signal quickly returns the VCO, as described above, to reduce the phase error to zero. The rate of returning (tracking rate) is limited primarily by the receiver bandwidth chosen. An optimum compromise therefore must be made between high signal-to-noise ratio (achieved by narrowing the bandwidth) and high Doppler tracking rate (achieved by broadening the bandwidth).

4.2.3 Computer Sub-System. The computer used in the acoustic Doppler system is a 16-bit NOVA 820 having an 800 nsec cycle time and 24K words of core storage. This sub-system included (a) two removable disk pack units capable of storing an additional 2.5 million 16-bit words, (b) an eight channel A/D converter, and (c) a Tektronix 4010 high speed video display terminal. Each disk was used for a specific purpose; one for program development and program storage, and the other for program operation and archiving. The "operations" disk contains the core image program files and their associated overlays which were called

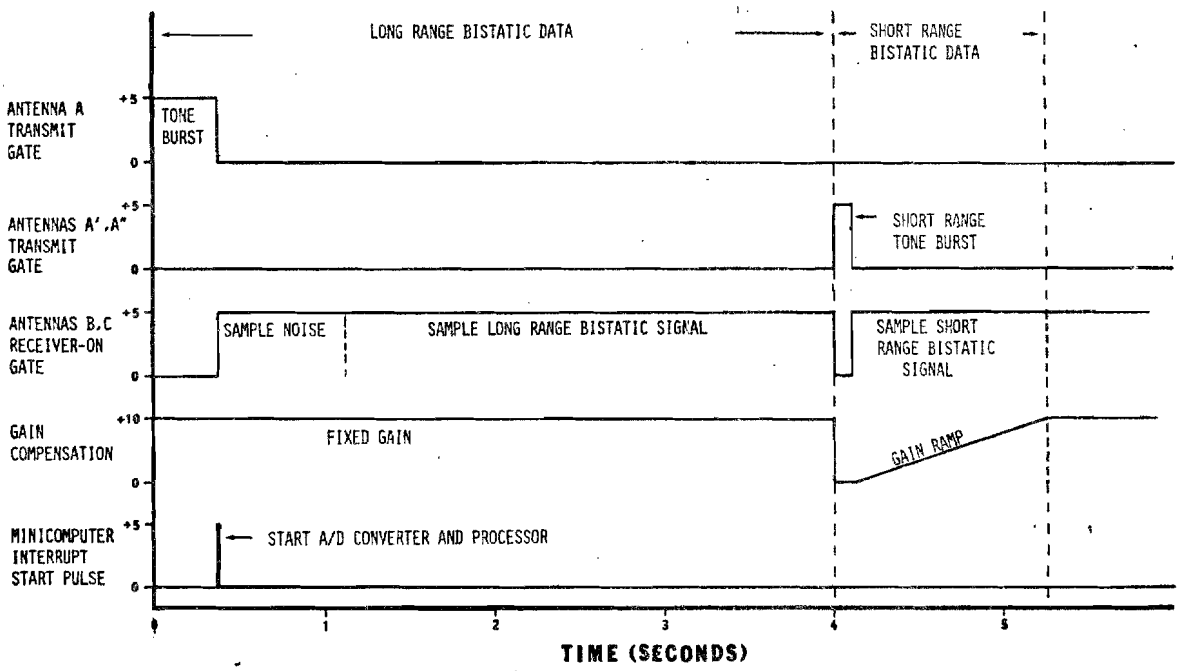

Figure 4.10 Timing diagram for Acoustic Doppler System.

during the Doppler processing, and an archiving file capable of storing up to three weeks of processed data. This archive information was used for off-line reconstruction of the state of the Doppler system, the computed wind profiles, the shear information, and the statistical analysis of the total system operation.

Figure 4.11 shows a block diagram of the complete hardware sub-system. Raw data were transferred from the sounder sub-system through an eight channel A/D converter. The inputs were sequentially quantized into 8 bit samples at a rate of 62.5 Hz per channel (i.e. one sample every 16 msec) and were stored on the disk until an entire profile scan was complete. When the processor was ready, raw data were recalled from the disk, processed in component form, translated into wind speed, direction and shear, and finally displayed both locally and in the control tower.

Figure 4.12 shows a block diagram of the computer software. The Doppler processing program was organized into four logically independent tasks:

1. Processor task
2. Sampling task
3. Tower display task
4. Local display task

These four tasks can operate simultaneously allowing optimum use of the central processing unit (CPU).

Initialization of the program was accomplished in the first overlay of the processor task. A list of about fifty system parameters, such as antenna spacing, receiver calibrations, timing requirements, and test thresholds was stored on the disk. The initialization routine read these "operator" parameters and translated them into "computer oriented" parameters. A list of settings for the thumbwheel switches on the digital timing generator was output on the video display terminal and checks were made to insure that no height gates were masked by the direct pulse from the transmitter.

When initialization was complete, the sampling task was activated. The sampling task awaited an interrupt from the sounder sub-system and then began sampling the input signals for a period of time long enough to cover the specified maximum height. These raw data were double buffered in core and stored on disk in a file accessible to the processor task. When data sampling was finished, the processor task was activated and the sampling task waited for the next interrupt from the sounder.

The processor task then read a complete data file from the disk and averaged these raw data gate by gate. The block averaged data were required to pass three tests before they were used to update the wind components. Before any data from a height gate were received, the ambient noise sensed by the sounder was measured and a "no-signal" signal-to-noise ratio (S/N) determined. When data from the height gates were received and averaged, the computed S/N was checked to determine if it was greater than the "no-signal" S/N before being accepted as valid. To be considered valid, the signal also had to pass a minimum signal test and a maximum signal test. Data from gates which did not pass all three tests were rejected. Information from gates for which valid data were received was used to update the wind components according to the following exponential averaging algorithm:

$$A_k = \frac{D_k + (n-1)\, A_{k-1}}{n}, \quad k = 1, 2, \ldots$$

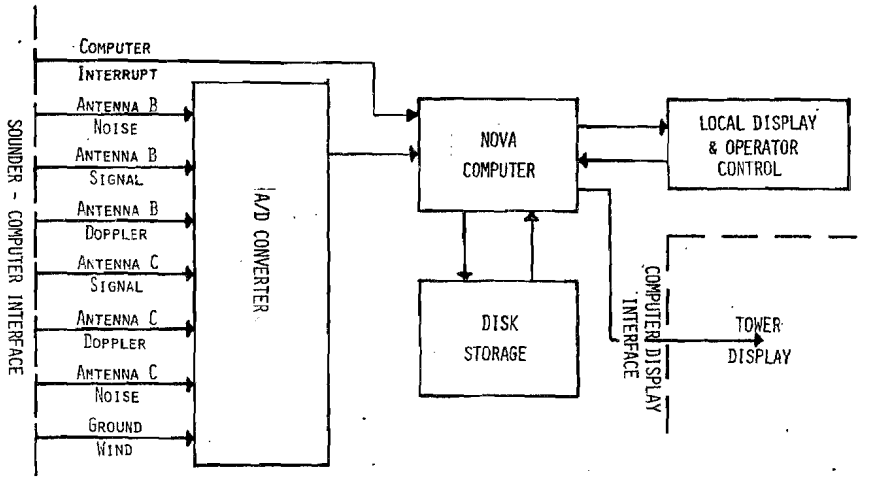

Figure 4.11 Block diagram of computer hardware.

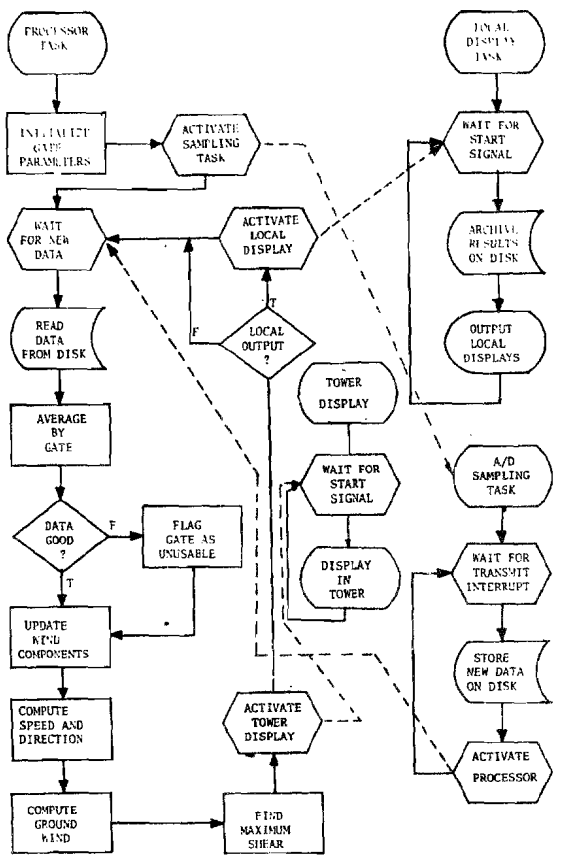

Figure 4.12 Block diagram of computer software.

where A_k was the updated component average for a given gate

A_{k-1} was the previous component average ($A_o = 0$)

D_k was the new Doppler data and

$$n = \begin{cases} k \text{ if } k < N \\ N \text{ if } k \geq N \end{cases}$$

where N was a number of pulse cycles comprising one "time constant" in this algorithm.

The wind speed and direction were then computed from the updated wind components. The ground wind components from an anemometer were also converted into ground wind speed and direction. The complete updated wind profile was then scanned to determine the maximum shear, which was then tested against a predetermined critical value to decide if the tower display shear warning light should be "on."

One of the input parameters was a reliability criterion which determined the confidence to be placed on a given exponentially averaged gate at a given time. If the reliability of the data in a gate dropped below a specified threshold, that gate was not considered in the shear calculations nor displayed on the local output.

Continuing through the processor loop, the tower display was next activated. During each processor loop (normally 10 sec) the updated shear summary was output to the tower display. This task required about 3 sec and was done simultaneously with the other tasks. The details of this task are covered in Section 4.2.4.

The parameters were then checked to determine whether or not the local display task was to be activated. If it was, then a complete graphical profile, a data table describing the profile, and a table of test results was output on the local video display terminal.

This same information was placed on the archive disk every 5 min. Data in the archiving file allowed complete reconstruction of all local display outputs at 5 min intervals for off-line analysis. A sample of part of the local display output can be seen in Figure 6.2.

During the processor and display task intervals, the sampling task accumulated a new data file on the disk. The processor task then waited for a go-ahead from the sampling task, if one had not already been received, and the complete cycle repeated itself ad infinitum or until an operator halted the program. Power failures, and sometimes even large fluctuations in the power supply can interrupt the computer operation. Automatic re-start capability was available, but was not included in this experimental system.

4.2.4 Display Sub-System. In one sense this portion of the system was the most critical. The display must relay information to a user. Failure to do so renders the previously discussed portions of the system useless. The primary goal of the tower display design shown in Figure 4.13 was to achieve an optimum balance between too much and too little information. If all of the wind information stored by the computer were displayed, the user might be needlessly confused. For this reason, the computer analyzed the stored data, selecting only the information which would (a) provide a warning of hazardous wind shear and (b) indicate the level and severity of the wind shear.

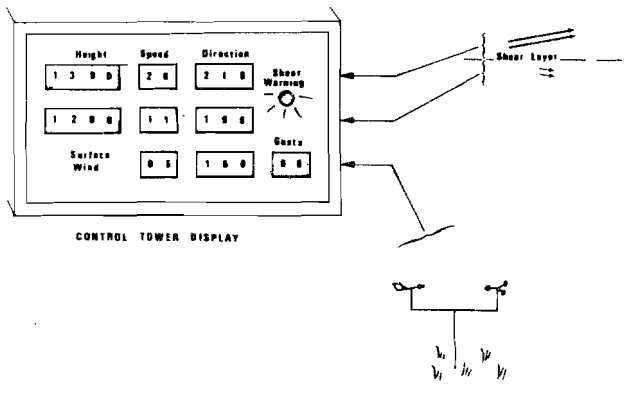

Figure 4.13 Control tower display unit showing the position of wind shear and ground wind readouts.

Each time the wind profile was updated (≈every 10 sec) the computer scanned the data to determine the maximum shear. This information was then displayed as the height, speed, and direction of the winds above and below the shear level. When the calculated shear value was above a critical value that might constitute a hazard to aircraft operations, the computer turned on a red warning light to draw attention to the display.

In addition to the shear information described above, the ground wind and gusts were displayed. This information was taken from a standard surface anemometer and processed for display in digital form by the computer. The objective of displaying the ground wind, information already available in another form in the control tower, was to provide all wind information on a single console in a compact and easily readable format.

The block diagram shown in Figure 4.14 shows the data flow between the computer and the tower display panel. The design and construction of the Remote Tower Display was accomplished by utilizing existing special programming considerations and flexibility built into the minicomputer. The operating system is designed to have a second teletype capable of asychronous transmission of 11-bit-even parity ASCII code at a rate of 110 baud. A second teletype transmitter, identical to the primary teletype transmitter, was built and installed on a special wiring board interfaced to the Echo Sounder Control Unit. The Remote Tower Display could be connected directly, either by use of a BNC cable to the interconnecting panel, or through a data coupler and regular telephone line.

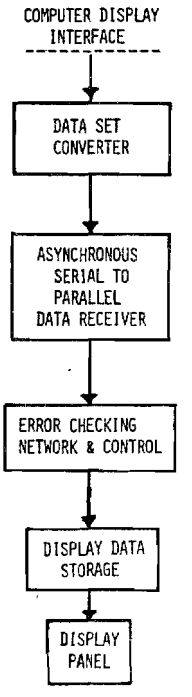

Figure 4.14 Block diagram of control tower display logic.

The Remote Tower Display provided a visual numeric readout of up to 32 digits. The unit operated from 110V a-c power and was completely self contained including power supplies, numeric readouts, eight segment drivers, oscillators, and receiver logic circuits. Two switches, OFF-ON power switch and BRIGHT-DIM display switch, were the only controls.

Computer stored data were automatically transmitted to the Remote Tower Display once during each sounder cycle. The data update rate could be varied with internal timing and error checking networks to insure that the 32 characters were correct and in proper order. These checks were made at both the transmit and receive terminals. The error checking network in the Remote Tower Display expected a continuous sequence of 32 characters with a character-to-character time no greater than 145 msec. The actual block length was 34 characters with the last two being blanks. These blanks caused the Remote Tower Display to load and display the newly received data block. If there were an error in

the number of characters sent, in the parity of the character, or in the inter-character time, the readout would not be changed and the last good data block continued to be displayed. If no good data blocks were received within 4 min, the entire display would go blank indicating a hardware failure in the computer, the sounder, the Remote Tower Display or an inoperative data coupler.

Operation of the display unit in the control tower indicated two problems that should be corrected in the next model. The controller needs a light intensity control that would allow him to adjust the brightness for changing ambient light. Second, the position of the wind speed and direction readout should be reversed so they agree with the standard format for wind readings used by the National Weather Service.

CHAPTER 5

SYSTEM CALIBRATION

5.1 INTRODUCTION

The calibration of the wind measuring acoustic Doppler system implies comparison with an accepted standard for wind measurement. When the present project was being proposed to the FAA in 1971, the best calibration of the system was the comparison of horizontal Doppler measured speed with that measured from a Boundary Layer Profiler (BLP) tethered kytoon supporting a three-cup anemometer. The comparison of the Doppler from a single axis, bistatic system and BLP measurements was very good, as shown in Figure 1.6.

This first calibration attempt was for winds at one height only (200 m) while the acoustic Doppler system is capable of measuring a profile of wind from 30 m up to altitudes of at least 500 or 600 m. It can measure the winds along this profile at 30 m increments and by averaging over some five discrete pulses, can provide the complete profile about once every minute. No other wind measuring device can achieve similar data rate and height resolution, so it was necessary to define those compromises that would be acceptable in achieving a reasonable calibration of the acoustic system.

The acoustic system senses winds only at levels above those measured by a surface anemometer, rendering surface measurements unacceptable for calibration. Other methods that can be used for comparison are: tower mounted anemometers, balloon borne anemometers, and radiosonde derived wind profiles. Instrumented towers higher than 150 m are rare and not readily accessible, limiting tower augmented calibration to lower levels of the region probed by the acoustic Doppler system. In addition, towers tend to produce undesirable acoustic echoes readily picked up in the sidelobes of most antennas. To avoid this, the distance between the tower and sounder must be kept large, reducing the confidence of the wind comparisons.

Tethered balloons offer an acceptable alternative as a platform for an anemometer; however, they too are not without problems. The lift of most easily deployed balloons is only enough to carry one lightweight anemometer, to heights of a few hundred meters. In addition, it is impossible to deploy a tethered balloon system when the winds are greater than about 5 m/sec. Therefore, a tethered balloon borne anemometer can only be used to measure light winds, at one level, within perhaps 300 m of the ground.

The third potential calibration standard is the rawinsonde. While these are not limited in height, their height resolution is very poor and they gave only an instantaneous point wind reading. Standard ascent rates used by the Weather Bureau provide only about two wind readings between the ground and the upper limit of the range of the acoustic Doppler. Slower ascent rates can be used; however, if the wind is strong the radiosonde balloon will usually travel so far away from the test site by the time the upper wind readings are taken that they are of questionable value.

Despite these formidable difficulties a rather good set of calibrations were performed, using, at different times, each of the standard sensors described above. The first calibration tests in 1971 were made at the NOAA Table Mountain field site and employed an anemometer suspended below a tethered balloon provided, and operated, by personnel from NCAR, as explained in Chapter 1.

The equipment used for this test is shown in Figure 1.5. Since the balloon borne anemometer could not be used to verify the profiling capability of the acoustic Doppler technique, the objective of these first measurements was to simply demonstrate that the correct winds could be measured at a given level. Figure 1.4 summarizes the results of these tests which were all performed with the three-axis monostatic system. The correlation coefficient (r) of 0.94 between the winds measured by the BLP (Boundary Layer Profiler or balloon supported anemometer) and the acoustic Doppler system (DOP) shows excellent agreement. The run numbers referred to in Figure 1.4 correspond to various antenna tilt angles employed during the test.

5.2 HASWELL CALIBRATION TESTS

The original plan proposed to the FAA was to calibrate the Doppler system during the WPL sponsored 1972 Haswell, Colorado, experiment, where anemometer data from a 150 m tower were routinely available. The timing of the Haswell experiment and changes in the sounder configuration made it necessary to modify this original plan. The configuration first proposed was based on a monostatic system, which had been successfully used for wind measuring to heights of 200 m during specific meteorological events. Its simplicity and excellent Doppler resolution angle made it highly favored for use in the airport wind monitoring system.

Several antenna configurations were tested at Haswell from 13 July to 31 July 1972. These configurations included the spaced monostatic (see Section 4.1.1) and a clustered monostatic (see Section 4.1.2). Backscattered intensity and Doppler shift data were recorded for 80 hr under a variety of weather conditions.

The Haswell field work was completed and the equipment returned to Boulder prior to the final analyses of the data. At this time when the weakness of the returns was recognized, it was too late to repeat the exercise with a bistatic configuration for tower comparison of the winds. During the few times when strong monostatic signal was received from 150 m, the Doppler and tower wind comparisons were quite good, agreeing with our earlier tests using the balloon system.

5.3 TABLE MOUNTAIN CALIBRATION TESTS

Analysis of the Haswell data demonstrated that the maximum range of the monostatic configuration (C_T scattering only)was less than 500 m and that signal fading was a problem of serious proportions.

Based on these findings, the system was modified to employ a bistatic approach with spaced antennas having beam patterns that would cover the total required range up to 1000 m. Early test results at the Table Mountain field site near Boulder, indicated that the expected stronger bistatic signals (C_V plus C_T scattering) could be received from elevations up to 1000 m.

A second series of calibration tests was then planned. To make these tests at Haswell would have required reactivating the tower anemometers and the analog recording equipment, in addition to moving the entire acoustic sounder back to Haswell. The cost of doing this for a single experiment would have been prohibitive in terms of both manpower and time, delaying the project by as much as two or three months.

While the Haswell site offered the potential of tower winds up to 150 m, previous calibration measurements up to 200 m, using kytoons (BLP) showed remarkably good agreement between the Doppler measured winds and the suspended anemometers. With this in mind, it was felt that radiosonde measurements of the wind to heights of 1000 m should be given primary consideration. GMD-1 radiosonde equipment was readily available in the Boulder area and extensive equipment relocation was not required to conduct the tests at Table Mountain.

The equipment was set up at Table Mountain in the configuration shown in Figure 5.1. Only one leg of the total system was used for these tests, hence, only a single component of the wind was measured (along 221°-41° azimuth). The GMD-1 and radiosonde launch area are shown in their relative positions. The radiosonde, of course, measured the total wind making it necessary to resolve these winds into the component along the azimuth 221°-41° before comparing the two sets of measured winds.

It was recognized that the planned bistatic configuration would be weak at low elevations where the scattering angle approached 90°. To test the effect of this weakness, two modes of operation were used during the Table Mountain exercise. The first consisted of pure bistatic where the winds at all height ranges were determined from the bistatic signal at two receivers, B_1 and B_2, spaced several hundred meters apart. The second mode made use of the dead time between the original transmitted pulse and the time when the first signals were received at the near antenna B_1. The far antenna B_2 was pulsed at the same time as the vertically pointed antenna, and during the dead time, monostatic returns were received along the sloping beam of antenna B_2. Proper switching of the signal from the various antennas could then be used to insure coverage over a height range from about 30 m up to 1000 m.

Acoustic data were collected on an analog tape recorder for later digitizing and processing in the CDC 3800 computer. Radiosonde data were recorded on standard GMD-1 strip charts and later reduced by hand for final computer processing.

An abbreviated log of the data runs is shown in Table 5.1. The 72T1 series of runs was plagued with radiosonde failure, hence, the acoustic records for these times were not digitized. During the 72T2 series, all of the equipment functioned properly and several runs were obtained with good radiosonde and acoustic Doppler data being collected for the same periods.

TABLE MOUNTAIN TEST CONFIGURATION

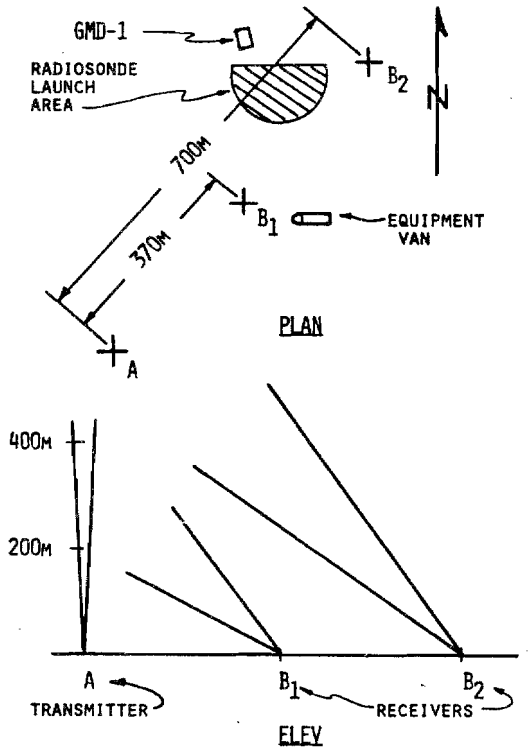

Figure 5.1 Sketch of the field layout for the calibration tests at Table Mountain, near Boulder, Colorado

Next, we discuss the acoustic Doppler calibration data taken at or near the radiosonde launches at 2232 MST* on 5 October 1972 and at 1105, 1135, 1400, 1434 and 1514 MST on 11 October 1972. A GMD-1 recorder failure during the 1208 launch on the 11th caused this run to be eliminated.

The six radiosonde wind profiles mentioned above are compared with the acoustic Doppler winds for the same time in Figures 5.2 to 5.7. Slow ascent balloons were used for all runs, insuring a large number (approximately twenty) of data points in the first 1 km. The program used for reducing the radiosonde wind data contained three smoothing options ranging from no smoothing to heavy smoothing, a feature which was useful for reducing the effect of spurious data points. At low elevation angles near the point of release, the GMD-1 often "lost" the balloon. When this happened the operators would note the time of "lock on"; however the lower portion of these records was unuseable.

While the slow ascent balloons significantly improved the resolution, they did produce the added complication that the wind profile had a large time dimension. In some cases nearly 15 min elapsed between the time of launch and the time when the balloon reached 1 km. The acoustic Doppler system measured this same profile in 8 sec. To adjust for this possible source of error the acoustic data from succeeding sets of pulses was averaged and matched with the radiosonde profiles as closely as possible in height and time. These time steps are noted in the figures which compare the two profiles.

*All times are Mountain Standard (MST)

TABLE 5.1

Table Mountain Data Log 72T

DATA RUN NO.	CONFIG.	START TIME (MST)	DURATION (MIN)	RADIOSONDES AT	COMMENTS
72T1A	Bist.	1045 4/10/72	62	1115	
72T1B	Bist.	1206 4/10/72	64		GMD-1 failure
72T1C	Bist.	1434 4/10/72	34		GMD-1 failure
72T1D	Bist	1200 5/10/72	30		No Radiosonde Calibration Run
72T1E	Mono-Bist.	1231 5/10/72	208	1218 1420	
72T1F	Bist.	1600 5/10/72	120		No Radiosonde Crew
72T2A	Bist.	2003 5/10/72	192	2232	Digitized: 2100-2315
72T2B	Bist.	1100 11/10/72	170	1105 1135 1208	Digitized: 1101-1300 Recorder failure
72T2C	Mono-Bist.	1350 11/10/72	84	1400 1434 1514	Digitized: 1350-1550

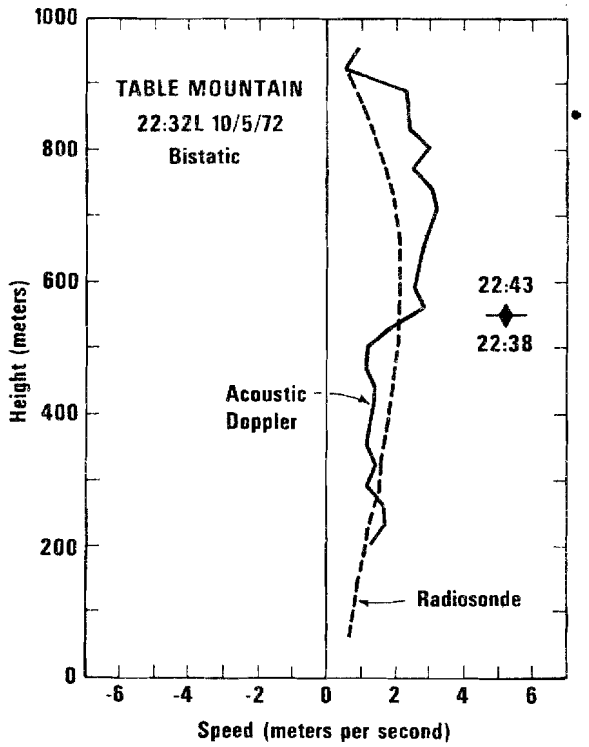

Figure 5.2 Comparison of radiosonde and acoustic Doppler derived wind profiles, run 72T2A.

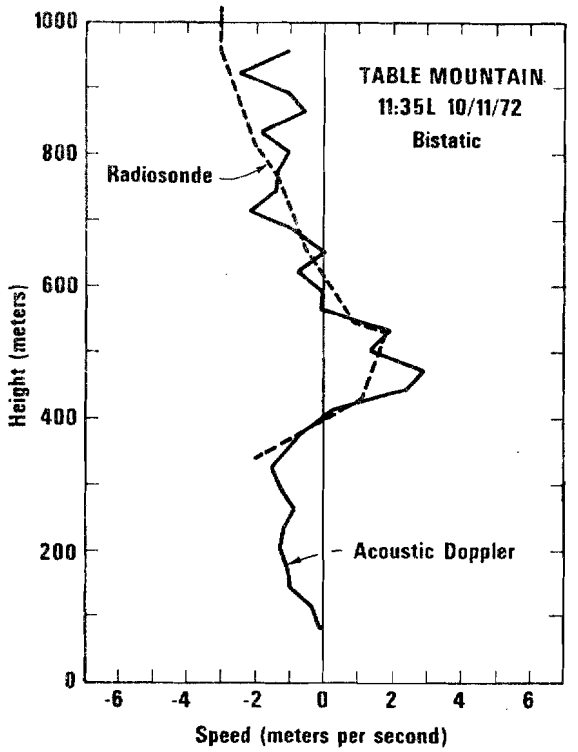

Figure 5.4 Comparison of radiosonde and acoustic Doppler derived wind profiles, run 72T2B.

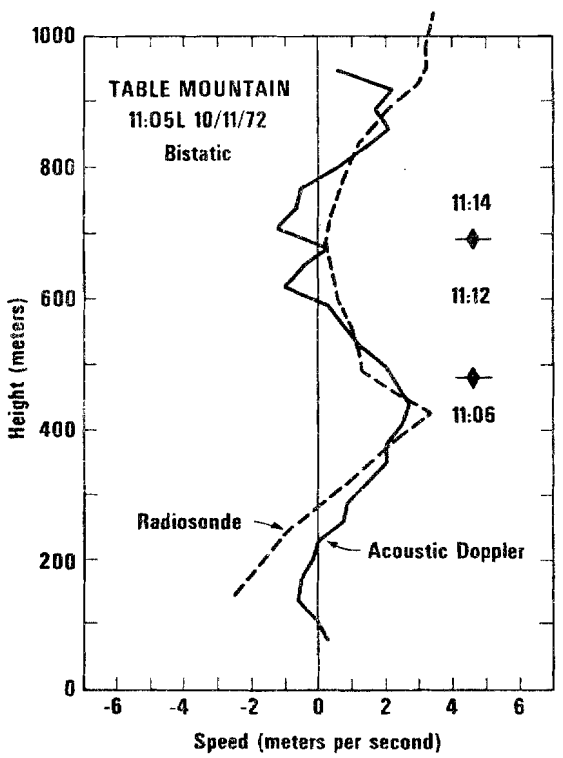

Figure 5.3 Comparison of radiosonde and acoustic Doppler derived wind profiles, run 72T2B.

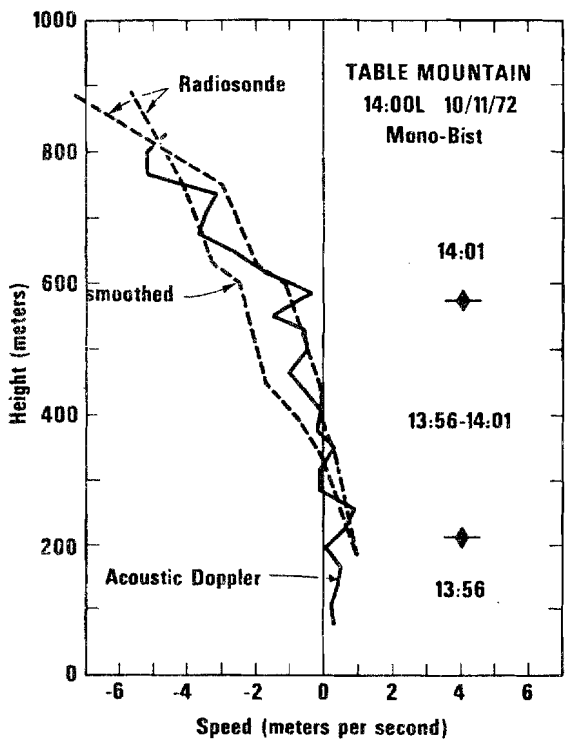

Figure 5.5 Comparison of radiosonde and acoustic Doppler derived wind profiles, run 72T2C.

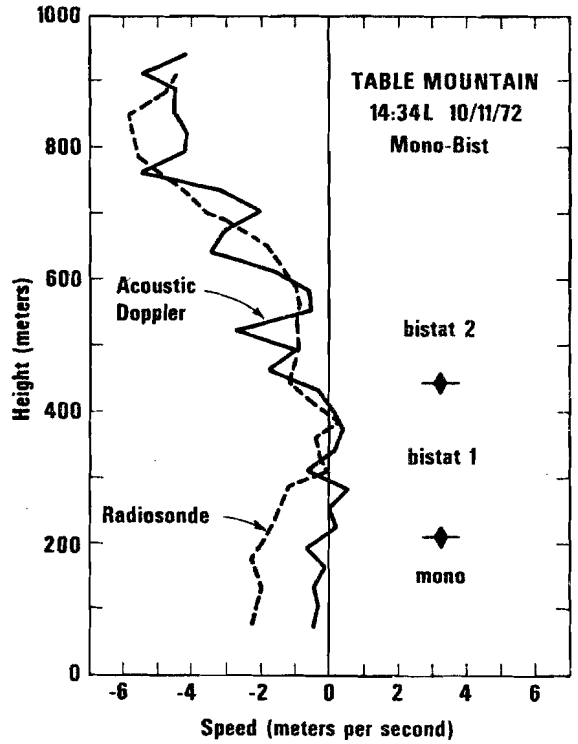

Figure 5.6 Comparison of radiosonde and acoustic Doppler derived wind profiles, run 72T2C.

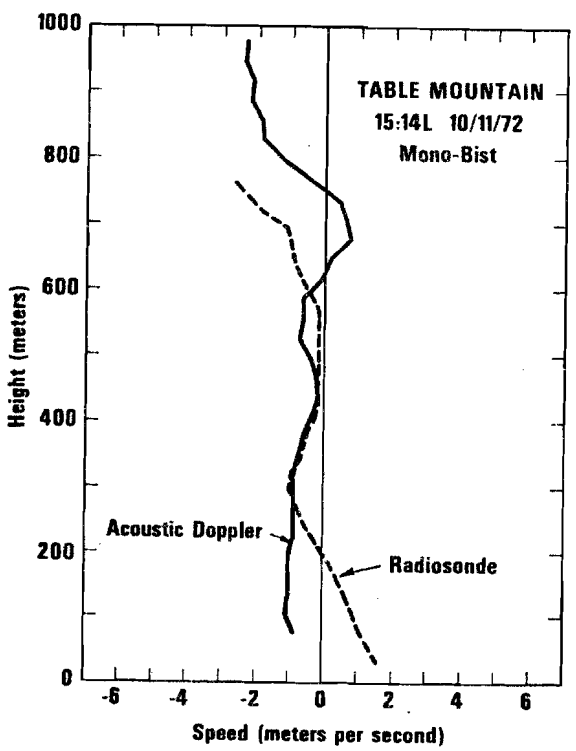

Figure 5.7 Comparison of radiosonde and acoustic Doppler derived wind profiles, run 72T2C.

The computer program used to reduce the acoustic Doppler data contains two variable length filters which produce different degrees of smoothing on the final wind profiles. The first filter, a running mean of 2 min maximum, was applied to the raw Doppler information; the primary purpose was to reduce the effect of noise spike tracking which might produce anomalous Doppler shifts. The second filter averaged over a maximum time of 5 min and was designed to measure the optimum scale of the wind eddies as they affect air traffic. Testing of these two filters could not be completed until the on-line NOVA computer was employed. Various filter lengths were used in the data shown in Figures 5.2 to 5.7, the values of each are also given in the discussion following the figures.

The radiosonde wind profile (dashed line) for 2232 MST, 5 October 1972 is shown in Figure 5.2. The solid line represents the winds measured by the acoustic Doppler. The full 2 min and 5 min filters were used on the Doppler profile and the heavy smoothing option was used on the radiosonde data. The lower portion of the acoustic Doppler curve represents the data prior to 2238; the upper portion, prior to 2243. The sharp gradient between 500 and 550 m may be the result of this time shift.

The data collected at 1105 is shown in Figure 5.3. In this case no smoothing was used on the radiosonde profile (dashed line) and only a 2 min filter length was used on the Doppler winds (solid line). The time shifts and valid times of the acoustic data are shown to the right of the profiles. This case, as did the previous one, employed only the two bistatic receivers, no monostatic pulse was used to fill in the lower elevations, explaining the lack of good agreement up to heights of 300 m.

Figure 5.4 shows the wind profile from a radiosonde taken 30 min later. The general shape of the profile is similar to that shown in Figure 5.3, suggestive of the time continuity between the two runs. Two minute averages were used for the Doppler data and light smoothing was used on the radiosonde winds.

The first combined monostatic-bistatic wind profile valid at 1400 on the 11th is shown in Figure 5.5. The Doppler shift data were smoothed over a 2 min period and the Doppler winds for a period of 5 min. Both smoothed and unsmoothed radiosonde profiles are plotted for this case. Again, the time shifts of the acoustic profile are shown on the right.

The second monostatic-bistatic profile is shown in Figure 5.6. The rather poor agreement at low levels is attributed to a calibration error in the monostatic receiver. This type of error was not a problem in the final Stapleton configuration because the receivers were locked together and BFO drift was automatically compensated for. The 2 and 5 min averaging routines were used on the Doppler data, and the radiosonde data was unsmoothed. This case is a good example of an unresolved problem encountered during the calibration tests. Note that the acoustic Doppler profile has a rather "spiky" appearance when compared with the radiosonde measured winds. This seems to occur even when the Doppler data have been heavily smoothed and the radiosonde not at all. When the radiosonde is used as the basis for comparison, it is impossible to determine if these spikes in the acoustic data are real or simply a function of the measurement instability. It can be argued that the radiosonde, by its very nature (a package suspended some 20 m below

a balloon) acts as a low pass filter as it ascends through the atmosphere. If the spikes seen in the acoustic record are real, then we must conclude that they are being removed by the filtering action of the radiosonde. This question can only be resolved over the entire 1 km height range by calibrating against a system like the English barrage balloon, which was used in Minnesota during the fall of 1973 by AFCRL.

The final radiosonde Doppler wind profiles, taken at 1514 on the 11th, are shown in Figure 5.7. Heavy smoothing was used on both profiles. The GMD-1 printer was only marginally operational for this case and the accuracy of the radiosonde winds must be questioned, as a great deal of interpolation was required before the data could be processed. This may explain the rather poor agreement at both the lower and upper levels.

The six profiles discussed above were used as the data base for estimating the statistical significance of the calibration tests. Data points were extracted at each 50 m increment of each profile throughout the range of heights where both radiosonde and Doppler profiles were available. These points were then used to generate the scatter diagram in Figure 5.8. If we assume that the radiosonde data are perfect (a rather tenuous assumption) and make them the independent variable, the linear regression line through the data follows the equation

$$DOP = 0.16 + 0.85\ RAD$$

where DOP represents the acoustic Doppler data and RAD the radiosonde measured data points. This regression line is shown as the solid curve in Figure 5.8, and can be compared with the theoretically perfect line of slope 1.0 and a zero intercept, shown by the long dashes. The 95% confidence limits on the regression line slope are 0.95 and 0.75, not including, but very close to 1.00. The 95% confidence limits on the mean of the zero y intercept are 0.35 and -0.0215, including zero. The standard error of estimate for the data sample is ± 0.89 m/sec This is well within the required ± 2.5 m/sec requirement for the accuracy of the Doppler system, as stated in Section 3.2.2.4 of the interagency agreement.

A direct comparison of the accuracy of the wind direction is impossible with this data set, as only a single wind component was measured by the Doppler. It should be noted that any directional error in the radiosonde data would be transferred to the data points used for the statistics when the component along 221° was extracted. This factor would tend to increase the spread of points in the scatter diagram.

Some data on wind direction were collected during the Haswell experiment and comparisons were made with both the tower and lower portions of the radiosonde profiles. These limited wind direction comparisons were very good, generally agreeing to within ± 5°, however, the data sample from Haswell was too small for a valid statistical test. It is worth noting that the accuracy of the wind direction is purely a function of the accuracy of the speed determination, since two measured orthogonal components are used to derive the direction of the total wind vector.

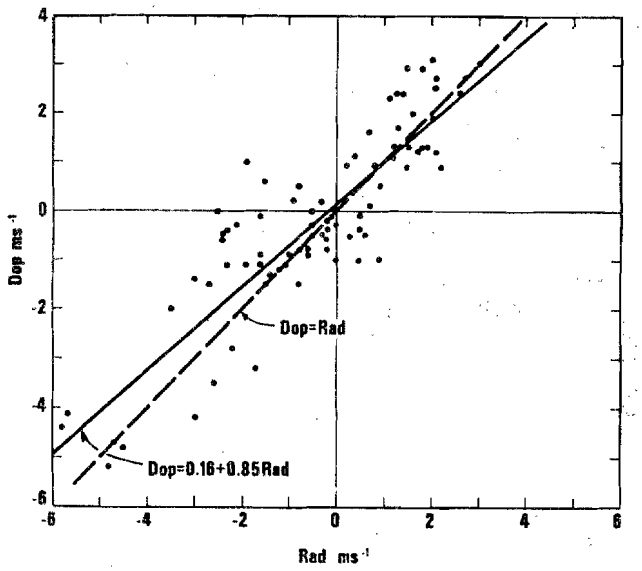

Figure 5.8 Scatter diagram of points taken from the acoustic Doppler and radiosonde wind profiles, both axes are in m/sec. See text for further explanation.

The continuity of the Doppler winds was checked by generating time height cross sections of the isotachs. An example of this check running from 1358 to 1409 on the 11th is shown in Figure 5.9. The radiosonde track at 1356 (see Figure 5.5) is superimposed on the contours to give a general idea of where the balloon penetrated this wind field. While the radiosonde profile is the only quantitative check on the accuracy of the wind, it is informative to see that no sharp discontinuities or unrealistic gradients appear.

5.4 RESULTS AND CONCLUSIONS ON THE CALIBRATION TESTS

For the data sample used, the statistical analysis demonstrates that the acoustic Doppler system is within the ± 5 knot limit specified in the FAA/NOAA agreement. The calibration test should, however, be considered minimal leaving several questions unresolved.

The highest wind speed encountered during the test was just under 6 m/sec (11.6 knots), leaving the system performance and accuracy at higher wind speeds untested. This deficiency was corrected during the Stapleton operation where standard radiosonde ascents were available for further comparison with the Doppler winds. On one occasion, winds of 13 m/sec were measured by the radiosonde at 600 m, in excellent agreement with the acoustic Doppler.

The problems inherent with the radiosonde profiles (i.e. lack of resolution or smoothing of the profile and infrequent single profiles with no indication of time continuity) will, of course, still be unresolved.

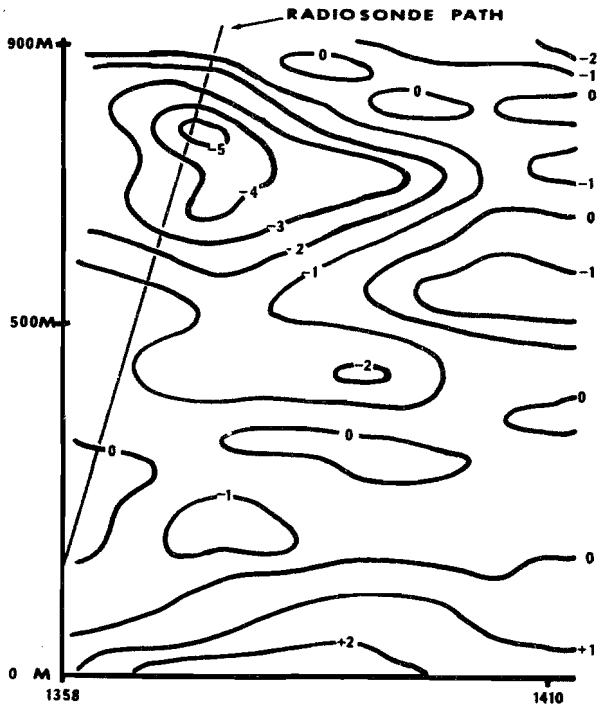

Figure 5.9 Time-height cross section of acoustic Doppler determined isotachs (m/sec) along the 221°-41° azimuths.

To fully calibrate the system the comparison measurements should have equal or better resolution in both space and time. This can be achieved with medium quality tower mounted anemometers; however, only a few towers in the U. S. are tall enough to reach even near the mid-range of the acoustic Doppler system. A second alternative is available, but would require considerable time and funds. This consists of a British designed system, having very accurate anemometers spaced along the tether cable of a large barrage balloon. The system has a range capability of between 1000 and 1500 m and would provide a continuous output of the winds at several levels. The device was operated for a short period at a field site in northern Minnesota during the late summer and fall of 1973. The system has now been returned to England, and no further U. S. tests are planned. If in the future the balloon system is again in the U. S., it could provide an ideal calibration standard for the acoustic Doppler system.

To summarize our efforts to calibrate the system indicate that the wind speed and direction can be measured to the tolerances specified in the original agreement (within 5 knots and 20 degrees). We cannot, at this time, tell how consistent the measurements will be under various operating conditions such as periods of very high ambient noise level and/or weak atmospheric scattering.

CHAPTER 6

AIRPORT OPERATIONAL TESTS

6.1 INTRODUCTION

The objective of airport testing was to place an experimental Acoustic Doppler Wind Measuring System in the operational environment of a large airport. This type of installation was deemed necessary to determine such factors as the effect of high level ambient background noise on the performance of the acoustic system, and to introduce operational personnel to new methods of measuring and using wind information. While it is difficult to make a qualitative assessment of the success of the airport operation, this should not detract from the importance of placing a new experimental device in a sometimes harsh operational setting. The lessons that are learned can save a great deal of time and expense during later phases when corrective measures become more costly and time consuming. In addition, the feedback from users is a great help toward improving the design of the system, insuring that the data will ultimately be presented in the best possible form.

6.2 SITE SELECTION

Any one of several major airports would have been suitable for the tests which culminated Phase II. The final decision was based primarily on logistics. To reduce the expense of moving men and equipment long distances, Denver, Colorado's, Stapleton International Airport, only 30 miles from the Boulder laboratory, was selected for the experiment.

Preparation for the airport tests started in March 1973. In consultation with local FAA representatives, two potential sites at Stapleton were selected. One was located in an open field west of the north end of the north-south runway. The second potential site was the east of the south end of the north-south runway. The second site was more centrally located; however, planned construction of commercial hangers in this area during the latter part of 1973 would have created an unacceptable amount of noise, and for this reason, the first site was selected. Figure 6.1 shows the general airport layout and the location of the antennas and the equipment van (the control tower and terminal complex are off the map to the left). The equipment van was located inside of the airport perimeter fence, affording some protection from potential vandalism. The antennas were placed in a city-owned field that was leased by a farmer. The presence of cattle and farm implements created minor problems, but nothing more serious than the occasional visit to the bunker by a cow seeking shelter from a storm.

6.3 INSTALLATION

Temporary bunkers, made by excavating the loose soil and erecting wooden retaining walls and wooden roofs, were emplaced during the spring of 1973. Unusually heavy rains complicated construction by causing soil erosion and occasional cave-ins of the bunker walls.

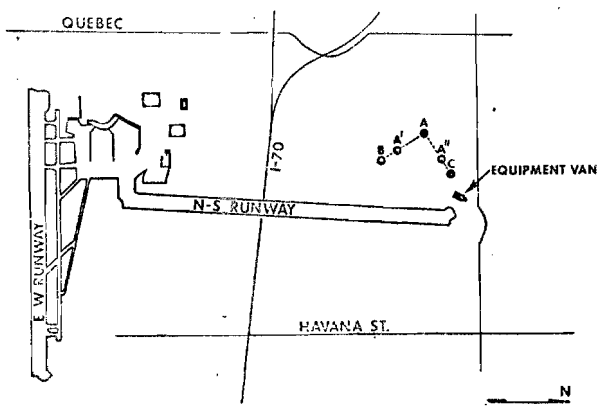

Figure 6.1 General layout of Stapleton International Airport showing the position of the Acoustic Doppler Wind Measuring System.

The bunkers were completed and the cables laid before moving the equipment van to the site in late August. The cable was placed in 6 inch deep trenches and covered to prevent damage by hawks. Leaking cable connectors and subsequent corrosion caused problems which delayed the final test.

We learned soon after the test started that the configuration first scheduled for the airport site (see Section 4.1.4) was not adequate due to the high background noise levels. Operations were delayed while the configuration was changed to that described in Section 4.1.5.

The system was operated in this mode for about 1 month, during which time modifications to the computer program were made. In late November, the display subsystem was placed in the control tower and operated on a nearly continuous basis until 23 December 1973. Work on the archiving portion of the computer program continued during this time, requiring that the display be turned off for brief periods. The antennas and bunkers were not designed to cope with snow, as the original test schedule called for operation during summer and early fall. The lack of snow removal devices resulted in further disruptions during two heavy snowstorms. The addition of heating elements imbedded in the antennas would have eliminated this problem.

6.4 RESULTS

The only available means of checking the accuracy of the winds measured by the acoustic Doppler system at the airport were the twice daily radiosondes taken by the National Weather Service. These data were collected and compared with the Doppler records on a

regular basis. Many of the comparisons showed only marginal agreement and some showed no agreement at all. Later analysis indicated that the total lack of agreement could usually be traced to some equipment malfunction. The distance between the radiosonde launch point and the Doppler site was nearly 3 miles. Judging from the difficulty experienced in the earlier Table Mountain calibration tests, where comparisons were made with a slow ascent radiosonde launched at the same location as the acoustic system, it is not surprising that the agreement between the Stapleton radiosonde winds and the Doppler winds was only marginal.

Despite these difficulties, some of the comparisons were excellent and indicated that when all systems were functioning properly very good wind measurements could be obtained. One example of the Doppler winds compared with the radiosonde winds is shown in Figure 6.2. This figure is a reproduction of the actual computer display printout, which is available at all times in the equipment van. The left side of the graph shows a plot of wind speed (m/sec vs. height (m); the right side of the graph shows the wind direction (degrees azimuth) vs height (m). The numbers in the top left corner of the graph are the calculated wind shear and ground wind in the same format that is transmitted to the control tower display (note the change of units to feet and knots). The valid time for this wind profile is given to the right of the tower display facsimile. In this case, the valid time was 04:56:00 Mountain Standard Time (MST) on 5 December. The radiosonde wind profile shown by the dashed lines was valid at 0500 MST on 5 December, 4 min after the valid time of the Doppler profile. The circled Xs' on the radiosonde wind profile indicate the actual data points that were reported. This diagram shows that the radiosonde provides only gross detail when compared with the acoustic Doppler winds. The wind profiles shown in Figure 6.2 represent measurement of the highest wind speeds that have been confirmed by an independent measurement. This is not a trivial point, because of the difficulty in finding an independent system that can operate in high winds at these altitudes, and in the good fortune of having both systems operating when strong winds occurred.

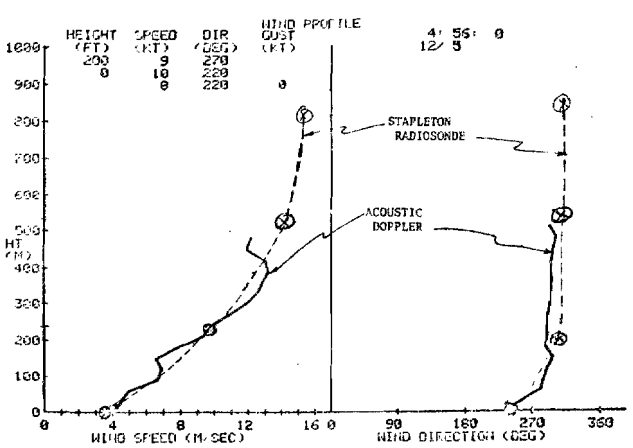

Figure 6.2 Comparisons of acoustic Doppler wind profile (04:56 MST 5 December 1973) with Stapleton Airport radiosonde wind profile (0500 MST, 5 December 1973).

Other examples of wind comparisons that have been made at Stapleton are shown in Figures 6.3 and 6.4. Note the lack of agreement, especially in Figures 6.4 of the ground winds. This is almost certainly due to the large separation distance between the measurement points. Due mostly to local terrain irregularities, surface winds tend to be less homogeneous over large distances than do winds aloft.

The gap near 500 ft on the Doppler profile shown in Figure 6.4 is the result of a still unsolved problem. This gap is near the point where the short range and long range bistatic systems overlap. As was mentioned in Section 4.2.1, the antenna beam patterns are too narrow for this application. Inefficiency of these beams near their outer limits occasionally result in such data gaps. This problem can only be eliminated by the development of antenna beams which have wider coverage in the vertical direction.

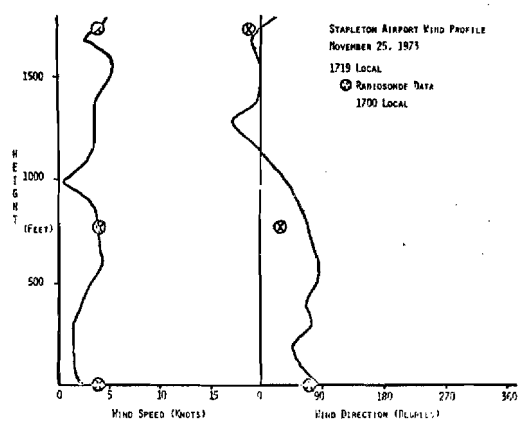

Figure 6.3 Reproduction of the acoustic Doppler wind profile (solid line) and the Stapleton radiosonde winds on the date shown. (Note the use of knots rather than m/sec.

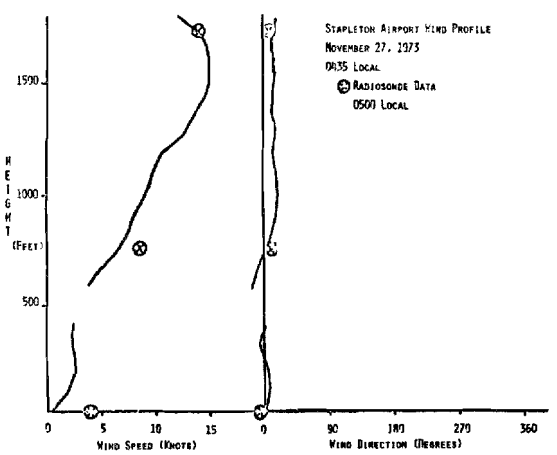

Figure 6.4 (See Figure 6.3).

To totally assess the effectiveness of the control tower display, the test period will need to be much longer. This type of wind information is new to the air traffic controllers, and I suspect that it will be essential for them to "live with it" for an extended period before they fully appreciate its usefulness, not to mention begin to trust the output and relay it to the pilots. This is an important aspect of introducing new technology to operational personnel and should not be relegated to the status of letting the user solve the problem of implementation. Training and educating will be essential, not only for the air traffic controllers, but also for the user: the pilots.

It was my impression that the controllers viewed the new instrumentation with curiousity. Their level of interest was such that they were very cooperative when asked to notify us when the display appeared to malfunction. In addition, they were very helpful in suggesting changes in the display light intensity, and asking for variable control so they could accommodate changes in the ambient background light.

I doubt that more than this could be expected from such a brief exposure. The important point is that the exposure was made and at least some exchange of ideas was started.

CHAPTER 7

SUMMARY

The need for more complete wind information in the mesoscale environment of airports has been established by the recognition that many landing incidents are wind related. There is a growing awareness that many short landings, missed approaches and, indeed, fatal crashes, previously blamed on pilot error, might well be the result of strong wind shear within the first few hundred meters above the ground. Our rather meager understanding of such wind shears suggests that they are transient - lasting only for periods of minutes up to a few hours. Our lack of knowledge in this area stems largely from the inadequate amount of data that can be collected with the radiosonde, which in practice is only used twice per day at fewer than 100 points in the United States. The radiosonde, designed for synoptic scale measurements, provides only about two or three wind measurements in the first 1 km above the ground Measurements on such gross time and spatial scales would completely miss a large percentage of the hazardous wind shears that occur. For this reason, not only are we left with inadequate data for establishing the nature and probability of occurrence of wind shear, but also we have no device that can provide adequate warning of hazardous conditions during landing operations.

The introduction of jumbo jets to the commercial fleet has added a second and equally perplexing problem for aircraft which must follow them in the approach pattern. The wing tip vortices shed by these large aircraft can prove fatal if encountered in the critical landing phase by a lighter aircraft. Among the many schemes which have been proposed for dealing with these hazardous vortices is to predict where they will be within a few minutes after they are generated, thus, making it possible to establish a minimum safe spacing between aircraft landings. Low-level winds and stability are the key to success for this proposed solution. In order to make accurate short term predictions of the vortex position, it is essential that the controlling wind field be known on a time scale equivalent to the desired forecast interval. Again, present wind measurements are inadequate for this task and we must look to new and unique methods for making higher resolution measurements.

Several ground based remote sensing devices show promise for providing a solution to this important wind measurement problem. An analysis of these techniques indicates that all of the proposed devices still have unknowns, such as availability of adequate tracers, ability to operate under all types of meteorological conditions and the accuracy with which measurements can be made. The status of these devices ranges from theory to experimental models.

Using as a guide the need to have a viable system in operation as soon as possible and the criteria that the device to be developed must show reasonable promise of success, the best selection appears to be the Acoustic Doppler System. Experiments have demonstrated that the acoustic technique can measure the winds at acceptable temporal and spatial scales and the device has reached at least the latter stages of experimental development. The acoustic system has recognizable shortcomings that cannot be fully assessed until prototype versions have been constructed and operated for extended periods in the airport environment. For example, it is known that heavy precipitation and strong surface winds will degrade or completely prevent the collection of good information.

The Acoustic Doppler Wind System described in this report is the culmination of nearly 3 years of designs and tests. It is the first such system which is capable of producing wind information on a real-time basis. To achieve this it was necessary to interface an acoustic sounder, having Doppler extraction capability, with an on-line computer. The entire concept as well as many of the system components are drawn from the latest state-of-the-art. The experimental system which was installed at Stapleton Airport was still undergoing modifications when the operational phase was started, and many desirable modifications were identified which could not be incorporated in the design.

Clearly, the experimental system is not yet optimum, but we are now in a position to isolate the major problem areas and to correct them before prototype development is started. A receiving antenna having a beam pattern shaped specifically for use with the multiple transmitter configuration is essential. Without such an antenna, the system will have unacceptably weak signal regions along the vertical, distorting the final wind profiles and producing gaps in the data. This does not appear to be an intractable problem and an intensive design and testing effort should yield a solution.

An equally critical problem, again involving the antenna sub-system, is the design of the antenna protective structure. The bunkers used during the Stapleton tests were crude and did not incorporate such features as snow removal provisions or protective berms to reduce the effect of ambient noise along the horizon. Since the bunker shape also affects the a antenna beam pattern, its design should be made an integral part of the antenna development effort. The success of protective devices can only be determined from operation under a wide variety of meteorological and background noise conditions, suggesting that more iterations will be needed when such data are collected during the prototype testing phase.

The Doppler Wind Measuring System used at Stapleton Airport was research oriented and designed for maximum flexibility so various parameters and the equipment configuration could be changed easily. Prototype equipment will not need, nor should it have, this same degree of flexibility. Many of the parameters that were tested can now be fixed. In doing this, the equipment will take on a different appearance and the operations and functions of the four sub-systems may be modified or transferred. For example, the acoustic sounder sub-system may be reduced to nothing more than the power amplifiers and a wideband receiver with the computer sub-system taking over the function of timing and Doppler extraction. Some testing of these modifications will be essential before the prototype design can be completed.

These equipment changes should not effect the basic operating principles of the system, and the results from the Stapleton tests will still be applicable. These tests have shown that an acoustic Doppler system can measure wind profiles in the environment of a major airport, and that such data can be transferred in real time to the user. Yet to be determined is how detrimental, in the long term, the effects of inclement weather and increased ambient noise will be. If severe weather proves to be an intractable problem, the ultimate system may require joint sensors (such as both electromagnetic and acoustic radar) to insure that wind profiles can be measured on a continuous basis.